Identification and characterization of proteins involved in proper functioning of UNC93B-Toll-like receptor complexes

Von der Fakultät für Lebenswissenschaften

der Technischen Universität Carolo-Wilhelmina

zu Braunschweig

zur Erlangung des Grades

einer Doktorin der Naturwissenschaften

(Dr. rer. nat.)

genehmigte

D i s s e r t a t i o n

von Elisa Reimer

aus Braunschweig

1. Referent:	Prof. Dr. Ralf-Rainer Mendel
2. Referentin:	Prof. Dr. Melanie M. Brinkmann
eingereicht am:	30.04.2014
mündliche Prüfung (Disputation) am:	25.07.2014

Druckjahr 2014

Vorveröffentlichungen der Dissertation

Teilergebnisse aus dieser Arbeit wurden mit Genehmigung der Fakultät für Lebenswissenschaften, vertreten durch den Mentor der Arbeit, in folgenden Beiträgen vorab veröffentlicht:

Publikationen

Bussey, K.A., **Reimer, E**.*, Todt, H.*, Denker, B., Gallo, A., Konrad, A., Ottinger, M., Adler, H., Stürzl, M., Brune, W., Brinkmann, M.M. The gammaherpesviruses KSHV and MHV68 modulate the TLR-induced proinflammatory cytokine response. *Journal of Virology*, 2014 (under revision)
*These authors contributed equally to this work

Tagungsbeiträge

Reimer, E., Brinkmann, M.M. Intracellular trafficking of the UNC93B-Toll-like receptor 9 complex. (Poster) 4th International PhD Symposium, HZI, Braunschweig (2010)

Reimer, E., Trupp, O., Brinkmann, M.M. Identification of proteins involved in proper functioning of the UNC93B-Toll-like receptor complexes. (Poster) 5th International PhD Symposium, HZI, Braunschweig (2011)

Reimer, E., Brinkmann, M.M. Regulation of endosomal Toll-like receptor signaling by the protein tyrosine phosphatase PTP1B. (Poster) 6th International Workshop "Interferon and Infection", HZI, Braunschweig (2013)

Bussey, K.A., Todt, H., **Reimer, E.**, Lau, U., Stürzl, M., Konrad, A., Brinkmann, M.M. Identification of KSHV ORFs that modulate the TLR-induced proinflammatory cytokine response. (Poster) 16th International Workshop on Kaposi's Sarcoma Herpesvirus (KSHV) and Related Agents, Puerto Vallarta, Mexico (2013)

Reimer, E., Ottinger, M., Brinkmann, M.M. Regulation of endosomal Toll-like receptor signaling by the protein tyrosine phosphatase PTP1B. (Poster) 43rd Annual Meeting of the German Society for Immunology (DGfI), Mainz (2013)

Reimer, E., Ottinger, M., Brinkmann, M.M. Regulation of endosomal Toll-like receptor signaling by the protein tyrosine phosphatase PTP1B. (Poster) The 14th Joint Scientific Meeting (LAVA, ESLAV and ECLAM), Cambridge, UK (2013)

Reimer, E., Ottinger, M., Brinkmann, M.M. Regulation of endosomal Toll-like receptor signaling by the protein tyrosine phosphatase PTP1B. (Talk) 6th International PhD Symposium, HZI, Braunschweig (2013)

Bussey, K.A., **Reimer, E.**, Todt, H., Gallo, A., Konrad, A., Stürzl, M., Adler, H., Brune, W., Brinkmann, M.M. The gammaherpesviruses KSHV and MHV68 modulate the TLR-induced proinflammatory cytokine response. (Poster) Innate Immunity to Viral Infections Keystone Symposium, Keystone, Colorado, USA (2014)

Table of contents

1. Introduction

1.1. Innate immunity

The innate immune system provides a first line of defense against invading pathogens. It includes physical barriers like the skin and other epithelial surfaces, humoral barriers like the complement system, and cellular barriers[1]. Innate immune cells include dendritic cells, monocytes, macrophages, granulocytes, and natural killer (NK) cells[2]. The innate immune system relies on a defined set of receptors and targets whole classes of pathogens in a nonspecific manner[3]. Cells and proteins of the innate immune system are constantly circulating in the body ready to immediately fight microbes at the site of infection. Activation of the innate immune system results in the elimination of pathogens and induction of the adaptive immune response which is mediated by the secretion of cytokines and upregulation of the expression of costimulatory molecules on antigen presenting cells (APC)[3].

The adaptive immune system is only found in vertebrates and, in contrast to the innate immune system, relies on highly specific antigen receptors which are expressed on B and T lymphocytes[1]. The adaptive immune response is usually inactive. A critical step for the induction of adaptive immunity is the interaction between activated APC and T lymphocytes. Upon activation, the adaptive immune system selectively expands antigen-specific B and T cells expressing unique antigen receptors[3]. This results in the specific elimination of pathogens or pathogen-infected cells and the development of an immunological memory which enables a more rapid response to specific pathogens upon further exposures[3].

1.1.1. Pattern recognition receptors

The innate immune system discriminates between self and nonself based on the recognition of invariant features of microorganisms[4]. Host recognition of these pathogen-associated molecular patterns (PAMPs) relies on germ-line encoded receptors called pattern recognition receptors (PRRs). PRRs do not only respond to molecules of microbial origin, but also sense host-derived molecules which are potentially dangerous, like for example nuclear proteins or nucleic acids which have been released from necrotic cells. These molecules are collectively termed damage (or danger)-associated molecular patterns (DAMPs). The class of PRRs which was first identified and is the best characterized is the class of Toll-like receptors (TLRs)[5,6]. Toll-like receptors are membrane-bound receptors which initiate immune responses upon the recognition of extracellular and endosomal PAMPs and DAMPs, like bacterial cell wall proteins or nucleic acids of microbial, but also of self origin. The second group of

PRRs is the group of C-type lectin receptors (CLRs). Like TLRs, most CLRs are transmembrane proteins. CLRs recognize carbohydrate structures and play a central role in innate immunity to fungal pathogens[7]. More recently, cytosolic PRRs have been discovered[8,9]. Cytosolic PRRs have evolved to sense nucleic acids of microbial and also host origin in the cytoplasm. The family of cytosolic PRRs comprises retinoic acid-inducible gene-I (RIG-I)-like receptors (RLRs) and cytosolic DNA sensors. RLRs sense cytoplasmic RNA and mediate antiviral responses, whereas cytosolic DNA sensors recognize cytoplasmic DNA upon viral or bacterial infections[10]. The activation of TLRs, CLRs, RLRs, and cytosolic DNA sensors induces the transcription of genes involved in inflammatory responses including proinflammatory cytokines and type I interferon (IFN)[10].

The last group of PRRs which has been described so far is the group of nucleotide-binding oligomerization domain (NOD)-like receptors (NLRs). The cytosolic NLRs sense PAMPs and DAMPs in the cytoplasm leading to the formation of multiprotein complexes called inflammasomes which consist of NLRs, apoptosis-associated speck-like protein containing a caspase recruitment domain (ASC), and caspase-1[11]. Caspase-1 is activated upon inflammasome formation and facilitates the maturation and secretion of the proinflammatory cytokines interleukin-1β (IL-1β) and IL-18[11].

1.1.2. Toll-like receptors

The Toll receptor was first identified to promote dorsoventral polarity in the development of the fruit fly *Drosophila melanogaster*[12]. A mutation in the *toll* gene resulted in abnormal embryonic development. Later, the group of Jules Hoffmann showed that the Toll receptor contributes to the host defense against fungal infections in *Drosophila melanogaster*[5]. The first human homolog of the *Drosophila* Toll protein, hToll, was described in 1997 by Ruslan Medzhitov and Charles Janeway[6]. This protein was identified as TLR4, the signaling receptor for lipopolysaccharide (LPS), by the group of Bruce Beutler who, together with Jules Hoffmann, was awarded with the Nobel Prize in Physiology or Medicine in 2011 *"for their discoveries concerning the activation of innate immunity"*[13,14]. Soon, further Toll homologs, collectively termed Toll-like receptors (TLRs), and their respective ligands were discovered[14].

TLRs are type I transmembrane proteins which consist of three different domains, an ectodomain, one transmembrane domain, and a cytoplasmic Toll-interleukin-1 receptor (TIR) domain. The N-terminal ectodomain consists of leucine-rich repeats (LRRs), which mediate ligand recognition, and the C-terminal cytoplasmic TIR domain mediates downstream signal transduction[15]. So far, 10 human and 12 murine TLRs have been

identified[16]. TLRs 1-9 are conserved in humans and mice. TLR10 has only been found in humans and TLRs 11, 12, and 13 are only expressed in mice (Table 1).

Table 1: Localization, species, and ligands of TLRs.

TLR	Localization	Species	Physiological ligands	Synthetic ligands
TLR1/ TLR2	Plasma membrane	Human and mouse	Triacetylated lipopeptides	Pam_3CSK_4
TLR2	Plasma membrane	Human and mouse	Lipoproteins, peptidoglycan, lipoarabinomannan, LTA	Not defined
TLR2/ TLR6	Plasma membrane	Human and mouse	Diacetylated lipopeptides, LTA, zymosan	Malp2, FSL-1
TLR3	Endolysosome	Human and mouse	dsRNA	Poly(I:C)
TLR4	Plasma membrane and endolysosome	Human and mouse	LPS, RSV fusion protein, MMTV envelope protein, mannan, glycosylinositol-phospholipids	Lipid A derivates
TLR5	Plasma membrane	Human and mouse	Flagellin	Not defined
TLR7	Endolysosome	Human and mouse	ssRNA	Poly(U), imidazoquinolines: imiquimod, resiquimod (R848)
TLR8	Endolysosome	Human and mouse	ssRNA	Poly(U), R848 (only in humans)
TLR9	Endolysosome	Human and mouse	DNA, hemozoin	CpG oligo-nucleotides
TLR10	Not defined	Human	Not defined	Not defined
TLR11	Endolysosome	Mouse	Profilin, flagellin	Not defined
TLR12	Endolysosome	Mouse	Profilin	Not defined
TLR13	Endolysosome	Mouse	Bacterial 23S rRNA	Not defined

LTA, lipoteichoic acid; Malp2, macrophage-activating lipopeptide 2; dsRNA, double-stranded RNA; Poly(I:C), polyinosinic-polycytidylic acid; LPS, lipopolysaccharide; RSV, respiratory syncytial virus; MMTV, mouse mammary tumor virus; ssRNA, single-stranded RNA; Poly(U), polyuridylic acid; rRNA, ribosomal RNA.

TLRs 1, 2, 4, 5, and 6 are primarily localized at the cell surface (Figure 1). They recognize microbial components such as lipopeptides, lipoproteins, lipopolysaccharide (LPS), and flagellin[13,17-20]. TLRs 3, 7, 8, 9, and 13 are mainly expressed intracellularly and have been described to recognize nucleic acids (Table 1)[21-25]. Most TLRs form

homodimers[26-30]. TLR2 heterodimerizes with TLR1 and TLR6 which extends its repertoire of ligands[31-33]. TLR11 can form heterodimers with TLR12[34].

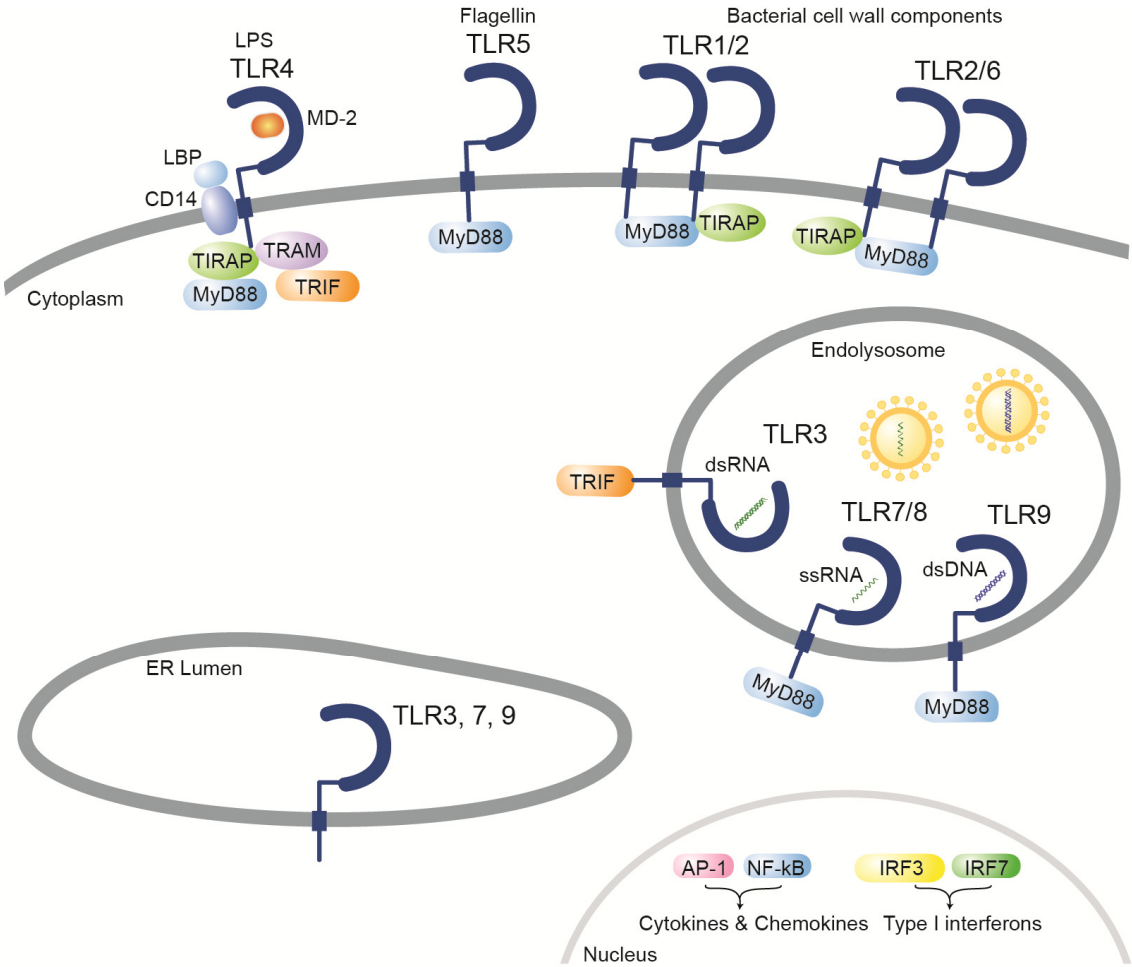

Figure 1: Toll-like receptors are localized at the cell surface or intracellularly. TLRs 1/2, 2/6, 4, and 5 are located at the plasma membrane. TLR1/2 and 2/6 recognize bacterial cell wall components, TLR4 recognizes LPS, and TLR5 recognizes flagellin. TLRs 3, 7/8, and 9 are located in the endolysosome and recognize nucleic acids. TLR3 senses double-stranded RNA, TLR7/8 sense single-stranded RNA, and TLR9 senses double-stranded DNA. Upon activation TLRs recruit specific adaptor proteins which lead to the production of proinflammatory cytokines and type I IFN.

Upon ligand recognition, TLRs recruit distinct TIR-domain-containing adaptor proteins including myeloid differentiation primary response gene 88 (MyD88), TIR domain-containing adaptor inducing IFNβ (TRIF, also known as TICAM1), TIR domain-containing adaptor protein (TIRAP, also known as MAL), and TRIF-related adaptor molecule (TRAM, also known as TICAM2) (Figure 1)[35]. The recruited adaptor molecules activate distinct signaling cascades which initiate proinflammatory cytokine and type I IFN responses (Figure 2). Signaling of cell surface TLR1/TLR2, TLR2/TLR6, and TLR5 mainly induces proinflammatory cytokine responses. In contrast, intracellular TLRs can induce proinflammatory cytokines as well as type I IFN[15]. TLR2 can also induce the production of type I IFN in response to vaccinia virus or mouse

cytomegalovirus upon internalization[36]. TLR4 forms a complex with myeloid differentiation factor 2 (MD-2). The TLR4-MD-2 complex initially signals from the cell surface upon delivery of LPS by the LPS-binding protein (LBP) and cluster of differentiation 14 (CD14) and is subsequently internalized into the endosomal compartment where it initiates an IFNβ response[37].

All TLRs, except TLR3, recruit MyD88. Upon TLR activation, MyD88 recruits IL-1 receptor-associated kinase 4 (IRAK4), IRAK1, IRAK2, and tumor necrosis factor receptor-associated factor 6 (TRAF6). The E3 ligase TRAF6 catalyzes the synthesis of K63-linked polyubiquitin chains which bind to TAK1-binding protein 2 (TAB2) and TAB3. TAB2 and TAB3 are components of the transforming growth factor β-activated kinase 1 (TAK1) complex and activate TAK1. The TAK1 complex simultaneously activates mitogen-activated protein kinases (MAPKs) and the IκB kinase (IKK) complex. The IKK complex consists of NF-κB essential modulator (NEMO), IKKα, and IKKβ and catalyzes the phosphorylation of IκB proteins. Degradation of IκB proteins facilitates translocation of the p50 and p65 subunits of NF-κB into the nucleus. Activation of the transcription factors nuclear factor kappa-light-chain-enhancer of activated B cells (NF-κB) and activator protein 1 (AP-1), which is activated by MAPKs, induces the production of proinflammatory cytokines like tumor necrosis factor (TNF), interleukin 6 (IL-6), and IL-12[15].

Recruitment of MyD88 by endosomal TLRs 7 and 9 can additionally lead to the activation of interferon regulatory factor 7 (IRF7) which triggers the production of type I IFN, a pathway that is especially important in plasmacytoid dendritic cells (pDC). Upon activation of TLR7 and TLR9, MyD88 leads to the recruitment of IRAK4 and TRAF6. This results in the activation of NF-κB, but also leads to IRAK1- and IKKα-dependent phosphorylation of IRF7 via TRAF3 activation. IRF7 initiates the production of type I IFN in the nucleus.

The adaptor molecule TRIF is used by TLR3 and the internalized TLR4-MD-2-LPS complex[38]. TRIF recruits TRAF6, TRAF3 and TNF receptor type 1-associated Death domain protein (TRADD) which interacts with Pellino-1 and receptor-interacting protein 1 (RIP1). RIP1 and TRAF6 activate the TAK1 complex which leads to the activation of MAPKs and NF-κB. Activation of TRAF3 additionally leads to the phosphorylation and activation of IRF3 via the TANK-binding kinase 1 (TBK1) and IKKε. Translocation of activated IRF3 leads to the production of type I IFN, mainly IFNβ[15].

TIRAP has been described as a sorting adaptor which links TLRs 2 and 4 on the plasma membrane to MyD88[15]. Recent evidence suggests that TIRAP also functions as a sorting adaptor for endosomal TLRs which signal via MyD88[39]. TRAM seems to

function exclusively in the TLR4 pathway and has been described as a sorting adaptor for the recruitment of TRIF to TLR4[15,35].

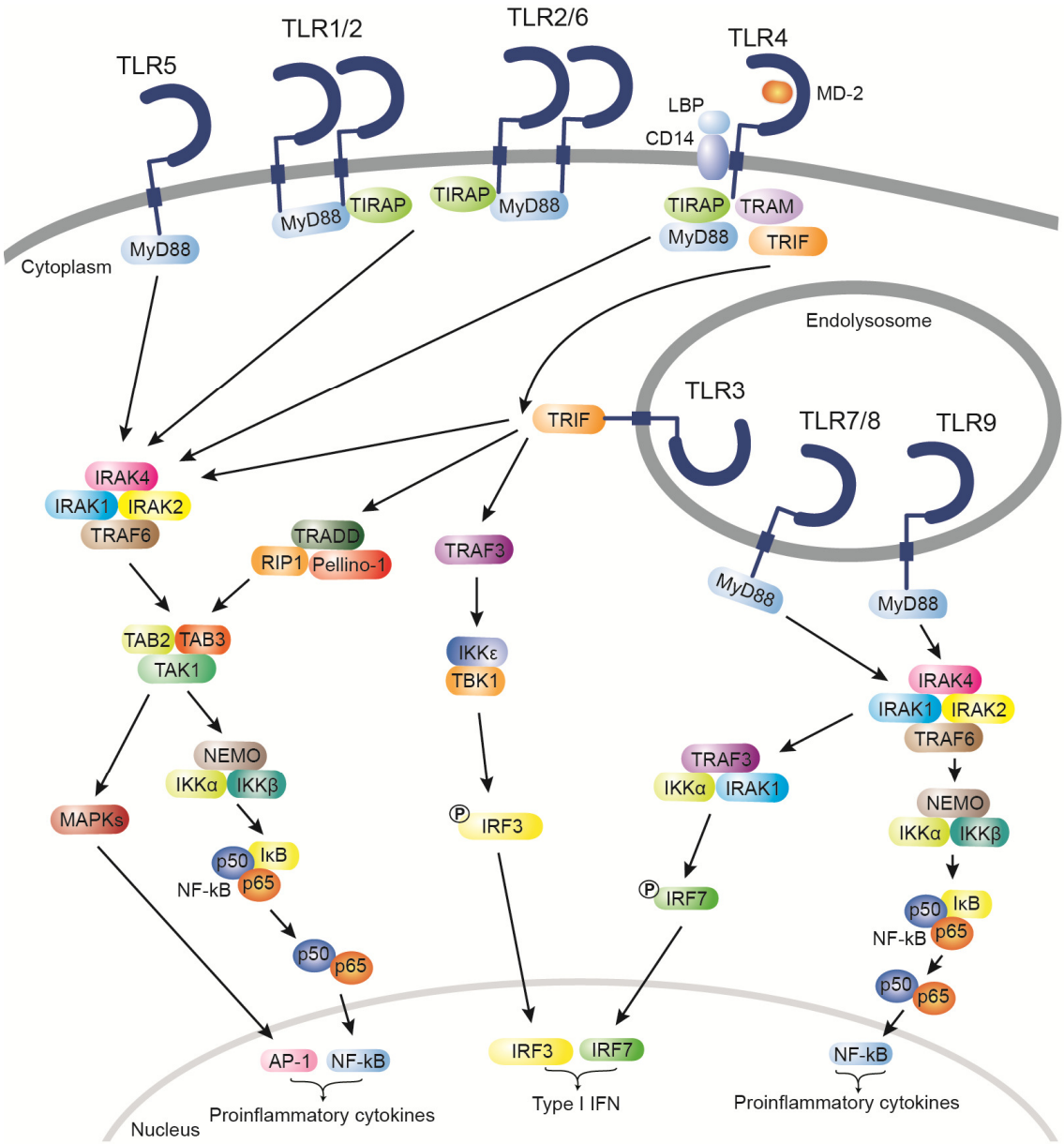

Figure 2: Schematic overview of TLR signaling. The adaptor protein MyD88 is used by all TLRs, except TLR3. MyD88 initiates signaling cascades which lead to the production of proinflammatory cytokines via the transcription factors AP-1 and NF-κB. Recruitment of MyD88 by TLR7 and 9 additionally activates the production of type I IFN via IRF7. TLR3 and the TLR4-MD-2-LPS complex use the adaptor molecule TRIF which initiates the production of pro-inflammatory cytokines and activates a type I IFN response via IRF3.

1.1.3. UNC93B regulates trafficking and signaling of intracellular TLRs

Nucleic acid-sensing intracellular TLRs reside in the endoplasmic reticulum (ER)[40]. Upon activation, TLRs 3, 7, and 9 rapidly relocalize to the endolysosomal compartment where they recognize and bind double-stranded RNA (dsRNA), single-stranded RNA (ssRNA), or double-stranded DNA (dsDNA), respectively, and initiate downstream

signal transduction[41]. Recent evidence suggests that RNA-DNA hybrids, which are essential intracellular replication intermediates generated during infection, are also recognized by TLR9 in dendritic cells[42]. The intracellular localization of nucleic acid-sensing TLRs is highly important to prevent autoimmunity caused by improper recognition of self nucleic acids[43,44]. It was shown that redirection of TLR9 to the cell surface by an exchange of its transmembrane and cytosolic domain with that of TLR4 facilitates the recognition of host genomic DNA by TLR9[43]. Similarly, the introduction of point mutations in the transmembrane domain of TLR9 ($TLR9^{TM\text{-}MUT}$) led to localization of $TLR9^{TM\text{-}MUT}$ to the plasma membrane where it recognized host genomic DNA and mice expressing $TLR9^{TM\text{-}MUT}$ developed systemic lethal inflammation[44]. Overexpression of TLR7 caused a fatal acute inflammatory pathology in mice[45-47]. Distinct motifs, which mediate the intracellular localization of nucleic-acid sensing TLRs, have been identified in the cytoplasmic linker region of TLR3 and the transmembrane regions of TLR7 and TLR9[48-51].

In a forward genetic screen using *N*-ethyl-*N*-nitrosourea (ENU) mutagenesis, mice with defects in signaling of intracellular TLRs 3, 7, and 9 and class I and II major histocompatibility complex (MHC)-restricted antigen presentation were identified[52]. Macrophages derived from these mice did not respond to stimulation of intracellular TLRs with Poly(I:C) (TLR3), resiquimod (TLR7), and CpG DNA (TLR9) and were termed “triple defect” (3d) mice. 3d mice are highly susceptible to infections with mouse cytomegalovirus (MCMV), *Listeria monocytogenes*, and *Staphylococcus aureus*. The cause for the 3d phenotype was mapped to one single histidine-to-arginine (H412R) point mutation in the *Unc93b* gene[52]. UNC93B (UNC-93 homolog B1 (*Caenorhabditis elegans*)) is a 598-amino-acid glycoprotein that localizes to the ER and is predicted to have twelve transmembrane domains with an N- and C-terminus facing the cytoplasm (Figure 3). Deficiency of UNC93B has been linked to herpes simplex virus-1 encephalitis (HSE) in children[53]. The H412R substitution is predicted to be located within the ninth transmembrane domain of UNC93B (Figure 3).

Wild type and mutant (H412R) UNC93B have similar half-lives (~4 h), but exhibit different migration patterns upon SDS-polyacrylamide gel electrophoresis (PAGE)[54]. Polyclonal antibodies raised against C-terminal or N-terminal peptides of UNC93B recognize wild type as well as mutant UNC93B[54]. In contrast to wild type UNC93B, which shows a diffuse band pattern, a more distinct band pattern is observed for mutant UNC93B. It has been shown that wild type, but not mutant, UNC93B interacts with the transmembrane domains of TLRs 3, 7, 9, and 13[54]. Chimeric TLR3 and TLR9 constructs in which the transmembrane domains of TLR3 or TLR9 were replaced with

the transmembrane domain of TLR4, were unable to interact with UNC93B, whereas chimeric TLR4 constructs containing the transmembrane domains of either TLR3 or TLR9 co-precipitated with UNC93B[54].

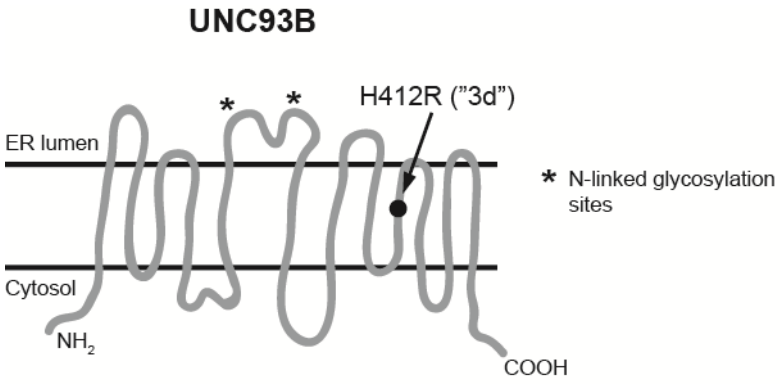

Figure 3: Predicted topology of UNC93B. UNC93B is an ER protein and is predicted to have twelve transmembrane domains with an N- and C-terminus facing the cytoplasm. The histidine-to-arginine (H412R) point mutation causing the 3d phenotype in mice is located in the ninth transmembrane domain of UNC93B. Predicted N-linked glycosylation sites are indicated (*).

UNC93B delivers intracellular TLRs from the ER to the endolysosomal compartment where they can bind their ligands and initiate downstream signal transduction (Figure 4)[55]. In cells derived from 3d mice, neither UNC93B nor TLR7 and 9 are able to leave the ER and therefore fail to respond to specific stimulation. In accordance with this observation, it has been shown that a portion of wild type UNC93B gained Endoglycosidase H (Endo H)-resistance in multiple cell types, whereas mutant (H412R) UNC93B failed to acquire Endo H resistant glycans, indicating that wild type UNC93B traffics through the Golgi apparatus[56]. N-linked glycosylation of wild type UNC93B was demonstrated using an UNC93B mutant in which an asparagine residue within a consensus N-linked glycosylation site was substituted (N251A)[56]. UNC93B was also linked to functioning of TLRs 11, 12, and 13[25,57-59]. Trafficking and signaling of cell surface TLRs is not affected by mutation of UNC93B[52,55].

UNC93B has been reported to mediate differential trafficking of endosomal TLRs[56,60,61]. TLR9 competes with TLR7 for UNC93B-dependent delivery to the endolysosome[60]. Trafficking of TLR9, but not TLR7, seems to be dependent on the N-terminal region of UNC93B[56,60]. UNC93B preferentially associates with TLR9. Mutation of aspartic acid at position 34 in UNC93B (D34A) biases the UNC93B-TLR association towards TLR7 and also TLR13 in dendritic cells (DC)[60]. Mice harboring the D34A mutation develop a spontaneous TLR7-dependent autoimmunity[61]. This study emphasizes the importance of UNC93B in the regulation of intracellular TLRs. At the ER, UNC93B facilitates

loading of TLR9 into coat protein complex II (COPII) vesicles and traffics in a complex with TLR9 through the Golgi apparatus[56,62]. In the same way, UNC93B mediates delivery of TLR3, TLR7, TLR11, and TLR13 to the endolysosome[56]. Acidic amino acids in the juxtamembrane region of nucleic acid-sensing TLRs seem to play an important role for their interaction with UNC93B as well as trafficking and signaling of these receptors[63]. TLR9 was initially thought to directly traffic from the ER via the Golgi apparatus to the endolysosomal compartment. However, recently small amounts of TLR9 were detected on the cell surface of human embryonic kidney (HEK) 293T cells transfected with TLR9 and UNC93B and immune cells such as splenic DC, B cells, and neutrophils which suggests that TLR9 traffics via the cell surface[56,64-66]. Internalization of UNC93B-TLR9 complexes from the cell surface to the endolysosome has been reported to be mediated by UNC93B-dependent recruitment of the adaptor protein 2 (AP-2) at the cell surface (Figure 5)[56]. In contrast, TLR7 does not travel via the cell surface and requires AP-4 for endosomal delivery after leaving the Golgi apparatus. Intracellular TLRs 3, 11, 12, and 13 seem to use the same route as TLR7[56].

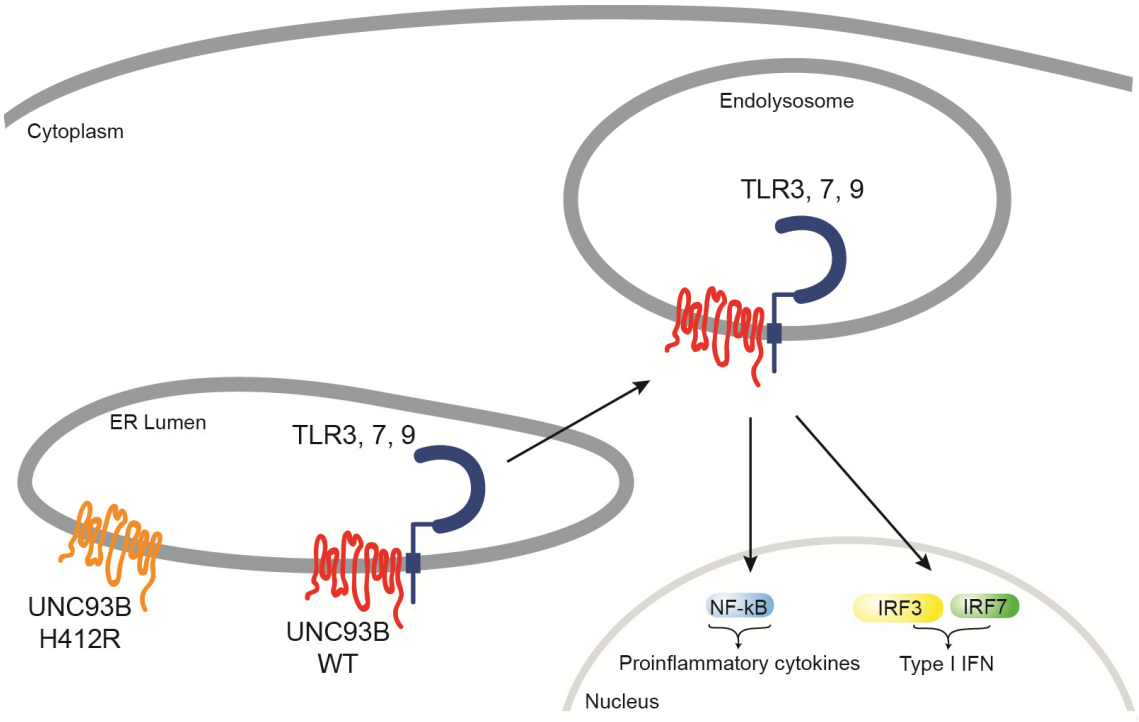

Figure 4: UNC93B mediates endosomal trafficking of intracellular TLRs. UNC93B interacts with the transmembrane domains of intracellular TLRs 3, 7, and 9 and delivers them from the ER to the endolysosome where TLRs initiate the production of proinflammatory cytokines and type I IFN upon ligand binding. Introduction of a single point mutation (H412R) in UNC93B disrupts binding between UNC93B and intracellular TLRs and both proteins fail to leave the ER.

Besides UNC93B, the ER chaperone proteins gp96 (also known as glucose-regulated protein of 94 kDa GRP94) and protein associated with TLR4 (PRAT4A) have been shown to mediate trafficking of intracellular TLRs. Heat shock protein gp96 is

necessary for the function of TLRs 1, 2, 4, 5, 7, and 9[67]. PRAT4A is required for trafficking of TLRs 1, 2, and 4 to the cell surface and trafficking of TLRs 7 and 9, but not TLR3, to the endolysosome[68]. gp96 and PRAT4A have been shown to work together and ensure proper folding of TLRs in the ER[69].

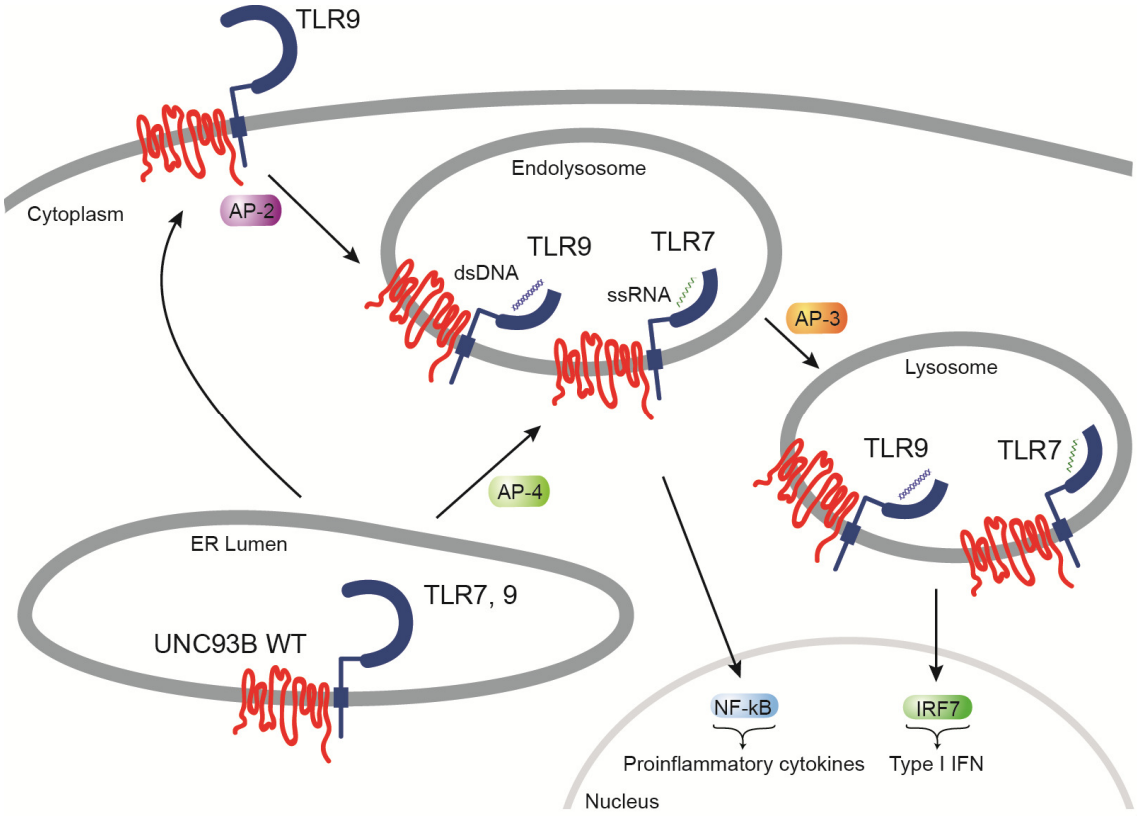

Figure 5: Proinflammatory cytokine and type I IFN responses upon stimulation of TLR9 and TLR7 are initiated from different endolysosomal compartments. In order to reach the endolysosomal compartment, TLR9 uses the secretory pathway and traffics together with UNC93B via the cell surface. At the cell surface, UNC93B recruits AP-2 which mediates endocytosis and endosomal delivery of the UNC93B-TLR9 complex. In the endolysosome, TLR9 binds to dsDNA and is proteolytically cleaved which facilitates the induction of a proinflammatory cytokine response via NF-κB. Upon AP-3-mediated delivery of TLR9 from the endolysosomal to the lysosomal compartment, it induces the production of type I IFN via the activation of IRF7. TLR7 in complex with UNC93B directly traffics from the ER to the endolysosome. This process is dependent on AP-4 and facilitates binding of TLR7 to ssRNA in the endolysosome.

Furthermore, the hepatocyte growth factor-regulated tyrosine kinase substrate (HRS) has been identified as a regulator for trafficking of TLRs 7 and 9 in a genome-wide RNA interference (RNAi) screen[70]. HRS is a component of the endosomal sorting complex required for transport (ESCRT) pathway which mediates lysosomal degradation of receptors upon their internalization from the cell surface. However, TLRs 7 and 9 seem to use a noncanonical ESCRT pathway for sorting and recycling rather than degradation. Ubiquitination of TLR9, and presumably TLR7, in a post-ER

compartment facilitates their recognition by HRS and delivery of these TLRs to the endolysosomal compartment[70].

In the endolysosome, the ectodomain of TLR9 is proteolytically cleaved to generate a functional receptor[71,72]. Proteolytic processing of the TLR9 ectodomain is a multistep event. The first cleavage step, which results in removal of the majority of the ectodomain, is mediated by asparagine endopeptidases or cathepsins. It is followed by a second trimming step which is completely cathepsin-dependent[73]. Cleavage of TLR9 has been shown in macrophages, B cells, conventional dendritic cells (cDC), and pDC[71,72,74]. Although proteolytic processing is not necessary for ligand binding, only processed TLR9 can recruit the adaptor protein MyD88. Binding of MyD88 to TLR9 is induced by a conformational change of the cytosolic TIR domains of preassembled TLR9 homodimers[72,75]. TLR3 and TLR7 are processed similarly to TLR9[73,76,77]. Besides intracellular localization of nucleic acid-sensing TLRs, the requirement for proteolytic processing provides an additional mechanism of protection against recognition of self nucleic acids. This seems especially important for TLR9 since it traffics via the cell surface on its way to the endolysosome[78]. Whether the N-terminal cleavage fragments of processed TLRs play a role in ligand binding and signaling is not clear. Two studies showed that deficiency of TLR9 can be rescued by expression of the C-terminal TLR9 cleavage fragment alone, suggesting that the N-terminal cleavage fragment of TLR9 is not required for TLR9 signaling[71,79]. On the other hand it was reported that a mutation in the N-terminus of TLR9 results in a signaling defect without affecting receptor dimerization or cleavage of TLR9[80]. Furthermore, it was shown that the N-terminal cleavage fragment of TLR9 remains associated with the truncated receptor and that it is required for signaling in response to DNA in bone marrow-derived (BM)-DC[64]. Structural analysis of TLR3 revealed binding sites for Poly(I:C) in N- as well as C-terminal regions of the TLR3 ectodomain[81]. Additionally, N- and C-terminal cleavage fragments of TLR3 have recently been reported to remain associated after proteolytic processing[82].

Upon ligand binding, TLRs 7 and 9 initiate the production of proinflammatory cytokines and type I IFN. The transcription of these two different classes of genes originates from two different types of endolysosomal compartments[83]. Activation of TLR9 with synthetic CpG oligonucleotides (ODN) results in the activation of different signaling pathways dependent on the type of CpG ODN[84-87]. Three different classes of CpG ODN have been identified: type A, type B, and type C CpG ODN. All of them contain immune stimulatory CpG motifs and have a phosphorothioate-stabilized backbone. Type A CpG

ODN are characterized by a phosphodiester central CpG-containing palindromic motif and a phosphorothioate 3`poly-G string. Type B CpG has a complete phosphorothioate backbone with at least one CpG dinucleotide. CpG C combines features of type A and type B CpG ODN. It has a full phosphorothioate backbone with a CpG-containing palindromic motif. CpG A aggregates in large multimeric complexes and strongly induces type I IFN. In contrast, CpG B remains monomeric and leads to the production of proinflammatory cytokines like TNF, IL-6, and IL12[78]. The ability of CpG A and CpG B to activate different immune pathways is caused by differential trafficking of these ODN to endosomal compartments[83]. In pDC, CpG A primarily traffics to early endosomes where it activates IRF7 and the production of type I IFN, whereas CpG B preferentially traffics to late endosomes where it activates NF-κB and the production of proinflammatory cytokines. Why these different types of CpG ODN end up in different endosomal compartments is not fully understood. If CpG B is complexed with cationic lipids, like the transfection reagent DOTAP, the localization of CpG B in pDC is altered to the early endosome which results in the activation of a type I IFN response[83]. Additionally, CpG A complexed with DOTAP can also induce the expression of type I IFN in cDC and macrophages indicating that functionally distinct signaling compartments exist not only in pDC, but also in cDC and macrophages.

The adaptor protein 3 (AP-3) has been shown to facilitate trafficking of TLR9, and probably TLR7, from the endosome to lysosome-related organelles (LRO) in pDC, a mechanism which is crucial for the TLR9-dependent type I IFN response (Figure 5)[88,89]. AP-3 directly interacts with TLR9 and mediates trafficking of the UNC93B-TLR9 complex from vesicle-associated membrane protein 3 (VAMP3)-positive endosomes to the lysosomal-associated membrane protein 2 (LAMP2)-positive LRO compartment[88]. AP-3-deficient mice did not produce type I IFN upon stimulation with ligands for TLR7 and TLR9, whereas the proinflammatory cytokine response was intact[88]. However, a second study reported that in addition to the lack of a type I IFN response, pDC derived from mutant mice also failed to produce proinflammatory cytokines in response to stimulation of TLRs 7 and 9 which would suggest a more general role of AP-3 for TLR trafficking[89].

1.1.4. Recognition of the murine herpesviruses mouse cytomegalovirus and murine herpesvirus 68 by TLRs

TLRs play an important role in the recognition of herpesviruses like mouse cytomegalovirus (MCMV) and murine herpesvirus 68 (MHV-68)[90]. Cell surface TLR2 and intracellular TLRs 3, 7, and 9 are involved in the recognition of the betaherpesvirus MCMV. TLR2 is important for the natural killer (NK) cell-mediated control of MCMV

in vivo[91]. It was shown that TLR2-deficient mice had elevated levels of MCMV in the spleen and liver after intraperitoneal infection. In inflammatory monocytes, TLR2 induces a type I IFN response upon recognition of MCMV[36]. Activation of the TLR2-dependent production of type I IFN requires receptor internalization and seems to be unique to inflammatory monocytes. In pDC, TLR9 is crucial for the induction of type I IFN and also mediates IL-12 responses and NK cell activation upon MCMV infection[92]. Intracellular TLRs 3 and 9 are essential for the recognition of MCMV *in vivo*[93]. Mice expressing a mutated, non-functional version of TLR9 ($TLR9^{CpG1}$) and mice deficient for TLR3 have been reported to be hypersusceptible to MCMV infection and to show impaired serum levels of type I IFN and IL-12p40 as well as impaired NK cell activation[93]. These effects were more pronounced in $TLR9^{CpG1}$ mice compared to TLR3-deficient mice. Furthermore, intraperitoneal infection with MCMV was lethal for $TLR9^{CpG1}$ mice, whereas TLR3-deficient mice showed no significant difference in survival rates compared to control animals, although they showed more signs of sickness than control animals[93]. This demonstrates that TLR9 is more important, but that TLR9 and TLR3 are both essential, for the innate immune response against MCMV infection. TLR7 also plays a role for the innate immune response upon MCMV infection[94]. In pDC, the type I IFN, IL-12, and TNF responses were impaired in pDC from TLR9-deficient, but not in pDC from TLR7-deficient mice. However, only in pDC from mice lacking TLR7 and TLR9, the type I IFN, IL-12, and TNF responses were completely abolished, indicating overlapping functions for TLR7 and TLR9 for the innate immune response against MCMV infection. Furthermore, mice deficient of TLR7 and TLR9 were more susceptible to MCMV infection *in vivo* than mice only lacking TLR9 upon intraperitoneal infection[94].

Cell surface TLR2 and intracellular TLR9 are involved in the recognition of the gammaherpesvirus MHV-68. An NF-κB reporter was activated by recognition of MHV-68 by murine TLR2 in transfected HEK 293T cells and IL-6 and type I IFN responses upon MHV-68 infection were reduced in TLR2-deficient mouse embryonic fibroblasts (MEF) and in TLR2-deficient mice *in vivo* compared to wild type controls[95]. TLR9 contributes to antiviral immunity against MHV-68 in dendritic cells[96]. Upon MHV-68 infection, TLR9-deficient dendritic cells secreted reduced levels of IL-12, IL-6, and IFNα compared to wild type cells and intraperitoneal infection of mice lacking TLR9 resulted in increased viral loads compared to wild type controls[96].

1.1.5. Cytosolic sensing of nucleic acids

During infections, pathogenic nucleic acids can access the cytoplasm of infected cells. Especially upon viral replication, RNA is generated in the cytosol. Cytosolic DNA does

not only occur during viral infections, but also upon infections with intracellular bacteria. Cytosolic nucleic acids are sensed by cytosolic PRRs in a TLR-independent manner. A variety of cytosolic PRRs detecting RNA or DNA in the cytoplasm has been discovered in the last few years (Figure 6)[16].

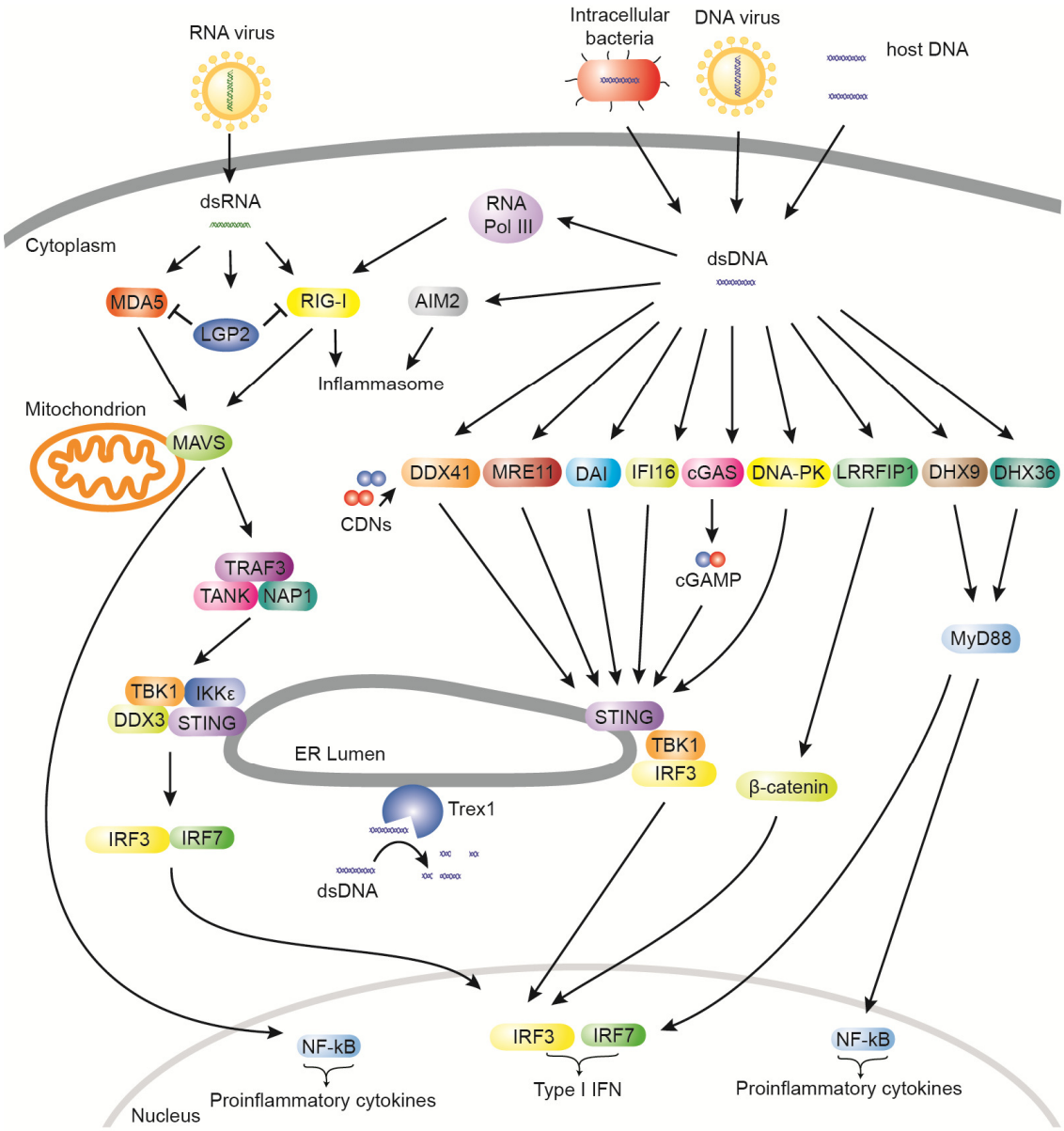

Figure 6: Overview of cytosolic sensing of nucleic acids. Cytosolic dsRNA is sensed by RIG-I and MDA5, which are regulated by LGP2, and induces the expression of proinflammatory cytokines and type I IFN via NF-κB or IRF3 and IRF7, respectively. Cytosolic DNA is sensed by RNA Pol III, AIM2, DDX41, MRE11, DAI, IFI16, cGAS, DNA-PK, LRRFIP1, DHX9, and DHX36. RNA Pol III converts dsDNA into dsRNA which is recognized by RIG-I. The cytosolic DNA sensor AIM2 as well as RIG-I induce the formation of inflammasomes. DDX41, MRE11, DAI, IFI16, cGAS, and DNA-PK activate the production of type I IFN via STING, TBK1, and IRF3 upon sensing of cytosolic DNA. LRRFIP1 activates β-catenin which induces an IRF3-mediated type I IFN response and DHX9 and DHX36 activate the NF-κB- and IRF7-mediated production of proinflammatory cytokines and type I IFN via MyD88. The ER-anchored exonuclease Trex1 digests cytosolic DNA and thereby negatively regulates STING-dependent cytosolic DNA responses.

Cytosolic RNA is detected by retinoic acid-inducible gene-I (RIG-I)-like receptors (RLRs). So far, three RLR family members have been identified, RIG-I, melanoma differentiation-associated gene-5 (MDA5), and laboratory of genetics and physiology 2 (LGP2)[8,97]. RLRs sense cytosolic dsRNA, a replication intermediate of RNA viruses. RLR signaling depends on the mitochondrial antiviral signaling protein (MAVS, also known as IPS-1 or CARDIF) which is located at the outer membrane of mitochondria and leads to activation of the transcription factors NF-κB, IRF3, and IRF7 and ultimately results in the production of proinflammatory cytokines and type I IFN[98].
RLRs are members of the DExD/H-box helicase superfamily. RIG-I and MDA5, but not LGP2, contain two caspase recruitment domains (CARD). The helicase domain mediates interaction with dsRNA and the CARD domains are required for downstream signal transduction. The role of LGP2 for cytosolic DNA sensing is not completely understood. It seems to have a regulatory effect on RIG-I and MDA5[99].
RIG-I specifically recognizes short RNA with blunt-ended base pairing and an uncapped 5`triphosphate end[100]. RIG-I preferentially recognizes short RNA molecules, whereas MDA5 preferentially recognizes long dsRNA[101]. It has also been shown that RIG-I recognizes dsRNA intermediates which have been transcribed from cytosolic B-form DNA by RNA polymerase III (Pol III)[102,103].
Whether viral RNA is recognized by TLRs or RLRs seems to be cell type dependent. It was shown that RIG-I and MDA5 are critical for the induction of a type I IFN response against RNA viruses in fibroblasts, macrophages, and cDC, whereas the TLR system was dispensable[104,105]. In contrast, intracellular TLRs were crucial for a type I IFN response against the RNA virus Newcastle disease virus (NDV) in pDC, while the production of type I IFN in pDC derived from RIG-I-deficient mice was not impaired[104]. This suggests that RLRs are the major sensors for viral RNA in fibroblasts, macrophages, and cDC, whereas in pDC TLRs play a more important role, although expression of RIG-I and MDA5 in pDC has been reported[106].

In contrast to the response to cytosolic RNA, which has been extensively studied for some time, the response to DNA has only recently come into focus when TBK1 and IRF3 were linked to the TLR- and RLR-independent recognition of cytosolic DNA[107,108]. The first direct cytosolic DNA sensor which was identified upstream of TBK1 and IRF3 was the DNA-dependent activator of IFN-regulatory factors (DAI, also known as ZBP1)[109]. DAI was shown to bind to dsDNA which enhances its association with IRF3 and TBK1. Knockdown of DAI in murine fibroblasts reduced their ability to induce an IFNβ response upon stimulation with cytosolic DNA[109]. However, a subsequent study showed that DAI is not essential for type I IFN responses to cytosolic DNA[110]. Recently,

DAI was reported to stimulate necrosis in MCMV-infected fibroblasts which activates an antiviral immune response[111].

The ER protein stimulator of interferon genes (STING, also known as MPYS, MITA, ERIS, or TMEM173) plays a crucial role for the TBK1/IRF3-mediated type I IFN response to cytosolic DNA[112-115]. STING has four N-terminal transmembrane domains, which mediate localization of STING to the ER membrane, and a large C-terminal cytoplasmic domain. It was shown that upon activation with dsDNA, the C-terminal domain of STING assembles with IRF3 and TBK1. This leads to TBK1-dependent phosphorylation of IRF3 and subsequent type I IFN production[116]. Upon activation, STING translocates with TBK1 from the ER to as yet undefined perinuclear vesicles in the cytosol[117].

Recently, the cyclic guanosine monophosphate-adenosine monophosphate (cGAMP) synthase (cGAS) was identified as a STING-dependent cytosolic DNA sensor[118,119]. Upon binding of DNA in the cytoplasm, cGAS facilitates the synthesis of cGAMP from adenosine triphosphate (ATP) and guanosine triphosphate (GTP). cGAMP acts as a second messenger and binds to STING. STING recruits TBK1, which phosphorylates IRF3 and leads to the production of type I IFN[116]. It has been shown that cGAMP spreads to neighboring cells via gap junctions where it can activate antiviral STING-dependent signaling[120]. This way, cells can rapidly initiate antiviral responses prior to the spread of the virus. However, the rapid spread and high amplification of innate immune signaling can also promote adverse effects. Excessive activation of STING *in vivo* has been linked to autoimmune diseases[121,122]. For this reason, STING-dependent signaling is usually tightly regulated. After activation, STING co-localizes with markers for autophagy and becomes phosphorylated[116,123]. A recent study suggests that after autophagy-dependent STING-mediated delivery of TBK1 to endolysosomal compartments and activation of IRF3, STING is subsequently phosphorylated by the autophagy-associated kinase UNC-51-like kinase 1 (ULK1) on a serine residue in the C-terminus (S366) of STING, which suppresses IRF3 phosphorylation and translocation[124]. Thereby, ULK1 negatively regulates STING-dependent signaling. ULK1 activity is usually suppressed by adenosine monophosphate-activated protein kinase (AMPK)-mediated phosphorylation. DNA stimulation leads to disassociation of ULK1 from its repressor AMPK, which is dependent on cyclic dinucleotides. Thus, although cyclic dinucleotides initially activate STING, they subsequently trigger negative regulation of STING to prevent persistent activation of immune responses. Besides ULK1, the autophagy-related gene 9a (Atg9a) and the three prime repair exonuclease 1 (Trex1) have been identified as negative regulators of STING signaling[122,123].

In addition to DAI, RNA Pol III, and cGAS, the human PYHIN proteins absent in melanoma 2 (AIM2) and IFNγ-inducible protein 16 (IFI16) have been identified as cytosolic DNA sensors[125-129]. PYHIN proteins have an N-terminal pyrin domain, which mediates protein-protein interactions and one or two C-terminal HIN domains which mediate DNA binding. AIM2 localizes to the cytoplasm and induces the assembly of a multimeric inflammasome complex with ASC and caspase 1 which activates the secretion of IL-1β in response to dsDNA[125-128]. The generation of AIM2-deficient mice revealed that AIM2 is essential for inflammasome activation upon infections with the bacterial pathogen *Francisella tularensis*, vaccinia virus, and MCMV[130]. Human IFI16 bind to dsDNA and induces a STING-dependent type I IFN response[129]. IFI16 has also been shown to induce inflammasome formation and the production of IL-1β upon nuclear sensing of DNA in Kaposi`s sarcoma-associated herpesvirus (KSHV) infected epithelial cells[131]. The murine homolog to IFI16 is the PYHIN protein p204. p204 has been shown to be crucial for DNA-induced IFNβ responses in murine macrophages[129].
The RNA helicases RIG-I, MDA5, and LGP2 of the DExD/H-box helicase family have been implicated as RNA sensors[8]. The DNA helicase DDX41, which is also a part of the DExD/H-box helicase family, has been shown to interact with dsDNA and to be essential for the STING- and TBK1-dependent induction of type I IFN[132]. Interestingly, in addition to its role as a cytosolic DNA sensor, DDX41 was recently reported to directly bind cyclic dinucleotides (CDNs) like STING. Knockdown of DDX41 resulted in defective activation of STING, TBK1, and IRF3 in response to cyclic dinucleotides[133]. This indicates a possible role for DDX41 as an essential signaling molecule for STING-dependent responses to CDNs.
Furthermore, the DExD/H-box helicases DHX9 and DHX36, as well as the leucine-rich repeat flightless-interacting protein 1 (LRRFIP1), and DNA-dependent protein kinase (DNA-PK) and meiotic recombination 11 (MRE11), which are both involved in the DNA damage response, have also been implicated in sensing cytosolic DNA[134-138].

DNA does not only appear in the cytoplasm upon infections, but also if endolysosomal degradation of exogenous DNA is impaired, or due to an imbalanced control of endogenous DNA products and turnover[139]. Cellular DNases usually prevent unwanted accumulation of DNA in the cytosol. DNase II digests pathogenic DNA or DNA derived from engulfed apoptotic cells in the lysosome of macrophages. In cells derived from DNase II-deficient mice, DNA can leak into the cytoplasm and stimulate cytosolic DNA sensors[140]. Another cellular DNase, Trex1, is the major 3`→5` DNA exonuclease in mammalian cells. Trex1 localizes to the cytoplasm, but is associated with the ER membrane via its C-terminal hydrophobic domain[141]. In humans, mutations in the

TREX1 gene are associated with Aicardi-Goutières syndrome (AGS), familial chilblain lupus, and systemic lupus erythematosus (SLE)[142-144]. Trex1 has been reported to degrade DNA replication byproducts and DNA derived from endogenous retroelements in the cytoplasm to prevent autoimmune responses[141,145]. Additionally, Trex1 has been shown to metabolize human immunodeficiency virus (HIV) DNA in infected cells and thereby prevents triggering of DNA sensors in HIV-infected cells[146]. Oxidized DNA has been shown to be less susceptible to Trex1-mediated degradation, leading to its accumulation in the cytoplasm and subsequent activation of the type I IFN response[147]. Trex1-deficient mice develop inflammatory myocarditis and exhibit a dramatically reduced survival[148]. Trex1-deficient mice can be completely rescued from mortality and autoimmune disease by crossing Trex1-deficient mice with STING-deficient mice[122]. This suggests Trex1 as a specific negative regulator of the cytosolic DNA response triggered through STING-dependent signaling. Trex1 also regulates lysosomal biogenesis and the IFN-independent activation of antiviral genes in macrophages[149]. Recently, expression of Trex1 has been found to be upregulated upon TLR or type I IFN stimulation of macrophages, cDC, and pDC[150,151]. These studies suggest that the expression of Trex1 is upregulated by proinflammatory stimuli in general and Trex1 thereby contributes to the regulation of the host immune response.

1.2. Protein tyrosine phosphatase 1B

Tyrosine phosphorylation is a fundamental post-translational mechanism regulating a large number of cellular processes including cellular signaling and communication, proliferation, differentiation, migration as well as gene regulation and transcription. Dysregulation of tyrosine phosphorylation is associated with the pathogenesis of numerous human diseases from cancer to immune deficiencies[152,153]. Tyrosine phosphorylation is regulated by protein tyrosine kinases and protein tyrosine phosphatases (PTPs). Protein tyrosine phosphatase 1B (PTP1B, also known as PTPN1) is the best characterized tyrosine phosphatase[153].

In humans, 107 PTP genes have been identified, 105 of which have a mouse ortholog[152]. PTPs are classified into four different families based on the amino acid sequences of their catalytic domains. Class I represents the largest PTP family and contains over 100 cysteine-based PTPs including PTP1B. Class I PTPs can be subdivided into “classical” PTPs and “dual specificity” PTPs. Dual specificity PTPs have the ability to dephosphorylate serine and threonine residues in addition to tyrosine residues. PTP1B belongs to the group of classical PTPs which only have an affinity for phosphotyrosine residues. The group of classical PTPs can be further subdivided into

receptor and non-receptor PTPs based on the presence of a transmembrane domain. PTP1B belongs to the group of non-receptor PTPs since it does not contain a transmembrane domain. However, PTP1B has a 35-residue C-terminal hydrophobic anchor sequence which mediates localization of PTP1B to the cytoplasmic face of the ER membrane[154,155]. Under certain circumstances, PTP1B can also be released from the ER, but the full-length ER-localized protein is the predominant form of PTP1B[156]. In addition to the N-terminal catalytic PTP domain and the C-terminal membrane anchor, PTP1B contains two tandem proline-rich motifs following the catalytic domain, which mediate interactions with other proteins[153]. So far, more than 30 substrates have been described for PTP1B with more suspect substrates remaining to be identified[157].

A role for PTP1B has been implicated in the regulation of trafficking of receptor tyrosine kinases (RTKs)[158]. When PTP1B was first identified, the insulin receptor, which belongs to the family of RTKs, was suggested as a substrate for PTP1B[159]. Further studies identified PTP1B as a negative regulator of the insulin receptor and its signaling[160-163]. Subsequently, direct interaction between PTP1B and the activated insulin receptor was shown[164,165]. The importance of PTP1B for the regulation of the insulin receptor was confirmed using PTP1B knockout ($PTP1B^{-/-}$) mice. $PTP1B^{-/-}$ mice have been generated independently by two different groups[166,167]. Both groups reported an enhanced insulin sensitivity of $PTP1B^{-/-}$ mice together with increased phosphorylation of the insulin receptor. Furthermore, due to the insulin hypersensitivity, $PTP1B^{-/-}$ mice were resistant to diet-induced obesity. These results indicate a major role for PTP1B in the modulation of insulin sensitivity and suggest PTP1B as a potential therapeutic target in the treatment of obesity and type 2 diabetes. However, specific targeting of PTP1B by small molecule inhibitors is complicated by its similarity to the closely related T cell PTP (TC-PTP, also known as PTPN2)[153].

Human PTP1B and TC-PTP have a sequence identity of about 74% in their catalytic domains[168]. Human PTP1B has a molecular weight of 50 kDa. For TC-PTP, two different splice variants are expressed in humans, a 48 kDa form and a 45 kDa form, which lacks the hydrophobic C-terminus. In mice, only the 45 kDa form of TC-PTP is expressed. Similar to PTP1B, the 48 kDa form of TC-PTP is targeted to the ER[169]. The 45 kDa form of TC-PTP primarily localizes to the nucleus but also has the ability to translocate to the cytoplasm[170]. In contrast to $PTP1B^{-/-}$ mice, which have a normal life span, knockout of TC-PTP is lethal and $TC\text{-}PTP^{-/-}$ mice die soon after birth[171]. Like PTP1B, TC-PTP has been implicated to play a role in the regulation of insulin signaling[172]. Although PTP1B and TC-PTP are highly related, they have been shown to act specifically and to play nonredundant roles in cellular signaling processes[173-175].

Because the interactions of phosphatases with their substrates are transient and therefore difficult to detect, a substrate trapping mutant of PTP1B (D181A) was developed for the identification of new substrates of PTP1B[176]. Compared to the wild type enzyme, the catalytic activity of the D181A mutant is reduced 10^5-fold. Thus, the D181A mutant of PTP1B can be used to isolate and study complexes of PTP1B with its substrates.

Using the D181A substrate-trapping mutant, the RTK epidermal growth factor receptor (EGFR) was identified as a substrate of PTP1B. It was shown that autophosphorylation of the EGFR is required for its interaction with PTP1B and co-expression with mutant PTP1B leads to intracellular accumulation of the EGFR and co-localization with PTP1B[176]. Upon EGF stimulation, the EGFR is endocytosed from the plasma membrane, ubiquitinated, and subsequently invaginated into multivesicular bodies (MVBs) where the receptors are degraded upon fusion of MVBs with lysosomes, a process that is mediated by ESCRT complexes[177]. In order to find out how PTP1B, which is localized at the ER membrane, can interact with cell surface RTKs like the EGFR, fluorescence resonance energy transfer (FRET) experiments were performed. FRET analysis revealed that PTP1B interacts with RTKs after internalization of the activated receptors from the cell surface and that PTP1B catalyzes dephosphorylation of RTKs at specific sites on the ER surface[178]. Direct sites of membrane contact between MVB and the ER facilitating the interaction between EGFR and PTP1B were shown by electron microscopy[179]. This study suggested that PTP1B plays a central role in the coordination of MVB maturation, which occurs during the movement of MVB from the periphery to the cell center, a hypothesis which fits well with a reported gradient of PTP1B activity from low at the cell periphery to high in the cell center[180]. Besides internalized RTKs, PTP1B likely dephosphorylates activated RTKs at the cell surface. Direct contact between ER-anchored PTP1B and plasma membrane-anchored RTKs has been shown by bimolecular fluorescence complementation (BiFC)[181,182].

In summary, PTP1B has been proposed to dephosphorylate activated RTKs at sites of membrane contact between the ER and the plasma membrane and upon trafficking of internalized RTKs in close proximity to the ER[158]. Furthermore, after their biosynthesis, RTKs can become autophosphorylated in a ligand-independent manner and the phosphorylation of these immature RTKs is particularly sensitive to PTP1B[183]. Thus, PTP1B might also be important to prevent ligand-independent activation of newly synthesized RTKs at the ER (Figure 7)[158].

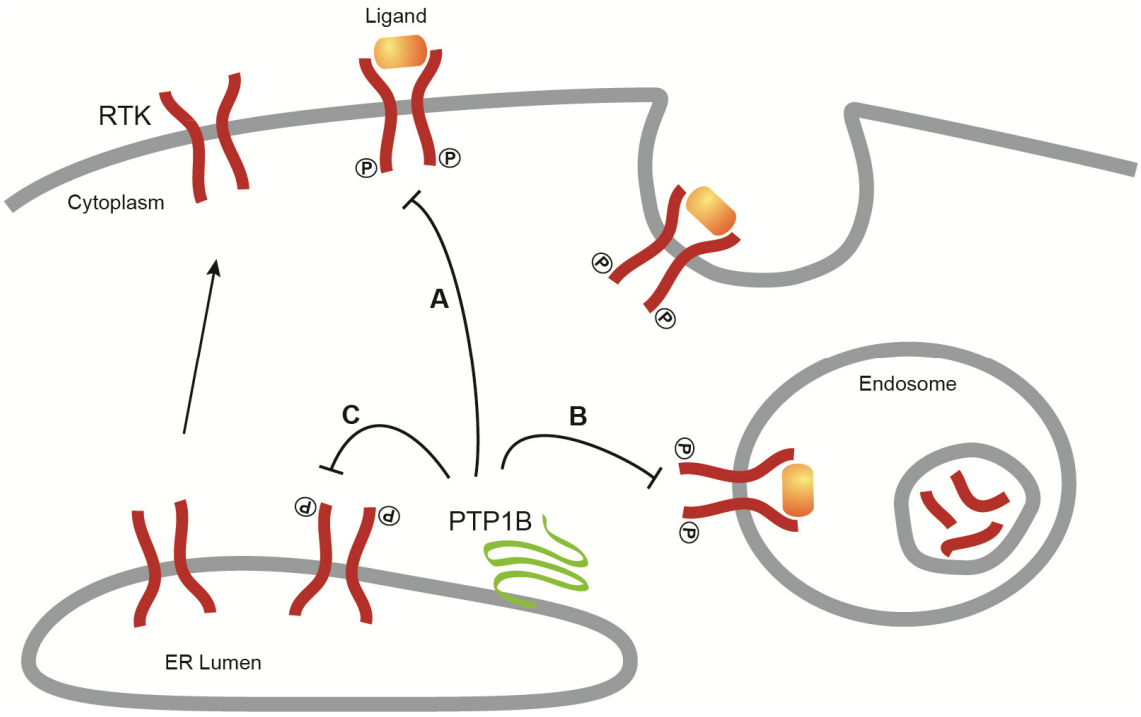

Figure 7: PTP1B regulates intracellular trafficking of receptor tyrosine kinases. Receptor tyrosine kinases (RTKs) become autophosphorylated upon ligand binding. PTP1B dephophorylates RTKs at the plasma membrane (A) or upon internalization (B) which down-regulates RTK signaling. PTP1B might also prevent ligand-independent activation of newly synthesized RTKs at the ER (C).

Further evidence for the central role of PTP1B in the regulation of RTK downregulation has been provided by a study which identified signal transducing adaptor molecule 2 (STAM2), an endosomal protein involved in sorting of activated RTKs for lysosomal degradation, as a substrate for PTP1B[184]. STAM2 is part of the ESCRT-0 complex which is implicated in the recognition of ubiquitinated endosomal RTKs. ESCRT-0 recruits ESCRT complexes I, II, and III, which mediate the internalization of RTKs, like the EGFR, into MVBs and target them for lysosomal degradation[185,186].

PTP1B has also been linked to several immune pathways. It has been shown that Janus kinase 2 (JAK2) and tyrosine kinase 2 (TYK2) are substrates of PTP1B[187]. TYK2 is involved in the signaling in response to colony-stimulating factor 1 (CSF-1, also known as macrophage colony-stimulating factor MSCF), a cytokine that is important for myeloid development. In the absence of PTP1B, the sensitivity of the CSF-1 receptor is increased which results in augmented monocytic development and an increased inflammatory activity in PTP1B-deficient macrophages *in vitro* and *in vivo*[188]. Additionally, nonredundant roles for PTP1B and TC-PTP were implicated in the regulation of IFNγ signaling, which is partially dependent on JAK2[174]. Splenic T cells from $TCPTP^{+/-}/PTP1B^{-/-}$ mice were able to produce higher amounts of IFNγ than T cells from $TCPTP^{+/+}/PTP1B^{-/-}$ or $TCPTP^{+/-}/PTP1B^{+/-}$ mice.

Recent evidence suggests that obesity can be considered as an inflammatory state[189]. It was shown that PTP1B is overexpressed in adipose tissues *in vivo* which is mediated by tissue inflammation and the proinflammatory cytokine TNF[190]. Additionally, chronic exposure to IL-6, another proinflammatory cytokine, leads to insulin resistance in wild type mice, whereas PTP1B$^{-/-}$ mice are protected against the effects of chronic IL-6 exposure[191]. Moreover, PTP1B$^{-/-}$ mice have been shown to be protected against age-induced obesity and insulin resistance due to a low grade of inflammation in adipose tissues[192]. Thus, PTP1B is important for the regulation of inflammation which is linked to obesity-induced metabolic changes.

Altogether, PTP1B has multiple functions and a variety of substrates which have been described since its discovery over 25 years ago. Besides its role in the regulation of metabolism, trafficking of RTKs, and inflammation, which have been summarized here, PTP1B has also been implicated as a key player in cancer and as a regulator of numerous additional signaling cascades[153].

1.3. Aim of the study

Immune sensing of foreign nucleic acids is important for the activation of the early immune response to infections as well as the subsequent activation of specific adaptive immune responses. Intracellular TLRs 3, 7, and 9 are a crucial part of the nucleic acid sensing machinery of the innate immune system and sense nucleic acids in the endolysosomal compartment. After their synthesis in the ER, intracellular TLRs traffic to the endolysosome in order to meet their ligands and initiate proinflammatory cytokine and type I IFN responses. The regulation of TLR localization and trafficking is also important to prevent autoimmunity.

The polytopic membrane protein UNC93B interacts with TLRs 3, 7, and 9 and delivers them from the ER to the endolysosome. The point mutation H412R in UNC93B disrupts binding of UNC93B to TLRs and UNC93B H412R as well as intracellular TLRs fail to leave the ER.

This study aims to investigate the role of UNC93B for innate immunity using two approaches:

1. A thorough comparison of innate immune cells derived from UNC93B H412R and UNC93B knockout mice.
2. The characterization of novel UNC93B interaction partners and their role for trafficking and signaling of intracellular TLRs and UNC93B.

To achieve the first aim, proinflammatory cytokine and type I IFN responses were analyzed upon stimulation of TLRs and cytosolic PRRs with synthetic agonists as well as upon herpesviral infection in macrophages and dendritic cells derived from wild type, UNC93B H412R, and UNC93B knockout mice.

To achieve the second aim, the novel UNC93B interaction partners Clptm, Trex1, and PTP1B were studied. The interaction of these proteins with UNC93B was verified by co-immunoprecipitation experiments. The functional role of Clptm for the TLR-dependent innate immune response was analyzed upon shRNA-mediated knockdown of Clptm in macrophages. The role of PTP1B for signaling of intracellular TLRs was analyzed upon TLR stimulation or herpesviral infection in macrophages and bone marrow cells from PTP1B-deficient mice, as well as upon stimulation of TLR9 *in vivo*. Furthermore, the role of PTP1B for intracellular trafficking and endosomal processing of TLR9 was investigated.

2. Materials and methods

2.1. Buffers and solutions

Annexin V binding buffer	10 mM HEPES/KOH, pH7.4 140 mM NaCl 2.5 mM $CaCl_2$ in H_2O
Digitonin lysis buffer	50 mM Tris-HCl, pH 7.4 150 mM NaCl 5 mM EDTA 1% digitonin in H_2O
Digitonin wash buffer	50 mM Tris-HCl, pH 7.4 150 mM NaCl 5 mM EDTA 0.2% digitonin in H_2O
HBS	20 mM HEPES 150 mM NaCl in H_2O, pH 7.4
MACS buffer	0.5% BSA 2 mM EDTA in PBS
NP-40 lysis buffer	50 mM Tris-HCl, pH 7.4 150 mM NaCl 0.5 mM EDTA 0.5-1% Nonidet P-40 (IGEPAL CA-630) in H_2O
PBS	137 mM NaCl 2.7 mM KCl 10 mM Na_2HPO_4 x 2 H_2O 1.8 mM KH_2PO_4 in H_2O, pH 7.4
RIPA 100 lysis buffer	20 mM Tris-HCl, pH 7.5 1 mM EDTA 100 mM NaCl 1% Triton X-100 0.5% sodium deoxycholate (DOC) 0.1% SDS in H_2O
SDS electrophoresis buffer	25 mM Tris base 192 mM glycine 0.1% SDS in H_2O

SDS loading buffer (4x)	250 mM Tris-HCl, pH 6.8 8% SDS 0.04% bromophenol blue 40% glycerol in H_2O add 10% 2-mercaptoethanol before use
SDS stacking gel, 7.5% acrylamide (for 2 gels)	5.9 ml H_2O 3 ml 1.5 M Tris-HCl, pH 8.8 3 ml 30% acrylamide-bisacrylamide 120 µl 10% SDS 16 µl TEMED 16 µl 25% APS
SDS separating gel, 5% acrylamide (for 2 gels)	2.3 ml H_2O 1 ml 0.5 M Tris-HCl, pH 6.8 0.68 ml 30% acrylamide-bisacrylamide 40 µl 10% SDS 8 µl TEMED 12 µl 25% ammonium persulfate (APS)
TBS	20 mM Tris base 137 mM NaCl in H_2O, pH 7.6
Transfer buffer (for tank blotting)	25 mM Tris base 192 mM glycine 0.05% SDS 20% methanol in H_2O

2.2. Constructs and DNA cloning

All constructs generated in this study are listed in Table 2. DNA was amplified from indicated templates by PCR with *Pfu* Polymerase and indicated primers (Table 2 and Table 3). cDNA was cloned into destination vectors using restriction sites as indicated. Trex1 D18N and PTP1B D181A point mutants were generated by sequential PCR with primers carrying the point mutation (Table 3, point mutation is underlined) followed by PCR with primers for ligation into pMSCV destination vectors. Wild type and D181A HA-PTP1B were cut from pMSCVpuro by restriction digest and ligated into pcDNA3.1(+) as indicated (Table 2). All constructs generated by PCR were completely sequenced. Expression of all constructs was verified by transfection of HEK 293T cells or retroviral transduction of BMDM followed by immunoblot analysis (2.7). All constructs which have been used, but were not generated in this study, are listed in Table 4. Plasmid DNA was prepared using the Plasmid Maxi Kit (Qiagen) according to the manufacturer`s instructions.

Table 2: List of constructs generated in this study.

Construct (Code)	Template	Primers	Restriction sites	Destination vector
Clptm-HA (L22)	HA-Clptm pMSCVhygro	150 + 153	*Bgl*II/*Hpa*I	pMSCVhygro
GFP-Clptm (L20)	HA-Clptm pMSCVhygro	39 + MB	*Bgl*II/*Eco*RI	pEGFP-C1
GFP-Clptm (L21)	GFP-Clptm pEGFP-C1	43 + MB	*Xho*I/*Eco*RI	pMSCVpuro
Clptm-GFP (L24)	HA-Clptm pMSCVhygro	150 + 40	*Bgl*II/*Sma*I	pEGFP-N1
Clptm-GFP (L23)	Clptm-GFP pEGFP-N1	150 + 152	*Bgl*II/*Eco*RI	pMSCVpuro
cherry-Trex1 (L33)	MGC Mouse Trex1 cDNA (MMM1013-65426, Open Biosystems)	64 + 61	*Eco*RI/*Xma*I	pmCherry-C1
cherry-Trex1 (L36)	cherry-Trex1 pmCherry-C1	63 + 61	*Hpa*I/*Hpa*I	pMSCVhygro
cherry-Trex1 1-235 (L34)	MGC Mouse Trex1 cDNA (MMM1013-65426, Open Biosystems)	64 + 62	*Eco*RI/*Xma*I	pmCherry-C1
cherry-Trex1 1-235 (L37)	cherry-Trex1 1-235 pmCherry-C1	63 + 62	*Hpa*I/*Hpa*I	pMSCVhygro
cherry-Trex1 236-314 (L35)	MGC Mouse Trex1 cDNA (MMM1013-65426, Open Biosystems)	65 + 61	*Eco*RI/*Xma*I	pmCherry-C1
cherry-Trex1 236-314 (L38)	cherry-Trex1 236-315 pmCherry-C1	63 + 61	*Hpa*I/*Hpa*I	pMSCVhygro
cherry-Trex1 D18N (L39)	cherry-Trex1 pMSCVhygro	66 + 67, 61 + 63	*Hpa*I/*Hpa*I	pMSCVhygro
HA-PTP1B (L41)	MGC Mouse Ptpn1 cDNA (EMM1002-3695563, Open Biosystems)	110 + 111	*Bgl*II/*Eco*RI	pMSCVpuro
HA-PTP1B D181A (L40)	HA-PTP1B pMSCVpuro	112 + 113, 110 + 111	*Bgl*II/*Eco*RI	pMSCVpuro
HA-PTP1B (L32)	HA-PTP1B pMSCVpuro		*Bam*HI/*Eco*RI	pcDNA3.1(+)
HA-PTP1B D181A (L31)	HA-PTP1B D181A pMSCVpuro		*Bam*HI/*Eco*RI	pcDNA3.1(+)
HA-PTP1B (L125)	HA-PTP1B pMSCVpuro	477 + 478	*Bgl*II/*Hpa*I	pMSCVhygro
mRuby2-HA-PTP1B (L163)	pcDNA3-mRuby2	407 + 409	*Bgl*II/*Bgl*II	HA-PTP1B pMSCVpuro

Table 3: List of primers used for DNA cloning.

No.	Name	Sequence, 5`→3`	T_m
MB	CleftLip*EcoRI*rev	GCTA*GAATTC*TAATCCTTTTTCTTGTCCTCTGC	64°C
39	*BglII*Clptmfor	GCAT*AGATCT*GCGGCGGCGCAGGAGGC	64°C
40	*SmaI*Clptmrev	GCTA*CCCGGG*CATCCTTTTTCTTGTCCTCTGC	60°C
43	*XhoI*GFPfor	GCAT*CTCGAG*GCCACCATGGTGAGCAAGGGCGAG	58°C
61	Trex*HpaIXmaI*rev	GCAT*CCCGGGGTTAAC*TTACTGCCCAGGTGAGGC	58°C
62	Trex705*HpaIXmaI*r	GCAT*CCCGGGGTTAAC*TTAAGTGCCGTACATGGGC	58°C
63	*HpaI*mCherryfor	GCAT*GTTAAC*CGCCACCATGGTGAGCAA	58°C
64	*EcoRI*Trexfor	GCAT*GAATTC*AGGCTCACAGACCCTGCC	58°C
65	*EcoRI*Trex706for	GCAT*GAATTC*ACCGGCTACCACTGGAACA	58°C
66	Trex D18N for	CCCTCATCTTCTTAAACCTGGAAGCCACTGGCCTGCC	
67	Trex D18N rev	GGCAGGCCAGTGGCTTCCAGGTTTAAGAAGATGAGGG	
110	*BglII*HAPTP1Bfor	GCAT*AGATCT*GCCACCATGTATCCGTACGACGTACCAGACTACGCAATCGAGGAGATGGAGAAGGAGTTCG	58°C
111	PTP1B*EcoRISalI*re	GCTA*GTCGACGAATTC*TCAGTGAAAACACACCCGG	58°C
112	PTP1B D181A for	CCACATGGCCTGCCTTTGGAGTCCCCGAGTCACCGGC	
113	PTP1B D181A rev	GCCGGTGACTCGGGGACTCCAAAGGCAGGCCATGTGG	
150	*BglII*ClptmStartf	GCAT*AGATCT*GCCACCATGGCGGCGGCGCAGGA	60°C
152	*EcoRI*GFPrev	GCTA*GAATTC*TTACTTGTACAGCTCGTCCAT	60°C
153	*HpaI*HAClptmrev	GCAT*GTTAAC*CTATGCGTAGTCTGGTACGTCGTACGGATAATCCTTTTTCTTGTCCTCTGC	60°C
407	*BglIIEcoRI*Ruby2f	GCAT*AGATCTGAATTC*GCCACCATGGTGTCTAAGGGCGAAG	58°C
409	CherRuby2*BglII*r	GCTA*AGATCT*CTTGTACAGCTCGTCCAT	54°C
477	*BglII*HAPTP1Bfor	GCAT*AGATCT*GCCACCATGTATCCGTACGACGTACC	60°C
478	PTP1B*HpaI*rev	GCTA*GTTAAC*TCAGTGAAAACACACCCGGT	60°C

Table 4: List of used vectors and constructs.

Construct/Vector (Code)	Vector backbone	Origin
VSV-G, retrovirus (V43)		M. Brinkmann
gag-pol, retrovirus (V44)		M. Brinkmann
HA-Clptm (L273)	pMSCVhygro	M. Brinkmann
pcDNA3.1(+) (V20)		Invitrogen
pcDNA3-mRuby2 (V17)	pcDNA3	Addgene, plasmid 40260
pEGFP-C1 (V2)		Clontech
pEGFP-N1 (V1)		Clontech
pmCherry-C1 (V4)		Clontech
pMSCVhygro (V27)		Clontech
pMSCVpuro (V28)		Clontech
pMSCVneo (V29)		Clontech
sh-control1	pMSCVpuro	see 2.15
sh-control2	pMSCVpuro	see 2.15
sh-UNC1	pMSCVpuro	see 2.15
sh-UNC2	pMSCVpuro	see 2.15
sh-UNC3	pMSCVpuro	see 2.15
sh-Clptm1	pMSCVpuro	see 2.15
sh-Clptm2	pMSCVpuro	see 2.15
TLR9-GFP (L15)	pMSCVpuro	M. Brinkmann
UNC93B-HA (L5)	pMSCVneo	M. Brinkmann
UNC93B-HA H412R (L6)	pMSCVneo	M. Brinkmann
UNC93B-GFP (L7)	pMSCVneo	M. Brinkmann
UNC93B-GFP H412R (L8)	pMSCVneo	M. Brinkmann

2.3. Cell lines and cell culture

The cell lines used in this study are listed in Table 5. All cell lines were cultured at 37°C in a humidified incubator with 7.5% CO_2. DMEM (high glucose, Gibco/Life Technologies) supplemented with 10% FCS (Sigma), 2 mM glutamine (Gibco/Life Technologies), 1% penicillin/streptomycin (P/S) (Gibco/Life Technologies), and 50 µM

2-mercaptoethanol (Gibco/Life Technologies) was used as the standard medium for all cell lines. Cells were trypsinized and split every 2-3 days. Stable cell lines generated by retroviral transduction (2.4) were put under selection with indicated antibiotics (Table 5).

Table 5: List of cell lines.

Cell line	Antibiotic, final concentration	Origin
HEK 293T		ATCC (CRL-11268)
BMDM, immortalized		M. Brinkmann[193] BEI Resources (NR-9456)
BMDM TLR9-GFP	Puromycin, 10 µg/ml	M. Brinkmann[74]
BMDM HA-PTP1B	Puromycin, 10 µg/ml	this study
BMDM HA-PTP1B	Hygromycin, 250 µg/ml	this study
BMDM HA-PTP1B D181A	Puromycin, 10 µg/ml	this study
BMDM TLR9-GFP + HA-PTP1B	Puromycin, 10 µg/ml; Hygromycin, 250 µg/ml	this study
BMDM GFP-Clptm	Puromycin, 10 µg/ml	this study
BMDM cherry-Trex1	Hygromycin, 250 µg/ml	this study
BMDM GFP-Clptm + cherry-Trex1	Puromycin, 10 µg/ml; Hygromycin, 250 µg/ml	this study
RAW 264.7 macrophages		ATCC (TIB-71)
RAW UNC93B-HA	G418, 750 µg/ml	M. Brinkmann
RAW UNC93B-HA H412R	G418, 750 µg/ml	M. Brinkmann
RAW HA-Clptm	Hygromycin, 250 µg/ml	M. Brinkmann
RAW Clptm-HA	Hygromycin, 250 µg/ml	this study
RAW GFP-Clptm	Puromycin, 10 µg/ml	this study
RAW Clptm-GFP	Puromycin, 10 µg/ml	this study
RAW cherry-Trex1	Hygromycin, 250 µg/ml	this study
RAW cherry-Trex1 1-235	Hygromycin, 250 µg/ml	this study
RAW cherry-Trex1 236-314	Hygromycin, 250 µg/ml	this study
RAW cherry-Trex1 + GFP-Clptm	Hygromycin, 250 µg/ml; Puromycin, 10 µg/ml	this study
RAW cherry-Trex1 1-235 + GFP-Clptm	Hygromycin, 250 µg/ml; Puromycin, 10 µg/ml	this study

RAW cherry-Trex1 236-314 + GFP-Clptm	Hygromycin, 250 µg/ml; Puromycin, 10 µg/ml	this study
RAW sh-control1	Puromycin, 10 µg/ml	this study
RAW sh-control2	Puromycin, 10 µg/ml	this study
RAW sh-UNC1	Puromycin, 10 µg/ml	this study
RAW sh-UNC2	Puromycin, 10 µg/ml	this study
RAW sh-UNC3	Puromycin, 10 µg/ml	this study
RAW sh-Clptm1	Puromycin, 10 µg/ml	this study
RAW sh-Clptm1	Puromycin, 10 µg/ml	this study

2.4. Preparation of retroviral particles for the generation of stable cell lines

2.4.1. Production of retroviral particles

Low passage HEK 293T cells were seeded in a 6 well plate or 10 cm dish. The cells were 70-90% confluent at the time of transfection. The following day, cells were transfected with a mix of DNA and Lipofectamine 2000 (Invitrogen), both diluted in OptiMEM (Invitrogen). The DNA mix contained plasmids encoding the retroviral envelope and packaging proteins VSV-G and gag-pol as well as the desired construct in a pMSCV retroviral expression vector. For a 10 cm dish, 4.8 µg of the expression construct in pMSCV, 3.6 µg of gag-Pol, 3.6 µg of VSV-G, and 60 µl of Lipofectamine 2000 were used for the transfection. 24-30 h post transfection, the medium containing viral particles was collected, filtered through a 0.45 µm membrane, aliquoted, and stored at -70°C.

2.4.2. Generation of stable macrophage cell lines by retroviral transduction

For the retroviral transduction of immortalized macrophage cell lines, cells were seeded in 6 well plates. Supernatants with viral particles were diluted in medium and 8 µg/ml of Polybrene (Santa Cruz) were added to increase the infection efficiency. Medium was removed and diluted supernatants containing viral particles were added onto the cells. Spin infection was carried out for 2 h at 2000 rpm at RT. After an additional incubation for 2 h at 37°C, the medium was replaced. Antibiotic selection was started one day post transduction.

2.5. Mice

All mouse strains used in this study are listed in Table 6.

To establish the UNC93B$^{-/-}$ mouse line in the HZI animal facility, *in vitro* fertilization (IVF) was performed with frozen Unc93b1$^{-/-}$ sperm (parental ES cell line: VGB6; background: C57BL/6NTac; ES cell clone 10049A-G9, obtained from the NCRR-NIH supported KOMP Repository (www.komp.org) and generated by Regeneron Pharmaceuticals, Inc. for the NIH funded Knockout Mouse Project (KOMP)[194]).

For this study, TLR9-GFP mice[74] were crossed with UNC93B$^{-/-}$ and PTP1B$^{-/-}$ mice to obtain TLR9-GFP/UNC93B$^{-/-}$ and TLR9-GFP/PTP1B$^{-/-}$ mouse strains and PTP1B$^{-/-}$ mice were crossed with IFNβ $^{\Delta\beta\text{-luc}/\Delta\beta\text{-luc}}$ reporter mice[195] to obtain IFNβ $^{+/\Delta\beta\text{-luc}}$/PTP1B$^{-/-}$ mice.

All animals were maintained under specific pathogen-free (SPF) conditions in the HZI central animal facility. Health monitoring was performed according to FELASA recommendations.

Table 6: List of mouse strains.

Mouse strain	Genetic background	Origin
C57BL/6J wild type		HZI animal facility
C57BL/6N wild type		HZI animal facility
UNC93B$^{-/-}$, UNC93B$^{+/-}$	C57BL/6N	KOMP Repository, HZI animal facility
3d	C57BL/6J	HZI animal facility[52]
TLR3$^{-/-}$	C57BL/6J	Mathias Hornef, MHH, Hannover[196]
TLR7$^{-/-}$	C57BL/6J	Sabine Stegemann-Koniszewski/Dunja Bruder, HZI animal facility[197]
TLR9$^{-/-}$	C57BL/6J	HZI animal facility[24]
TLR9-GFP	C57BL/6J	HZI animal facility[74]
PTP1B$^{-/-}$ (PTPN1$^{-/-}$)	C57BL/6J	Jackson Laboratory (MMRRC, stock number: 032240-JAX), HZI animal facility[167]
TLR9-GFP/PTP1B$^{-/-}$	C57BL/6J	this study, HZI animal facility
TLR9-GFP/UNC93B$^{-/-}$	C57BL/6J	this study, HZI animal facility
IFNβ$^{+/\Delta\beta\text{-luc}}$/PTP1B$^{-/-}$	C57BL/6J	this study, HZI animal facility

2.6. Generation of primary BMDM, FL-DC, and total bone marrow cells

Primary bone marrow-derived macrophages (BMDM) were cultivated in DMEM (high glucose) supplemented with 10% FCS, 2 mM glutamine, 1% P/S, 50 µM 2-mercaptoethanol, and 5% self-made MCSF. Flt3 ligand-induced dendritic cells (FL-DC) and total bone marrow (BM) cells were cultured in RPMI (Gibco/Life Technologies) supplemented with 10% FCS, 2 mM glutamine, 1% P/S, and 50 µM 2-mercaptoethanol. For the generation of FL-DC, 2.5% of self-made Flt3 ligand were added to the culture medium. Primary BMDM, FL-DC, and total BM cells were cultured at 37°C and 7.5% CO_2.

For the preparation of MCSF, 3T3-MCSF cells (M. Brinkmann) were grown in tissue culture flasks in DMEM supplemented with 10% FCS without P/S. Cell supernatant was collected and centrifuged for 5 min at 2000 rpm. The supernatant was filtered through a 0.2 µm membrane, aliquoted, and stored at -70°C. For the preparation of Flt3 ligand, B16 Flt-3L cells[198] were grown in FL-DC medium. Cell supernatant was collected and centrifuged at 3000 rpm for 10 min. The supernatant was transferred into new tubes and centrifuged at 3000 rpm for 10 min. The supernatant was filtered through a 0.2 µm membrane, aliquoted, and stored at -70°C. Optimal amounts of self-made MCSF and Flt3 ligand for the generation of BMDM and FL-DC were determined by flow cytometry phenotypic analysis of macrophages and dendritic cells (cDC and pDC), respectively.

For bone marrow preparation, femur and tibia were removed from the mouse and the bone marrow was extruded from the opened bone with DMEM or RPMI using a syringe and a 0.5 x 16mm, 25 G x 5/8'' needle. Cells were resuspended to obtain a single cell suspension followed by centrifugation for 5 min at 1000 rpm.

For the generation of BMDM, pellets were resuspended in medium containing MCSF and transferred into a 10 cm dish (day 0). On day 1, non-adherent cells were transferred into 6-7 10 cm or 3 15 cm dishes. On day 3, fresh medium was added to the cells. On day 5, the medium was completely replaced by fresh medium. Cells were used for experiments on days 7 or 8 using medium without MCSF.

For FL-DC or total BM cells, pellets of bone marrow cells were resuspended in 0.5 ml of Red Blood Cell Lysing Buffer (Sigma-Aldrich) and incubated for 1-2 min at RT. Medium was added and cells were centrifuged for 5 min at 1000 rpm, resuspended in medium, and counted with Tuerk`s Solution. For experiments with total BM cells, these cells were directly seeded in 96 well plates. To generate FL-DC, cell numbers were

adjusted to 1.5 x 10^6 cells/ml, 2.5 % of Flt3 ligand were added, and cells were cultured in tissue culture flasks (day 0). FL-DC were used for experiments on day 8.

The genotypes of all mice used for the preparation of primary cells were confirmed by genotyping or immunoblotting.

2.7. Immunoblotting

If not specified elsewhere, cells were lysed in RIPA 100 lysis buffer supplemented with protease inhibitors (Complete EDTA-free, Roche) for at least 10 min on ice followed by centrifugation for 10 min at 14,000 g and 4°C to remove cell debris.
Prior to SDS-Polyacrylamide gel electrophoresis (SDS-PAGE), SDS loading buffer was added to cell lysates and lysates were subjected to a 7.5% SDS-PAGE (10% for Figure 21B). Proteins were transferred to a nitrocellulose membrane (Protran BA85, pore size 0.45 µm, GE Healthcare) by tank blotting at 0.35 A for 1 h.
For immunoblots shown in Figure 22, Figure 25B, Figure 42A, and Figure 43A, Bolt LDS Sample Buffer and Bolt Sample Reducing Agent (Life Technologies) were added to cell lysates instead of SDS loading buffer and lysates were separated by Bolt 4-12% Bis-Tris Gels (Life Technologies) using Bolt MOPS SDS Running Buffer (Life Technologies). Proteins were transferred to a nitrocellulose membrane using Bolt Transfer Buffer (Life Technologies) supplemented with 20% methanol as described above.

Membranes were blocked with 5% milk powder in TBS/0.1% Tween 20 (TBS-T) for 1 h at RT or overnight at 4°C. Antibodies were diluted in 5% milk powder in TBS-T (Table 7). Membranes were incubated with diluted antibodies for 1 h at RT and subsequently washed three times with TBS-T for 10 min. For detection of peroxidase activity and immunoblot imaging, membranes were incubated with Lumi-Light Western Blotting Substrate (Roche) for 1 min and chemiluminescence was visualized on chemiluminescence films (GE Healthcare). If signals were very weak, membranes were reincubated with Super Signal West Femto Chemiluminescent Substrate (Thermo Scientific) for 1 min.

Antibodies against the N-terminal (aa 1-354) and C-terminal (aa 530-664) region of murine Clptm were generated according to the generation of antibodies against murine UNC93B described by Brinkmann et al.[54]. N-terminal Clptm peptides were as follows: 1N, C-HPDPRQKALYRRLA; 2N, C-RMINKYKRRRFQKTK; 3N, C-KFDAVSGDYYPIIY

FND. C-terminal Clptm peptides were as follows: 1C, C-QRWIYRVDPTRVNEFG; 2C, C-GEDVSAAAS RAQASTAAGA; 3C, C-QPQEAPPKPAEDKKKD.

Table 7: List of antibodies used for immunoblotting.

Antibody	Species	Source	Order number	Dilution
Primary antibodies				
Anti-α-tubulin	mouse, monoclonal	Sigma-Aldrich	T6199	1:1000
Anti-GFP	rabbit, polyclonal	Abcam	ab290	1:6000
Anti-PTP1B Antibody	rabbit, polyclonal	Millipore	ABS40	1:500
Anti-GFP HRP (B-2)	mouse, monoclonal	Santa Cruz	sc-9996 HRP	1:1000
Anti-HA-Peroxidase High Affinity (3F10)	rat, monoclonal	Roche	12013819001	1:4000
Anti-RFP (5F8)	rat, monoclonal	Chromtek	5F8	1:1000
Anti-uncC, 6055 4th or final bleed	rabbit, polyclonal	M. Brinkmann[54]		1:2000
Anti-uncC, 6055 purified from 6th bleed	rabbit, polyclonal	M. Brinkmann[54]		1:1000
Anti-ClptmC, 6804 3rd bleed	rabbit, polyclonal	M. Brinkmann		1:5000
Anti-ClptmC, 6804 purified from final bleed	rabbit, polyclonal	M. Brinkmann		1:2000
Secondary antibodies				
Anti-mouse IgG + IgM (H+L)-HRPO (A4a)	goat, polyclonal	Dianova	115-035-068	1:5000
Anti-rabbit IgG (H+L)-HRPO (B4c)	goat, polyclonal	Dianova	111-035-045	1:20000
Anti-rat IgG (H+L)-HRPO (C4c)	goat, polyclonal	Dianova	112-035-062	1:5000

2.8. Stimulation of PRRs

2.8.1. PRR agonists

Pam_3CSK_4, FSL-1, Poly(I:C) (HMW), R848, Poly(U), and 5`ppp-dsRNA were purchased from Invivogen. LPS was purchased from Sigma-Aldrich.

CpG oligonucleotides (ODN) and ISD 45bp[107] and ISD 85bp[141] were synthesized by Eurofins MWG Operon and reconstituted in endotoxin-free water (Table 8).

To obtain double stranded ISD, equal amounts of forward and reverse ODN were mixed and incubated for 10 min at 95°C followed by cooling at RT.

Table 8: List of oligonucleotides used for PRR stimulation. Bases in capital letters are phosphodiester, bases in lower case are phosphorothioate.

Name	Sequence, 5`→3`
CpG 1826, type B	tccatgacgttcctgacgtt
CpG 1585, type A	ggGGTCAACGTTGAgggggg
CpG 2336, type A	gggGACGACGTCGTGgggggg
CpG 2216, type A	ggGGGACGATCGTCgggggg
GpC 2216 control	ggGGGAGCATGCTCgggggg
ISD 45bp forward	TACAGATCTACTAGTGATCTATGACTGATCTGTACATGATCTACA
ISD 45bp reverse	TGTAGATCATGTACAGATCAGTCATAGATCACTAGTAGATCTGTA
ISD 85bp forward	ACATCTAGTACATGTCTAGTCAGTATCTAGTGATTATCTAGACATA CATGATCTATGACATATATAGTGGATAAGTGTGGACATC
ISD 85bp reverse	GATGTCCACACTTATCCACTATATATGTCATAGATCATGTATGTCT AGATAATCACTAGATACTGACTAGACATGTACTAGATGT

2.8.2. Stimulation of PRRs with PRR agonists for cytokine measurements by ELISA

To stimulate cell surface and intracellular TLRs as well as cytosolic PRRs, primary BMDM, FL-DC, RAW 264.7 macrophages, and total BM cells were seeded in 96 well plates and stimulated with TLR agonists.

1.5 x 10^5 primary BMDM per well were seeded in 96 well plates. When the cells were adherent, they were stimulated with PRR agonists for 16 to 18 h as indicated in figure legends. 5 x 10^5 FL-DC per well were seeded in 96 well plates (round bottom) and stimulated or transfected with indicated PRR agonists for 18 h. 1 x 10^5 RAW 264.7 macrophages stably expressing shRNAs were seeded per well in 96 well plates. When the cells were adherent, they were stimulated with indicated TLR agonists for 4 h. 1 x 10^6 total BM cells per well were seeded in 96 well plates (round bottom) and stimulated or transfected with indicated TLR agonists for 22 h.

For stimulation of cells with Pam_3CSK_4, FSL-1, LPS, Poly(I:C), R848, CpG 1826, and CpG 2336, stimuli were diluted directly into the medium and added to the cells. For stimulation with Poly(U), 5`ppp-dsRNA, ISD 85bp, or ISD45bp, cells were transfected

with 200 ng of RNA/DNA and 1.2 µl of DOTAP (Roche) diluted in HBS according to the manufacturer's instructions. Transfection mixes were diluted in medium and added to the cells (final volume: 200 µl per well, final DNA/RNA concentration: 1 µg/ml).
After stimulation, supernatants were stored at -20°C for analysis of proinflammatory cytokine and type I IFN responses by ELISA as described in 2.10.

2.8.3. Stimulation of TLR9 for qPCR analysis

To analyze the TLR9-dependent type I IFN response in macrophages, primary BMDM were stimulated with two different kinds of CpG A. 1.5 x 10^6 primary BMDM in 1 ml per well were seeded in a 6 well plate. When the cells were adherent, they were transfected with 6.8 µg of CpG 1585 or CpG 2336 and 30 µl of DOTAP (Roche) diluted in HBS according to the manufacturer's instructions per well (final concentration of CpG DNA: 1 µM). After 6 h of incubation, cells were lysed in 350 µl of RLT buffer with 2-mercaptoethanol per well. RNA isolation and qPCR analysis of IFNα4 mRNA expression were carried out as described in 2.17.

2.8.4. Stimulation of TLRs for immunoblot analysis of PTP1B expression levels

1.5 x 10^6 primary BMDM were seeded per well of a 6 well plate. The next day, cells were stimulated with 100 ng/ml LPS, 1 µM of CpG 1826, or 1 µM of R848. BMDM were incubated with TLR agonists for 6, 12, or 24 h, lysed in 200 µl RIPA 100 lysis buffer, and protein levels of PTP1B were determined by immunoblotting as described in 2.7 using an antibody against endogenous PTP1B.

2.9. Viral infections with MCMV-GFP and MHV-68

2.9.1. Viruses

MCMV-GFP[199] was purified as described by Scheibe et al.[200]. MHV-68 WUMS strain was purchased from ATCC (VR-1465) and purified from infected M2-10B4 cells as described by Bussey et al.[201]. Purified viruses were titered using the median tissue culture infective dose ($TCID_{50}$) method on M2-10B4 cells.

2.9.1. Viral infections for cytokine measurements by ELISA

Primary BMDM, FL-DC, or total BM cells were seeded in 96 well plates as described in 2.8.2. For viral infections of the cells with MCMV-GFP or MHV-68 at indicated MOIs, respective amounts of virus were added into the medium. Cells were incubated with

viruses for 16 to 22 h as indicated in figure legends. Supernatants were frozen at -20°C for analysis of proinflammatory cytokine and type I IFN responses by ELISA as described in 2.10.

2.9.2. MCMV infection for qPCR analysis

To analyze the type I IFN response in macrophages, primary BMDM were infected with MCMV-GFP at an MOI of 0.5. 1.5 x 10^6 primary BMDM per well were seeded in a 6 well plate. Prior to infection, the medium was removed from adherent cells. MCMV-GFP was diluted in 2.5 ml of medium per well. Spin infection was carried out for 30 min at 2000 rpm and 4°C followed by incubation at 37°C for 2 or 6 h. Cells were lysed in 350 µl of RLT buffer with 2-mercaptoethanol per well. RNA isolation and qPCR analysis of IFNα4 mRNA expression were carried out as described in 2.17.

2.10. ELISA

2.10.1. TNF ELISA

To quantify amounts of secreted TNF in cell culture supernatants or mouse serum, 96 well plates (NUNC, Maxisorp) were coated with 50 µl of Purified Hamster Anti-Mouse/Rat TNF antibody (BD Biosciences, #557516), diluted to a concentration of 2 µg/ml in PBS, overnight at 4°C. Wells were blocked with 200 µl of 2% BSA in PBS for 1 h at 37°C, followed by incubation with 50 µl of diluted samples or standard for 1 h at 37°C. Recombinant Mouse TNF (BD Bioscience, #554589) with concentrations ranging from 31.25 to 2000 pg/ml was used as a standard. For detection of TNF, plates were incubated with 50 µl of Biotin Rabbit Anti-Mouse/Rat TNF antibody (BD Biosciences, #557432), diluted to a concentration of 1 µg/ml, for 45 min at RT followed by incubation with 50 µl of HRP-Conjugated Streptavidin antibody (Thermo Scientific, #N100), diluted 1:4000 (0.31 µg/ml), for 30 min at RT. Antibodies, samples, and standard were diluted in 2% BSA in PBS. After each incubation step, plates were washed 3-4 times with 200 µl PBS/0.01% Triton X-100 per well. To develop the assay, 50 µl of TMB substrate solution (Sigma-Aldrich) were added to each well and incubated for 5 to 15 min at RT followed by addition of 50 µl stop solution (1 N H_2SO_4) per well. Absorption was measured at a wavelength of 450 nm.

2.10.2. IFNα ELISA

To measure amounts of IFNα in cell culture supernatants from FL-DC or total bone marrow cells, 96 well plates (NUNC, Maxisorp) were coated with 50 µl of Rat Anti-Mouse Interferon Alpha antibody (PBL Assay Science, #22100-1), diluted to a

concentration of 2.5 µg/ml in PBS, overnight at 4°C. For blocking, 200 µl of 1% BSA in PBS were used per well and incubation was carried out for 2 h at RT followed by incubation with of 50 µl of standard or diluted samples per well overnight at 4°C. Mouse Interferon Alpha A (PBL Assay Science, #12100-1) with concentrations ranging from 78.12 to 5000 pg/ml was used as a standard. For detection of IFNα, plates were incubated with 50 µl of Rabbit Anti-Mouse Interferon Alpha antibody (PBL Assay Science, #32100-1), diluted to a final concentration of 16 ng/ml. Incubation was carried out for 4 h at RT. After detection, plates were incubated with 50 µl of Peroxidase-conjugated AffiniPure $F(ab')_2$ Fragment Donkey Anti-Rabbit IgG (H+L) (Jackson Immunoresearch, #711-036-152), diluted to a final concentration of 80 ng/ml per well, for 1.5 h at RT. Antibodies, samples, and standard were diluted in 1% BSA in PBS. After each incubation step, plates were washed 3-4 times with 200 µl PBS/0.05% Tween 20 per well. The assay was developed as described in 2.10.1. For detection of IFNα in cell culture supernatants from BMDM or mouse serum, the more sensitive ELISA Kit from PBL Assay Science was used as described in 2.10.4.

2.10.3. IL-6 and IL-12p40 ELISA

For detection of IL-6 and IL-12p40 in cell culture supernatants or mouse serum, the BD OptEIA™ Mouse IL-6 and Mouse IL-12(p40) ELISA Sets (BD Biosciences, #555240 and #555165) were used according to the manufacturer's instructions with the modification that instead of using 100 µl, plates were incubated with 50 µl of diluted antibodies, standard, and diluted samples.

2.10.4. IFNα and IFNβ ELISA

To detect type I IFN secreted by BMDM upon viral infection or in mouse serum, the VeriKine Mouse Interferon Alpha and Mouse Interferon Beta ELISA Kits (PBL Assay Science, #42120-2 and #42400-2) were used according to the manufacturer's specifications.

2.11. Microarray

Primary BMDM derived from wild type and UNC93B$^{-/-}$ mice were seeded in 12 well plates and infected with MCMV-GFP at an MOI of 0.5 the following day. Spin infection was carried out for 30 min at 2000 rpm and 4°C followed by incubation at 37°C for 2 or 6 h. Uninfected cells and cells 2 or 6 h post infection were lysed in RLT buffer and total RNA was prepared using the RNeasy Mini Kit (Qiagen). RNA quality was assessed with an Agilent 2100 Bioanalyzer using the Agilent RNA 6000 Pico Kit. RNA integrity

numbers (RIN) of all samples used for microarray analysis were 10. Gene expression analysis was performed using the Whole Mouse Genome Microarray, 4x44k (Agilent). RNA quality control, microarray, and data analysis were performed by the HZI Microarray Core unit.

2.12. Large scale immunoprecipitation and mass spectrometry analysis of UNC93B and Clptm

For large scale immunoprecipitation and mass spectrometry analysis using UNC93B as a bait, RAW 264.7 macrophages stably expressing wild type UNC93B-Flag-TEV-HA or mutant UNC93B-myc-TEV-HA H412R were lysed and subjected to an anti-HA immunoprecipitation. Proteins were released by digestion with TEV protease, separated by liquid chromatography, and analyzed by mass spectrometry (LC-MS/MS) as described by Brinkmann et al.[54].

Large scale immunoprecipitation and mass spectrometry analysis using Clptm as a bait was carried out with RAW 264.7 macrophages stably expressing HA-Clptm as described for UNC93B except for TEV protease digest. UNC93B and Clptm large scale immunoprecipitation experiments were performed by M. Brinkmann prior to this study.

2.13. PNGase F assay

RAW 264.7 macrophages stably expressing Clptm-GFP were lysed in 1% NP-40 lysis buffer for 30 min on ice followed by centrifugation for 10 min at 14,000 g and 4°C to remove cell debris. For digestion with PNGase F (New Englang Biolabs), Denaturing Buffer was added to 50 µl of cell lysates and samples were incubated for 1 h at 37°C. According to the manufacturer`s instructions, G7 Reaction Buffer, 10% NP-40 and 0.5 µl PNGase F were added and incubated with the lysate for another hour at 37°C. Samples were analyzed by immunoblotting as described in 2.7.

2.14. Co-immunoprecipitation

2.14.1. Co-immunoprecipitations with macrophages

One confluent 10 cm dish of cells was lysed in 1 ml 1% digitonin lysis buffer or 0.5% NP-40 lysis buffer supplemented with protease inhibitors (Complete EDTA-free, Roche) as indicated in figure legends for at least 1 h or 30 min at 4°C, respectively. Lysates were centrifuged for 10 min at 14,000 g and 4°C to remove cell debris. An aliquot was taken as input lysate and put aside for immunoblot analysis. 0.5-1 ml of cell lysate were used per immunoprecipitation.

Lysates were mixed with antibodies for immunoprecipitation as indicated (Table 9) and incubated for at least 3 h or overnight at 4°C. 20-30 µl of Protein A beads, equilibrated in lysis buffer, were added per IP and incubation was carried out for 1.5 h or overnight at 4°C. Lysates and beads were centrifuged for 2 min at 2500 rpm and 4°C and washed 3-5 times with 0.5-1 ml of 0.2% digitonin wash buffer or 0.5% NP-40 lysis buffer. SDS loading buffer was added to beads and input lysates followed by 0.5 to 1 h shaking at 37°C. Input lysates and immunoprecipitations were subjected to SDS-PAGE and analyzed by immunoblotting as described in 2.7.

For anti-HA immunoprecipitations, 50 µl of Anti-HA Affinity Matrix (Roche, 13053900), equilibrated in lysis buffer, were added to cell lysates and incubated for 1 to 1.5 h at 4°C (Figure 22D-F and Figure 23C). To precipitate GFP fusion proteins, the GFP-Trap (Chromotek) was used as an alternative to immunoprecipitations with antibodies (Figure 23B). The GFP-Trap is a GFP-binding protein coupled to agarose beads. Control beads (Chromotek) were used for control precipitations. 50 µl of GFP-Trap or control beads, equilibrated in lysis buffer, were added per sample and incubated for 1.5 h at 4°C. Washing and preparation of samples was carried out as described above.

2.14.2. Co-immunoprecipitations with HEK 293T cells

HEK 293T cells were seeded in 6 well plates. The following day, cells were transfected with 1.25 µg of each of the indicated expression constructs in pMSCV (total amount of DNA: 2.5 µg) and 10 µl of Lipofectamine 2000 (Invitrogen) according to the manufacturer's instructions. 48 h post transfection, cells were lysed in 500 µl of 0.5% NP-40 lysis buffer per well. Sample preparation an co-immunoprecipitations were performed as described in 2.14.1

Table 9: List of antibodies used for co-immunoprecipitations.

Antibody	Origin	Dilution	Experiment
Anti-uncC, 6055 4th bleed	M. Brinkmann	1:150-1:200	Figure 19B, Figure 23A
Anti-ClptmC, 6804 3rd bleed	M. Brinkmann	1:150-1:200	Figure 19A, Figure 23A
Anti-TLR7	Imgenex (IMG-5632)	1:150	Figure 23A
Anti-ClptmC, 6804 prebleed (serum control)	M. Brinkmann	1:150-1:500	Figure 19A+B, Figure 21B, Figure 23A
Anti-GFP	Abcam (ab290)	1:500	Figure 21B, Figure 22A-C
Anti-GFP (B-2)	Santa Cruz (sc-9996)	1:50	Figure 42A

2.15. shRNA knockdown of UNC93B and Clptm in RAW 264.7 macrophages

Protein expression of UNC93B and Clptm in RAW 264.7 macrophages was knocked down using a miR30-based shRNA approach[202]. miR30 is a naturally occurring microRNA and is commonly used as pri-miRNA backbone in which the coding region of the mature miR30 miRNA is replaced with sequences encoding shRNAs targeting the gene of interest. 97bp oligonucleotides containing the 5`flanking stem sequence of miR30, the sequence of the UNC93B or Clptm target site (sense orientation), the miR30 loop sequence, the sequence of the UNC93B or Clptm target site (antisense orientation), and the 3`flanking stem sequence of miR30 were designed (T. Wüstefeld, HZI) and synthesized by Eurofins MWG Operon (Table 10). Three and two shRNAs targeting UNC93B and Clptm were used, respectively. shRNAs targeting the human retinoblastoma protein (sh-control1) or Renilla Luciferase (sh-control2) were used as controls (obtained from T. Wüstefeld/L. Zender, HZI).

Table 10: Sequences of miR30 based shRNAs. The sequences of the target sites in UNC93B, Clptm, and controls are shown in red (sense orientation) and blue (antisense orientation). The miR30 loop sequence is shown in green. 5`and 3` flanking miR30 sequences are underlined.

shRNA	Sequence, 5`→3` (5`miR30-sense-loop-antisense-3`miR30)
sh-control1	TGCTGTTGACAGTGAGCGCGCAGTTCGATATCTACTGAAATAGTGAAGCC ACAGATGTATTTCAGTAGATATCGAACTGCTTGCCTACTGCCTCGGA
sh-control2	TGCTGTTGACAGTGAGCGCAGGAATTATAATGCTTATCTATAGTGAAGCCA CAGATGTATAGATAAGCATTATAATTCCTATGCCTACTGCCTCGGA
sh-UNC1	TGCTGTTGACAGTGAGCGCCACCAGGATGTCCCAGAAGTATAGTGAAGC CACAGATGTATACTTCTGGGACATCCTGGTGATGCCTACTGCCTCGGA
sh-UNC2	TGCTGTTGACAGTGAGCGACAGGATGTCCCAGAAGTACTATAGTGAAGCC ACAGATGTATAGTACTTCTGGGACATCCTGGTGCCTACTGCCTCGGA
sh-UNC3	TGCTGTTGACAGTGAGCGAAGGCAGGACTTCATCTTCACCTAGTGAAGCC ACAGATGTAGGTGAAGATGAAGTCCTGCCTCTGCCTACTGCCTCGGA
sh-Clptm1	TGCTGTTGACAGTGAGCGACCGGATGATCAACAAATACAATAGTGAAGCC ACAGATGTATTGTATTTGTTGATCATCCGGGTGCCTACTGCCTCGGA
sh-Clptm2	TGCTGTTGACAGTGAGCGCCACCACAGCTCTTCATCAACTTAGTGAAGCC ACAGATGTAAGTTGATGAAGAGCTGTGGTGTTGCCTACTGCCTCGGA

The miR30 backbone was excised from the retroviral vector MLP carrying the extending miR30 flanking sequence (obtained from T. Wüstefeld/L. Zender, HZI) and ligated into the retroviral vector pMSCVpuro with *Bgl*II and *Age*I. The ordered shRNA oligonucleotides targeting UNC93B or Clptm were amplified by PCR using primers

adding *Xho*I and *Eco*RI restriction sites to the 5` and 3`flanking miR30 precursor sequences. The PCR products were digested with *Xho*I and *Eco*RI and ligated into *Xho*I and *Eco*RI digested pMSCVpuro containing the miR30 backbone. shRNA sequences were verified by sequencing.

Retroviral particles were produced with pMSCVpuro retroviral vectors containing control shRNAs or shRNAs targeting UNC93B or Clptm as described in 2.4.1. RAW 264.7 macrophage cell lines stably expressing respective shRNAs were generated by retroviral transduction and put under selection with Puromycin as described in 2.4.2. Six days after retroviral transduction, cells were seeded and stimulated with TLR agonists as described in 2.8.2.

2.16. Live cell imaging

Immortalized BMDM expressing GFP-Clptm and cherry-Trex1, TLR9-GFP and Ruby-PTP1B, or primary BMDM derived from TLR9-GFP/WT or TLR9-GFP/PTP1B$^{-/-}$ mice were seeded in 8 well coverglass cell culture chambers (Sarstedt). Cells were maintained in phenol-red free DMEM (high glucose, 25 mM HEPES) supplemented with 10% FCS, 2 mM glutamine, and 1% P/S. Cells were incubated with 50 nM lysotracker red (Life Technologies) or stimulated with 1 µM CpG 1826 or CpG 1826-Alexa647 (Eurofins MWG Operon, 2.8.1) for the indicated time periods. Medium containing CpG 1826-Alexa647 was replaced prior to imaging in order to reduce background fluorescence. Images were taken using a Nikon ECLIPSE Ti-E inverted microscope equipped with a spinning disc confocal device (UltraView VOX, Perkin Elmer), solid state diode lasers (Perkin Elmer), an OrcaR2 CCD camera (Hamamatsu), and a Nikon 60x 1.4 N.A. planapochromat objective. During imaging, cells were maintained in a climate chamber (EMBLEM, Germany) at 37°C and 5% CO_2. Image processing was performed using Volocity and Photoshop.

2.17. Real-time quantitative PCR

2.17.1. RNA isolation

Total RNA was purified from RLT lysates of primary BMDM (2.8.3) or MEF (2.20) using the RNeasy Mini Kit (Qiagen) according to the manufacturer`s instructions. RNA was quantified using a NanoDrop (Thermo Scientific). Ratios of the readings at 260 nm and 280 nm (A_{260}/A_{280}) were between 1.9 and 2.1 indicating a good RNA quality.

2.17.2. qPCR analysis of IFNα4, PTP1B, and TLR9 mRNA expression

To analyze mRNA expression of IFNα4, PTP1B, and TLR9, real-time quantitative PCR (qPCR) analysis was performed with RNA isolated from primary BMDM or MEF (2.17.1). The Universal ProbeLibrary (UPL, Roche) was used for qPCR assays and primers were designed using the UPL Probe Finder software (Version 2.50, Roche) (Table 11). The murine ribosomal protein L8 (Rpl8) was used as a housekeeping gene. Primers were synthesized by Eurofins MWG Operon.

qPCR assays were performed using the EXPRESS One-Step SuperScript qRT-PCR Kit (Life Technologies). For MEF, 100 ng of RNA were used per reaction, for primary BMDM, 100 to 200 ng of RNA were used per reaction. Reactions were set up in duplicates in 96 multiwell plates for qPCR (Roche) as follows:

EXPRESS SuperScript qPCR SuperMix Universal (2x)	10 µl
EXPRESS SuperScript Mix for One-Step qPCR	2 µl
Forward primer (20 µM)	0.4 µl
Reverse primer (20 µM)	0.4 µl
UPL probe (10 µM)	0.4 µl
RNA	100-200 ng
H_2O	up to 20 µl

Plates were sealed with sealing foil and centrifuged for 2 min at 2000 rpm. qPCR analysis was carried out using the LightCycler 96 (Roche) with the following program setup:

cDNA synthesis	15 min	60°C	
Denauration	5 min	95°C	
Amplification	10 s	95°C	65 cycles
	30 s	60°C	
	1 s	72°C	
Cooling	30 s	40°C	

C_t values were obtained using the LightCycler 96 software (Roche). Relative quantification was performed according to the $2^{-\Delta\Delta Ct}$ method using Rpl8 as reference gene[203]: $\Delta\Delta C_t = (C_{t,\text{gene of interest}} - C_{t,\text{reference}})_{\text{treated}} - (C_{t,\text{gene of interest}} - C_{t,\text{reference}})_{\text{untreated}}$, relative mRNA induction of gene of interest = $2^{-\Delta\Delta Ct}$.

Table 11: List of primers and probes used for qPCR analysis.

Gene of interest	Forward primer	Reverse primer	UPL probe
Rpl8	caacagagccgttgttggt	cagcctttaagataggcttgtca	#5
IFNα4	tcaagccatccttgtgctaa	gtcttttgatgtgaagaggttcaa	#3
PTP1B	acctgtggggatgaagacag	cttcagtgtctggactcatgct	#13
TLR9	gaatcctccatctcccaacat	ccagagtctcagccagcact	#79

2.18. Flow cytometry

2.18.1. Determination of proportions of cDC, pDC, B cells, and T cells in FL-DC cultures or lymphoid organs

To determine proportions of cDC and pDC in FL-DC cultures, FL-DC derived from wild type and PTP1B$^{-/-}$ mice were analyzed by flow cytometry. 1 x 10^6 cells were centrifuged for 6 min at 1200 rpm in a 5 ml FACS tube and washed once with 1 ml of PBS. Supernatants were poured off and cells were resuspended in 100 µl of PBS containing premixed antibodies in specific dilutions (Table 12). Cells were incubated with antibodies for 15 min at 4°C followed by addition of 1 ml of PBS per sample. Cells were centrifuged and washed with PBS once more. Supernatants were poured off and cells were resuspended in 50 µl of PBS. 50 µl of LIVE/DEAD Fixable Aqua Dead Cell Stain (Life Technologies) prediluted in PBS were added to the cells. The final dilution of LIVE/DEAD Fixable Aqua Dead Cell Stain was 1:1000. Cells were incubated with LIVE/DEAD Fixable Aqua Dead Cell Stain for 30 min at 4°C followed by addition of 1 ml of PBS. Cells were centrifuged for 6 min at 1200 rpm and again washed with 1 ml of PBS. Supernatants were poured off, cells were resuspended in PBS and data was acquired with a LSR II flow cytometer and FACSDiva software (BD Biosciences). FCS files were exported and data were analyzed with FlowJo software (Version 10, Tree Star, Inc.).

For the analysis of proportions of B cells, T cells, cDC, and pDC in lymphoid organs, bone marrow, spleen and inguinal lymph nodes were prepared from wild type and PTP1B$^{-/-}$ mice. For bone marrow preparation femur and tibia were removed from the mouse and the bone marrow was extruded from the opened bone with RPMI using a syringe and a 0.5 x 16mm, 25 G x 5/8'' needle. To prepare single cell suspensions for flow cytometry analysis, bone marrow, spleens, and inguinal lymph nodes were collected in 4 ml RPMI and passed through a 100 µm cell strainer. Cells were centrifuged for 5 min at 1500 rpm at RT. Bone marrow and splenic cells were

resuspended in 0.5 ml or 1 ml of Red Blood Cell Lysing Buffer (Sigma-Aldrich) for bone marrow from one mouse or per spleen, respectively. Lysis of red blood cells was carried out for 1-2 min at RT. 15 or 30 ml of medium were added, respectively, and cells were again centrifuged for 5 min at 1500 rpm. Total bone marrow cells, splenocytes and cells from inguinal lymph nodes were resuspended in medium and counted with Tuerk`s Solution.

Preparation of cells for analysis by flow cytometry was carried out as described for FL-DC with an additional blocking step to block Fc-receptors prior to antibody staining. Cells were resuspended in 100 µl of PBS (after they had been washed with PBS) and 1 µg of Mouse BD Fc Block (BD Biosciences) was added. Cells were incubated with Mouse BD Fc Block for 10 min at 4°C followed by addition of 1 ml of PBS and centrifugation for 6 min at 1200 rpm. Supernatant was poured off and cells were stained with two different sets of antibodies as described above (Table 12).

Table 12: List of antibodies used for flow cytometry analysis.

Antibody	Source	Order number	Dilution
cDC/pDC FL-DC (Figure 33)			
Anti-Human/Mouse B220 PerCp-Cy5.5	eBioscience	45-0452	1:500
Anti-Mouse CD11b PE	eBioscience	12-0112	1:4000
Anti-Mouse CD11c APC	eBioscience	17-0114	1:400
Anti-Mouse Siglec-H FITC	eBioscience	11-0333	1:1000
B and T cells lymphoid organs (Figure 41)			
Anti-Mouse CD3 PE	BD Biosciences	555275	1:200
Anti-Mouse CD4 FITC	eBioscience	11-0042	1:500
Anti-Mouse CD19 APC	BD Biosciences	550992	1:200
Anti-Mouse CD8α PE-Cy7	BioLegend	100722	1:1000
cDC/pDC lymphoid organs (Figure 41)			
Anti-Human/Mouse B220 PerCp-Cy5.5	eBioscience	45-0452	1:500
Anti-Mouse CD11b PE	eBioscience	12-0112	1:4000
Anti-Mouse CD11c PE-Cy7	BioLegend	117318	1:1000
Anti-mPDCA-1 FITC	Miltenyi Biotec	130-091-961	1:10
Anti-Mouse Siglec-H APC (eFluor 660)	eBioscience	51-0333	1:1000

2.18.2. Determination of proportions of dead and apoptotic FL-DC after treatment with inhibitors

In order to analyze amounts of dead and apoptotic cells in wild type FL-DC after treatment of the cells with PTP Inhibitor XXII or z-FA-fmk, cells were stained with

Annexin V, which binds to phosphatidylserine exposed on the surface of apoptotic cells, and 7-Aminoactinomycin (7-AAD), a fluorescent intercalator which undergoes a spectral shift upon association with DNA. 1 x 10^6 unstimulated wild type FL-DC treated with PTP Inhibitor XXII, z-FA-fmk or DMSO were collected in a 5 ml FACS tube. 1 ml of PBS was added. Cells were centrifuged for 5 min at 1500 rpm and washed with 1 ml of PBS. Supernatants were poured off and cells were resuspended in 250 µl of Annexin V binding buffer. 5 µl of Annexin V FITC (BD Biosciences, 556419) and 2.5 µl of 7-AAD (Sigma, 0.1 mg/ml) were added per sample. Incubation was carried out for 15 min at RT. 250 µl of Annexin V binding buffer were added and cells were directly analyzed by flow cytometry.

2.19. Treatment of FL-DC with PTP1B Inhibitors

To study the role of the enzymatic function of PTP1B, FL-DC derived from wild type and PTP1B$^{-/-}$ mice were treated with specific PTP1B inhibitors, stimulated with TLR agonists, and amounts of IFNα in supernatants were determined by ELISA. To verify that IFNα responses upon stimulation with TLR agonists were dependent on TLRs, cells were treated with z-FA-fmk which inhibits processing and signaling of TLR7 and TLR9[71]. PTP1B inhibitors MSI-1436 (Ohr Pharma-ceutical) and PTP Inhibitor XXII (Merck, 539741) and the cysteine protease inhibitor z-FA-fmk (Sigma-Aldrich, C1480) were reconstituted in DMSO.

5 x 10^5 FL-DC in a volume of 50 µl per well were seeded in 96 well plates (round bottom). 50 µl of medium containing indicated concentrations of PTP Inhibitor XXII, z-FA-fmk or respective amounts of DMSO were added and cells were incubated for 4 h at 37°C. After pretreatment of the cells with inhibitors, they were stimulated with CpG 2336 and Poly(U). CpG 2336 was directly diluted into 50 µl medium and added to the cells. For stimulation with Poly(U), cells were transfected with 150 ng of RNA and 1.2 µl of DOTAP (Roche) diluted in HBS according to the manufacturer's instructions. The transfection mix was diluted in 50 µl medium and added to the cells (final RNA concentration: 1 µg/ml). Cells were stimulated for 6 h at 37°C. After stimulation, supernatants were stored at -20°C for the analysis of IFNα in supernatants by ELISA as described in 2.10.2.

2.20. Preparation and retroviral transduction of MEF

Mouse embryonic fibroblasts (MEF) were cultivated in DMEM (high glucose) supplemented with 15% FCS, 2 mM glutamine, 1% P/S, 1% NEAA, and 50 µM 2-mercaptoethanol. For preparation of wild type and PTP1B$^{-/-}$ MEF, breeding pairs

were set up for wild type and PTP1B$^{-/-}$ mice. Every day, female mice were checked for vaginal plug to verify that mating had occurred. 13.5 days after the plug check had been positive (day 0.5), the pregnant female was euthanized. Both uterine horns containing the embryos were removed and washed twice in 70% ethanol and twice in PBS for 1 min, respectively. Single embryos were separated by opening the uterine wall with scissors. Using two pairs of forceps, the amniotic sac and placenta were removed from the embryo. Next, liver, heart, and head were removed from the embryo. Embryos were placed in a new 15 cm dish and 100 µl of 0.15% trypsin were added onto the embryo. Each embryo was thoroughly minced with two scalpels and incubated for 5 to 10 min at 37°C. Cells were carefully resuspended in 5 ml of medium and another 20 ml of medium were added. Cells were cultivated at 37°C and 7.5% CO_2 (day 0). On day 3, 15 ml of medium were removed and replaced by fresh medium. When cells were confluent, they were frozen or cultured for several passages until growth stopped.

For retroviral transduction, MEF were seeded in 6 well plates and transduced with empty vector (pMSCVpuro), wild type HA-PTP1B, or HA-PTP1B D181A in pMSCVpuro as described for macrophage cell lines in 2.4.2. Antibiotic selection with 5 µg/ml Puromycin was started one day after transduction. 3 days after transduction, 2 x 10^5 cells per well were seeded in 12 well plates. The next day, MEF were lysed in 350 µl of RLT buffer with 2-mercaptoethanol per well for qPCR analysis or in 200 µl of RIPA 100 lysis buffer for immunoblot analysis. RNA isolation and qPCR analysis of PTP1B and TLR9 expression were carried out as described in 2.17. Immunoblot analysis of PTP1B was carried out as described in 2.7.

2.21. *In vivo* experiments

To measure type I IFN and proinflammatory cytokine responses upon stimulation of TLR9 *in vivo*, wild type, PTP1B$^{-/-}$, and TLR9$^{-/-}$ mice were injected with CpG DNA and serum levels of IFNα, IL-12p40, TNF, and IL-6 were determined by ELISA.

For induction of IFNα and IL-12p40 responses, mice were challenged with CpG A. Wild type, PTP1B$^{-/-}$, and TLR9$^{-/-}$ mice were intravenously injected with a total volume of 200 µl containing 10 µg CpG 2216 or GpC 2216 control (2.8.1) complexed with 30 µl DOTAP (Roche) in PBS. 6 h post injection, mice were sacrificed and total blood was collected from the heart.

To measure TNF and IL-6 responses, mice were challenged with CpG B. Wild type, PTP1B$^{-/-}$, and TLR9$^{-/-}$ mice were intraperitoneally injected with 60 µg of CpG 1826 in a total volume of 200 µl in PBS. 2 h post injection, mice were sacrificed and total blood was collected from the heart.

For serum preparation, blood was kept at RT for at least 1 h, centrifuged for 8 min at 5000 rpm, and supernatants were collected. Serum levels of IFNα and proinflammatory cytokines were determined by ELISA as described in 2.10.

2.22. Cell sorting

2.22.1. Magnetic-activated cell sorting (MACS)

pDC were sorted from FL-DC derived from wild type and PTP1B$^{-/-}$ mice or splenocytes by magnetic-activated cell sorting (MACS) using the Plasmacytoid Dendritic Cell Isolation Kit II, LS columns, and MidiMACS or QuadroMACS separator (Miltenyi Biotec). Using the Plasmacytoid Dendritic Cell Isolation Kit II, murine pDC are isolated based on negative selection. Non-pDC are magnetically labeled with antibodies targeting different markers which are not expressed by murine pDC. Magnetically labeled cells are retained on the MACS column in the magnetic field of the MACS separator, whereas unlabeled pDC pass through the column.

For the preparation of splenocytes, spleens were isolated from wild type and PTP1B$^{-/-}$ mice, passed through a 70 µm cell strainer and erythrocytes were lysed as described in 2.18.1. Isolation of pDC from FL-DC cultures or splenocytes with the Plasmacytoid Dendritic Cell Isolation Kit II was performed according to the manufacturer`s instructions. Up to 1 x 10^8 cells were used per column. After MACS, the enrichment of pDC sorted from FL-DC cultures was verified by flow cytometry analysis of proportions of pDC and cDC according to 2.18.1. Upon MACS, the percentage of pDC was enriched from 30-40% to 80-90% as verified by flow cytometry analysis.

Wild type and PTP1B$^{-/-}$ pDC were stimulated with Poly(U), CpG 2336, or infected with MCMV as described in 2.8.2 and 2.9.1. Levels of IFNα, TNF, and IL-6 were determined by ELISA as described in 2.10.

2.22.2. Fluorescence-activated cell sorting (FACS)

Siglec-H-positive pDC were sorted from FL-DC derived from wild type and PTP1B$^{-/-}$ mice by fluorescence-activated cell sorting (FACS) in order to measure type I IFN responses upon TLR stimulation by ELISA. To analyze processing of TLR9-GFP in dendritic cells, cDC and pDC were sorted from FL-DC derived from TLR9-GFP/WT, TLR9-GFP/UNC93B$^{-/-}$, and TLR9-GFP/PTP1B$^{-/-}$ mice using specific antibodies against CD11b and B220.

4-6 x 10^7 FL-DC were centrifuged for 6 min at 1200 rpm in 15 ml tubes. Supernatants were poured off and cells were washed with 15 ml of PBS. Cells were resuspended in 4 ml of PBS containing diluted antibodies (Table 13) and incubated for 15 min at 4°C

followed by addition of 10 ml PBS. Cells were centrifuged for 6 min at 1200 rpm and washed with 15 ml PBS. Supernatants were poured off and cells were resuspended in 1 ml of FL-DC medium. Sorting of Siglec-H$^+$ pDC or B220$^-$CD11b$^+$ cDC and B220$^+$CD11b$^-$ pDC was performed by the HZI Flow Cytometry and Cell Sorting unit.

FACS-sorted pDC from wild type and PTP1B$^{-/-}$ mice were stimulated with Poly(U), CpG 2336, or infected with MCMV as described in 2.8.2 and 2.9.1. Levels of IFNα, TNF, and IL-6 were measured by ELISA as described in 2.10.
Sorted cDC and pDC derived from TLR9-GFP/WT, TLR9-GFP/UNC93B$^{-/-}$, and TLR9-GFP/PTP1B$^{-/-}$ mice were used to analyze proteolytic processing of TLR9-GFP as described in 2.23.

Table 13: List of antibodies used for cell sorting.

Antibody	Source	Order number	Dilution
Sorting of pDC from FL-DC (3.4.7)			
Anti-Mouse Siglec-H FITC	eBioscience	11-0333	1:1000
Sorting of cDC/pDC from FL-DC (Figure 43)			
Anti-Mouse CD45R/B220 APC-Cy7	BD Biosciences	561102	1:150
Anti-Mouse CD11b PE	eBioscience	12-0112	1:1000

2.23. Analysis of TLR9-GFP proteolytic processing

In order to find out whether proteolytic endosomal processing of TLR9 in macrophages, cDC, and pDC is intact in the absence of PTP1B, BMDM derived from TLR9-GFP/WT and TLR9-GFP/PTP1B$^{-/-}$ mice or cDC and pDC sorted from FL-DC derived from TLR9-GFP/WT, TLR9-GFP/UNC93B$^{-/-}$, and TLR9-GFP/PTP1B$^{-/-}$ mice were analyzed by anti-GFP immunoblotting.
One confluent 10 cm dish of BMDM derived from TLR9-GFP/WT or TLR9-GFP/ PTP1B$^{-/-}$ mice was treated with 10 µM z-FA-fmk (Sigma-Aldrich, C1480) for 15 h and lysed in 1 ml RIPA 100 lysis buffer. 4.5 x 10^6 - 8.5 x 10^6 cDC and pDC sorted from FL-DC derived from TLR9-GFP/WT, TLR9-GFP/UNC93B$^{-/-}$, and TLR9-GFP/PTP1B$^{-/-}$ mice by FACS (2.22.2) were lysed in 80 µl RIPA 100 lysis buffer. Lysates of BMDM and sorted cDC and pDC were analyzed by immunoblotting as described in 2.7.

3. Results

3.1. Characterization of innate immune signaling by UNC93B knockout mice

3.1.1. BMDM and FL-DC derived from UNC93B$^{-/-}$ mice do not express UNC93B

Until today, 3d mice have been used to study the role of UNC93B for innate immunity. These mice have been generated using *N*-ethyl-*N*-nitrosourea (ENU) mutagenesis, which induces genomic point mutations. 3d mice fail to respond to stimulation of TLRs 3, 7, and 9. The 3d phenotype was mapped to a single point mutation, H412R, in the *Unc93b* gene[52]. However, due to ENU mutagenesis, 3d mice carry additional mutations, which makes the characterization of 3d mice more difficult[204]. The fact that UNC93B H412R is still expressed and localizes to the ER in 3d mice further complicates the usage of these mice for studying UNC93B biology. Recently, UNC93B knockout (UNC93B$^{-/-}$) mice were made publicly available. These mice have not been characterized yet. Studying UNC93B$^{-/-}$ mice may reveal additional functions of UNC93B mediated by regions of the protein which are not affected by the H412R mutation.

3d mice were generated on the C57BL/6J (B6J) background, whereas UNC93B$^{-/-}$ mice were generated on the C57BL/6N (B6N) background. Both of these wild type strains initially had the same origin, but were separated over 60 years ago. To exclude the possibility that potential differences between UNC93B$^{-/-}$ and 3d mice arise from the different genetic backgrounds of these mouse lines, both wild type strains were included in the following studies.

Prior to any functional experiments, the absence of UNC93B in primary bone marrow-derived macrophages (BMDM) and Flt3 ligand-induced dendritic cells (FL-DC) derived from UNC93B$^{-/-}$ mice was verified by immunoblot analysis (Figure 8, A and B). Expression of UNC93B could not be detected in cells derived from UNC93B$^{-/-}$ mice using an antibody against the C-terminus of murine UNC93B. Cells derived from wild type, heterozygous UNC93B$^{+/-}$, and TLR9$^{-/-}$ mice showed comparable levels of UNC93B. As shown in earlier studies, a more distinct band pattern was observed for UNC93B in cells derived from 3d mice[54]. This characteristic band pattern allows easy distinction between wild type and mutant (H412R) UNC93B.

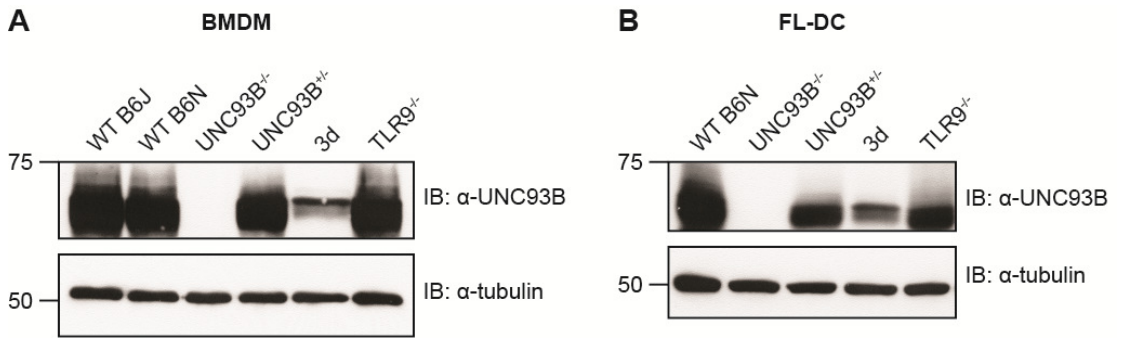

Figure 8: Immunoblot analysis of UNC93B protein expression in primary BMDM and FL-DC. Immunoblot analysis of UNC93B protein expression in primary BMDM (A) and FL-DC (B) generated from B6J or B6N wild type (WT), UNC93B$^{-/-}$, UNC93B$^{+/-}$, 3d, and TLR9$^{-/-}$ mice. UNC93B was detected using an antibody against UNC93B. Loading of equal amounts of protein was verified by anti-tubulin immunoblot.

3.1.2. Knockout of UNC93B abrogates proinflammatory cytokine responses upon stimulation of intracellular TLRs in primary BMDM

BMDM derived from 3d (UNC93B H412R) mice do not respond to stimulation of TLRs 3, 7, and 9, whereas signaling of cell surface TLRs (e.g. TLR2 and TLR4) is intact. In order to analyze whether BMDM derived from UNC93B$^{-/-}$ mice exhibit the same phenotype, primary BMDM from B6J and B6N wild type, UNC93B$^{-/-}$, UNC93B$^{+/-}$, 3d, and TLR9$^{-/-}$ mice were stimulated with different concentrations of TLR agonists and the production of the proinflammatory cytokine TNF was measured by ELISA. Upon stimulation of cell surface TLRs 1/2, 2/6, and 4 with Pam_3CSK_4, FSL-1, and LPS, respectively, BMDM derived from UNC93B$^{-/-}$ mice produced comparable amounts of TNF as BMDM derived from wild type mice (Figure 9, A-C). However, BMDM derived from UNC93B$^{-/-}$ mice did not secrete detectable amounts of TNF upon stimulation of intracellular TLRs 3, 7, and 9 with Poly(I:C), R848, and CpG 1826, respectively (Figure 9, D-F). Compared to wild type BMDM, BMDM derived from heterozygous UNC93B$^{+/-}$ mice did not show an impaired production of TNF upon stimulation of cell surface or intracellular TLRs, indicating that one functional allele of UNC93B is sufficient to induce a proinflammatory cytokine response. TNF responses of BMDM derived from 3d and TLR9$^{-/-}$ mice were similar to those of wild type BMDM upon stimulation of cell surface TLRs. As expected, BMDM derived from 3d mice did not respond to stimulation of intracellular TLRs. The TNF response of BMDM derived from TLR9$^{-/-}$ mice upon stimulation of the intracellular TLRs 3 and 7 with Poly(I:C) and R848 was comparable to wild type BMDM, but, as expected, like BMDM derived from 3d mice, BMDM derived from TLR9$^{-/-}$ mice did not respond to stimulation of TLR9 with CpG 1826.

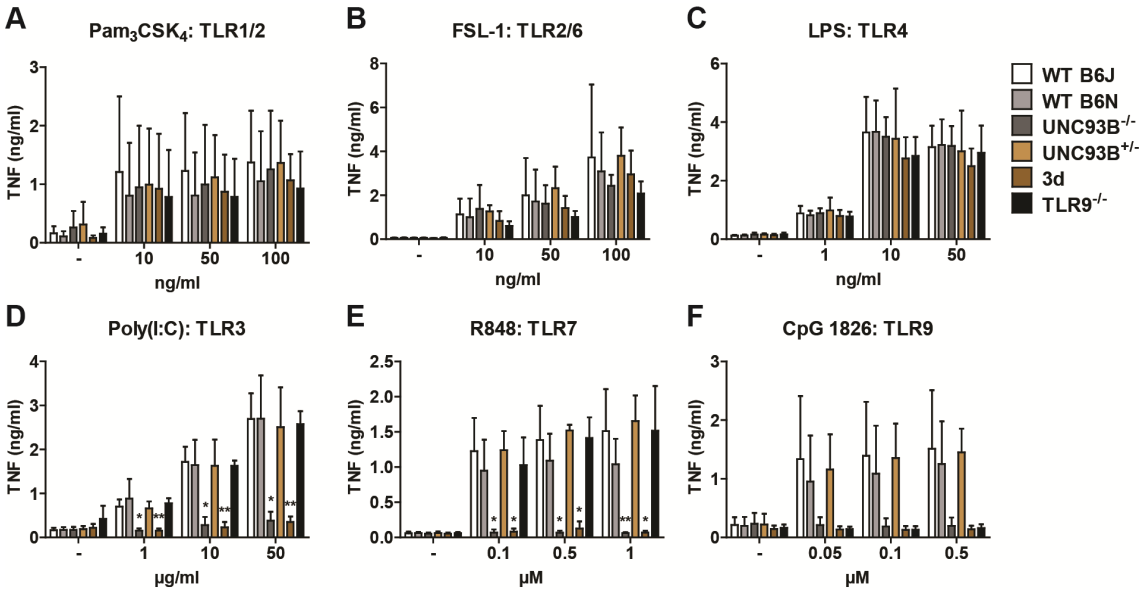

Figure 9: BMDM derived from UNC93B$^{-/-}$ mice do not secrete TNF in response to agonists of intracellular TLRs. Primary BMDM derived from B6J or B6N wild type (WT), UNC93B$^{-/-}$, UNC93B$^{+/-}$, 3d, and TLR9$^{-/-}$ mice were stimulated with indicated concentrations of TLR agonists for 16 h (A-F). TNF levels in supernatants were determined by ELISA. Results are shown as mean ± S.D. of 3 independent experiments. Statistical significance compared to respective wild type controls was determined by two-tailed, unpaired t test; *, p<0.05; **, p<0.01.

In agreement with the results for TNF, the production of IL-6, another proinflammatory cytokine, by BMDM derived from UNC93B$^{-/-}$ mice was comparable to wild type BMDM upon stimulation of cell surface TLRs 1/2, 2/6, and 4 (Figure 10, A-C), but abrogated upon stimulation of intracellular TLRs 3, 7, and 9 (Figure 10, D-F). IL-6 responses of BMDM derived from heterozygous UNC93B$^{+/-}$ mice were comparable to those of wild type BMDM. BMDM derived from 3d and TLR9$^{-/-}$ mice produced comparable amounts of IL-6 to wild type BMDM upon stimulation of cell surface TLRs. As expected, BMDM derived from 3d mice did not respond to stimulation of intracellular TLRs 3, 7 and 9. BMDM derived from TLR9$^{-/-}$ mice did not respond to stimulation of TLR9 with CpG 1826, but upon stimulation of intracellular TLRs 3 and 7 with Poly(I:C) and R848, respectively, amounts of secreted IL-6 were comparable to wild type BMDM.

Thus, BMDM derived from UNC93B$^{-/-}$ mice exhibit a phenotype resembling the previously described 3d phenotype, whereas BMDM derived from UNC93B$^{+/-}$ mice behave like wild type BMDM.

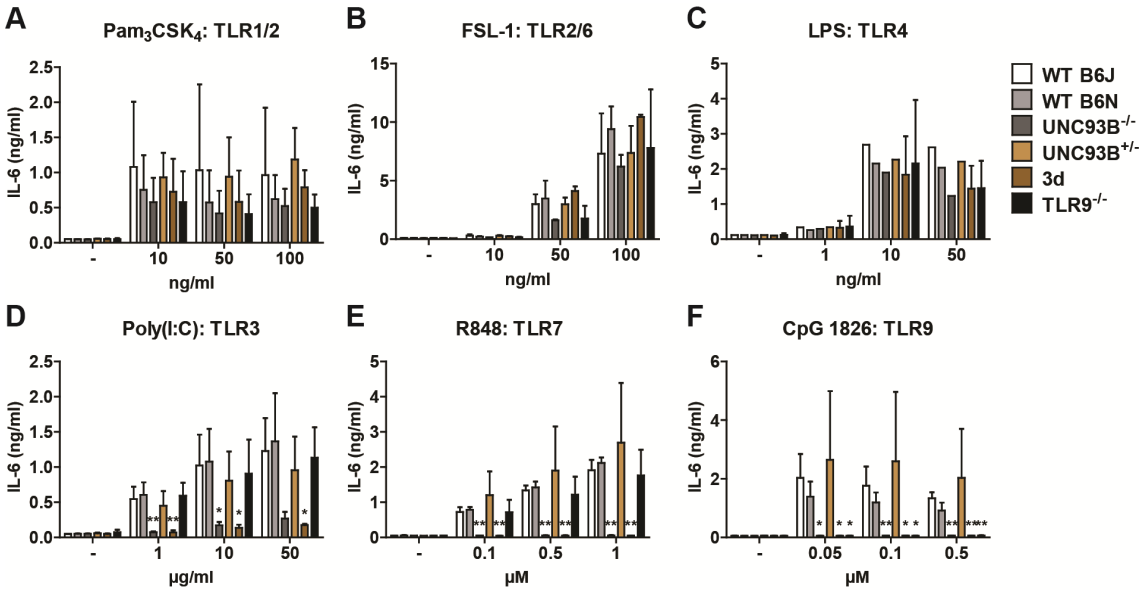

Figure 10: BMDM derived from UNC93B$^{-/-}$ mice do not produce IL-6 in response to stimulation of intracellular TLRs. Primary BMDM derived from B6J or B6N wild type (WT), UNC93B$^{-/-}$, UNC93B$^{+/-}$, 3d, and TLR9$^{-/-}$ mice were stimulated with indicated concentrations of Pam_3CSK_4 (A, n=3), FSL-1 (B, n=2), LPS (C, n=1 for WT B6J, WT B6N, UNC93B$^{-/-}$, and UNC93B$^{+/-}$, n=3 for 3d and TLR9$^{-/-}$), Poly(I:C) (D, n=3), R848 (E, n=3), or CpG 1826 (F, n=3) for 16 h. IL-6 levels in supernatants were determined by ELISA. Results are shown as mean ± S.D. of n (as specified) independent experiments. Statistical significance compared to respective wild type controls was determined by two-tailed, unpaired t test; *, p<0.05; **, p<0.01.

3.1.3. Intracellular TLRs only play a minor role for recognition of the murine herpesviruses MCMV and MHV-68 in primary BMDM

Intracellular TLRs are important for the recognition of herpesviruses. It has been shown that TLR9 is crucial for the type I interferon (IFN) response against the betaherpesvirus mouse cytomegalovirus (MCMV) in FL-DC and that TLR 3, 7, and 9 are involved in the recognition of MCMV *in vivo*[92-94]. A role for TLR9 has also been implicated in the recognition of the gammaherpesvirus murine herpesvirus 68 (MHV-68) in FL-DC[96]. To assess the role of UNC93B and intracellular TLRs for the recognition of the DNA viruses MCMV and MHV-68, primary BMDM derived from B6J and B6N wild type, UNC93B$^{-/-}$, UNC93B$^{+/-}$, 3d, and TLR9$^{-/-}$ mice were infected with MCMV and MHV-68 at different multiplicities of infection (MOIs) and proinflammatory cytokine responses were measured by ELISA. In contrast to stimulation of BMDM with synthetic TLR agonists, infection of BMDM with MCMV or MHV-68 leads to the production of amounts of type I IFN high enough to be detected by ELISA. Therefore, IFNα and IFNβ responses of primary BMDM infected with MCMV or MHV-68 were measured as well.

Infection of primary BMDM with MCMV induced the release of the proinflammatory cytokines TNF and IL-6 (Figure 11, A and B). This cytokine response was independent of TLR9, as BMDM derived from TLR9$^{-/-}$ mice generated cytokine responses comparable to those of wild type BMDM. However, recognition of MCMV seemed to be

at least partially dependent on intracellular TLRs, since BMDM derived from 3d mice showed reduced TNF and IL-6 levels compared to wild type and TLR9$^{-/-}$ BMDM, although this effect was not statistically significant. Again, as observed with synthetic TLR agonists (Figure 9 and Figure 10), the phenotype of BMDM derived from UNC93B$^{-/-}$ mice resembled the phenotype of BMDM generated from 3d mice, whereas BMDM derived from UNC93B$^{+/-}$ mice behaved like wild type BMDM.

In contrast to MCMV, levels of proinflammatory cytokines secreted upon infection of primary BMDM with MHV-68 were close to the detection limit, even with an MOI of 5 (Figure 11, C and D). Many viruses have developed strategies to evade the immune system of their hosts. MHV-68 is able to downregulate proinflammatory cytokine responses upon infection of primary BMDM and thereby prevents the secretion of TNF and IL-6 (Bussey et al., submitted)[201].

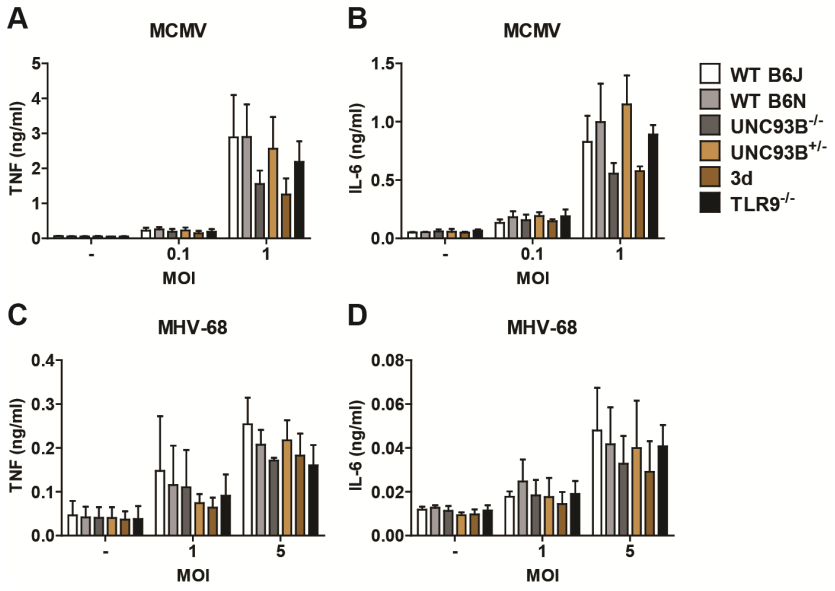

Figure 11: Primary BMDM elicit proinflammatory cytokine responses upon recognition of MCMV, but not MHV-68, which are partially dependent on intracellular TLRs. Primary BMDM from B6J or B6N wild type (WT), UNC93B$^{-/-}$, UNC93B$^{+/-}$, 3d, and TLR9$^{-/-}$ mice were infected with MCMV-GFP (A, B) or MHV-68 (C, D) at indicated MOIs for 16 h. Levels of TNF (A, C) and IL-6 (B, D) in supernatants were determined by ELISA. Results are shown as mean ± S.D. of 3 independent experiments. Statistical significance compared to respective wild type controls was determined by two-tailed, unpaired t test.

Upon infection of primary BMDM with MCMV, IFNα and IFNβ were detected in cell supernatants by ELISA (Figure 12, A and B). In contrast to the proinflammatory cytokine responses, type I IFN responses triggered by infection with MCMV seemed to be completely independent of intracellular TLRs and UNC93B as BMDM derived from UNC93B$^{-/-}$, UNC93B$^{+/-}$, 3d, and TLR9$^{-/-}$ mice all produced amounts of IFNα and IFNβ comparable to the amounts produced by wild type BMDM. Thus, the type I IFN

response upon infection of primary BMDM with MCMV is most likely mediated by cytosolic PRRs.

Similar to proinflammatory cytokine responses, infection of primary BMDM with MHV-68 did not lead to the production of measurable amounts of type I IFN (data not shown).

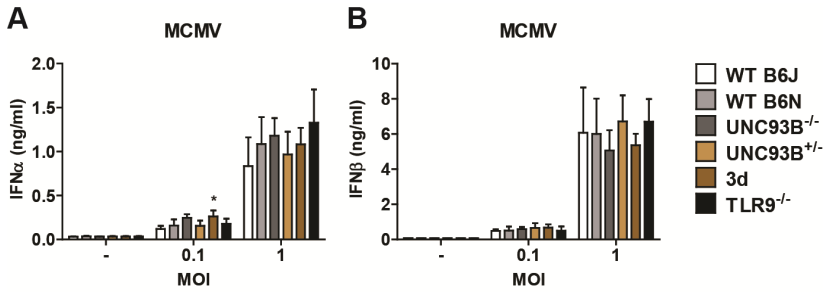

Figure 12: Type I IFN responses of primary BMDM upon MCMV infection are independent of intracellular TLRs. Primary BMDM from B6J or B6N wild type (WT), UNC93B$^{-/-}$, UNC93B$^{+/-}$, 3d, and TLR9$^{-/-}$ mice were infected with MCMV-GFP at MOI 0.1 and 1 for 16 h. Levels of IFNα (A) and IFNβ (B) in supernatants were determined by ELISA. Results are shown as mean ± S.D. of 3 independent experiments. Statistical significance compared to respective wild type controls was determined by two-tailed, unpaired t test; *, p<0.05.

In the *in vitro* studies performed so far there was no evidence for a difference between cells derived from the B6J and the B6N wild type mouse strain. Therefore, only one of the wild type strains was included in the following experiments.

Protein levels of UNC93B in cells derived from heterozygous UNC93B$^{+/-}$ and wild type mice did not significantly differ (Figure 8) and BMDM derived from UNC93B$^{+/-}$ mice did not show any difference in the TLR responses compared to cells derived from wild type mice (Figure 9 - Figure 12). This suggests that BMDM derived from UNC93B$^{+/-}$ mice do not differ from wild type BMDM and that only a complete loss of UNC93B leads to a different phenotype. Therefore, cells derived from heterozygous UNC93B$^{+/-}$ mice were omitted in the following studies.

3.1.4. MCMV infection leads to the induction of proinflammatory cytokines and type I IFN followed by induction of ISGs in BMDM

In addition to the ELISA experiments, innate immune responses upon MCMV infection of BMDM derived from wild type and UNC93B$^{-/-}$ mice were also analyzed using the microarray technology. The microarray experiment allowed analysis of transcript regulation of about 40,000 genes simultaneously. In this study, we focused on the regulation of genes which are involved in the innate immune response, among them proinflammatory cytokines, type I IFN, and IFN-stimulated genes (ISGs). Expression of ISGs is induced by IFN and mediates numerous antiviral effector functions[205].

Microarray analysis also allowed to distinguish between different subtypes of IFNα (IFNα1, IFNα2, IFNα4, IFNα5, IFNα7, IFNα11, IFNα12, IFNα13, IFNα14, and IFNαA), whereas detection of IFNα by ELISA (Figure 12) did not differentiate between different IFNα subtypes.

As expected, microarray analysis revealed that mRNA levels of proinflammatory cytokines and type I IFN were upregulated 2 h post infection (Figure 13). This in turn led to transcriptional activation of ISGs which were highly upregulated 6 h post infection. The expression of most proinflammatory cytokines and type I IFN was already downregulated 6 h post infection.

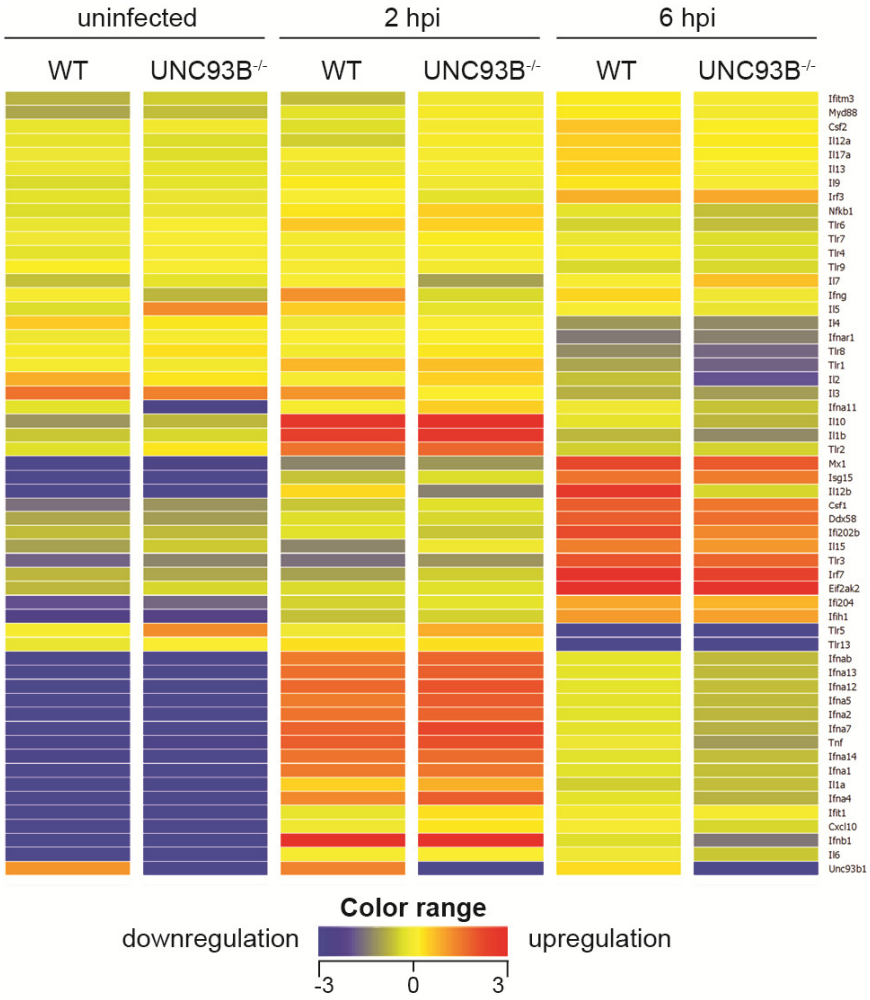

Figure 13: Infection of primary BMDM with MCMV leads to mRNA induction of proinflammatory cytokines and type I IFN followed by mRNA induction of ISGs. Primary BMDM derived from B6N wild type (WT) or UNC93B$^{-/-}$ mice were left untreated or spin infected with MCMV-GFP at an MOI of 0.5. RNA was isolated and mRNA expression was analyzed by microarray analysis in uninfected cells and 2 h or 6 h post infection (hpi). Shown are mRNA expression profiles of selected cytokines and interferon-stimulated genes (ISGs).

The expression patterns for the selected genes appeared very similar for BMDM from wild type and UNC93B$^{-/-}$ mice. This indicates that the response to MCMV by primary BMDM is largely independent on UNC93B and intracellular TLRs. These findings are in agreement with the type I IFN ELISA results described in 3.1.3 (Figure 12). 2 h post MCMV infection, TNF and IL-6 mRNA expression was induced to a similar extent in BMDM derived from UNC93B$^{-/-}$ and wild type mice. However, 6 h post infection, TNF and IL-6 mRNA levels in wild type BMDM were slightly higher than in BMDM derived from UNC93B$^{-/-}$ mice. This result is in agreement with the TNF and IL-6 ELISA result described in 3.1.3 as TNF and IL-6 levels were slightly impaired in BMDM derived from UNC93B$^{-/-}$ mice compared to wild type BMDM (Figure 11).

In summary, the microarray experiment shows a rapid induction of proinflammatory cytokine and type I IFN expression upon MCMV infection of primary BMDM within 2 h post infection. The produced type I IFN in turn activates upregulation of the expression of ISGs, which was detected 6 h post infection.

3.1.5. Intracellular TLRs are crucial for type I IFN responses upon infection or stimulation of FL-DC with MCMV and MHV-68

Plasmacytoid dendritic cells (pDC) are important mediators of antiviral immunity and produce high amounts of type I IFN in response to stimulation of intracellular TLR7 and TLR9[206]. pDC lack intracellular TLR3 and predominantly express TLRs 7 and 9[106,207,208]. *In vitro*, pDC can be generated by cultivation of bone marrow cells with Flt3 ligand which stimulates the differentiation of bone marrow cells to dendritic cells[209]. After 10 days of *in vitro* culture in the presence of Flt3 ligand, Flt3 ligand-induced dendritic cells (FL-DC) consist of about 40% pDC and 60% conventional dendritic cells (cDC)[210]. Upon viral infection, pDC produce large amounts of IFNα, whereas cDC secrete only low amounts of IFNα[210].

In order to study the importance of UNC93B and intracellular TLRs for the type I IFN response in dendritic cells, FL-DC were generated from wild type, UNC93B$^{-/-}$, 3d, TLR7$^{-/-}$, and TLR9$^{-/-}$ mice. Cells were transfected with the single stranded RNA Poly(U) to stimulate TLR7, stimulated with CpG 2336, an agonist for TLR9, or infected with MCMV or MHV-68 and amounts of IFNα were determined by ELISA. In addition, in order to find out if UNC93B also plays a role for the TLR-independent type I IFN response in FL-DC, cells were stimulated with agonists for cytosolic DNA or RNA sensors. A role of UNC93B for the function of cytosolic PRRs has not been described so far.

The absence of TLR7 and TLR9 in FL-DC of respective knockout mice was verified by stimulation with Poly(U) and CpG 2336, respectively. Upon stimulation of TLR7 with

Poly(U), FL-DC from wild type and TLR9$^{-/-}$ mice secreted comparable amounts of IFNα (Figure 14A). As expected, FL-DC generated from UNC93B$^{-/-}$, 3d, and TLR7$^{-/-}$ mice did not produce detectable amounts of IFNα upon stimulation of TLR7. Upon stimulation of TLR9 with CpG 2336, FL-DC from wild type and TLR7$^{-/-}$ mice, but not FL-DC derived from UNC93B$^{-/-}$, 3d, and TLR9$^{-/-}$ mice, produced up to 100 ng/ml of IFNα (Figure 14B).
In contrast to primary BMDM, intracellular TLRs 7 and 9 are crucial for the recognition of MCMV in FL-DC[94]. Upon MCMV infection, wild type FL-DC produced high amounts of IFNα, but IFNα responses were completely abolished when UNC93B was missing (UNC93B$^{-/-}$) or not functional (3d) (Figure 14C). Compared to wild type FL-DC, FL-DC derived from TLR9$^{-/-}$ mice produced 10- or 6-fold less IFNα upon infection with MCMV at MOI 0.5 or MOI 1, respectively, but FL-DC from TLR7$^{-/-}$ mice did not show a significant reduction of the IFNα response upon MCMV infection. This confirms that TLR9 is the major receptor for recognition of MCMV in FL-DC which has been described previously and is consistent with the finding that TLR9 is essential for the type I IFN response against MCMV in vivo[92,93]. In contrast to FL-DC from UNC93B$^{-/-}$ and 3d mice, which showed IFNα responses that were reduced to the background level, FL-DC derived from TLR9$^{-/-}$ mice still induced the production of up to 18 ng/ml IFNα. This suggests that TLR7 does contribute to the IFNα response against MCMV and is consistent with the finding that TLR7 and TLR9 have overlapping functions for the immune response to MCMV in pDC and *in vivo*[94]. Only if TLR7 and TLR9 are not functional, like in FL-DC from 3d or UNC93B$^{-/-}$ mice, the cells are completely unable to respond to the infection (Figure 14C).
IFNα responses by FL-DC upon infection with MHV-68 were about 5-fold lower than those observed for infection with MCMV. Infection of wild type FL-DC with MHV-68 led to the production of up to 20 ng/ml IFNα at an MOI of 2, but FL-DC derived from UNC93B$^{-/-}$ and 3d mice did not produce measurable amounts of IFNα upon infection with MHV-68 (Figure 14D). The role of TLR7 for the recognition of MHV-68 seemed to be more prominent than for the recognition of MCMV. Compared to wild type FL-DC, a 2-fold reduction in amounts of secreted IFNα was observed for FL-DC derived from TLR7$^{-/-}$ mice infected with MHV-68 at MOI 0.5 or 2. However, this effect was not statistically significant. FL-DC derived from TLR9$^{-/-}$ mice showed a 3-fold reduction in the amounts of secreted IFNα compared to wild type FL-DC upon infection with MHV-68 at the two tested MOIs. The observation that TLR9 is important for the IFNα response upon infection of FL-DC with MHV-68 is consistent with previous findings[96]. A role for TLR7 for the recognition of MHV-68 has not been described so far. Thus, similar to the IFNα response upon MCMV infection, the IFNα response upon MHV-68 infection of FL-DC was only completely abrogated when TLR7 and TLR9 were absent

and there was no difference in IFNα responses between FL-DC derived from UNC93B$^{-/-}$ or 3d mice.

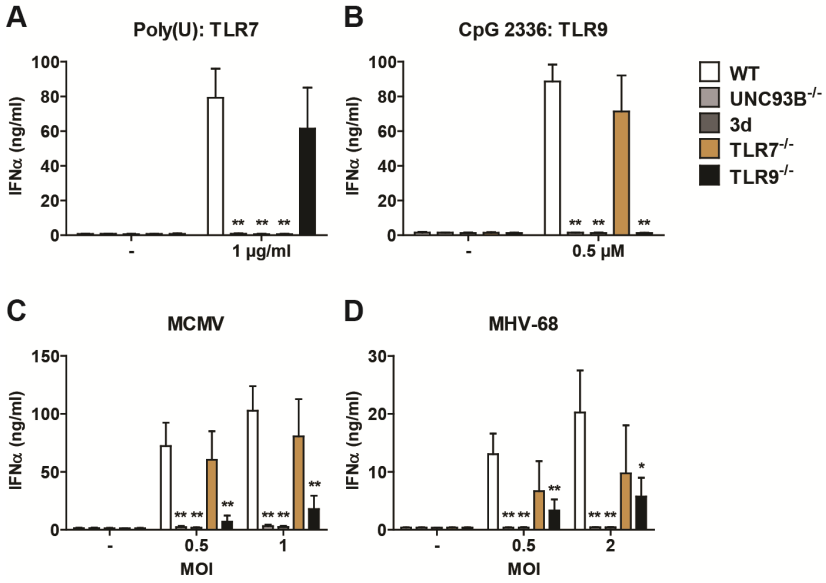

Figure 14: Type I IFN responses of FL-DC upon MCMV or MHV-68 infection are dependent on UNC93B and intracellular TLRs. FL-DC from wild type (WT), UNC93B$^{-/-}$, 3d, TLR7$^{-/-}$, and TLR9$^{-/-}$ mice were transfected with Poly(U) (A), stimulated with CpG 2336 (B), or infected with MCMV-GFP (C) or MHV-68 (D) at indicated MOIs for 18 h. Levels of IFNα in supernatants were determined by ELISA. Results are shown as mean ± S.D. of 3 independent experiments for FL-DC from UNC93B$^{-/-}$ mice or 4 independent experiments for FL-DC derived from wild type, 3d, TLR7$^{-/-}$, and TLR9$^{-/-}$ mice. Statistical significance compared to wild type controls was determined by two-tailed, unpaired t test; *, p<0.05; **, p<0.01.

To stimulate signaling pathways downstream of cytosolic DNA and RNA sensors in dendritic cells, FL-DC derived from wild type, UNC93B$^{-/-}$, 3d, and TLR9$^{-/-}$ mice were transfected with interferon stimulatory DNA (ISD) or the RIG-I ligand 5`triphosphate double stranded RNA (5`ppp-dsRNA)[211]. ISD lacks any kind of CpG motif and is supposed to stimulate cytosolic DNA sensors in a TLR9-independent manner[107]. Two different kinds of ISD have been described, a 45-base pair (45bp) and a 85-base pair (85bp) ISD, and both were used to stimulate cytosolic DNA sensors in FL-DC[107,141].

As a control for FL-DC derived from TLR9$^{-/-}$ mice, cells were stimulated with the TLR9 ligand CpG 2336. As observed earlier (Figure 14B), wild type FL-DC produced high amounts of IFNα upon stimulation with CpG 2336, whereas FL-DC derived from UNC93B$^{-/-}$, 3d, and TLR9$^{-/-}$ mice did not respond to stimulation of TLR9 (Figure 15A).

Transfection of FL-DC with the 85bp and the 45bp ISD led to the production of 5 and 16 ng/ml of IFNα in wild type FL-DC, respectively (Figure 15, B and C). This suggests that the 45bp ISD is a more potent stimulator than the 85bp ISD. Surprisingly, FL-DC derived from UNC93B$^{-/-}$, 3d, and TLR9$^{-/-}$ mice did not respond to stimulation with the 45bp or 85bp ISD, indicating that the IFNα responses to both forms of ISD were

dependent on TLR9. However, a previous study showed that the IFNα response upon transfection of FL-DC with 45bp ISD is completely abrogated in STING-deficient mice, indicating that the ISD response is completely dependent on cytosolic DNA sensors and independent of TLR9[117].

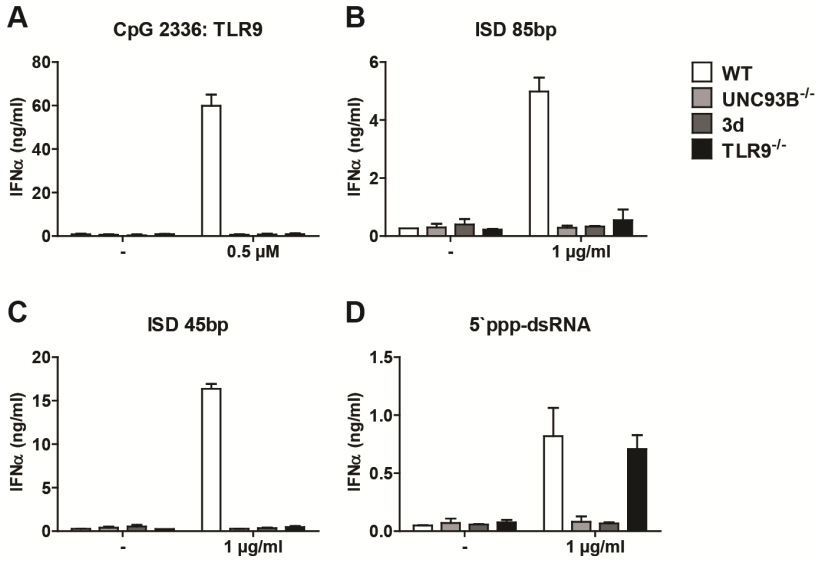

Figure 15: Sensing of ISD in FL-DC is dependent on TLR9. FL-DC derived from wild type (WT), UNC93B$^{-/-}$, 3d, and TLR9$^{-/-}$ mice were stimulated with CpG 2336 (A) or transfected with 45bp ISD (B), 85bp ISD (C), or 5`ppp-dsRNA (D) for 18 h. Levels of IFNα in supernatants were determined by ELISA. Results are shown as mean ± S.D. of 2 independent experiments for CpG 2336 and ISD 85bp or one representative experiment with duplicates for ISD 45bp and 5`ppp-dsRNA.

Stimulation of FL-DC with 5`ppp-dsRNA led to the production of IFNα in FL-DC derived from wild type and TLR9$^{-/-}$ mice as expected (Figure 15D). Surprisingly, this response was also dependent on intracellular TLRs, indicated by the complete absence of an IFNα response in FL-DC derived from UNC93B$^{-/-}$ and 3d mice. Since FL-DC derived from TLR9$^{-/-}$ mice produced IFNα levels comparable to those of wild type FL-DC, this response was most likely mediated by intracellular TLRs 3 or 7, which are dependent on UNC93B. Since 5`ppp-dsRNA is a double stranded RNA molecule, it could be sensed by TLR3. TLR3 is not expressed in pDC, whereas cDC which constitute up to 60% of the cells in FL-DC cultures express TLR3 and are able to produce small amounts of IFNα [106,207,208]. Since the amounts of IFNα secreted by FL-DC derived from wild type and TLR9$^{-/-}$ mice upon stimulation with 5`ppp-dsRNA were very low compared to stimulation with CpG 2336 or ISD (Figure 15, A-C), this response was very likely mediated by cDC in a TLR3-dependent manner. However, to clarify this, FL-DC derived from TLR3$^{-/-}$ and TLR7$^{-/-}$ mice should be included in further experiments. In addition, in order to find out which type of dendritic cells mediates the IFNα responses

to ISD and 5`ppp-dsRNA, these experiments should be repeated with pDC and cDC sorted from FL-DC cultures.

Together, these data verify that the intracellular TLRs 7 and 9 are responsible for the type I IFN response upon infection of FL-DC with MCMV and that TLR9 plays a more important role for this process than TLR7. The importance of TLR9 for the IFNα response against MHV-68 in FL-DC was also confirmed. Additionally, TLR7 was shown to be involved in the recognition of MHV-68 in FL-DC. In agreement with these results, UNC93B is crucial for the recognition of MCMV and MHV-68 in FL-DC. A new role for UNC93B for the PRR response to cytosolic DNA or RNA could not be demonstrated. However, it was shown for the first time that the IFNα response upon stimulation of FL-DC with ISD was dependent on TLR9.
As observed for BMDM (Figure 9 - Figure 12), we did not find differences in FL-DC derived from UNC93B$^{-/-}$ and 3d mice (Figure 14 and Figure 15).

In summary, the experiments performed with BMDM and FL-DC derived from UNC93B$^{-/-}$ and 3d mice lead to the conclusion that upon stimulation of TLRs or cytosolic PRRs innate immune cells derived from UNC93B$^{-/-}$ and 3d mice exhibit the same phenotype.

3.2. Identification of novel UNC93B interaction partners

3.2.1. Identification of novel UNC93B interaction partners by large scale immunoprecipitation and mass spectrometry analysis

UNC93B is crucial for the trafficking and signaling of intracellular TLRs. It delivers intracellular TLRs 3, 7, and 9 from the ER to the endolysosomal compartment where they can bind their ligands and initiate proinflammatory cytokine and type I IFN responses[55]. How trafficking of UNC93B-TLR complexes is regulated is not well understood. The identification and characterization of novel UNC93B interaction partners could give important insights into the regulation of UNC93B-TLR trafficking.

RAW 264.7 macrophages stably expressing wild type UNC93B-Flag-TEV-HA WT or mutant UNC93B-myc-TEV-HA H412R were lysed with the mild detergent digitonin and subjected to an anti-HA immunoprecipitation. Proteins were released by digestion with TEV protease, separated by liquid chromatography, and analyzed by mass spectrometry (LC-MS/MS)[54]. TLRs 3, 7, 9, and 13 bound to wild type, but not mutant

UNC93B. Besides TLRs 3, 7, 9, and 13, mass spectrometry analysis revealed many proteins which interacted with both wild type and mutant UNC93B (Table 14, V Appendix). Several highly interesting candidates among these potential UNC93B interacting proteins were further analyzed in this study: the uncharacterized protein cleft lip and palate associated transmembrane protein (Clptm), the protein tyrosine phosphatase 1B (PTP1B) known to regulate endosomal receptor trafficking, and three prime repair exonuclease 1 (Trex1), which is involved in the innate immune response to cytosolic DNA (Figure 16A) (peptides found by large scale immunoprecipitation and mass spectrometry analysis, V Appendix).

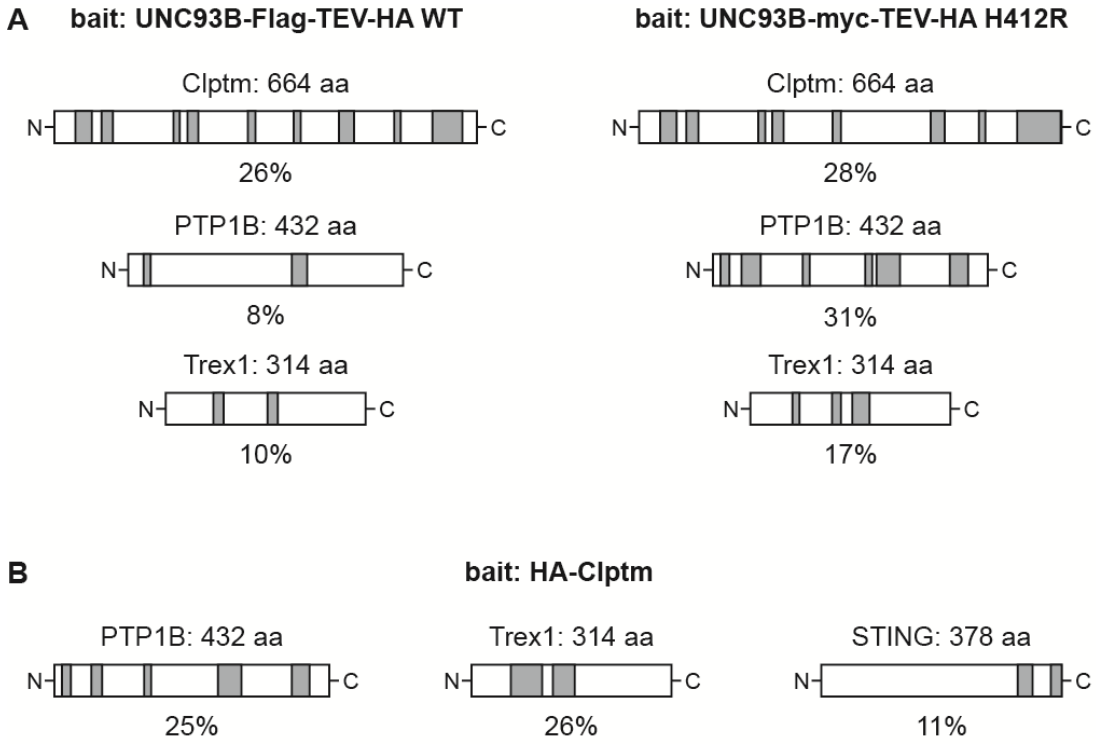

Figure 16: UNC93B and Clptm interaction partners in RAW 264.7 macrophages. RAW 264.7 macrophages stably expressing tagged versions of wild type (UNC93B-Flag-TEV-HA WT) and mutant (UNC93B-myc-TEV-HA H412R) UNC93B (A) and Clptm (HA-Clptm) (B) were lysed with 1% digitonin and immunoprecipitated with an anti-HA antibody. Proteins were separated by liquid chromatography and analyzed by mass spectrometry (LC-MS/MS). Cleft lip and palate associated transmembrane protein (Clptm) was found to interact with wild type and mutant UNC93B-HA. Protein tyrosine phosphatase 1B (PTP1B) and three prime repair exonuclease 1 (Trex1) were found to interact with wild type and mutant UNC93B-HA and HA-Clptm. Stimulator of interferon genes (STING) was found to interact with HA-Clptm. Peptides identified by mass spectrometry analysis are depicted in grey. Peptide coverage is shown in percent.

Peptides for cleft lip and palate associated transmembrane protein (Clptm) were recovered in immunoprecipitations with wild type and mutant UNC93B (Figure 16A). Clptm was initially identified as HS9 Ag, a molecule involved in intrathymic T cell development, on thymic stromal cells[212]. Subsequently, the *Clptm1* gene was found to be disrupted by translocation in a family that had a history of cleft lip and palate[213].

However, a link between the *Clptm1* gene and the etiology of cleft lip and palate has never been confirmed. Furthermore, mutations in the *Clptm1* gene were found in prostate cancer cell lines[214]. Clptm is predicted to have 5 transmembrane domains with a large luminal N-terminus (aa 1-354) and a cytosolic C-terminus (aa 530-664) by the TMHMM 2.0 programme of the CBS prediction servers (Figure 17A). To gain insight into possible functions of Clptm, RAW 264.7 macrophages stably expressing HA-tagged Clptm were generated, lysed, and subjected to an anti-HA immuno-precipitation. Proteins interacting with HA-Clptm were analyzed by LC-MS/MS (Table 15, V Appendix). Among the proteins listed in Table 15 PTP1B, Trex1, and stimulator of interferon genes (STING), which is a key regulator of the response to cytosolic DNA, were identified as binding partners of Clptm (Figure 16B) (peptides found by large scale immunoprecipitation and mass spectrometry analysis, V Appendix).

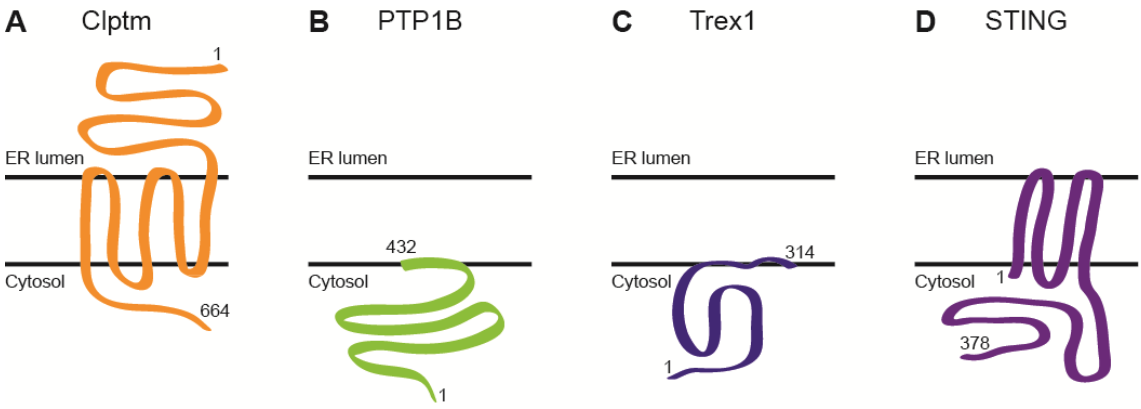

Figure 17: Predicted topology of UNC93B and Clptm interaction partners. Clptm has five predicted transmembrane domains with a large luminal N-terminus (aa 1-354) and a cytosolic C-terminus (aa 530-664) (A). PTP1B and Trex1 are C-terminally anchored to the cytosolic side of the ER via a 35- or 79-residue domain, respectively (B, C). STING is reported to have four transmembrane domains with a short cytosolic N-terminus (aa 1-19) and a large cytosolic C-terminal domain (aa 137-378) (D).

Protein tyrosine phosphatase 1B (PTP1B) was identified as an interacting partner of wild type and mutant UNC93B as well as Clptm (Figure 16). PTP1B is the best characterized tyrosine phosphatase (1.2). It is attached to the cytoplasmic face of the ER membrane via its hydrophobic C-terminal 35-residue domain (Figure 17B)[154]. Among other functions, PTP1B has been reported to regulate trafficking of receptor tyrosine kinases which made PTP1B a highly interesting candidate for this study[158].

The three prime repair exonuclease 1 (Trex1) interacted with wild type and mutant UNC93B and Clptm (Figure 16, A and B). Trex1 is the major 3`→5` DNA exonuclease in mammals and has been described as a negative regulator of the cytosolic DNA response[122]. Trex1 has been reported to interact with the cytosolic side of the ER membrane via its 79-residue hydrophobic C-terminal domain (Figure 17C)[141].

The membrane protein stimulator of interferon genes (STING) was only identified as an interaction partner of Clptm (Figure 16B). STING is an ER resident protein with four predicted transmembrane domains and a large C-terminal domain (aa 137-378) facing the cytosolic side of the ER (Figure 17D)[215]. STING is known to be a crucial player in the cytosolic DNA response[216].

The interaction between Trex1 and STING with UNC93B and Clptm has been extensively investigated in a separate study (Olga Trupp, bachelor thesis 2011: The DNA exonuclease Trex-1 interacts with Cleft lip and palate associated transmembrane protein (Clptm), a component of the UNC93B1/Toll-like receptor complex).

3.3. Characterization of the role of Clptm and Trex1 for TLR- and UNC93B-mediated immune responses

3.3.1. Clptm interacts with wild type and mutant UNC93B

Clptm is a poorly characterized protein which is predicted to have five transmembrane domains (CBS prediction servers, TMHMM 2.0) (Figure 17A). To study the subcellular localization of Clptm and its interaction with UNC93B, Trex1, STING, and PTP1B, different expression constructs of Clptm were generated. Clptm was N-terminally as well as C-terminally tagged with the HA epitope tag or fused to GFP. RAW 264.7 macrophage cell lines stably expressing HA-Clptm, Clptm-HA, GFP-Clptm, or Clptm-GFP were established by retroviral transduction. Expression of endogenous Clptm as well as HA-Clptm, Clptm-HA, GFP-Clptm, and Clptm-GFP in RAW 264.7 macrophages was verified by immunoblotting with a polyclonal rabbit antibody raised against C-terminal peptides of Clptm (Figure 18, A and B).

Clptm is predicted to have six putative N-linked glycosylation sites all of which are located within predicted luminal domains of Clptm (CBS prediction servers, NetNGlyc 1.0) (Figure 18C). Potential glycosylation sites (consensus sequence NxS/T) are N^{28}GS, N^{119}AT, N^{161}GS, N^{241}IT, N^{295}ES, and N^{413}ET. In order to show whether Clptm is glycosylated, lysates of RAW 264.7 macrophages stably expressing Clptm-GFP were digested with PNGase F, a glycosidase which catalyzes the cleavage of N-linked oligosaccharides from glycoproteins. Immunoblot analysis revealed that endogenous Clptm as well as Clptm-GFP were glycosylated, since treatment of cell lysates with PNGase F resulted in a shift of both protein bands to bands of lower molecular weights (Figure 18D). This indicates that Clptm traffics through the Golgi apparatus where it is modified by glycosylation. Addition of the large GFP moiety does not influence Golgi trafficking of the GFP-Clptm fusion protein. Glycosylation of Clptm was also observed

in wild type RAW 264.7 macrophages and RAW 264.7 macrophages stably expressing GFP-Clptm (data not shown).

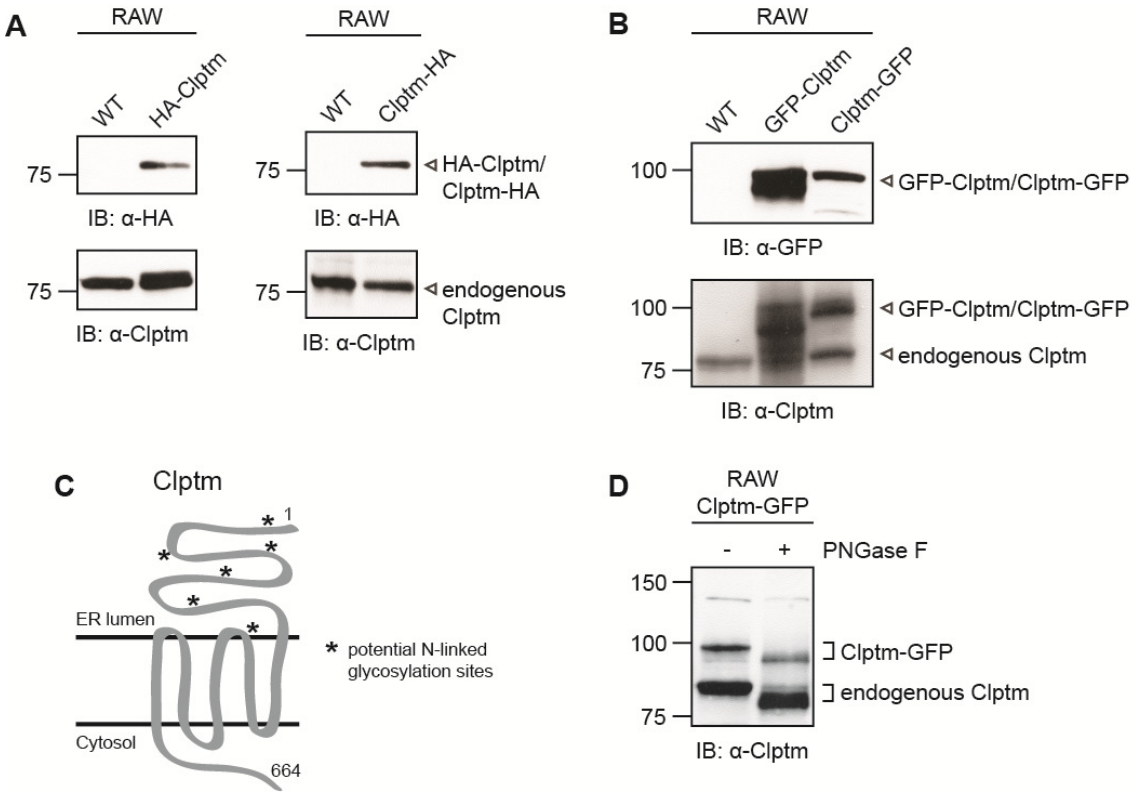

Figure 18: HA-Clptm, Clptm-HA, GFP-Clptm, and Clptm-GFP are expressed and Clptm is glycosylated in macrophages. RAW 264.7 macrophages stably expressing HA-Clptm or Clptm-HA (A) and GFP-Clptm or Clptm-GFP (B) were lysed and expression of Clptm fusion proteins was analyzed by immunoblotting with the indicated antibodies. Predicted N-linked glycosylation sites of Clptm are indicated (*) (C). RAW 264.7 macrophages stably expressing Clptm-GFP were lysed with 1% NP-40. Lysates were left untreated or treated with PNGase F for 1 h at 37°C (D).

To verify the interaction between UNC93B and Clptm identified by large scale immunoprecipitation and LC-MS/MS analysis (Figure 16A), individual co-immunoprecipitations were performed with lysates of RAW 264.7 macrophages stably expressing wild type or mutant UNC93B-HA or HA-Clptm. Cells were lysed under mild conditions and subjected to immunoprecipitations with an anti-Clptm or anti-UNC93B antibody. Expression of wild type and mutant UNC93B-HA and HA-Clptm in input lysates was verified by anti-HA immunoblotting (Figure 19, A and B). Upon immunoprecipitation of endogenous Clptm, wild type and mutant (H412R) UNC93B-HA could be detected by anti-HA immunoblotting (Figure 19A). Vice versa, HA-Clptm co-precipitated with endogenous UNC93B in RAW 264.7 macrophages stably expressing HA-Clptm (Figure 19B). These results confirm an interaction between UNC93B and Clptm as initially shown by large scale immunoprecipitation and LC-MS/MS.

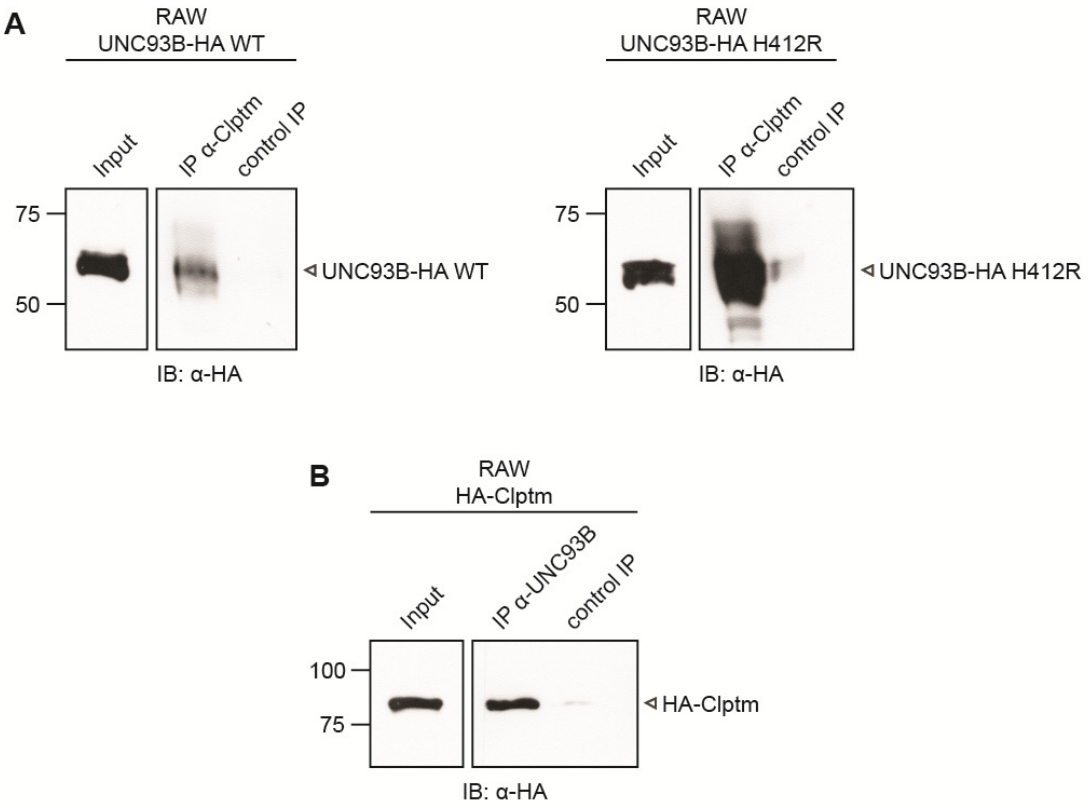

Figure 19: Wild type and mutant UNC93B-HA interact with endogenous Clptm and HA-Clptm interacts with endogenous UNC93B in RAW 264.7 macrophages. RAW 264.7 macrophages stably expressing wild type (WT) or mutant (H412R) UNC93B-HA (A) or HA-Clptm (B) were lysed with 1% digitonin and subjected to an immunoprecipitation with anti-Clptm or anti-UNC93B, respectively. Rabbit serum was used as control. Immunoprecipitated UNC93B-HA or HA-Clptm were detected with an anti-HA antibody.

3.3.2. Knockdown of Clptm in macrophages does not impair the TNF response upon TLR stimulation

In order to find out whether Clptm plays a role for TLR signaling, a knockdown of Clptm was performed in RAW 264.7 macrophages using an shRNA approach. Knockdown of UNC93B was performed as a control. Two or three independent shRNAs were used for knockdown of Clptm and UNC93B, respectively. Additionally, control shRNAs targeting the human retinoblastoma protein (sh-control1) and Renilla luciferase (sh-control2) were included. Successful knockdown of Clptm and UNC93B in RAW 264.7 macrophages was verified by immunoblotting with anti-Clptm and anti-UNC93B antibodies (Figure 20A). Expression of sh-UNC1, sh-UNC2, or sh-UNC3 efficiently downregulated protein levels of UNC93B compared to cells expressing the control shRNAs (sh-control1, sh-control2). sh-UNC2 mediated the strongest knockdown of UNC93B (Figure 20A). Compared to the control shRNAs, protein levels of Clptm were equally reduced upon expression of sh-Clptm1 and sh-Clptm2. Protein levels of Clptm were not affected by knockdown of UNC93B and vice versa (Figure 20A).

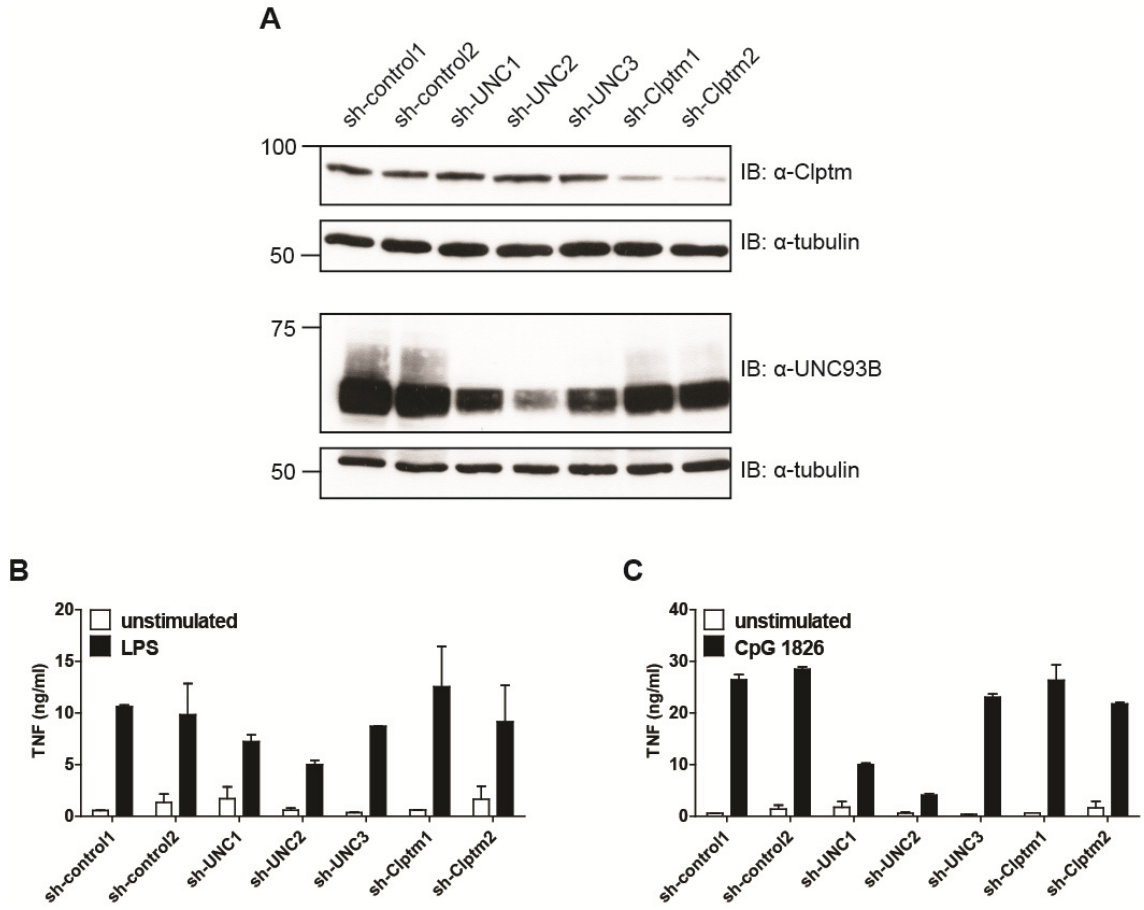

Figure 20: Knockdown of Clptm in RAW 264.7 macrophages does not have an effect on the TNF response upon TLR stimulation. RAW 264.7 macrophages stably expressing indicated shRNAs were lysed and protein levels of Clptm and UNC93B were analyzed by immunoblotting with anti-Clptm or anti-UNC93B antibodies (A). Loading of equal amounts of protein was confirmed by anti-tubulin immunoblots. Cells expressing indicated shRNAs were stimulated with 10 ng/ml of LPS (B) or 0.2 µM CpG 1826 (C) for 4 h. Levels of TNF in supernatants were determined by ELISA. Results are shown as mean ± S.D. of one representative experiment with duplicates.

Next, the RAW 264.7 macrophage cell lines stably expressing UNC93B- or Clptm-specific shRNAs or control shRNAs were stimulated with LPS or CpG 1826 and the amount of TNF in supernatants was determined by ELISA. Compared to the amounts of TNF secreted by cells expressing control shRNAs, knockdown of UNC93B led to an up to 2-fold reduction of the TNF response upon LPS stimulation of TLR4 (Figure 20B). Knockdown of Clptm with sh-Clptm1 and sh-Clptm2 did not impair the TNF production in response to LPS stimulation. As expected, upon stimulation of TLR9 with CpG 1826, knockdown of UNC93B with sh-UNC1 or sh-UNC2 led to a 3- or more than 6-fold reduction of the elicited TNF responses compared to responses of cells expressing control shRNAs, respectively (Figure 20C). Although the efficiency of the UNC93B knockdown with sh-UNC1 and sh-UNC3 seemed to be comparable by immunoblotting, knockdown of UNC93B with sh-UNC3 did not lead to a reduction of the TNF response upon stimulation of TLR9 to a degree as seen with sh-UNC1. TNF levels upon

stimulation with CpG 1826 were not affected by knockdown of Clptm with sh-Clptm1 or sh-Clptm2 (Figure 20C).

This indicates that Clptm may not be involved in the proinflammatory cytokine response upon stimulation of cell surface TLR4 and intracellular TLR9 in macrophages. It is also possible that the shRNA-mediated knockdown of Clptm was not strong enough and that the remaining protein level of Clptm was sufficient to mediate a proinflammatory cytokine response.

3.3.3. Clptm co-localizes with Trex1 in macrophages and interacts with the luminal domain of Trex1

As described in 3.2.1, the DNA exonuclease Trex1 was found to interact with UNC93B and Clptm (Figure 16). Further interaction studies of UNC93B, Clptm, and Trex1 revealed interactions between endogenous Clptm and UNC93B with endogenous Trex1 (Olga Trupp, bachelor thesis 2011).

Trex1 was shown to co-localize with the ER-marker calnexin by immuno-fluorescence[141]. In order to analyze localization of Trex1 and Clptm by live cell imaging, monomeric cherry (mcherry) was N-terminally fused to Trex1 and BMDM stably expressing GFP-Clptm and cherry-Trex1 were generated by retroviral transduction. Co-localization of GFP-Clptm with cherry-Trex1 at the ER was demonstrated by live cell imaging (Figure 21A).

Trex1 is composed of two different domains. The N-terminal domain (aa 1-235) mediates its exonuclease function and the hydrophobic C-terminal domain (aa 236-314) attaches Trex1 to the cytoplasmic face of the ER membrane (Figure 17C). In order to find out which domain of Trex1 mediates interaction with Clptm, N- and C-terminally truncated versions of Trex1 were generated and N-terminally fused to mcherry. RAW 264.7 macrophage cell lines stably expressing GFP-Clptm and either full length or the N- or C-terminal truncated versions of cherry-Trex1 were established and expression of cherry-Trex1 constructs was verified by immunoblotting with an anti-RFP antibody which recognizes mcherry (Figure 21B). Upon anti-GFP immuno-precipitation, full length as well as the C-terminally truncated version of Trex1, were detected by immunoblotting. The hydrophobic C-terminal domain of Trex1, which anchors the protein in the ER membrane, did not co-precipitate with GFP-Clptm.

These results confirm the interaction between Clptm and Trex1 found by large scale immunoprecipitation and LC-MS/MS analysis and suggest that the luminal exonuclease domain of Trex1, but not the C-terminal domain, interacts with Clptm at the ER.

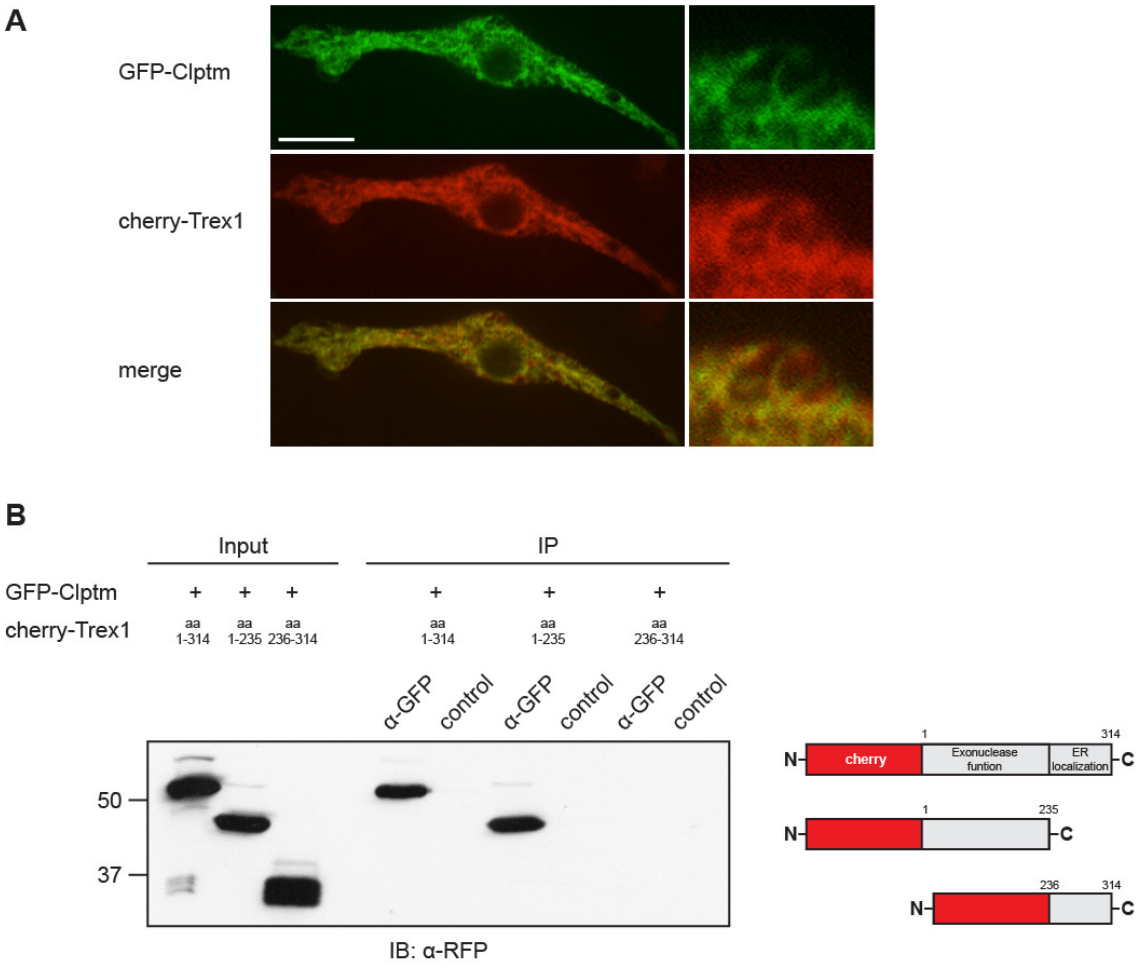

Figure 21: Clptm and Trex1 co-localize and Clptm interacts with the luminal domain of Trex1 in macrophages. BMDM stably expressing GFP-Clptm and cherry-Trex1 were analyzed by live cell imaging (A). Scale bar, 10 µm. RAW macrophages stably expressing GFP-Clptm and either full-length or truncated versions of cherry-Trex1 (cherry-Trex1 1-314, cherry-Trex1 1-235, and cherry-Trex1 236-314) were lysed with 1% digitonin and subjected to an immunoprecipitation with an anti-GFP antibody. Rabbit serum was used as control. Immunoprecipitated cherry-Trex1 constructs were detected with an anti-RFP antibody (B).

The immunoprecipitation experiments conducted with UNC93B, Clptm, and Trex1 confirmed interactions between all these proteins (Figure 19, Figure 21, and Olga Trupp, bachelor thesis 2011). A role for Clptm for the TLR-dependent proinflammatory cytokine response could not be shown in initial experiments. However, Clptm could be important for the type I IFN response upon TLR stimulation. Unfortunately, Clptm knockout mice are not available which is why we could not study the role of Clptm for the TLR-dependent type I IFN response in pDC.

3.4. Characterization of the role of protein tyrosine phosphatase PTP1B for TLR and innate immune signaling

3.4.1. PTP1B interacts with UNC93B, TLR9, TLR7, and Clptm

Protein tyrosine phosphatase 1B (PTP1B) was identified as an interacting partner of UNC93B and Clptm in large scale immunoprecipitations (Figure 16). To confirm interaction of UNC93B and Clptm with PTP1B, individual co-immunoprecipitations were performed.

Human embryonic kidney (HEK) 293T cells were co-transfected with HA-PTP1B and either wild type or mutant (H412R) UNC93B-GFP. Expression of HA-PTP1B in input lysates was verified by anti-HA immunoblotting (Figure 22, A and D) and expression of wild type and mutant UNC93B-GFP was verified by anti-GFP immunoblotting (data not shown and Figure 22D). Upon anti-GFP immunoprecipitation, HA-PTP1B was detected by immunoblotting when co-expressed with wild type or mutant UNC93B-GFP (Figure 22A). In the reverse experiment, wild type as well as mutant UNC93B-GFP was detected after anti-HA immunoprecipitation when co-expressed with HA-PTP1B (Figure 22D).

In order to analyze whether Clptm interacts with PTP1B, HEK 293T cells were co-transfected with HA-PTP1B and Clptm-GFP or empty vector. Expression of the transfected constructs in input lysates was verified by immunoblotting (Figure 22, B and E, and data not shown). HA-PTP1B co-precipitated with Clptm-GFP upon anti-GFP immunoprecipitation (Figure 22B). Vice versa, GFP-Clptm co-precipitated with HA-PTP1B upon anti-HA immunoprecipitation (Figure 22E).

At this point it is not clear whether the interaction between UNC93B and PTP1B is direct or indirect. Since UNC93B has been shown to interact with TLR9 via its transmembrane domain[54], it was also analyzed whether PTP1B interacts with TLR9. For this reason, anti-HA and anti-GFP immunoprecipitations were performed with HEK 293T cells co-transfected with HA-PTP1B and TLR9-GFP. In both cases, HA-PTP1B or TLR9-GFP were detected by immunoblotting only when co-expressed with TLR9-GFP or HA-PTP1B, respectively (Figure 22, C and F). Expression of HA-PTP1B and TLR9-GFP in input lysates was confirmed by immunoblotting (Figure 22, C and F, and data not shown).

Together, the co-immunoprecipitation experiments performed with lysates of transfected HEK 293T cells indicate that PTP1B interacts with wild type and mutant (H412R) UNC93B, Clptm, and TLR9.

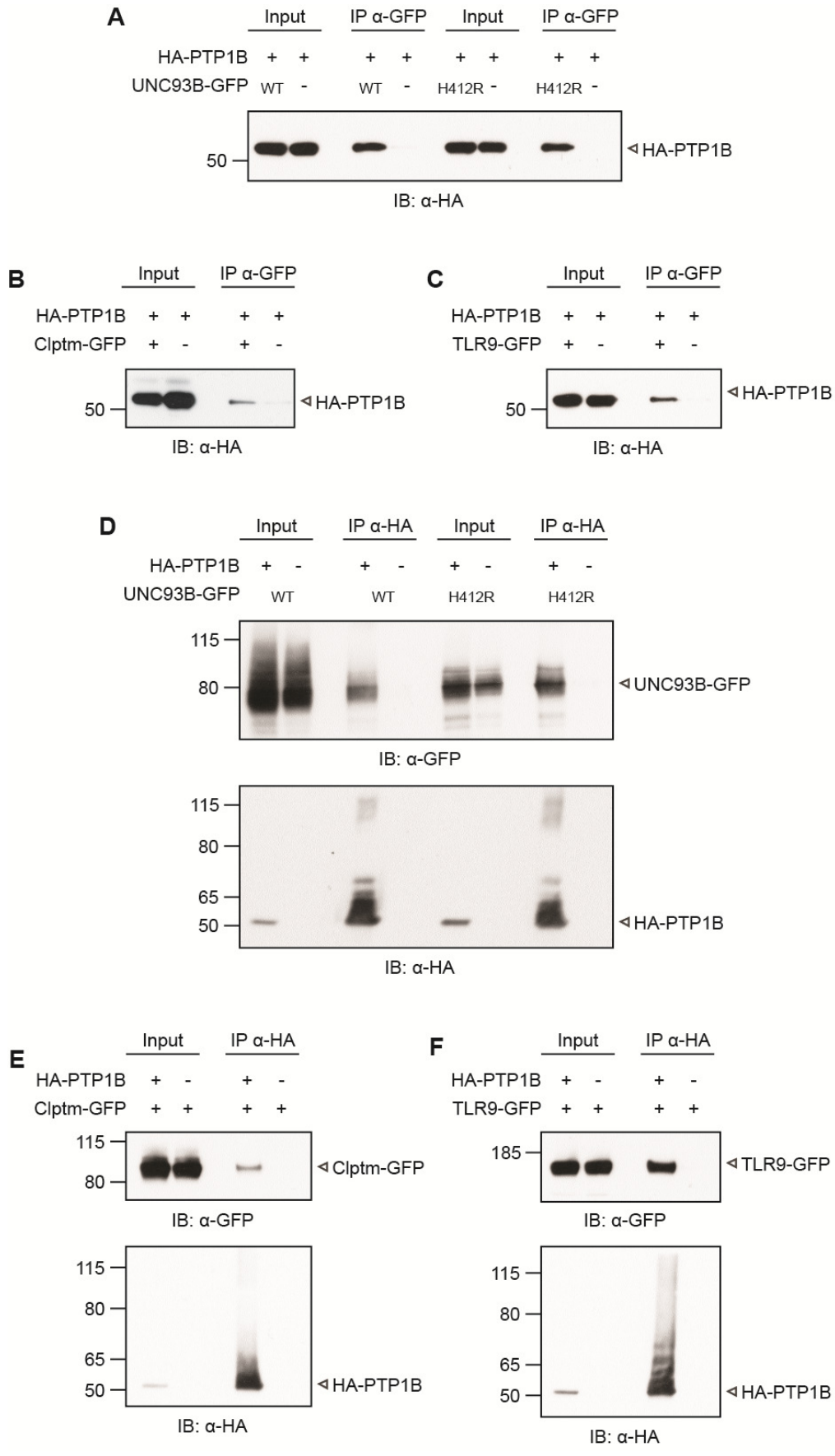
A
Input
IP α-GFP
Input
IP α-GFP
HA-PTP1B + + + + + + + +
UNC93B-GFP WT - WT - H412R - H412R -
50
HA-PTP1B
IB: α-HA
B
Input
IP α-GFP
HA-PTP1B + + + +
Clptm-GFP + - + -
50
HA-PTP1B
IB: α-HA
C
Input
IP α-GFP
HA-PTP1B + + + +
TLR9-GFP + - + -
50
HA-PTP1B
IB: α-HA
D
Input
IP α-HA
Input
IP α-HA
HA-PTP1B + - + - + - + -
UNC93B-GFP WT WT H412R H412R
115
80
UNC93B-GFP
IB: α-GFP
115
80
65
50
HA-PTP1B
IB: α-HA
E
Input
IP α-HA
HA-PTP1B + - + -
Clptm-GFP + + + +
115
80
Clptm-GFP
IB: α-GFP
115
80
65
50
HA-PTP1B
IB: α-HA
F
Input
IP α-HA
HA-PTP1B + - + -
TLR9-GFP + + + +
185
TLR9-GFP
IB: α-GFP
115
80
65
50
HA-PTP1B
IB: α-HA

Figure 22: Wild type and mutant UNC93B-GFP, Clptm-GFP, and TLR9-GFP interact with HA-PTP1B in HEK 293T cells. HEK 293T cells were transfected with HA-PTP1B and empty vector (-) or together with wild type (WT) or mutant (H412R) UNC93B-GFP (A), Clptm-GFP (B), or TLR9-GFP (C). Expression of HA-PTP1B in input lysates was verified by anti-HA immunoblotting. Cells were lysed with 0.5% NP-40 and immunoprecipitation was performed with an anti-GFP antibody. HA-PTP1B was detected by immunoblotting with an anti-HA antibody (A-C). HEK 293T cells were transfected wild type (WT) or mutant (H412R) UNC93B-GFP (D), Clptm-GFP (E), or TLR9-GFP (F) together with empty vector (-) or with HA-PTP1B. Expression of the different constructs in input lysates was verified by anti-GFP and anti-HA immunoblotting. Immunoprecipitation was performed with an anti-HA antibody. GFP fusion proteins were detected by immunoblotting with an anti-GFP antibody. Co-immunoprecipitated HA-PTP1B was detected by anti-HA immunoblotting (D-F).

HEK 293 cells do not express endogenous TLR9[208]. However, HEK 293 cells stably expressing human or murine TLR9 reporter constructs are commercially available (Invivogen) and functional, which indicates that UNC93B is expressed in HEK 293 cells. In order to analyze the interactions between PTP1B, UNC93B, intracellular TLRs, and Clptm in a more relevant cell type, co-immunoprecipitation experiments were performed in murine BMDM. TLR9 is proteolytically cleaved in the endolysosome in order to generate a functional receptor[71]. In contrast to HEK 293T cells, BMDM express endogenous TLR9 and TLR9 as well as TLR9-GFP are processed in BMDM. In lysates of BMDM expressing TLR9-GFP, full-length as well as the C-terminal TLR9-GFP cleavage fragment can be detected by anti-GFP immunoblotting (Figure 23).

Immortalized BMDM stably expressing TLR9-GFP and HA-PTP1B were lysed under mild conditions. For the analysis of the interaction between HA-PTP1B and TLR7, UNC93B, and Clptm, lysates were subjected to immunoprecipitations with antibodies against the respective proteins. To analyze whether HA-PTP1B interacts with TLR9-GFP, precipitations were performed with a GFP-binding protein coupled to agarose beads (GFP-Trap) or an anti-HA antibody. The expression of HA-PTP1B and TLR9-GFP in input lysates was confirmed by immunoblotting (Figure 23, A-C). HA-PTP1B co-precipitated with endogenous TLR7, UNC93B, and Clptm (Figure 23A). For the control immunoprecipitation rabbit serum was used instead of the antibodies against endogenous TLR7, UNC93B, and Clptm. This control only showed a very weak band upon anti-HA immunoblotting (Figure 23A). TLR7 and TLR9 both bind to UNC93B, which explains why detected signals for TLR9-GFP (full length and C-terminal cleavage fragment) were detected upon anti-TLR7 and anti-UNC93B immunoprecipitation and anti-GFP immunoblotting (Figure 23A). The signal detected for TLR9-GFP by anti-GFP immunoblotting upon anti-Clptm immunoprecipitation suggests a weak interaction of Clptm with TLR9-GFP.

Because of the lack of an antibody able to detect endogenous TLR9, the GFP-Trap was used to precipitate TLR9-GFP in immortalized BMDM stably expressing TLR9-GFP and HA-PTP1B. HA-PTP1B was detected after precipitation of TLR9-GFP

with the GFP-Trap, but not with control beads (Figure 23B). Interaction between TLR9-GFP and HA-PTP1B was further verified by detection of full length TLR9 after anti-HA immunoprecipitation of HA-PTP1B in BMDM stably expressing TLR9-GFP and HA-PTP1B (Figure 23C). In the absence of HA-PTP1B, TLR9-GFP did not precipitate with anti-HA beads, verifying the specificity of the TLR9-PTP1B co-immunoprecipitation (Figure 23C).

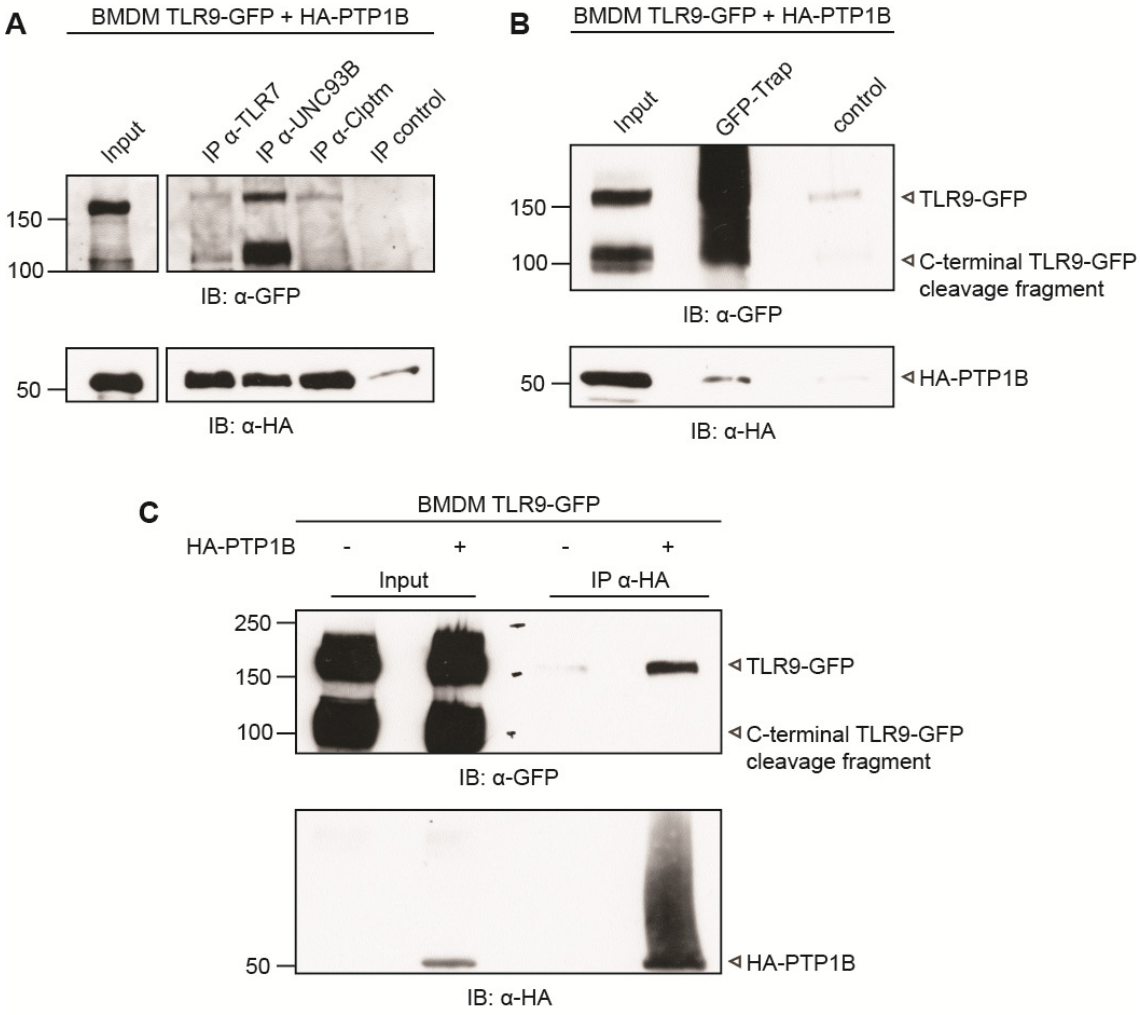

Figure 23: HA-PTP1B interacts with TLR7, UNC93B, Clptm, and TLR9-GFP in immortalized BMDM. BMDM stably expressing TLR9-GFP and HA-PTP1B were lysed with 1% digitonin. Immunoprecipitations for TLR7, UNC93B, and Clptm were performed with the indicated antibodies. Rabbit serum was used as control (A). TLR9-GFP was precipitated with GFP-Trap or control beads (B). Lysates of BMDM stably expressing TLR9-GFP alone or TLR9-GFP together with HA-PTP1B were subjected to an immunoprecipitation with an anti-HA antibody (C). HA-PTP1B was detected by immunoblotting with an anti-HA antibody. TLR9-GFP and its C-terminal cleavage fragment were detected with an anti-GFP antibody.

Altogether, these data demonstrate that HA-tagged PTP1B interacts with endogenous UNC93B, Clptm, and TLR7, as well as with TLR9-GFP in BMDM. However, at this point we cannot draw any conclusions about the nature of these interactions. To address, for example, the question whether PTP1B directly interacts with TLR9 or,

rather likely, via UNC93B, co-immunoprecipitations would need to be performed in BMDM derived from UNC93B$^{-/-}$ or TLR9$^{-/-}$ mice.

3.4.2. Ruby-PTP1B and TLR9-GFP partially co-localize in BMDM

PTP1B is anchored to the cytosolic side of the ER membrane via a hydrophobic C-terminal 35-residue region. In order to analyze whether PTP1B co-localizes with TLR9 in the ER or endosomes by live cell imaging, the red fluorescent protein mRuby2 was fused to HA-PTP1B. Immortalized BMDM stably expressing TLR9-GFP were retrovirally transduced with Ruby-PTP1B and cells were imaged unstimulated and upon stimulation with CpG DNA. As previously shown, TLR9-GFP localized to the ER as well as the endosomal compartment in unstimulated cells (Figure 24A)[41,62,74]. This is consistent with the observation that cleavage of TLR9 is present in unstimulated cells (Figure 23). Ruby-PTP1B was mainly located in the perinuclear region indicating ER localization. Occasionally, Ruby-PTP1B was also detected in endosomal structures (Figure 24A). The localization of TLR9-GFP and Ruby-PTP1B did not change upon CpG stimulation (Figure 24B). Stimulation of the cells with fluorescently labeled CpG 1826 allowed the visualization of CpG DNA-containing endosomes. TLR9-GFP clearly localized to endosomes filled with CpG DNA (Figure 24C). In contrast, Ruby-PTP1B did not accumulate in endosomes.

Live cell imaging of TLR9-GFP and Ruby-PTP1B indicates that both proteins partially co-localize in the ER. However, a large portion of TLR9-GFP localizes to the endosomal compartment and endosomal localization of Ruby-PTP1B was only observed occasionally.

We previously observed that the localization of the UNC93B-GFP construct differs from the reported localization of UNC93B in macrophages (data not shown)[52,55]. Therefore, UNC93B was not included in the co-localization experiments with Ruby-PTP1B conducted by live cell imaging.

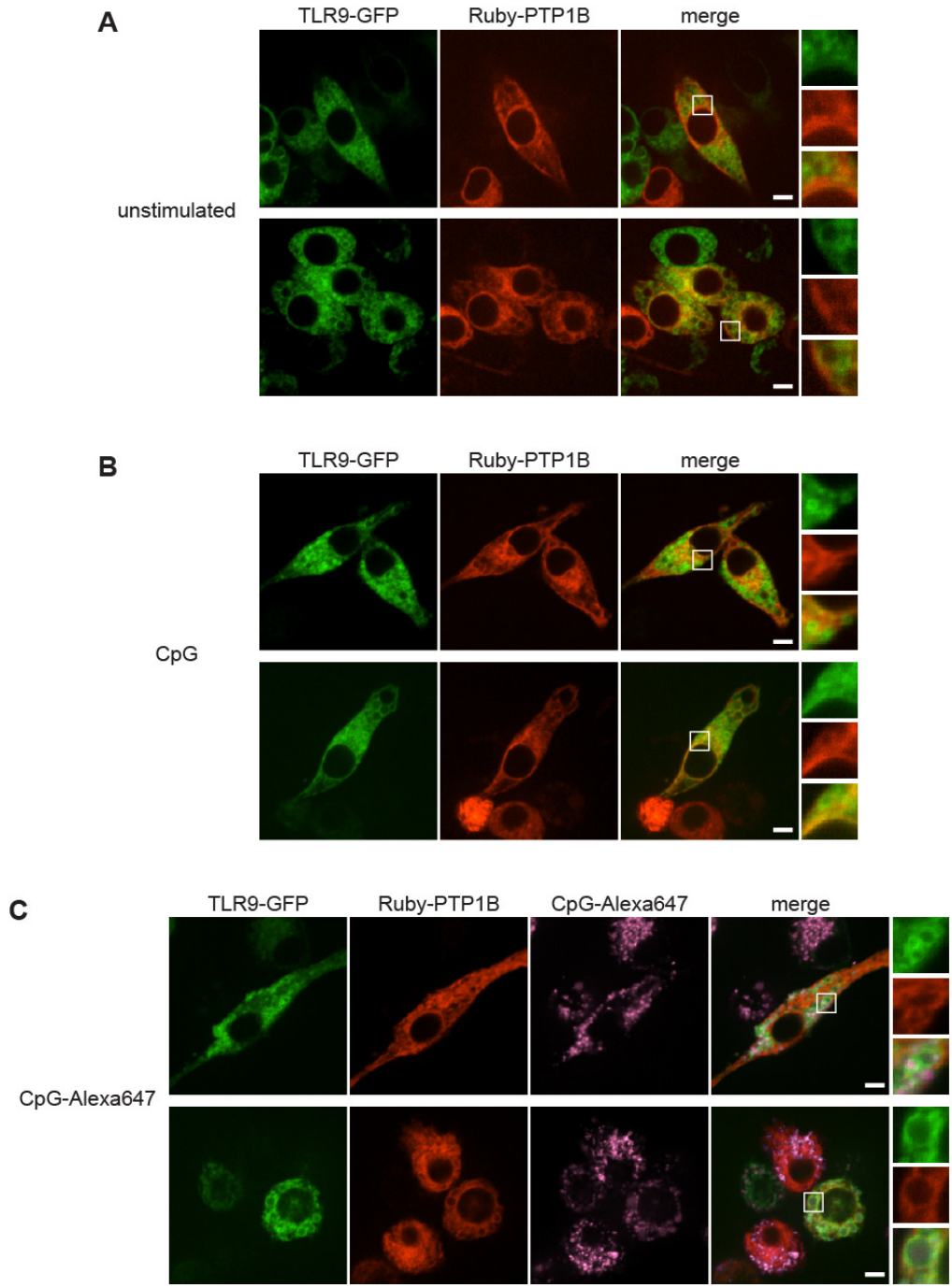

Figure 24: Ruby-PTP1B localizes to the ER where it partially co-localizes with TLR9-GFP in BMDM. Immortalized BMDM stably expressing TLR9-GFP were retrovirally transduced with Ruby-PTP1B and left unstimulated (A), stimulated with 1 µM CpG 1826 (B), or 1 µM CpG 1826-Alexa647 (C) for 2 h and analyzed by confocal microscopy. Scale bar, 5 µm.

3.4.3. The expression of PTP1B in BMDM is upregulated upon TLR stimulation

Analysis of gene expression profiles for UNC93B and PTP1B (BioGPS) revealed similar expression patterns for both proteins. UNC93B and PTP1B are highly expressed in lymphoid organs and innate immune cells including B cells, dendritic

cells, and macrophages (Figure 25A). The fact that PTP1B is highly expressed in immune cells indicates a link between PTP1B and innate immunity.

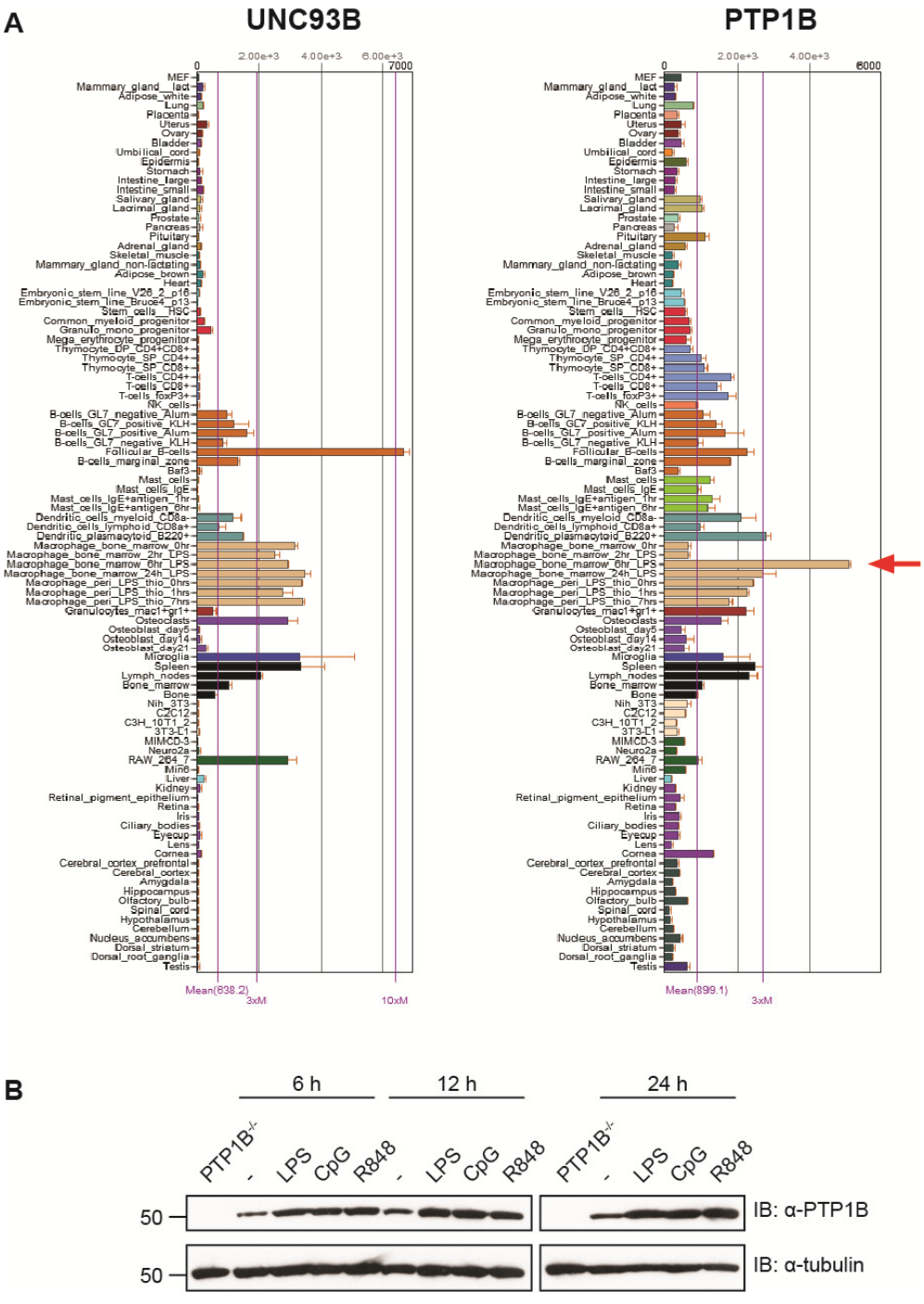

Figure 25: PTP1B protein levels are upregulated upon TLR stimulation in BMDM. Gene expression profiles for UNC93B and PTP1B were obtained from BioGPS (A). Primary BMDM were stimulated with LPS (100 ng/ml), CpG 1826 (1 µM), or R848 (1 µM) for 6, 12, and 24 h (B). Expression of PTP1B was analyzed by anti-PTP1B immunoblotting. BMDM derived from PTP1B$^{-/-}$ mice were used as a negative control. Loading of equal amounts of proteins was verified by anti-tubulin immunoblotting.

Furthermore, the gene expression profile for PTP1B suggested that gene expression of PTP1B is upregulated upon stimulation with the TLR ligand LPS (Figure 25A, red arrow). In order to analyze protein levels of PTP1B in unstimulated and TLR agonist stimulated BMDM, primary BMDM were stimulated with the TLR4 agonist LPS, the TLR9 agonist CpG 1826, and the TLR7 agonist R848 and lysed 6, 12, and 24 h post stimulation. Immunoblot analysis of PTP1B showed that protein levels of endogenous PTP1B were upregulated upon stimulation with all TLR agonists tested (Figure 25B). Primary BMDM derived from PTP1B$^{-/-}$ mice were used to verify the specificity of the PTP1B antibody. Upregulation of PTP1B expression upon TLR stimulation supports the idea that PTP1B may be involved in innate immune signaling.

3.4.4. Knockout of PTP1B does not impair proinflammatory cytokine responses upon TLR stimulation in BMDM

To investigate the role of PTP1B for signaling of intracellular TLRs in macrophages, primary BMDM derived from wild type, PTP1B$^{-/-}$, and TLR9$^{-/-}$ mice were stimulated with TLR agonists and amounts of the proinflammatory cytokines TNF and IL-6 in supernatants were measured by ELISA.

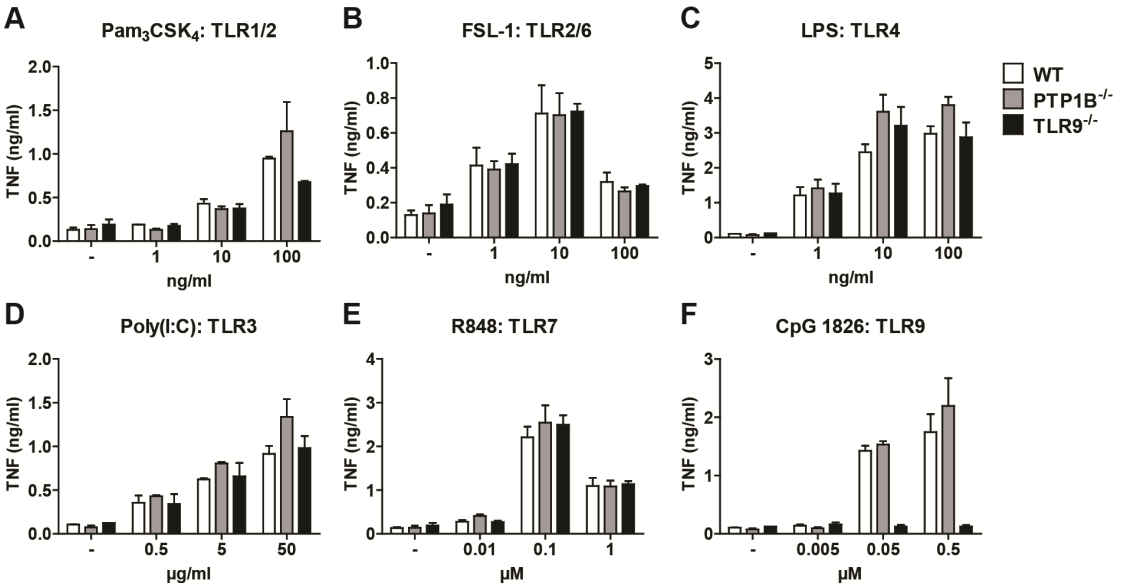

Figure 26: TNF responses in primary BMDM derived from PTP1B$^{-/-}$ mice are not impaired upon TLR stimulation. Primary BMDM derived from wild type (WT), PTP1B$^{-/-}$, and TLR9$^{-/-}$ mice were stimulated with indicated concentrations of TLR agonists for 18 h (A-F). TNF levels in supernatants were determined by ELISA. Shown is one representative experiment with duplicates as mean ± S.D. out of 3 independent experiments.

Stimulation of cell surface TLRs 1/2, 2/6, and 4 with Pam_3CSK_4, FSL-1, and LPS, respectively, did not reveal considerable differences in TNF or IL-6 responses between BMDM derived from wild type, PTP1B$^{-/-}$, and TLR9$^{-/-}$ mice (Figure 26, A-C and

Figure 27, A-C). Upon stimulation of intracellular TLRs 3, 7, and 9 with Poly(I:C), R848, and CpG 1826, the amounts of produced TNF and IL-6 did not differ between BMDM derived from wild type and PTP1B$^{-/-}$ mice (Figure 26, D-F and Figure 27, D-F). As expected, BMDM derived from TLR9$^{-/-}$ mice did not secrete TNF or IL-6 in response to stimulation of TLR9 with CpG 1826. Upon stimulation of TLR3 with Poly(I:C) or TLR7 with R848, BMDM derived from TLR9$^{-/-}$ mice secreted amounts of TNF and IL-6 comparable to wild type and PTP1B$^{-/-}$ mice.

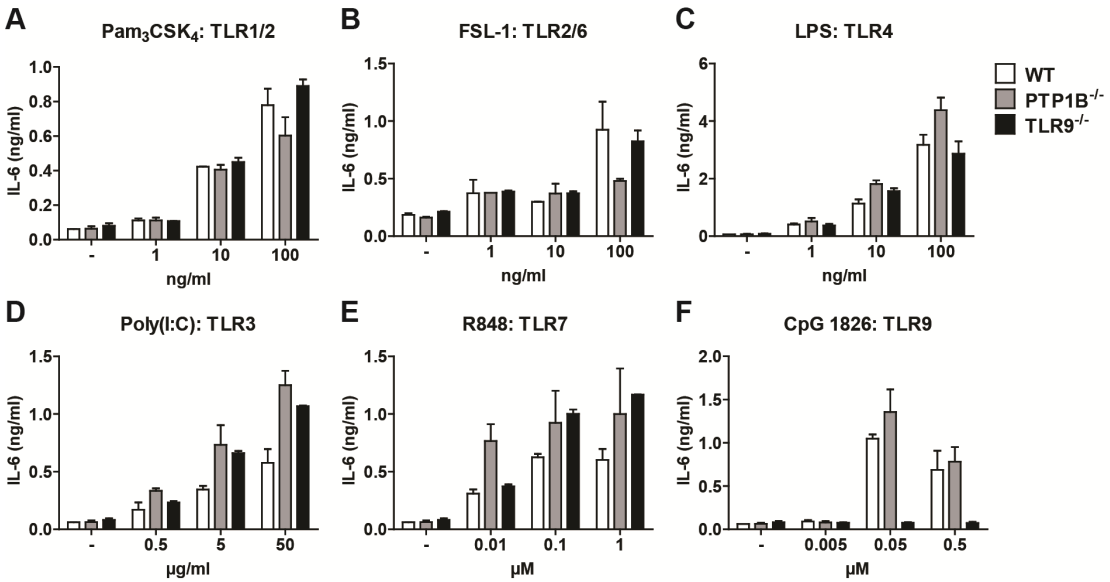

Figure 27: IL-6 responses in primary BMDM derived from PTP1B$^{-/-}$ mice are not impaired upon TLR stimulation. Primary BMDM derived from wild type (WT), PTP1B$^{-/-}$, and TLR9$^{-/-}$ mice were stimulated with indicated concentrations of TLR agonists for 18 h (A-F). IL-6 levels in supernatants were determined by ELISA. Shown is one representative experiment with duplicates as mean ± S.D. out of 3 independent experiments.

To further study TLR responses of BMDM derived from wild type, PTP1B$^{-/-}$, and TLR9$^{-/-}$ mice, production of the proinflammatory cytokine IL-12p40 upon stimulation of cell surface and intracellular TLRs was analyzed by ELISA. Stimulation of TLR1/2 with Pam_3CSK_4 and TLR2/6 with FSL-1 only led to the production of extremely low amounts of IL-12p40 in primary BMDM, which did not allow any conclusion from this data set (not shown). Upon stimulation of TLR4 and intracellular TLRs 3, 7, and 9 with LPS, Poly(I:C), R848, and CpG 1826, respectively, no prominent differences in IL-12p40 levels were observed between BMDM derived from wild type and PTP1B$^{-/-}$ mice (Figure 28, A-D). BMDM derived from TLR9$^{-/-}$ mice responded like BMDM derived from wild type and PTP1B$^{-/-}$ mice upon stimulation of TLR4, TLR3, and TLR7, but, as expected, did not secrete IL-12p40 in response to stimulation of TLR9 with CpG 1826.

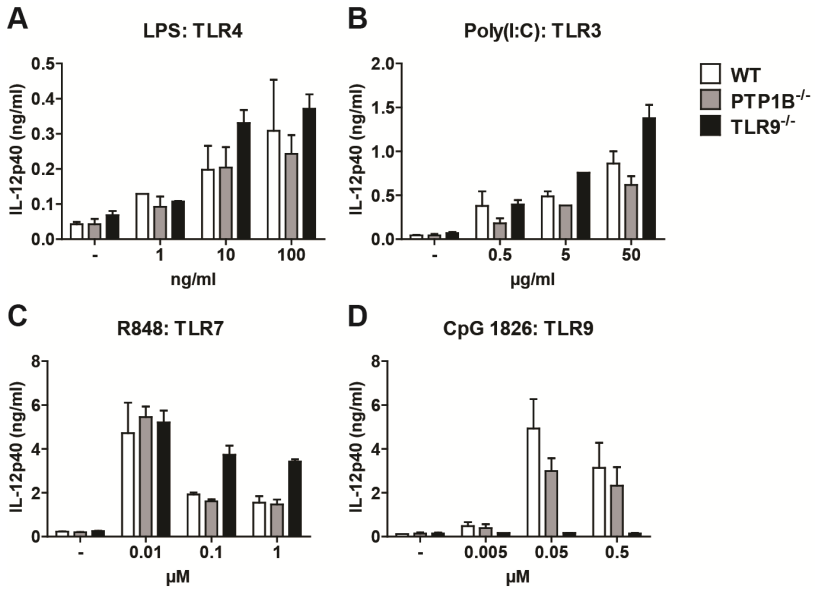

Figure 28: IL-12p40 responses in primary BMDM derived from PTP1B$^{-/-}$ mice are not impaired upon TLR stimulation. Primary BMDM derived from wild type (WT), PTP1B$^{-/-}$, and TLR9$^{-/-}$ mice were stimulated with indicated concentrations of TLR agonists for 18 h (A-D). IL-12p40 levels in supernatants were determined by ELISA. Shown is one representative experiment with duplicates as mean ± S.D. out of 3 independent experiments.

In summary, we found no difference in proinflammatory cytokine levels of TNF, IL-6, and IL-12p40 between BMDM derived from wild type and PTP1B$^{-/-}$ mice. Therefore, we conclude that PTP1B does not play a role for the proinflammatory cytokine response upon stimulation of cell surface or intracellular TLRs in macrophages.

3.4.5. PTP1B regulates the type I IFN response upon MCMV infection of BMDM

To investigate the role of PTP1B for the type I IFN response in macrophages in the context of viral infection, BMDM derived from wild type, PTP1B$^{-/-}$, 3d, and TLR9$^{-/-}$ mice were infected with MCMV and amounts of TNF, IFNα, and IFNβ in supernatants were determined by ELISA. Consistent with the data shown for UNC93B$^{-/-}$ mice (Figure 11, A and B), the TNF response upon infection with MCMV was only slightly reduced in BMDM derived from TLR9$^{-/-}$ or 3d mice (Figure 29A). The TNF response upon MCMV infection of BMDM derived from PTP1B$^{-/-}$ mice was not impaired compared to wild type BMDM. In contrast, the IFNα response upon MCMV infection was almost completely abolished in PTP1B$^{-/-}$ BMDM (Figure 29B). Since the IFNα response in BMDM derived from TLR9$^{-/-}$ and 3d mice was intact, we conclude that the phenotype observed in BMDM derived from PTP1B$^{-/-}$ mice is not linked to the TLR9 response in BMDM. A similar picture as for IFNα was observed for the IFNβ response, but less pronounced. Upon infection with MCMV, BMDM derived from TLR9$^{-/-}$ and 3d mice produced amounts of IFNβ comparable to wild type BMDM, whereas BMDM derived from

PTP1B$^{-/-}$ mice secreted a significantly lower amount of IFNβ than wild type BMDM (Figure 29C).

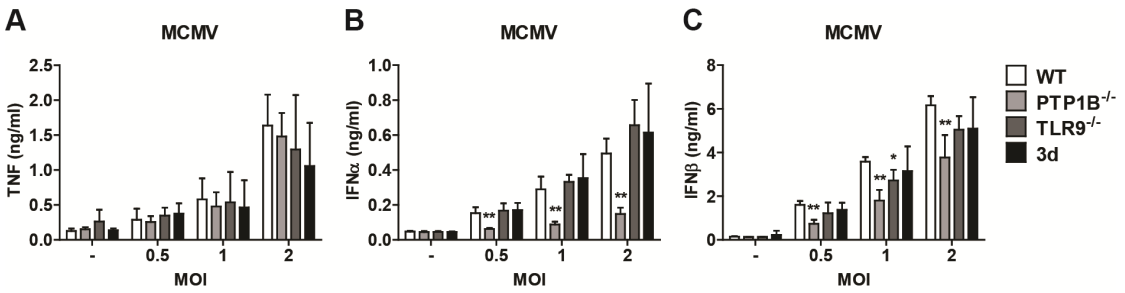

Figure 29: Type I IFN responses upon MCMV infection are impaired in primary BMDM derived from PTP1B$^{-/-}$ mice. Primary BMDM from wild type (WT), PTP1B$^{-/-}$, TLR9$^{-/-}$, and 3d mice were infected with MCMV-GFP at MOI 0.5, 1, or 2 for 18 h. Levels of TNF (A), IFNα (B), and IFNβ (C) in supernatants were determined by ELISA. Results are shown as mean ± S.D. of 3 independent experiments. Statistical significance compared to wild type controls was determined by two-tailed, unpaired t test; *, p<0.05; **, p<0.01.

These data show that PTP1B regulates the IFNα and IFNβ response upon MCMV infection in BMDM. However, since TLR9 does not play a role for the type I IFN response upon MCMV infection of BMDM, we conclude that this effect is independent of intracellular TLRs. This suggests a role for PTP1B in the regulation of cytosolic PRRs or a general role in the regulation of type I IFN responses. Consistent with the hypothesis that PTP1B is important for the regulation of cytosolic DNA sensors, BMDM derived from STING-deficient mice do not produce IFNα or IFNβ in response to MCMV infection (Baca Chan, unpublished results). Since STING is the key regulator for the cytosolic DNA response[216], this suggests that in BMDM MCMV is detected by cytosolic DNA sensors upstream of STING.

3.4.6. Knockout of PTP1B does not have an effect on the TLR9-dependent IFNα response in BMDM

The IFNα response upon MCMV infection of primary BMDM was significantly impaired in the absence of PTP1B, but not in the absence of TLR9 (Figure 29B). This indicates that PTP1B regulates the IFNα response upon MCMV infection of BMDM in a TLR9-independent manner. In addition to intracellular TLRs 3, 7, and 9, MCMV also activates other PRRs[90]. The production of type I IFN in response to MCMV infection is partially dependent on TLR2 in murine bone marrow cells[36] and in the absence of STING, BMDM do not produce type I IFN upon MCMV infection (Baca Chan, unpublished results). Upon TLR9 stimulation with CpG ODN, BMDM only produce very low amounts of type I IFN which cannot be detected by ELISA. To study whether PTP1B has a role for the TLR9-dependent type I IFN response in BMDM, qPCR analysis upon MCMV

infection or stimulation with two different kinds of CpG A was carried out with IFNα4-specific primers. Macrophages produce small amounts of type I IFN upon transfection with CpG A in a TLR9-dependent manner. In contrast, CpG B, which has a different backbone, does not induce a type I IFN response, but activates TLR9-dependent NF-κB signaling, leading to the production of proinflammatory cytokines[78].

To confirm the result that PTP1B, but not TLR9, is required for the IFNα response by primary BMDM upon MCMV infection described in 3.4.5, primary BMDM derived from wild type, PTP1B$^{-/-}$, and TLR9$^{-/-}$ mice were first infected with MCMV and the expression of IFNα4 2 h and 6 h post infection was analyzed by qPCR. Compared to wild type BMDM, the relative induction of IFNα4 in BMDM derived from PTP1B$^{-/-}$ mice was impaired 2 h as well as 6 h after MCMV infection (Figure 30, A and B). The relative IFNα4 mRNA expression in BMDM derived from TLR9$^{-/-}$ mice 2 h and 6 h post infection was comparable to BMDM derived from wild type mice. Thus, qPCR analysis of the IFNα4 response in primary BMDM confirmed the ELISA results shown in Figure 29B that PTP1B, but not TLR9, regulates the IFNα response upon MCMV infection.

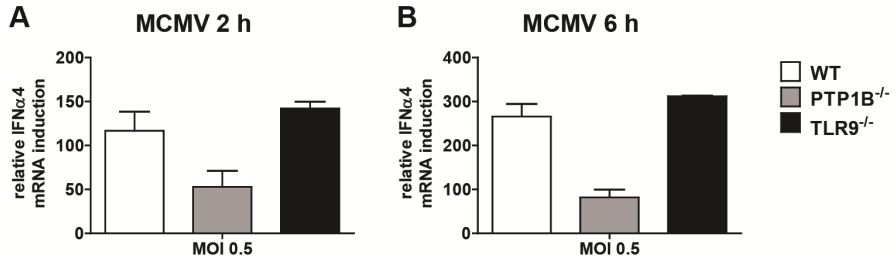

Figure 30: The IFNα4 response upon MCMV infection is impaired in the absence of PTP1B in primary BMDM. Primary BMDM were generated from wild type (WT), PTP1B$^{-/-}$, and TLR9$^{-/-}$ mice. Cells were spin infected with MCMV-GFP at MOI 0.5 for 2 h (A) or 6 h (B). qPCR was carried out with 200 ng RNA and IFNα4-specific primers. Data were normalized to Rpl8 and fold induction was calculated relative to uninfected cells. Results are shown as mean ± S.D. of one experiment in duplicates.

To find out whether PTP1B regulates the TLR9-dependent IFNα response in BMDM, primary BMDM derived from wild type, PTP1B$^{-/-}$, and 3d mice were transfected with the A type CpG ODN 2336 and 1585 and the expression of IFNα4 6 h post transfection was analyzed by qPCR. Since experiments were performed with different amounts of RNA, results of two independent experiments are shown in separate graphs (Figure 31). Transfection of BMDM with CpG 2336 or CpG 1585 induced a potent IFNα4 response in wild type BMDM (Figure 31, A-D). However, the relative induction of IFNα4 mRNA expression upon stimulation with CpG 2336 or 1585 did not differ between BMDM derived from wild type and from PTP1B$^{-/-}$ mice. Stimulation of BMDM derived from 3d mice, which lack functional TLR9, with CpG 2336 or CpG 1585 only

marginally induced IFNα4 mRNA expression as expected. In accordance with previous studies[83], transfection of BMDM with CpG 1826, a B type CpG ODN, did not elicit a potent IFNα4 response in BMDM (data not shown).

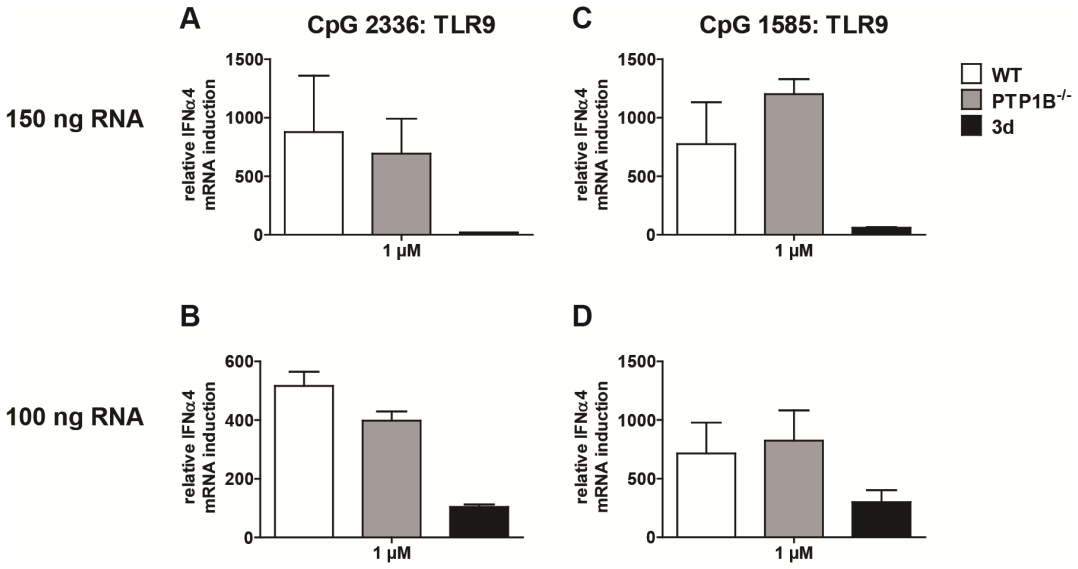

Figure 31: PTP1B does not regulate the TLR9-dependent IFNα4 response in primary BMDM. Primary BMDM were generated from wild type (WT), PTP1B$^{-/-}$, and 3d mice. Cells were transfected with CpG 2336 (A, B) or CpG 1585 (C, D) for 6 h. qPCR was carried out with 150 ng (A, C) or 100 ng (B, D) RNA and IFNα4-specific primers. Data were normalized to Rpl8 and fold induction was calculated relative to untransfected cells. Results are shown as mean ± S.D. of 2 independent experiments in duplicates, respectively.

Together with the results described in 3.4.5, these data suggest that PTP1B is important for the type I IFN response upon MCMV infection, but is not involved in the TLR9-dependent IFNα response in primary BMDM.

3.4.7. Knockout of PTP1B affects differentiation of bone marrow cells into FL-DC

Plasmacytoid dendritic cells (pDC) produce high amounts of type I IFN in response to stimulation of TLR7, TLR9, and upon viral infection. Up to 40% of pDC can be generated by culturing bone marrow cells for 8 days in the presence of Flt3 ligand[209]. The Flt3 ligand is a growth factor which stimulates differentiation of bone marrow cells into dendritic cells. The majority of cells in Flt3 cultures that do not display the phenotype of pDC are conventional dendritic cells (cDC). cDC can only produce very small amounts of type I IFN upon TLR stimulation or viral infection. Because of their ability to produce high amounts of type I IFN, FL-DC were the cells of choice to further study the impact of PTP1B on the type I IFN response upon TLR stimulation and MCMV infection.

FL-DC were generated from bone marrow of wild type and PTP1B$^{-/-}$ mice by culturing with Flt3 ligand for 8 days. The absence of PTP1B in FL-DC derived from PTP1B$^{-/-}$ mice was verified by immunoblotting with a PTP1B-specific antibody (Figure 32A). Surprisingly, the total number of FL-DC differed substantially between cells derived from wild type and PTP1B$^{-/-}$ mice. Cell numbers of wild type and PTP1B$^{-/-}$ cells were determined on day 0, directly after preparation of the bone marrow, and on day 8, when they were used for experiments. On day 0, around 6 x 10^7 cells per mouse were obtained from the bone marrow preparation of wild type and PTP1B$^{-/-}$ mice. On day 8 however, more than twice as many cells were counted in PTP1B$^{-/-}$ cultures compared to wild type cultures (Figure 32B).

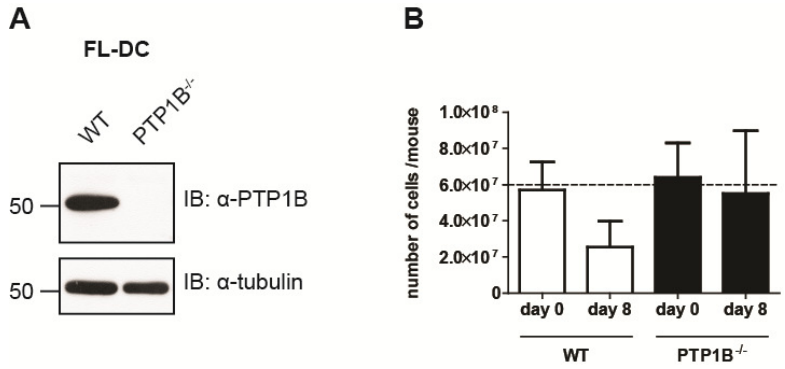

Figure 32: Cell numbers of cells derived from PTP1B$^{-/-}$ mice are higher than cell numbers of cells derived from wild type mice after 8 days of culture with Flt3 ligand. Immunoblot analysis of PTP1B protein expression in FL-DC generated from wild type (WT) and PTP1B$^{-/-}$ mice (A). PTP1B was detected using an antibody against endogenous PTP1B. Loading of equal amounts of protein was verified by anti-tubulin immunoblot. Bone marrow was prepared from wild type (WT) and PTP1B$^{-/-}$ mice (B). Cell numbers were determined directly after bone marrow preparation (day 0) and after 8 days of culture with Flt3 ligand. Data are shown as mean ± S.D. of 24 mice, respectively.

The Flt3 receptor is a receptor tyrosine kinase (RTK) and a number of RTKs are regulated by PTP1B[158,217]. Therefore, the difference in FL-DC cell numbers obtained from wild type and PTP1B$^{-/-}$ mice most likely results from the fact that the Flt3 receptor is not functioning normally in the absence of PTP1B.

When identical numbers of FL-DC from wild type and PTP1B$^{-/-}$ mice were seeded and stimulated with TLR agonists or ligands for intracellular DNA or RNA sensors, cells derived from PTP1B$^{-/-}$ mice consistently showed higher IFNα responses than wild type FL-DC (Figure 35). For this reason, FL-DC derived from wild type and PTP1B$^{-/-}$ mice were analyzed by flow cytometry using antibodies against CD11c, CD11b, B220, and Siglec-H and percentages of pDC and cDC populations were determined. pDC and cDC are positive for CD11c, which is a marker for dendritic cells. cDC are positive for CD11b and negative for B220. Vice versa, pDC are negative for CD11b and positive for

B220. Furthermore, cells were stained with an antibody against Siglec-H, a specific marker for murine pDC. Flow cytometry analysis of wild type and PTP1B$^{-/-}$ FL-DC revealed higher amounts of pDC in PTP1B$^{-/-}$ samples (Figure 33, A and B). FL-DC cultures from wild type mice contained about 30% of pDC (CD11b^{-} B220^{+}CD11c^{+}Siglec-H^{+}), whereas FL-DC cultures from PTP1B$^{-/-}$ mice contained about 40% of pDC and less cDC (CD11b^{+}B220^{-}CD11c^{+}Siglec-H^{-}).

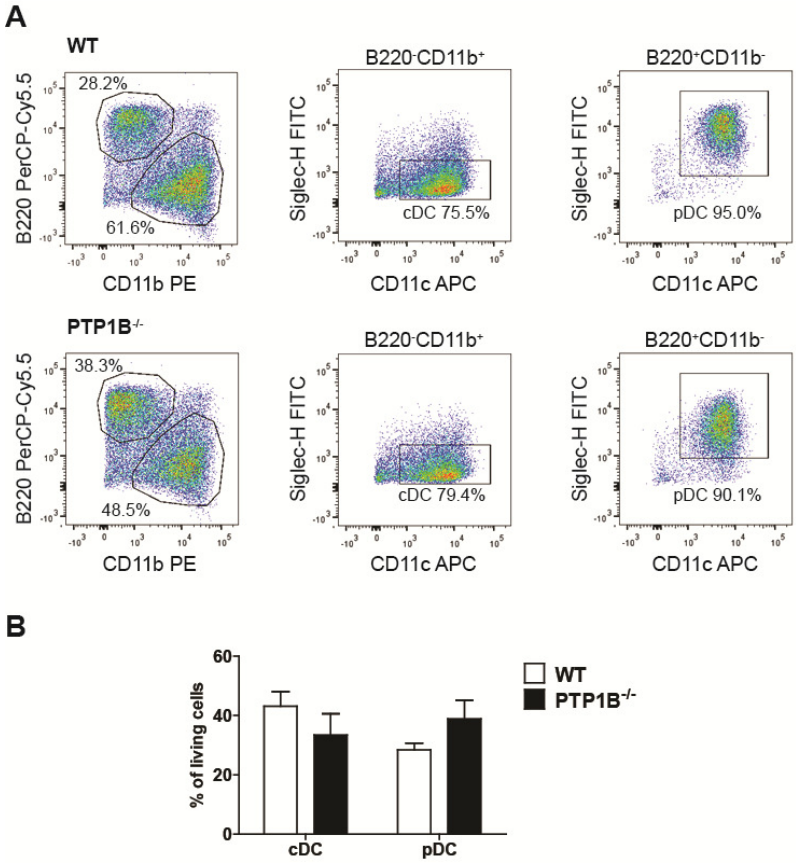

Figure 33: FL-DC derived from PTP1B$^{-/-}$ mice contain higher numbers of pDC than FL-DC from wild type mice. *In vitro* generated FL-DC from wild type (WT) and PTP1B$^{-/-}$ mice were stained with antibodies against CD11b, B220, CD11c, and Siglec-H and analyzed by flow cytometry. Representative dot plots are shown for FL-DC from WT and PTP1B$^{-/-}$ mice (A). Portions of cDC (CD11b^{+}B220^{-}CD11c^{+}Siglec-H^{-}) and pDC (CD11b^{-}B220^{+}CD11c^{+}Siglec-H^{+}) were calculated relative to the amount of living cells (B). Results are shown as mean ± S.D. of 2 independent experiments.

It seems very likely that the increased IFNα responses seen in FL-DC from PTP1B$^{-/-}$ mice were caused by the elevated numbers of pDC. Therefore, pDC were sorted from wild type and PTP1B$^{-/-}$ FL-DC by magnetic-activated cell sorting (MACS) and fluorescence-activated cell sorting (FACS). For MACS, FL-DC were incubated with a mix of antibodies against non-pDC and cells were sorted based on negative selection. For FACS, FL-DC were sorted using Siglec-H as a specific marker for pDC. Sorted pDC were stimulated with TLR agonists or ligands for intracellular DNA or RNA

sensors. However, even after sorting, cells from PTP1B$^{-/-}$ mice secreted higher amounts of IFNα and also TNF and IL-6 than wild type cells in response to all stimuli (data not shown).

In conclusion, the data obtained for the IFNα response by FL-DC suggest that compared to wild type FL-DC, FL-DC from PTP1B$^{-/-}$ mice produce higher amounts of IFNα in response to TLR stimulation or MCMV infection. This stands in conflict with the observation that the type I IFN response upon MCMV infection in BMDM is impaired in the absence of PTP1B (Figure 29 and Figure 30). However, since the Flt3 receptor is regulated by PTP1B, we conclude that FL-DC generated from PTP1B$^{-/-}$ mice do not behave normally and therefore cannot be used to study the role of PTP1B for type I IFN responses. For this reason we were looking for other options or cell types to evaluate the role of PTP1B for TLR-dependent type I IFN responses.

3.4.8. Inhibition of PTP1B with a specific inhibitor reduces the TLR-dependent IFNα response in a PTP1B-independent manner

Due to the fact that PTP1B regulates trafficking of the Flt3 receptor, FL-DC were not an ideal system to study the role of PTP1B for the type I IFN response. Therefore, FL-DC derived from wild type mice were treated with PTP1B inhibitors. Many different PTP1B inhibitors are commercially available. Two different inhibitors were used in this study to inhibit PTP1B in wild type FL-DC, MSI-1436 (trodusquemine) and PTP Inhibitor XXII. MSI-1436 and PTP Inhibitor XXII are selective, allosteric, and noncompetitive inhibitors of PTP1B with an IC_{50} of approximately 1 μM and 4 μM, respectively. MSI-1436 has been successfully used for the treatment of obesity and type 2 diabetes in mice[218]. Recently, a phase I clinical trial for MSI-1436 has been completed.

Upon pretreatment of wild type FL-DC with 10 μM MSI-1436 for 4 h and subsequent TLR stimulation for 6 h in presence of the inhibitor, there was no effect on the IFNα response compared to FL-DC which had been treated with DMSO. However, flow cytometry analysis upon staining of MSI-1436-treated FL-DC with the DNA intercalator propidium iodide, which stains the DNA of dead cells, revealed that a dose of 20 μM MSI-1436 resulted in cell death (data not shown).

We therefore first tested whether PTP inhibitor XXII induced apoptosis or cell death. Cells were treated with 50 or 150 μM of PTP Inhibitor XXII, z-FA-fmk, or DMSO as control, stained with 7-Aminoactinomycin (7-AAD) and Annexin V, and analyzed by flow cytometry. 7-AAD is a DNA intercalator and Annexin V binds to phosphatidylserine exposed on the cell surface of apoptotic cells. Staining of DMSO-treated FL-DC with 7-AAD and Annexin V revealed a large population of about 62-68% of dead cells

positive for 7-AAD and Annexin V (Figure 34). Around 30% of living cells, which were negative for 7-AAD and Annexin V, were found in DMSO-treated FL-DC cultures. Upon treatment of wild type FL-DC with 50 or 150 µM of PTP Inhibitor XXII, the amount of dead cells was only slightly increased to around 70%. The amount of dead cells in FL-DC cultures, which had been treated with z-FA-fmk, was around 66%. Apoptotic cells should appear negative for 7-AAD and positive for Annexin V. However, populations of apoptotic cells were not identified in this experiment. Thus, PTP Inhibitor XXII did not induce apoptosis and did also not induce extensive cell death and was therefore used for functional experiments in wild type FL-DC.

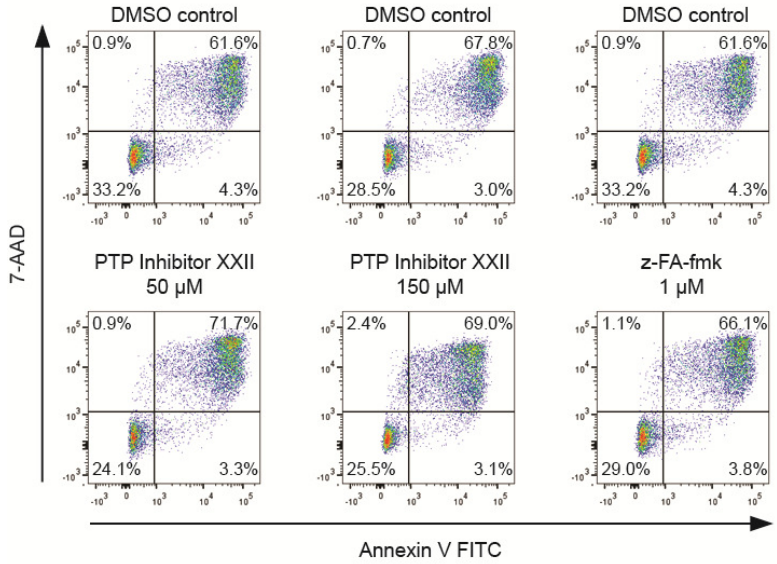

Figure 34: Treatment of FL-DC with PTP Inhibitor XXII does not induce apoptosis. FL-DC from wild type mice were treated with indicated concentrations of PTP Inhibitor XXII, z-FA-fmk, or DMSO as control for 10 h. Cells were stained with 7-AAD and Annexin V and analyzed by flow cytometry. Percentages of living cells are depicted in lower left quadrants and percentages of dead cells are depicted in upper right quadrants.

To study the role of PTP1B for the TLR-dependent IFNα response in pDC, FL-DC were pretreated with PTP Inhibitor XXII for 4 h and subsequently stimulated with the TLR9 ligand CpG 2336 or transfected with the TLR7 ligand Poly(U) to initiate the production of IFNα. Amounts of IFNα in supernatants were measured by ELISA. Treatment of FL-DC with 10 µM PTP Inhibitor XXII did not affect IFNα responses upon TLR stimulation (data not shown). Upon treatment of FL-DC with 50 µM or 150 µM PTP Inhibitor XXII, the IFNα responses upon stimulation of TLR9 or TLR7 were reduced (Figure 35, A-D). Treatment of FL-DC with z-FA-fmk, an inhibitor of TLR9 and TLR7 endosomal processing, confirmed that the IFNα responses upon stimulation with CpG 2336 and Poly(U) were dependent on TLR9 and TLR7, respectively (Figure 35, E and F).

To ensure that the observed inhibitory effect was PTP1B-specific, PTP1B$^{-/-}$ FL-DC were included in the experiment. As described in 3.4.7, FL-DC derived from PTP1B$^{-/-}$ mice generally showed higher IFNα responses compared to wild type cells (Figure 35, A-F). However, similar to wild type FL-DC, they also showed reduced IFNα responses upon TLR stimulation in the presence of PTP inhibitor XXII (Figure 35, A-D).

This leads to the conclusion that the inhibitory effect of PTP Inhibitor XXII on the IFNα response in wild type FL-DC was unspecific. In summary, the two tested PTP1B inhibitors were not suitable to study the type I IFN response upon TLR stimulation in primary cells.

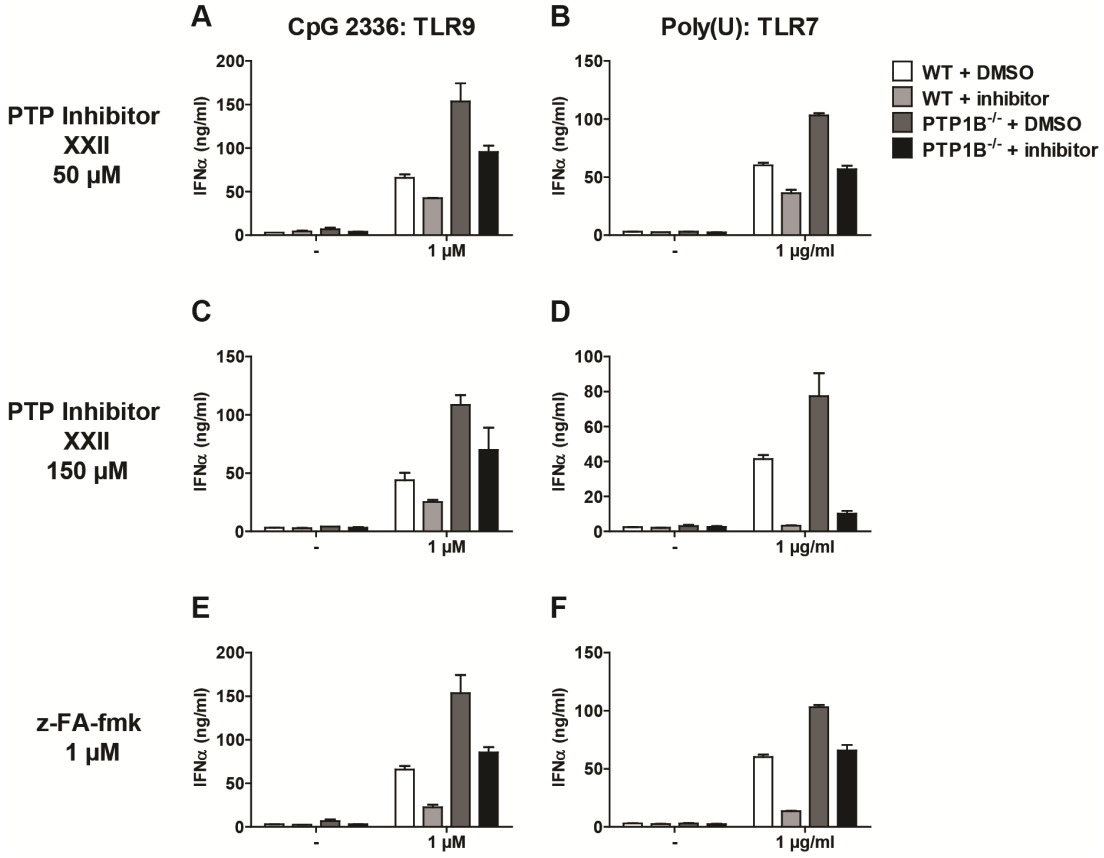

Figure 35: Treatment of wild type FL-DC with a PTP1B inhibitor leads to unspecific downregulation of the IFNα response upon TLR stimulation in FL-DC. FL-DC derived from wildtype (WT) or PTP1B$^{-/-}$ mice were incubated with 50 µM (A, B) or 150 µM (C, D) of PTP Inhibitor XXII or 1 µM z-FA-fmk (E, F) for 4 h. Subsequently, cells were stimulated with 1 µM CpG 2336 (A, C, E) or transfected with 1 µg/ml of Poly(U) (B, D, F) for additional 6 h in presence of the inhibitor. Levels of IFNα in supernatants were determined by ELISA. Results are shown as mean ± S.D. of one representative experiment in duplicates.

3.4.9. IFNα responses of total BM cells from PTP1B$^{-/-}$ mice are impaired upon TLR stimulation or infection with MCMV

FL-DC from PTP1B$^{-/-}$ mice could not be used to study type I IFN responses, and treatment of wild type FL-DC with PTP1B inhibitors either induced cell death or was not specific. We therefore chose different sources of primary pDC. pDC are the main source of type I IFN. In mice, pDC are present in lymphoid organs including the spleen and bone marrow. Hence, pDC were isolated from spleens of wild type and PTP1B$^{-/-}$ mice with a negative selection approach using MACS. Unfortunately, cell numbers of splenic pDC after isolation were extremely low (less than 0.5% of total splenocytes) which made this approach inapplicable to study type I IFN responses in PTP1B$^{-/-}$ cells.

Next, total bone marrow (BM) cells from wild type, PTP1B$^{-/-}$, TLR9$^{-/-}$, and 3d mice were stimulated with agonists for TLR9 or TLR7 or were infected with MCMV, and amounts of secreted IFNα in supernatants were measured by ELISA. Upon stimulation of TLR9 with CpG 2336 or TLR7 with Poly(U), IFNα responses in cells from PTP1B$^{-/-}$ mice were decreased compared to cells from wild type mice (Figure 36, A and B). As expected, total BM cells from TLR9$^{-/-}$ mice did not respond to stimulation of TLR9, but produced amounts of IFNα similar to those produced by total BM cells from wild type mice upon stimulation of TLR7, and total BM cells from 3d mice did not respond to stimulation of TLR9 or TLR7 (Figure 36, A and B). However, due to the high variability of the measured IFNα responses, especially by the control cells from wild type mice, none of these effects was statistically significant.

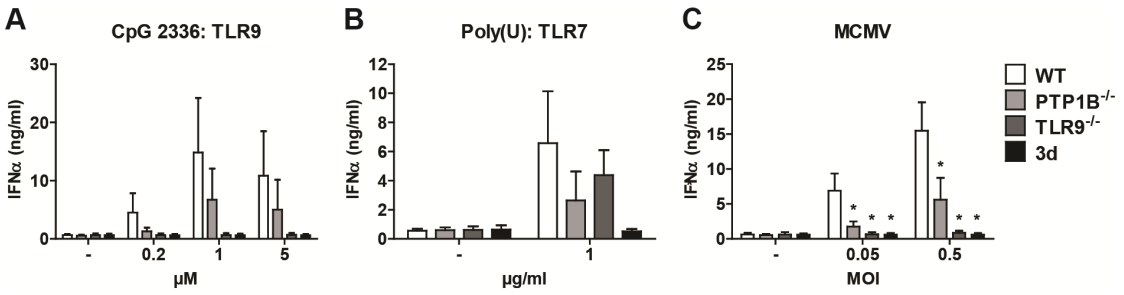

Figure 36: The IFNα response by total BM cells from PTP1B$^{-/-}$ mice is impaired upon TLR stimulation or MCMV infection. Total BM cells were prepared from wild type (WT) (n=3), PTP1B$^{-/-}$ (n=3), TLR9$^{-/-}$ (n=2), and 3d (n=2) mice. Cells were stimulated with CpG 2336 (A), transfected with Poly(U) (B), or infected with MCMV-GFP (C) for 22 h. Levels of IFNα in supernatants were determined by ELISA. Results are shown as mean ± S.D. of n (as specified) independent experiments. Statistical significance compared to wild type controls was determined by two-tailed, unpaired t test; *, $p<0.05$.

Upon MCMV infection, total BM cells from PTP1B$^{-/-}$ mice produced significantly lower amounts of IFNα than total BM cells from wild type mice (Figure 36C). Total BM cells from TLR9$^{-/-}$ and 3d mice did not respond to infections with MCMV indicating that the

recognition of MCMV by pDC in total BM cells is completely dependent on TLR9 (Figure 36C).

We next analyzed the proinflammatory cytokine responses in total BM cells from wild type, PTP1B$^{-/-}$, TLR9$^{-/-}$, and 3d mice. TNF and IL-6 levels in supernatants of total BM cells upon stimulation with the TLR9 ligand CpG 2336 or the TLR7 ligand Poly(U) or upon infection with MCMV were determined by ELISA. Compared to total BM cells from wild type mice, TNF as well as IL-6 responses were not decreased in total BM cells from PTP1B$^{-/-}$ mice upon stimulation of TLR7 or TLR9 or upon MCMV infection (Figure 37, A-F). Total BM cells from TLR9$^{-/-}$ and 3d mice did not produce TNF or IL-6 in response to stimulation of TLR7 or 9 and secreted only very low amounts of TNF and IL-6 upon infection with MCMV.

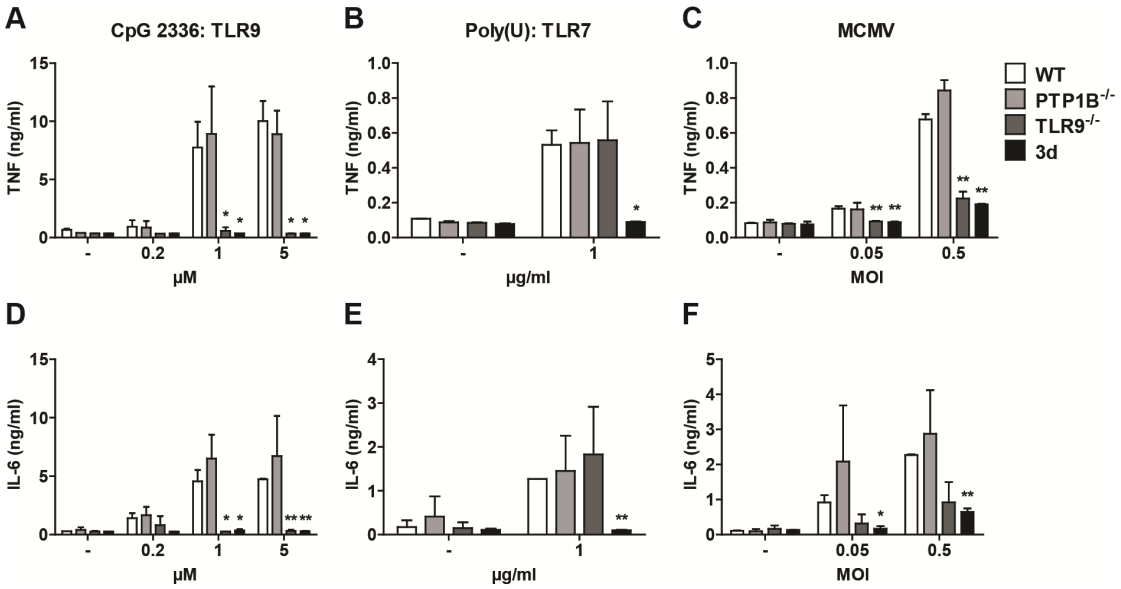

Figure 37: TNF and IL-6 responses upon TLR stimulation or MCMV infection are not impaired in total BM cells from PTP1B$^{-/-}$ mice. Total BM cells were prepared from wild type (WT), PTP1B$^{-/-}$, TLR9$^{-/-}$, and 3d mice. Cells were stimulated with CpG 2336 (A, D), transfected with Poly(U) (B, E) or infected with MCMV (C, F) for 22 h. Levels of TNF (A-C) and IL-6 (D-F) in supernatants were determined by ELISA. Results are shown as mean ± S.D. of 2 independent experiments. Statistical significance compared to wild type controls was determined by two-tailed, unpaired t test; *, p<0.05; **, p<0.01.

In contrast to BMDM (Figure 29A), proinflammatory cytokine responses upon MCMV infection were almost completely dependent on TLR9 in total BM cells. This suggests that intracellular PRRs do not play an important role for viral infection with MCMV in total BM cells.

Thus, PTP1B regulates the IFNα response, but not the proinflammatory cytokine response, upon stimulation of TLR7 and 9 and upon the TLR9-dependent recognition of MCMV in total BM cells.

3.4.10. MEF express low amounts of PTP1B, but do not express TLR9

Although mouse embryonic fibroblasts (MEF) do not produce high amounts of IFN, they can be used to study type I IFN responses. Especially the IFNβ response upon stimulation of cytosolic DNA or RNA sensors is often analyzed in MEF. The use of MEF has some advantages in comparison to the use of other kinds of primary cells. First, large numbers of cells can be obtained from one single embryo and MEF can be passaged several times before they stop proliferating. Second, MEF can easily be immortalized and, in contrast to primary BMDM or FL-DC, they can efficiently be transduced with retroviruses for the generation of stable cell lines. These characteristics should allow analysis of the role of the enzymatic function of PTP1B for its effect on type I IFN responses by transduction of immortalized PTP1B$^{-/-}$ MEF with a catalytically inactive mutant (D181A) of PTP1B. However, we first had to verify whether MEF express PTP1B and TLR9.

MEF were prepared from embryos of wild type and PTP1B$^{-/-}$ mice 13.5 days post coitum (d.p.c.). To verify mRNA expression of PTP1B in MEF, qPCR analysis was carried out with PTP1B-specific primers on RNA from wild type and PTP1B$^{-/-}$ MEF and BMDM. qPCR analysis of PTP1B mRNA expression confirmed expression of endogenous PTP1B in wild type MEF (Figure 38A). The PTP1B mRNA expression in primary BMDM was 2.6-fold higher than in MEF. The specificity of the chosen primer/probe combination was validated with MEF and BMDM from PTP1B$^{-/-}$ mice.

To analyze protein expression of PTP1B in MEF, immunoblotting using a PTP1B-specific antibody was performed with lysates of wild type MEF, PTP1B$^{-/-}$ MEF, and PTP1B$^{-/-}$ MEF stably expressing empty vector or wild type or mutant (D181A) HA-PTP1B. Protein expression of endogenous PTP1B in MEF from wild type mice was not detected by anti-PTP1B immunoblotting (Figure 38B). In contrast, using the PTP1B-specific antibody, endogenous PTP1B was detected in BMDM by immunoblotting (Figure 25B). In MEF, PTP1B was only detected by immunoblotting in MEF stably expressing wild type HA-PTP1B or the catalytically inactive HA-PTP1B D181A (Figure 38B). Together, these data indicate that PTP1B is only weakly expressed in MEF and cannot be detected by immunoblotting with the available PTP1B antibody.

To find out whether the TLR9-dependent type I IFN response to CpG DNA can be studied in MEF, total RNA from wild type MEF and MEF from PTP1B$^{-/-}$ mice was analyzed for expression of TLR9 by qPCR. No signal for TLR9 mRNA expression was detected in MEF from wild type or PTP1B$^{-/-}$ mice by qPCR using TLR9-specific primers (data not shown). In contrast, mRNA expression of TLR9 in BMDM was detected as

expected. For this reason MEF were not used to investigate the role of PTP1B for the TLR-dependent type I IFN response.

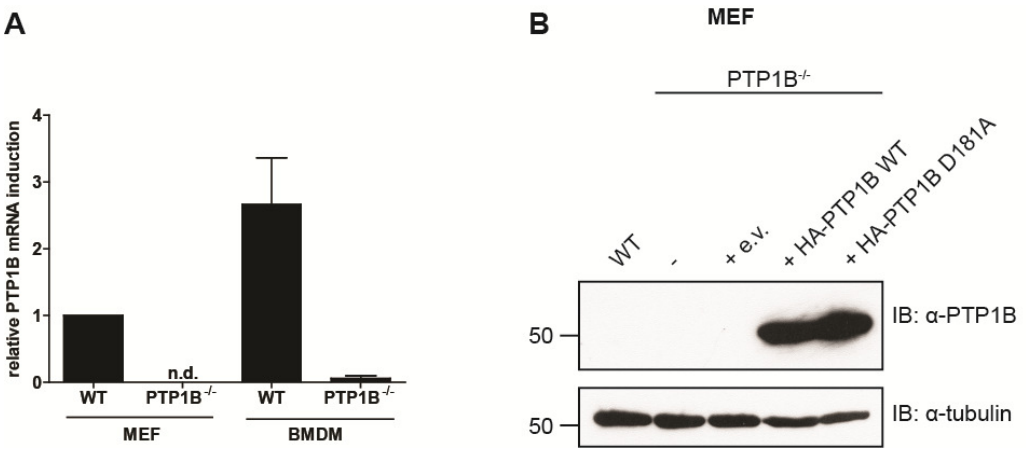

Figure 38: Expression of endogenous PTP1B in MEF can be detected by qPCR, but not by immunoblotting. Primary MEF (n=1) and BMDM (n=2) were generated from wild type (WT) and PTP1B$^{-/-}$ mice. qPCR was carried out with 100 ng RNA and PTP1B-specific primers. Data were normalized to Rpl8 and fold induction was calculated relative to wild type MEF (A). Shown are mean ± S.D. of n (as specified) independent experiments. n.d., not detected. PTP1B$^{-/-}$ MEF were left untransduced (-) or transduced with empty vector (e.v.), wild type HA-PTP1B, or catalytically inactive HA-PTP1B D181A (B). Cells were lysed and an anti-PTP1B antibody was used for immunoblotting. Loading of equal amounts of protein was verified by anti-tubulin immunoblotting.

3.4.11. PTP1B plays an important role for the TLR9-dependent IFNα and IL-12p40 response *in vivo*

In vivo, injection of CpG DNA in mice leads to the production of IFNα. This response has been described to be exclusively mediated by pDC[219,220]. To study the role of PTP1B for the TLR9-dependent type I IFN and proinflammatory cytokine response *in vivo*, wild type and PTP1B$^{-/-}$ mice were challenged with CpG DNA and serum levels of IFNα, IL-12p40, TNF, and IL-6 2 or 6 h post injection were measured by ELISA. Upon intravenous injection (i.v.) of CpG A 2216, PTP1B$^{-/-}$ mice showed significantly reduced serum levels of IFNα and IL-12p40 compared to wild type mice (Figure 39, A and B). As expected, CpG A challenge of TLR9$^{-/-}$ mice did not lead to the production of relevant amounts of IFNα or IL-12p40. The control oligonucleotide GpC 2216 contains two GpC dinucleotides instead of CpG motifs and was used as a negative control. As expected, GpC 2216 did not elicit an IFNα or IL-12p40 response.

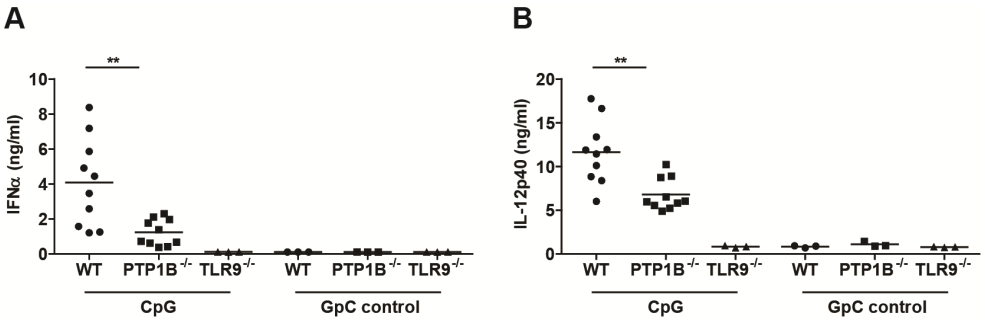

Figure 39: IFNα and IL-12p40 responses are impaired in PTP1B$^{-/-}$ mice upon *in vivo* administration of CpG 2216. Wild type (WT), PTP1B$^{-/-}$, and TLR9$^{-/-}$ mice were intravenously injected with 10 µg CpG 2216 or GpC 2216 control complexed with 30 µl DOTAP in PBS. Serum levels of IFNα (A) and IL-12p40 (B) 6 h post injection were determined by ELISA. Results are from 3 independent experiments with each point representing an individual mouse. **, p<0.01 by two-tailed, unpaired t test.

Additionally, mice were challenged intraperitoneally (i.p.) with CpG B to analyze TNF and IL-6 responses upon stimulation of TLR9. Serum levels of TNF were comparable between wild type and PTP1B$^{-/-}$ mice (Figure 40A). However, serum levels of IL-6 were significantly elevated in PTP1B$^{-/-}$ mice compared to wild type mice (Figure 40B). The TNF and IL-6 responses to CpG B were strictly TLR9-dependent, as TLR9$^{-/-}$ mice did not produce TNF or IL-6 upon challenge with CpG B.

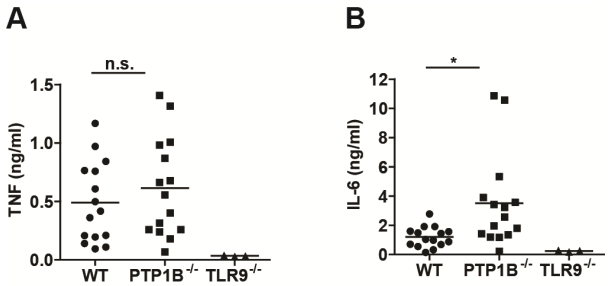

Figure 40: TNF and IL-6 responses are not reduced in PTP1B$^{-/-}$ mice upon *in vivo* administration of CpG 1826. Wild type (WT), PTP1B$^{-/-}$, and TLR9$^{-/-}$ mice were intraperitoneally injected with 60 µg CpG 1826 in PBS. Serum levels of TNF (A) and IL-6 (B) 2 h post injection were determined by ELISA. Results are from 3 independent experiments with each point representing an individual mouse. *, p<0.05 by two-tailed, unpaired t test; n.s., not significant.

To make sure that the differences in immune responses upon CpG challenge *in vivo* did not arise from differences in the amount of immune cells between wild type and PTP1B$^{-/-}$ mice, immune cell populations in lymphoid organs were analyzed by flow cytometry. Single cell suspensions were prepared from spleen, lymph nodes, and bone marrow of wild type and PTP1B$^{-/-}$ mice and cells were stained with antibodies to identify B cell, T cell, cDC, and pDC populations (Figure 41). In the spleen pDC only made up around 0.25% of total cells (Figure 41B), which explains the low yield of pDC that was obtained upon splenic pDC isolation by MACS (3.4.9). It has been reported that

PTP1B$^{-/-}$ mice show significantly increased numbers of B cells in lymph nodes and bone marrow compared to wild type mice[221]. In the spleens of PTP1B$^{-/-}$ mice, the authors of this study detected a slight but not significant decrease of B cells compared to wild type mice[221]. In accordance with these findings, we detected a significant increase in the proportion of B cells (CD3^{-}CD19^{+}) in lymph nodes from PTP1B$^{-/-}$ mice compared to wild type mice (Figure 41A). In contrast, the proportion of B cells in the spleens from PTP1B$^{-/-}$ mice was significantly decreased compared to wild type mice. The proportions of CD4^{+} T cells (CD3^{+}CD19^{-}CD4^{+}CD8α^{-}) in spleen and lymph nodes were equal between wild type and PTP1B$^{-/-}$ mice, but there was a slight but significant increase in the proportion of CD8^{+} T cells (CD3^{+}CD19^{-}CD4^{-}CD8α^{+}) in the spleens of PTP1B$^{-/-}$ mice compared to wild type mice (Figure 41A). The proportions of CD8^{+} T cells in lymph nodes did not show significant differences between wild type and PTP1B$^{-/-}$ mice. The proportions of cDC (CD11c^{+}CD11b^{+}B220^{-}) and pDC (CD11c^{+}Siglec-H^{+}mPDCA^{+}) in bone marrow, spleen, and lymph nodes did not significantly differ between wild type and PTP1B$^{-/-}$ mice (Figure 41B).

Together, the *in vivo* experiments performed with PTP1B$^{-/-}$ mice suggest an important role of PTP1B for the TLR9-dependent IFNα and IL-12p40 responses *in vivo*. Flow cytometry analysis of cell populations in lymphoid organs showed that there are small differences in B cell and T cell populations in spleen and lymph nodes between wild type and PTP1B$^{-/-}$ mice. However, since pDC are the main source for IFNα it is very unlikely that the observed effects can be attributed to abnormalities of immune cell populations in PTP1B$^{-/-}$ mice.

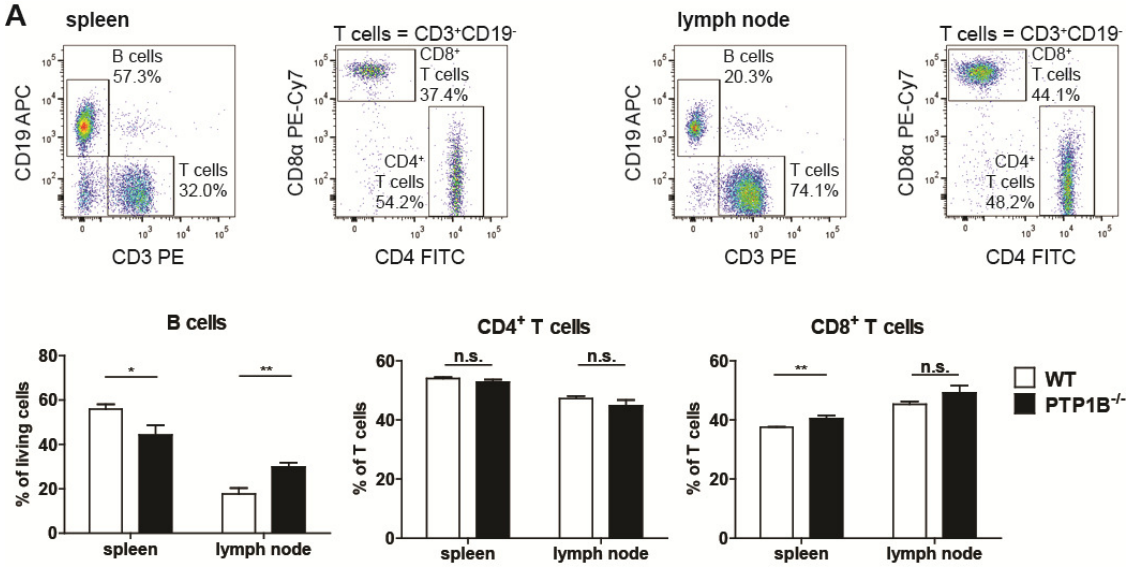

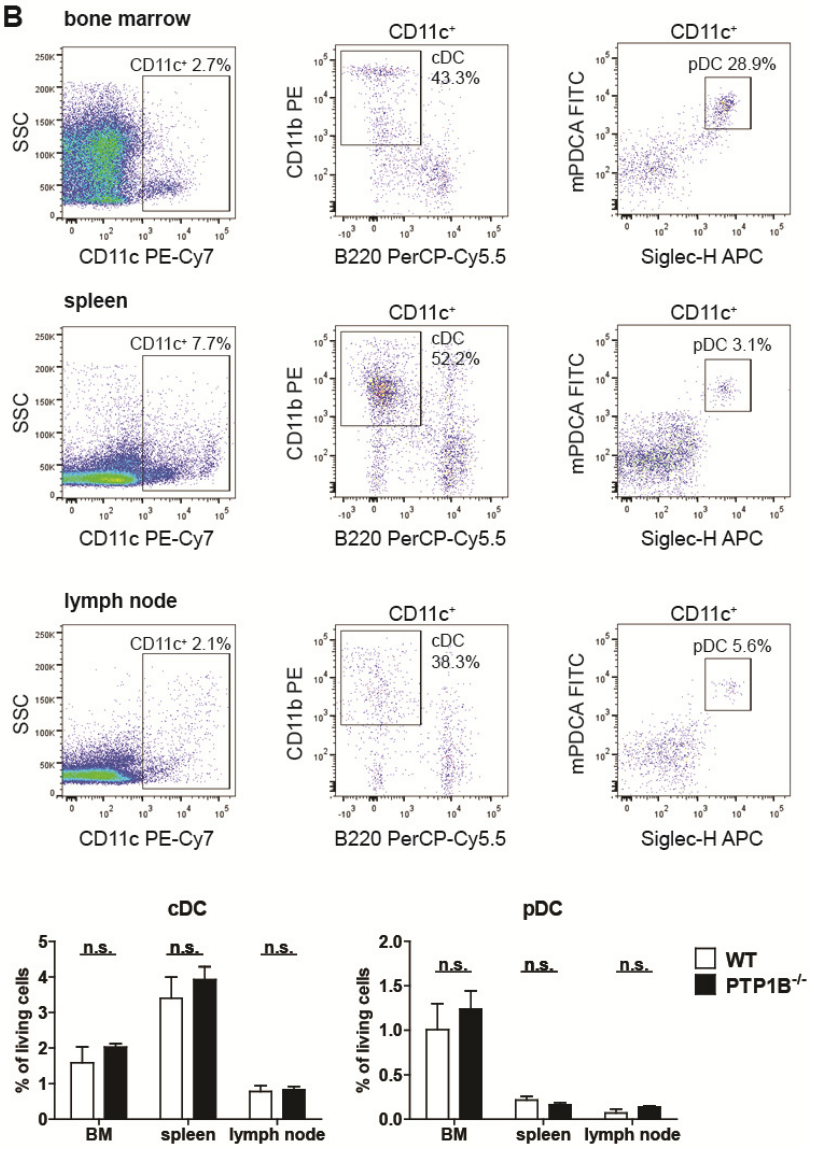

Figure 41: Knockout of PTP1B does not have an effect on cDC and pDC populations in mice. Single cell suspensions from spleen and inguinal lymph nodes of wild type (WT) and PTP1B$^{-/-}$ mice were stained with antibodies against CD3, CD19, CD4, and CD8α and analyzed by flow cytometry (A). Portions of B cells (CD3$^-$CD19$^+$) were calculated relative to the amount of living cells. Portions of CD4$^+$ T cells (CD3$^+$CD19$^-$CD4$^+$CD8α$^-$) and CD8$^+$ T cells (CD3$^+$CD19$^-$CD4$^-$CD8α$^+$) were calculated relative to the amount T cells (CD3$^+$CD19$^-$). Single cell suspensions from bone marrow, spleen, and inguinal lymph nodes of WT and PTP1B$^{-/-}$ mice were stained with antibodies against CD11c, CD11b, B220, Siglec-H, and mPDCA and analyzed by flow cytometry (B). Portions of cDC (CD11c$^+$CD11b$^+$B220$^-$) and pDC (CD11c$^+$Siglec-H$^+$mPDCA$^+$) were calculated relative to the amount of living cells. Results are shown as mean ± S.D. of organs from 3 different mice, respectively. *, p<0.05; **, *p*<0.01 by two-tailed, unpaired t test; n.s., not significant.

3.4.12. Trafficking and processing of TLR9 and its interaction with UNC93B are not dependent on PTP1B

TLR9 traffics from the ER to the endolysosomal compartment where it is proteolytically cleaved and initiates the production of proinflammatory cytokines and type I IFN upon binding of DNA. PTP1B could regulate TLR responses in different ways: it could, for example, mediate binding between UNC93B and TLR9, regulate endolysosomal trafficking of TLR9, or facilitate proteolytic processing of TLR9. Trafficking of TLR9 can be analyzed with TLR9-GFP, a fluorescent version of TLR9[74]. Cleavage of TLR9-GFP can easily be analyzed by the detection of full-length TLR9-GFP and the C-terminal TLR9-GFP cleavage fragment upon anti-GFP immunoblotting. To gain insight into how PTP1B regulates TLR responses, TLR9-GFP mice were crossed with PTP1B$^{-/-}$ mice. These mice were used to study trafficking and processing of TLR9 in the absence of PTP1B.

TLR9 binds UNC93B in the ER and traffics together with UNC93B from the ER to the endolysosome. If binding to UNC93B is disrupted, TLR9 cannot leave the ER[55]. To test whether UNC93B and TLR9 still interact in the absence of PTP1B, interaction between these two proteins was assessed by co-immunoprecipitation in primary BMDM derived from TLR9-GFP/PTP1B$^{-/-}$ and TLR9-GFP/WT mice. Endogenous UNC93B and PTP1B in input lysates were detected by immunoblotting with an UNC93B- or PTP1B-specific antibody, respectively (Figure 42A). UNC93B was recovered after an anti-GFP immunoprecipitation of TLR9-GFP in BMDM derived from TLR9-GFP/WT as well as TLR9-GFP/PTP1B$^{-/-}$ mice, indicating that UNC93B interacts with TLR9-GFP independently of PTP1B.

To analyze whether trafficking of TLR9-GFP is still intact in the absence of PTP1B, primary BMDM from TLR9-GFP/WT and TLR9-GFP/PTP1B$^{-/-}$ mice were analyzed by live cell imaging. Unstimulated cells were incubated with lysotracker, a dye that labels acidic organelles like lysosomes in living cells. A large portion of TLR9-GFP was found in the ER and in lysotracker-positive compartments in BMDM from TLR9-GFP/WT as well as TLR9-GFP/PTP1B$^{-/-}$ mice (Figure 42B). To promote trafficking of TLR9-GFP to the endolysosomal compartment, cells were incubated with fluorescently labeled CpG DNA. Upon TLR9 stimulation, TLR9-GFP almost exclusively localized to CpG DNA-positive endolysosomes (Figure 42C). Again, BMDM derived from TLR9-GFP/WT and TLR9-GFP/PTP1B$^{-/-}$ mice showed a similar subcellular distribution, indicating that endosomal trafficking of TLR9-GFP is intact in the absence of PTP1B.

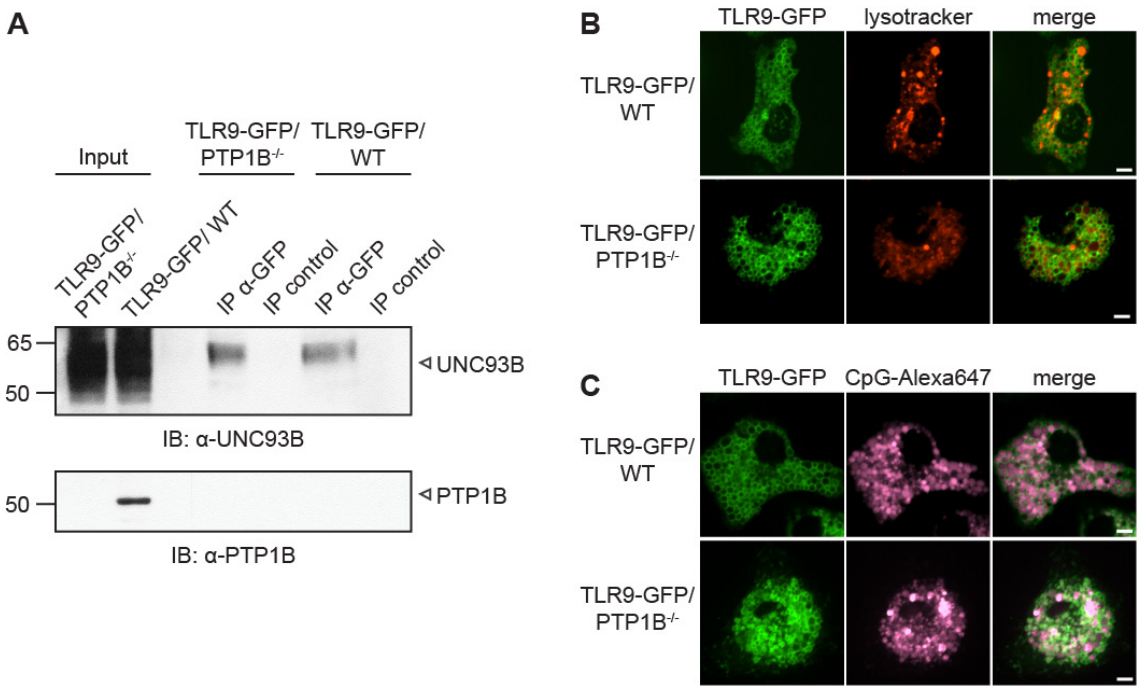

Figure 42: Interaction with UNC93B and trafficking of TLR9-GFP are intact in primary BMDM from TLR9-GFP/PTP1B$^{-/-}$ mice. Primary BMDM derived from TLR9-GFP/WT and TLR9-GFP/PTP1B$^{-/-}$ mice were lysed in 0.5% NP-40 and subjected to an anti-GFP immunoprecipitation. Beads without addition of antibody were used as control. Endogenous UNC93B was detected by anti-UNC93B immunoblotting (A). Knockout of PTP1B was verified by anti-PTP1B immunoblotting. Cells were incubated with lysotracker and left unstimulated (B) or stimulated with 1 µM CpG-Alexa647 (C) for 3.5 h and analyzed by confocal microscopy. Scale bar, 5 µm.

TLR9 needs to be proteolytically cleaved by cathepsins in the endolysosomal compartment in order to initiate signal transduction. To find out whether cleavage of TLR9 occurs in the absence of PTP1B, primary BMDM derived from TLR9-GFP/WT and TLR9-GFP/PTP1B$^{-/-}$ mice were treated with the cathepsin inhibitor z-FA-fmk or DMSO and lysates were analyzed by anti-GFP immunoblotting. The C-terminal cleavage fragment of TLR9-GFP was detected in TLR9-GFP/WT as well as in TLR9-GFP/PTP1B$^{-/-}$ cells (Figure 43A). Inhibition of TLR9 cleavage with z-FA-fmk led to the accumulation of a high molecular weight form of TLR9 which has been described in earlier studies[71,72]. However, the C-terminal TLR9-GFP cleavage fragment was still present after treatment of the cells with z-FA-fmk for 15 h indicating that it is very stable and has a long half-life.

Cleavage of TLR9-GFP was also assessed in pDC and cDC sorted from FL-DC derived from TLR9-GFP/WT, TLR9-GFP/UNC93B$^{-/-}$, and TLR9-GFP/PTP1B$^{-/-}$ mice. Full length TLR9-GFP and the C-terminal TLR9-GFP cleavage fragment were detected in lysates of pDC and cDC from TLR9-GFP/WT and TLR9-GFP/PTP1B$^{-/-}$ FL-DC upon anti-GFP immunoblotting (Figure 43B). As expected, the C-terminal TLR9-GFP

cleavage fragment was not detected in pDC and cDC sorted from TLR9-GFP/ UNC93B$^{-/-}$ FL-DC.

Collectively, these data suggest that trafficking and processing of TLR9 are independent of PTP1B.

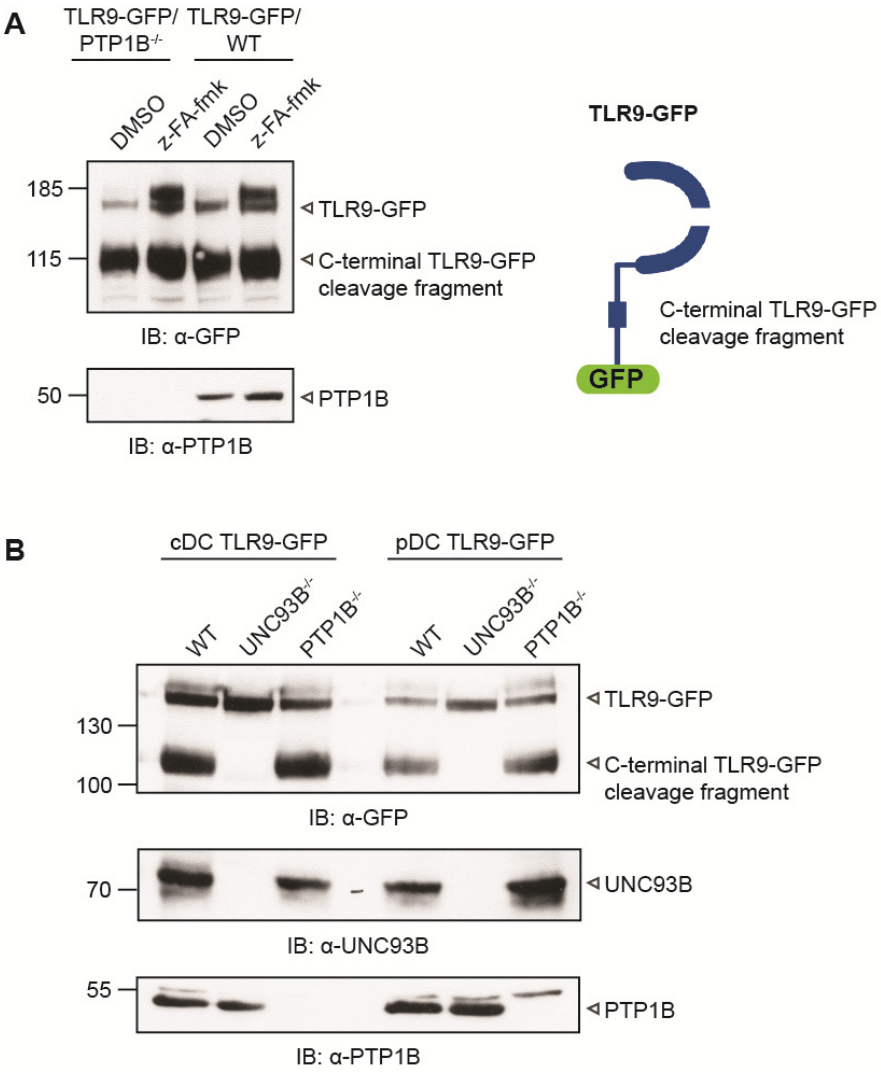

Figure 43: Processing of TLR9-GFP in primary BMDM, pDC, and cDC is independent of PTP1B. Primary BMDM from TLR9-GFP/WT and TLR9-GFP/PTP1B$^{-/-}$ mice were incubated with 10 µM z-FA-fmk or DMSO for 15 h (A). cDC (B220^{-}CD11b^{+}) and pDC (B220^{+}CD11b^{-}) were sorted from TLR9-GFP/WT, TLR9-GFP/UNC93B$^{-/-}$, and TLR9-GFP/PTP1B$^{-/-}$ FL-DC by FACS (B). TLR9-GFP and its C-terminal cleavage fragment were detected by anti-GFP immunoblotting. Knockouts of UNC93B and PTP1B were verified by anti-UNC93B and anti-PTP1B immunoblotting, respectively.

3.4.13. UNC93B, TLR9, and Clptm could be potential substrates of PTP1B

PTP1B regulates trafficking of RTKs by dephosphorylation of tyrosine residues. TLR9 has been shown to be tyrosine phosphorylated in response to stimulation with CpG DNA[222,223]. Where exactly TLR9 is phosphorylated is not clear. A tyrosine-based motif in the cytoplasmic tail of TLR9 (Y^{888}NEL) was shown to be required for the TNF response, but not for the type I IFN response, upon TLR9 stimulation with CpG DNA in macrophages[223]. Although Y^{888} was not phosphorylated itself, TLR9 could not be phosphorylated and induce a TNF response upon stimulation with CpG DNA when Y^{888} was substituted with alanine. This indicates that the structure of the Y^{888}NEL motif is important for phosphorylation of TLR9 and its ability to induce the production of TNF.

To identify potentially phosphorylated tyrosine residues in UNC93B and TLR9, UNC93B and TLR9 peptide sequences were screened for potential tyrosine phosphorylation sites. Seven putative tyrosine phosphorylation sites in UNC93B were found by bioinformatic analysis (CBS prediction servers, NetPhos 2.0). Potential tyrosine phosphorylation sites in UNC93B are: Y^{8}, Y^{52}, Y^{94}, Y^{99}, Y^{159}, Y^{182}, and Y^{191}, with high scores for Y^{94} and Y^{99} (Figure 44A). For TLR9, three potential phosphorylation sites were found by bioinformatic analysis: Y^{180}, Y^{321}, and Y^{980} (Figure 44B). However, Y^{180} and Y^{321} are part of the luminal TLR9 ectodomain which makes it very unlikely that these two tyrosine residues are dephosphorylated by PTP1B, because the catalytic domain of PTP1B faces the cytoplasm. Y^{980} is part of the cytoplasmic domain of TLR9 which makes it accessible for PTP1B.

Clptm, which binds to UNC93B, PTP1B, and possibly TLR9, could be another potential substrate of PTP1B (Figure 19, Figure 22, and Figure 23). Bioinformatic analysis of the Clptm peptide sequence revealed eleven potential tyrosine phosphorylation sites: Y^{146}, Y^{165}, Y^{229}, Y^{265}, Y^{276}, Y^{284}, Y^{292}, Y^{335}, Y^{463}, Y^{471}, and Y^{546} (CBS prediction servers, NetPhos 2.0) (Figure 44C). Eight of these predicted phosphorylation sites are located within the large predicted luminal N-terminus of Clptm which makes them inaccessible for PTP1B. The residual three predicted tyrosine phosphorylation sites are located in predicted cytosolic domains of Clptm where they would be accessible for PTP1B.

It has been described that PTP1B has a high affinity for tandem phosphotyrosine (pTyr)-containing peptides[224]. Analysis of the UNC93B peptide sequence revealed three tandem pTyr motifs: Y^{52}Y, Y^{158}Y, and Y^{190}Y. All of the three tandem pTyr motifs include one tyrosine residue which had also been identified as putative phosphorylation site by bioinformatic analysis. Based on the predicted membrane topology of UNC93B, Y^{52}Y and Y^{190}Y would be accessible for PTP1B (Figure 44A). Analysis of the TLR9 peptide sequence revealed only one tandem pTyr motif (Y^{179}Y) which is one of the potential phosphorylation sites located in the ectodomain of TLR9 (Figure 44B). Clptm

contains two tandem pTyr motifs (YY^{276}, YY^{292}) which are located in the N-terminal domain of Clptm facing the luminal side of the ER (Figure 44C). It has further been shown that an acidic and a basic residue, flanking the tandem pTyr motif on the N- and the C-terminal side, respectively, contribute to the high affinity of PTP1B for tandem pTyr motifs and that (E/D)-pY-pY-(R/K) is a consensus substrate recognition motif for PTP1B[187,224]. However, none of the tandem pTyr motifs identified in UNC93B ($RY^{52}YR$, $RY^{158}YT$, and $KY^{190}YE$), TLR9 ($CY^{179}YK$), and Clptm ($DYY^{276}P$, $DYY^{292}P$) completely matches these criteria.

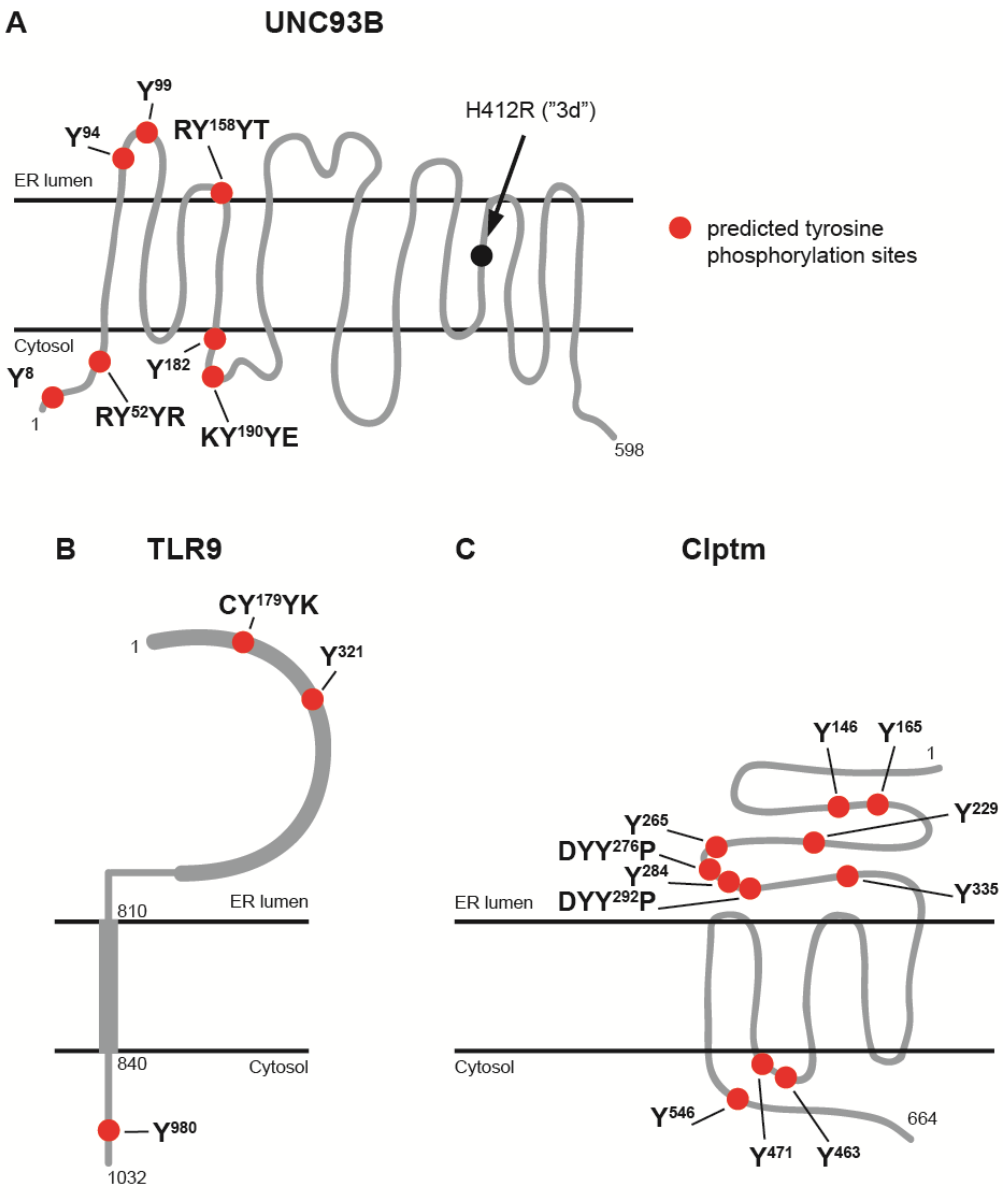

Figure 44: UNC93B, TLR9, and Clptm have several potential tyrosine phosphorylation sites. Potential tyrosine phosphorylation sites in UNC93B (A), TLR9 (B), and Clptm (C) identified by bioinformatic analysis (CBS prediction servers, NetPhos 2.0) are highlighted in red.

In order to find out whether UNC93B, Clptm, or TLR9 are phosphorylated, we tried to detect phosphorylation of endogenous UNC93B, endogenous Clptm, UNC93B-GFP, and TLR9-GFP in immortalized and primary BMDM upon immunoprecipitation with anti-UNC93B, anti-Clptm, or anti-GFP antibodies by immunoblotting using an antibody against pTyr. Unfortunately, we were not successful in showing phosphorylation of UNC93B, Clptm, or TLR9 in preliminary experiments.

In summary, UNC93B, TLR9, and Clptm could be potential substrates of PTP1B. However, in preliminary experiments we could not yet show whether UNC93B, Clptm, or TLR9 are phosphorylated and are indeed substrates of PTP1B.

4. Discussion

4.1. Characterization of innate immune signaling by UNC93B knockout mice

TLRs are located on the cell surface or intracellularly and recognize structurally conserved microbial features. Upon ligand binding, activated TLRs induce a potent innate immune response which leads to the elimination of infected cells and the activation of a specific adaptive immune response. The recognition of nucleic acids by intracellular TLRs in the endolysosome has been well documented[21-24,41,43], but how exactly the trafficking of intracellular TLRs from the ER to the endolysosome is regulated is not completely understood. The polytopic ER resident membrane protein UNC93B binds to the transmembrane domains of nucleic acid-sensing TLRs 3, 7, and 9 and delivers them from the ER to the endolysosomal compartment where they can bind their ligands and initiate the production of proinflammatory cytokines and type I IFN[54,55]. A single histidine-to-arginine point mutation in UNC93B (H412R) causes defective signaling of nucleic acid-sensing TLRs[52]. Mice carrying the H412R point mutation were termed “triple defect” (3d) mice because they fail to respond to agonist stimulation of TLRs 3, 7, and 9[52]. The H412R mutation disrupts binding of UNC93B to intracellular TLRs and UNC93B as well as TLR7 and TLR9 fail to leave the ER[54,55]. 3d mice have exclusively been used to study the role of UNC93B for the trafficking of intracellular TLRs. However, since mutated UNC93B is still present in the ER of cells derived from 3d mice, it could still fulfill yet unknown functions besides the regulation of intracellular TLR trafficking. Additionally, ENU mutagenesis usually induces various point mutations which further complicates the characterization of UNC93B in cells derived from 3d mice. UNC93B knockout (UNC93B$^{-/-}$) mice were only recently made publicly available which offers the possibility to further study the function of UNC93B. In this study, innate immune responses were compared between innate immune cells derived from UNC93B$^{-/-}$ and 3d mice. Proinflammatory cytokine and type I IFN responses were analyzed upon stimulation of TLRs and cytosolic PRRs with synthetic ligands and upon herpesviral infections in primary macrophages and dendritic cells derived from wild type, UNC93B$^{-/-}$, and 3d mice.

An antibody raised against C-terminal peptides of UNC93B specifically detected endogenous UNC93B in BMDM and FL-DC and confirmed the absence of UNC93B in BMDM and FL-DC derived from UNC93B$^{-/-}$ mice (Figure 8). Upon stimulation of TLRs with synthetic agonists, BMDM derived from UNC93B$^{-/-}$ mice responded exactly as BMDM derived from 3d mice. Like BMDM derived from wild type and 3d mice, BMDM from UNC93B$^{-/-}$ mice secreted the proinflammatory cytokines TNF and IL-6 in response

to stimulation of cell surface TLRs. In contrast, BMDM derived from UNC93B$^{-/-}$ and 3d mice did not respond to stimulation of intracellular TLRs, whereas wild type BMDM induced the production of TNF and IL-6 in response to stimulation of TLRs 3, 7, and 9 (Figure 9 and Figure 10). Cells derived from heterozygous UNC93B$^{+/-}$ mice expressed similar protein levels of UNC93B as wild type cells (Figure 8) and did not show differences to wild type BMDM upon stimulation of TLRs with synthetic agonists of cell surface and intracellular TLRs (Figure 9 and Figure 10). The UNC93B$^{+/-}$ data lead to the conclusion that only a complete loss of UNC93B leads to the 3d phenotype.

To assess the role of UNC93B in the context of viral infections, primary BMDM and FL-DC were infected with the murine herpesviruses mouse cytomegalovirus (MCMV) and murine herpesvirus 68 (MHV-68) followed by the analysis of proinflammatory cytokine and type I IFN responses. Previous studies showed that intracellular TLRs 3, 7, and 9 are involved in the recognition of MCMV[93,94]. MCMV infection induced the production of comparable amounts of TNF, IL-6, IFNα, and IFNβ by BMDM derived from UNC93B$^{-/-}$ and 3d mice (Figure 11 and Figure 12). There were no significant differences in TNF, IL-6, IFNα, and IFNβ responses between BMDM derived from UNC93B$^{-/-}$ and 3d mice compared to BMDM from wild type and TLR9$^{-/-}$ mice. However, upon MCMV infection, BMDM derived from UNC93B$^{-/-}$ and 3d mice produced 30-55% less TNF and IL-6 than wild type BMDM (Figure 11, A and B). This suggests that type I IFN response in BMDM upon MCMV infection is completely independent of intracellular TLRs, whereas the production of proinflammatory cytokines depends on intracellular TLRs to a limited extend. Studies which reported the involvement of intracellular TLRs in proinflammatory cytokine and type I IFN responses upon MCMV infection mainly focus on pDC and *in vivo* studies[93,94]. The impairment of TNF and IL-6 responses upon MCMV infection of BMDM from UNC93B$^{-/-}$ and 3d mice indicates that intracellular TLRs are at least partially involved in the proinflammatory cytokine response against MCMV in BMDM, although the absence of TLR9 alone did not have an effect on TNF and IL-6 levels. To clarify the role of intracellular TLRs 3, 7, and 9 for proinflammatory cytokine responses upon MCMV infection of BMDM, BMDM derived from TLR3$^{-/-}$ and TLR7$^{-/-}$ mice should be included in further experiments.

Herpesviral DNA is recognized by intracellular TLRs in the endolysosome or by PRRs in the cytosol[90]. The first cytosolic DNA sensor which was identified to recognize MCMV is AIM2[130]. However, the activation of AIM2 leads to inflammasome formation, which results in the secretion of IL-1β and IL-18, and does not contribute to TNF, IL-6, or type I IFN responses. MDA5, RNA Polymerase III, RIG-I, DAI, IFI16, and DHX9 and DHX36 have been linked to the innate immune recognition of herpes simplex virus

(HSV) and human cytomegalovirus (HCMV)[90]. Therefore, it is likely that at least some of the cytosolic PRRs, which have been described to detect HSV or HCMV, are also involved in the detection of MCMV. Preliminary data suggest that the production of TNF, IL-6, IL-12p40, IFNα, and IFNβ upon MCMV infection of BMDM is impaired in the absence of STING (Baca Chan, unpublished results). STING is a key regulator of the cytosolic DNA response and acts downstream of cytosolic DNA sensors including cGAS, DAI, IFI16, DDX41, MRE11, and DNA-PK. In order to show that pro-inflammatory cytokine and type I IFN responses upon MCMV infection of BMDM are dependent on cytosolic PRRs, BMDM derived from STING-deficient mice could be included in further experiments. The observation that intracellular TLRs do not play an important role for the proinflammatory cytokine and no role for the type I IFN response upon MCMV infection of BMDM was further supported by a microarray experiment that was conducted with MCMV infected BMDM from wild type and UNC93B$^{-/-}$ mice 2 and 6 h post infection (Figure 13). However, the microarray experiment was only performed once and should be confirmed by at least one more experiment. Furthermore, BMDM derived from 3d mice should be included in the experiment in order to compare the induction of genes involved in the innate immune response between BMDM derived from UNC93B$^{-/-}$ and 3d mice.

In contrast to MCMV, BMDM which had been infected with MHV-68 produced very low amounts of TNF and IL-6 even at high MOIs (Figure 11) and no IFNα production was detected upon MHV-68 infection of BMDM (data not shown). Based on this observation, we recently showed that BMDM infected with MHV-68 do not secrete TNF or IL-6 upon TLR stimulation (Bussey et al., submitted)[201]. This demonstrates that MHV-68 can manipulate proinflammatory cytokine responses to evade recognition by the innate immune system.

pDC secrete high amounts of IFNα upon activation of TLRs 7 or 9, but they do not express TLR3[106,206,207]. TLR7 and TLR9 contribute to the innate immune response against MCMV in pDC[92,94]. In this study, MCMV infection induced the secretion of high amounts of IFNα in FL-DC derived from wild type or TLR7$^{-/-}$ mice, but the IFNα response was significantly impaired in FL-DC from TLR9$^{-/-}$ mice (Figure 14C). In FL-DC from UNC93B$^{-/-}$ and 3d mice, the IFNα response was reduced to the background level. This result confirms the observation of an earlier study which showed that pDC from TLR9$^{-/-}$, but not from TLR7$^{-/-}$ mice, produce significantly lower amounts of type I IFN than wild type pDC, whereas the type I IFN response is completely abolished in pDC from mice deficient of TLR9 and TLR7[94]. The authors concluded that TLR7 can partially compensate the TLR9 deficiency, which most likely also applies to the observations

described here. Only upon MCMV infection of FL-DC from UNC93B$^{-/-}$ or 3d mice, when TLR7 and TLR9 were not functional, the IFNα response was completely abrogated (Figure 14C). How exactly TLR7, which is a sensor for single-stranded RNA, senses MCMV in the endolysosome is not clear. HCMV, another betaherpesvirus, has been reported to deliver viral mRNAs, which are packaged within the infectious virions, to the host cell[225]. Therefore, TLR7 most likely senses virion- or replication-associated viral RNA upon MCMV infection[90]. Overlapping functions of TLR7 and TLR9 were also shown for TNF and IL-12p40 responses in MCMV infected pDC[94]. Analyses of proinflammatory cytokine levels upon MCMV infection of FL-DC were not included in this study. However, to see whether intracellular TLRs and UNC93B in addition to the type I IFN response also mediate proinflammatory cytokine responses, it would be interesting to analyze TNF, IL-6, and IL-12p40 levels in supernatants of MCMV infected FL-DC.

The amounts of secreted IFNα upon infection of FL-DC with MHV-68 were lower than the IFNα amounts secreted upon MCMV infection, but the response pattern was similar. MHV-68 induced the production of IFNα in wild type FL-DC, whereas it did not induce an IFNα response in FL-DC from UNC93B$^{-/-}$ or 3d mice (Figure 14D). A role for TLR9 has previously been implicated in the recognition of MHV-68 in FL-DC[96]. We also observed a significantly impaired but measurable IFNα response upon MHV-68 infection of FL-DC derived from TLR9$^{-/-}$ mice (Figure 14D). Since MHV-68 infection did not induce an IFNα response in FL-DC from UNC93B$^{-/-}$ and 3d mice, at least one more UNC93B-dependent sensor must be involved in the recognition of MHV-68 in FL-DC. This role could be fulfilled by TLR7. Upon infection with MHV-68, the amount of secreted IFNα by FL-DC from TLR7$^{-/-}$ mice was 2-fold lower than the amount of IFNα secreted by wild type FL-DC (Figure 14D). To our knowledge TLR7 has not been implicated in the recognition of MHV-68 so far. This result suggests that, in addition to TLR9, TLR7 is involved in the type I IFN response upon MHV-68 infection of FL-DC and that similar to the recognition of MCMV, TLR7 and TLR9 have overlapping functions in the recognition of MHV-68. IL-6 and IL-12 proinflammatory cytokine responses upon MHV-68 infection are also dependent on TLR9 in FL-DC[96]. To investigate the role of TLR7 for proinflammatory cytokine responses upon MHV-68 infection of FL-DC, TNF, IL-6, and IL-12 levels in supernatants of infected FL-DC should be determined.

In addition to TLRs, cytosolic DNA and RNA sensors were also stimulated in FL-DC. Surprisingly, IFNα responses in FL-DC upon transfection with ISD or 5`ppp-dsRNA were dependent on UNC93B and the response upon ISD stimulation was also

dependent on TLR9 (Figure 15). ISD is described to be recognized by cytosolic DNA sensors in a TLR-independent manner in FL-DC and BMDM[107]. A previous study showed that the IFNα response in FL-DC upon transfection with ISD was completely dependent on STING[117]. 5`ppp-dsRNA is a ligand for the cytosolic RNA sensor RIG-I[211]. Why IFNα responses upon stimulation of FL-DC with ISD and 5`ppp-dsRNA were dependent on UNC93B is not clear. The interpretation of these results is complicated by the fact that FL-DC are not a homogenous cell population. FL-DC are a mix of about 40% pDC and 60% cDC, but the proportions can vary between different preparations. pDC are the main producers of IFNα in FL-DC cultures, but cDC also produce small amounts of type I IFN upon stimulation[210]. Therefore, the possibility that especially the low IFNα response, which was observed upon stimulation of FL-DC with 5`ppp-dsRNA, was mediated by cDC and not by pDC cannot be excluded. If the response to 5`ppp-dsRNA was mediated by cDC, it could be dependent on TLR3, which is expressed in cDC, but not in pDC. Analysis of the proteome of cDC and pDC confirmed expression of STING in cDC as well as in pDC[106]. To study the role of intracellular TLRs and UNC93B for the type I IFN response upon stimulation with ISD or 5`ppp-dsRNA in pDC or cDC, the experiment should be repeated with pDC and cDC sorted from FL-DC cultures including cells derived from TLR3-, TLR7-, and STING-deficient mice.

In summary, we conclude that at least in the experiments described here, the phenotype of innate immune cells from UNC93B$^{-/-}$ mice does not differ from the phenotype observed for cells derived from 3d mice. Additionally, we suggest a previously undescribed role for TLR7 for the recognition of the gammaherpesvirus MHV-68 in FL-DC and overlapping functions of TLR7 and TLR9 in the recognition of MHV-68 in FL-DC.

4.2. Characterization of the role of Clptm and Trex1 for TLR- and UNC93B-mediated immune responses

To improve our understanding of the regulation of UNC93B-TLR complexes, novel UNC93B interaction partners were identified and characterized in this study. Clptm is an uncharacterized protein which was found to interact with wild type and mutant (H412R) UNC93B by large scale immunoprecipitation and mass spectrometry analysis (Figure 16A). The interaction between Clptm and wild type as well as mutant UNC93B in macrophages was confirmed by co-immunoprecipitation experiments (Figure 19). A recent study, which systemically investigated the human innate immune signaling

network regulating the production of type I IFN, also found Clptm as UNC93B interaction partner[226]. In this study, 58 proteins with known functions in the regulation of type I IFN production, including UNC93B, were used as baits to get insight into the human innate immunity interactome for type I IFN. The interaction between human UNC93B and Clptm was verified by co-immunoprecipitation in HEK 293T cells[226]. This study supports our finding that Clptm interacts with UNC93B and indicates that human UNC93B and human Clptm also interact.

Since, to our knowledge, Clptm knockout mice do not exist, a stable shRNA-mediated knockdown of Clptm was performed in macrophages in order to find out whether Clptm regulates the TLR-dependent proinflammatory cytokine response. Protein expression of Clptm was efficiently reduced upon expression of two different shRNAs targeting Clptm (Figure 20A). Besides control shRNAs targeting unrelated proteins, three shRNAs targeting UNC93B, which is known to be crucial for innate immune responses mediated by intracellular TLRs 3, 7, and 9, were included as positive controls. The shRNA-mediated knockdown of UNC93B was also successful (Figure 20A). As expected, compared to macrophages stably expressing control shRNAs, the TNF response in macrophages stably expressing sh-UNC1 and sh-UNC2 was impaired upon stimulation of TLR9 (Figure 20C). Surprisingly, in comparison to macrophages expressing control shRNAs, the TLR4-dependent TNF response was also impaired in BMDM stably expressing shRNAs targeting UNC93B, but to a lesser extent than upon TLR9 stimulation (Figure 20B). This stands in contrast to the data obtained with BMDM derived from UNC93B$^{-/-}$ or 3d mice (Figure 9C). Why the shRNA knockdown of UNC93B affected TNF levels upon stimulation of TLR4 in macrophages is not clear. Before macrophages were stimulated with TLR agonists, they were counted and identical cell numbers were seeded. Usually, the seeding of equal amounts of cells was verified by lysis and the determination of protein amounts in these lysates. However, seven different stable shRNA-expressing macrophage cell lines were generated here, and not all of them always showed exactly the same growth behavior. These differences in the growth rates could be the cause for the observed differences in the proinflammatory cytokine responses upon TLR stimulation. The possibility of off-target effects, which are a major disadvantage using shRNAs, can also not be excluded. However, since at least a slight downregulatory effect on the TLR4-dependent TNF response upon expression of all three UNC93B-targeting shRNAs was observed, it is not very likely that this downregulation was mediated by off-target effects. In this study, only one representative experiment is shown and especially upon stimulation of TLR4, the standard deviations were quite high for some of the samples. However, a slight downregulatory effect on the TLR4-dependent TNF response upon expression of

UNC93B-targeting shRNAs was observed in other experiments as well. To find out whether this is a significant effect, more experiments should be conducted in order to reduce standard deviations and to perform statistical analysis. TLR4- and TLR9-dependent TNF responses upon stimulation with the specific agonists LPS and CpG 1826 did not differ between macrophages expressing Clptm-targeting shRNAs and control shRNA (Figure 20, B and C). Thus, a regulatory function of Clptm for cell surface TLR4 and intracellular TLR9 signaling could not be shown. To find out whether proinflammatory cytokine responses of other TLRs besides TLR4 and TLR9 are regulated by Clptm, additional TLR agonists for the stimulation of TLR3 and TLR7 should be included in further experiments. Furthermore, other proinflammatory cytokines could be tested and the cells could be infected with MCMV to investigate whether Clptm has a role for proinflammatory cytokine responses upon viral infection of macrophages. However, protein knockdowns are never complete and thus there is always the possibility that the remaining protein level of Clptm is sufficient to regulate innate immune responses. Another disadvantage of the shRNAs is the variability in the efficiency of the knockdown. To circumvent this problem, stable cell lines expressing the different shRNA constructs were generated in this study. However, although the cells were always kept under antibiotic selection, the efficiency of the protein knockdowns decreased after a few passages.

Unfortunately, Clptm knockout mice are not available and primary cells such as FL-DC cannot efficiently be transduced with retroviruses. For this reason the role of Clptm for TLR-dependent type I IFN responses in FL-DC or pDC could not be studied. However, the role of Clptm for the TLR-dependent type I IFN response could be studied in macrophage reporter cell lines stably expressing Clptm-targeting shRNAs. To study the IFNα response, RAW macrophages stably expressing an IFNα4-turboGFP reporter construct could be used. The IFNβ response could be studied in immortalized BMDM generated from IFNβ$^{+/\Delta\beta\text{-luc}}$ reporter mice which express luciferase under transcriptional control of the IFNβ promoter[195]. Alternatively to an shRNA knockdown of Clptm, the use of the recently described clustered regularly interspaced short palindromic repeat (CRISPR)-Cas knockout system might be more effective to stably disrupt gene expression of Clptm[227].

In summary, apart from the observation that Clptm interacts with UNC93B, a role for Clptm for TLR-dependent innate immune signaling could not be shown in this study.

The exonuclease Trex1 was found to interact with HA-tagged wild type and mutant UNC93B and Clptm by large scale immunoprecipitation and mass spectrometry analysis (Figure 16). Trex1 has been reported to interact with the cytosolic side of the

ER membrane[141]. Trex1 co-localized with Clptm at the ER (Figure 21A). Interactions between Trex1 and Clptm as well as UNC93B were verified by co-immunoprecipitation in macrophages (Olga Trupp, bachelor thesis 2011). Using N- and C-terminally truncated versions of Trex1, it was further shown that Clptm interacts with the luminal exonuclease domain of Trex1, but not with the hydrophobic membrane anchor domain (Figure 21B). This was unexpected, since the C-terminally truncated version of Trex1 (aa 1-235) has been reported to localize diffusely throughout the cell because of its missing ER anchor, whereas the N-terminally truncated version of Trex1 (aa 236-314) as well as full-length Trex1 localize to the ER[141]. However, in this report, the localization of the C- and N-terminally truncated versions of Trex1 has only been analyzed in transfected HeLa cells[141]. Therefore, the localization of the truncated versions of Trex1, which were generated in this study, should be verified by co-localization experiments in macrophages using an ER marker. Co-localization of the truncated versions of Trex1 with Clptm should also be analyzed.
Trex1 digests cytosolic DNA and is a negative regulator of the ISD response. If UNC93B or Clptm are important for the function of Trex1, the type I IFN response upon ISD stimulation should be upregulated in macrophage reporter cell lines (RAW IFNα4-turboGFP or immortalized BMDM generated from IFNβ$^{+/\Delta\beta\text{-luc}}$ reporter mice) stably expressing shRNAs targeting UNC93B or Clptm. To study the role of UNC93B or Clptm for the function of Trex1, type I IFN response upon ISD stimulation could alternatively be analyzed by qPCR in MEF or BMDM derived from UNC93B$^{-/-}$ mice or upon CRISPR-Cas knockout of Clptm.

The ER resident protein STING is a key regulator of the response to cytosolic DNA and was found to interact with Clptm (Figure 16B). The interaction between STING and Clptm was verified by co-immunoprecipitation in macrophages, an interaction between STING and wild type UNC93B was not detected (Olga Trupp, bachelor thesis 2011). Since Clptm interacts with STING, Clptm could play a role in sensing cytosolic DNA. The IFNβ response upon stimulation of cytosolic PRRs is often analyzed in MEF which can easily be transduced with retroviruses. In order to investigate the role of Clptm for the STING-dependent type I IFN response, wild type MEF transduced with shRNAs targeting Clptm could be used to study the role of Clptm for the localization and trafficking of STING and for the type I IFN response upon stimulation of cytosolic PRRs.

In all co-immunoprecipitation experiments for the investigation of interactions between the ER proteins UNC93B, Clptm, Trex1, and STING in macrophages, cells were lysed

with the mild detergent digitonin in order to preserve weak protein interactions. These co-immunoprecipitation experiments should be repeated with a stronger detergent, for example NP-40, to ensure complete solubilization of the ER membrane.
In order to investigate whether UNC93B is important for the localization of Clptm, Trex1, or STING, localization studies could be performed in cells derived from UNC93B$^{-/-}$ mice.

In summary, in this study, interactions between wild type and mutant (H412R) UNC93B and Clptm, between Trex1 and Clptm as well as wild type UNC93B, and between Clptm and STING in macrophages were shown by co-immunoprecipitation. This indicates that all these proteins form a large complex in the ER membrane. The relevance of these interactions for the innate immune response needs to be elucidated in further studies.

4.3. Characterization of the role of protein tyrosine phosphatase PTP1B for TLR and innate immune signaling

Protein tyrosine phosphatase PTP1B was identified as an interaction partner of wild type and mutant (H412R) UNC93B and Clptm (Figure 16). PTP1B terminates signaling of receptor tyrosine kinases (RTKs) by dephosphorylation and thereby regulates endocytosis and endosomal trafficking of RTKs[158].
The interactions of HA-PTP1B with wild type and mutant UNC93B, Clptm, TLR7, and TLR9-GFP were confirmed by co-immunoprecipitations in transfected HEK 293T cells and immortalized macrophages (Figure 22 and Figure 23). So far, it is not clear which of the demonstrated interactions are direct interactions and which interactions are indirect interactions mediated by another protein. In order to get an idea of how PTP1B could regulate innate immune signaling, it would be helpful to find out whether PTP1B directly interacts with UNC93B or with TLR9. HEK 293 cells do not express endogenous TLR9[208]. The fact that an interaction between UNC93B-GFP and HA-PTP1B was observed in transfected HEK 293T cells therefore indicates that UNC93B and PTP1B interact in the absence of TLR9. This suggests an indirect interaction between TLR9 and PTP1B via UNC93B. However, we cannot draw this conclusion yet since it is not clear whether HEK 293T cells express endogenous UNC93B. The fact that HEK 293 cells stably expressing human or murine TLR9 reporter constructs are commercially available and functional indicates that UNC93B is expressed in HEK 293 cells and that human UNC93B, which has 90% amino acid identity with murine UNC93B[54], can mediate trafficking of murine TLR9. On the other

hand, we did not detect cleavage of TLR9 in HEK 293T cells transfected with TLR9-GFP. This suggests that signaling of at least murine TLR9 in HEK 293T cells differs from TLR9 signaling in murine immune cells. Proteolytic cleavage of TLR9 is required for TLR9 signaling in murine cells, but cleavage of TLR9 may not be necessary to induce downstream signaling in HEK 293T cells[71,72]. It was shown that UNC93B acquires Endo H resistance when it is transiently expressed in HEK 293T cells indicating that Golgi trafficking of murine UNC93B is intact in HEK 293T cells[78]. To find out whether PTP1B directly interacts with TLR9-GFP or with UNC93B, co-immunoprecipitations can be performed with lysates of BMDM derived from TLR9-GFP/UNC93B$^{-/-}$ or TLR9$^{-/-}$ mice, respectively. Cells derived from UNC93B$^{-/-}$ mice can also be used to analyze whether Clptm still interacts with PTP1B in the absence of UNC93B. Unfortunately, the antibody for detection of endogenous PTP1B is not very sensitive and did not precipitate or detect precipitated PTP1B in first preliminary co-immunoprecipitation experiments using lysates of BMDM from UNC93B$^{-/-}$ or TLR9$^{-/-}$ mice. Nevertheless, given that TLR9 has no functional relevance in HEK 293T cells, further interaction studies should focus on the co-immunoprecipitation experiments with BMDM from UNC93B$^{-/-}$ and TLR9$^{-/-}$ mice. In BMDM derived from TLR9-GFP/PTP1B$^{-/-}$ mice the interaction between UNC93B and TLR9-GFP was intact, indicating that PTP1B is not required for their interaction (Figure 42).

Full-length, but not the C-terminal cleavage fragment of TLR9-GFP co-precipitated with HA-PTP1B in BMDM (Figure 23C). Co-precipitation of HA-PTP1B with TLR9-GFP was observed in multiple experiments, whereas the reverse experiment was only performed once. After a long exposure (data not shown) the C-terminal TLR9-GFP cleavage fragment was detected upon precipitation of HA-PTP1B in BMDM stably expressing TLR9-GFP and HA-PTP1B, but also in the control experiment using BMDM stably expressing TLR9-GFP only. If PTP1B interacts with full-length, but not the C-terminal cleavage fragment of TLR9, this could indicate that PTP1B, unlike the UNC93B-TLR9 complex, does not traffic to the endolysosome where TLR9 is proteolytically cleaved. Further co-immunoprecipitation experiments using PTP1B as a bait need to be performed to convincingly show that PTP1B only interacts with full-length TLR9 and not with the TLR9 C-terminal cleavage fragment and whether this interaction is mediated by UNC93B. A truncated version of TLR9-GFP, which comprises only the C-terminal cleavage fragment of TLR9, could be used for co-immunoprecipitation experiments in transfected HEK 293T cells or upon retroviral transduction of immortalized TLR9-deficient BMDM. Furthermore, the interaction of PTP1B with UNC93B, TLR9, and Clptm should also be studied in FL-DC or sorted pDC. The question whether PTP1B traffics to the endolysosome was addressed by co-localization experiments with

TLR9-GFP and Ruby-PTP1B. Analysis of BMDM expressing TLR9-GFP and Ruby-PTP1B by live cell imaging revealed that PTP1B, as previously described, localizes to the ER and only occasionally localizes to endosomes (Figure 24). Co-staining with an ER marker and a marker for endosomes could clarify if PTP1B actually localizes to endosomal structures in BMDM. Unfortunately, ER markers for live cell imaging and the visualization of endosomes upon fixation of BMDM do not work well, which makes it difficult to visualize both structures in the same experiment. Together, these data do not indicate that PTP1B traffics to the endolysosomal compartment. However, direct sites of membrane contact between the ER and endosomes facilitate the dephosphorylation of endosomally localized RTKs by PTP1B[179]. Therefore, PTP1B could regulate endosomally localized TLRs although it does not traffic to endosomes itself.

The expression of PTP1B in BMDM was upregulated upon TLR stimulation, indicating that PTP1B is involved in innate immune signaling (Figure 25). To test whether PTP1B is upregulated specifically upon TLR stimulation or upon activation of innate immune responses in general, expression levels of PTP1B in BMDM could also be analyzed upon stimulation with agonists for cytosolic PRRs or upon viral infection.

Using BMDM derived from PTP1B$^{-/-}$ mice, it was clearly demonstrated that PTP1B does not play a role for proinflammatory cytokine responses upon stimulation of cell surface or intracellular TLRs or upon MCMV infection (Figure 26 - Figure 29). In contrast, compared to wild type BMDM, type I IFN responses were downregulated upon MCMV infection of BMDM derived from PTP1B$^{-/-}$ mice (Figure 29). The production of IFNα in BMDM derived from PTP1B$^{-/-}$ mice was almost completely abrogated, whereas the IFNβ response was only slightly but significantly reduced compared to wild type BMDM. Why the impairment of the IFNα response in the absence of PTP1B was stronger than the impairment of the IFNβ response is not clear. A role of PTP1B for the IFNα response upon MCMV infection of BMDM was confirmed by qPCR (Figure 30). In order to clarify the role of PTP1B for the IFNβ response upon MCMV infection of BMDM, the mRNA induction of IFNβ in the presence and absence of PTP1B should be analyzed as well. Because the effect on the type I IFN response observed in the absence of PTP1B was independent of TLRs, we conclude that PTP1B regulates the type I IFN response upon stimulation of cytosolic DNA sensors or has a general role for the regulation of type I IFN responses. In order to find out which PRRs are involved in the recognition of MCMV in BMDM, we started to test proinflammatory cytokine and type I IFN responses upon MCMV infection in BMDM derived from mice

which are deficient of adaptor proteins used by one or more PRRs. These experiments are still ongoing and will be helpful to understand how exactly MCMV is sensed in BMDM. In order to analyze innate immune responses upon MCMV infection of BMDM in the absence of STING, the *Goldenticket* mouse can be used. The *Goldenticket* mouse carries a single point mutation in *Sting* resulting in a non-functional (null) allele that fails to produce detectable protein[228]. Using BMDM generated from mice deficient of MyD88 (all TLRs except TLR3), TRIF (TLR3/TLR4), MAVS (RLRs), MyD88/TRIF (all TLRs), and MyD88/TRIF/MAVS (all TLRs and RLRs), or from *Goldenticket* mice (cytosolic DNA sensors), preliminary data suggest that especially STING is crucial for INFα and IFNβ responses against MCMV in BMDM (Baca Chan, unpublished results). This supports the hypothesis that PTP1B regulates type I IFN signaling downstream of cytosolic DNA sensors. In addition, results obtained from BMDM derived from MAVS$^{-/-}$ mice suggest that RLRs such as RIG-I and MDA5 also play an important role at least for the IFNα response upon MCMV infection in macrophages (Baca Chan, unpublished results). The data presented in this study show that MCMV infection does not affect the TNF response in BMDM derived from PTP1B$^{-/-}$ mice (Figure 29A). However, we observed that TNF, IL-6, and IL-12p40 responses were impaired in BMDM derived from *Goldenticket* mice compared to wild type BMDM (Baca Chan, unpublished results), which is in contrast with our hypothesis that PTP1B only regulates type I IFN responses upon stimulation of cytosolic DNA sensors. Upon activation, STING translocates from the ER to a perinuclear compartment[117]. The analysis of STING trafficking in BMDM derived from PTP1B$^{-/-}$ mice could therefore be helpful to find out whether PTP1B plays a role for the regulation of STING and co-immunoprecipitation experiments with macrophages could reveal if PTP1B and STING interact. Furthermore, the role of PTP1B for cytosolic PRRs should be studied in BMDM or MEF derived from PTP1B$^{-/-}$ mice upon agonist stimulation of cytosolic DNA or RNA sensors, for example with ISD.

The recognition of MCMV is not dependent on TLRs in BMDM. Analysis of the TLR9-dependent IFNα4 response by qPCR indicates that PTP1B does not play a role for the TLR9-dependent IFNα response in BMDM (Figure 31). Following experiments should also include the analysis of IFNβ mRNA induction. To further address the question whether PTP1B is involved in the TLR9-dependent type I IFN response, PTP1B$^{-/-}$ mice were crossed with IFNβ$^{\Delta\beta\text{-luc}}$ mice which express luciferase under transcriptional control of the IFNβ promoter[195]. This luciferase reporter system is very sensitive and in contrast to ELISA experiments facilitates the detection of low amounts of IFNβ[195]. Cells generated from IFNβ$^{+/\Delta\beta\text{-luc}}$/PTP1B$^{-/-}$ mice will allow us to easily study whether PTP1B plays a role for the IFNβ response upon TLR9-specific stimulation of BMDM.

Since the Flt3 receptor is a RTK which is dependent on PTP1B, FL-DC derived from PTP1B$^{-/-}$ mice could not be used to study the role of PTP1B for the TLR-dependent type I IFN response in FL-DC. Therefore, wild type FL-DC were treated with PTP1B inhibitors. Because PTP1B is regarded as a novel therapeutic target for the treatment of type 2 diabetes and obesity, a variety of PTP1B inhibitors are commercially available. Unfortunately, the downregulation of the IFNα response that was observed upon stimulation of TLRs 7 and 9 in FL-DC which had been treated with a PTP1B inhibitor was not specific, since IFNα responses were also downregulated in FL-DC derived from PTP1B$^{-/-}$ mice (Figure 35). The possibility that the treatment of FL-DC with PTP inhibitor XXII induces cell death was ruled out by flow cytometry analysis (Figure 34). PTP1B is closely related to TC-PTP and the catalytic sites of both phosphatases are highly conserved which makes the design of specific inhibitors with a high selectivity for PTP1B over TC-PTP difficult. In order to see a downregulation of IFNα responses upon TLR stimulation, FL-DC were treated with relatively high doses of PTP inhibitor XXII (12.5- to 37.5-fold of the IC_{50}). Therefore, in addition to PTP1B, the treatment of FL-DC with PTP inhibitor XXII might have inhibited other PTPs, especially TC-PTP, as well. In future experiments, further PTP1B inhibitors could be tested in order to inhibit PTP1B in FL-DC. These inhibitors should be carefully titrated to ensure that potentially observed effects are not caused by the induction of cell death or are unspecific side effects. Alternatively to flow cytometry analysis, the colorimetric MTT (3-(4,5-dimethylthiazol-2-yl)-2,5-diphenyltetrazolium bromide) assay could be used to easily test the cell viability upon treatment of the cells with different doses of inhibitors[229].

Since FL-DC could not be used, the role of PTP1B for the type I IFN response upon stimulation of TLR7 and TLR9 was investigated in total BM cells. TLR-dependent IFNα, but not proinflammatory cytokine responses, were impaired in total BM cells from PTP1B$^{-/-}$ mice compared to BM cells from wild type mice (Figure 36 and Figure 37). Since pDC are the main source for IFNα, this suggests a role of PTP1B for the TLR7- and TLR9-dependent IFNα response in pDC. In accordance with these results, the TLR9-dependent IFNα response, but not TNF or IL-6 responses, was significantly impaired in the absence of PTP1B *in vivo* (Figure 39A and Figure 40). These experiments convincingly demonstrate that PTP1B regulates the IFNα response upon stimulation of TLR7 or TLR9 in pDC. In addition to IFNα, decreased TLR9-dependent IL-12p40 levels were observed in the sera of PTP1B$^{-/-}$ mice compared to sera from wild type mice (Figure 39B). Whether this effect was mediated by pDC is not clear, since IL-12 is also secreted by other types of antigen presenting cells (APC) in response to stimulation of TLR9. However, upon MCMV infection *in vivo*, pDC are the main source

for IL-12[230]. In order to find out whether PTP1B is important for IL-12 responses upon TLR stimulation in general, levels of IL-12p40 should also be determined in supernatants of total BM cells upon stimulation of TLR7 or TLR9. The fact that the IFNα response upon injection of CpG DNA was not completely abrogated in PTP1B$^{-/-}$ mice supports the idea that PTP1B regulates TLR9 signaling in pDC, but not in other types of APC which also produce small amounts of type I IFN upon stimulation of TLR9. TNF responses upon i.p. injection of CpG DNA did not differ between wild type and PTP1B$^{-/-}$ mice and IL-6 levels in sera from PTP1B$^{-/-}$ mice were slightly elevated compared to sera from wild type mice (Figure 40). TNF and IL-6 in response to stimulation of TLR9 are mainly secreted by macrophages and B cells and not by pDC. Therefore, the increased number of B cells that was observed in lymph nodes of PTP1B$^{-/-}$ mice compared to wild type mice in accordance with previous studies (Figure 41A) could explain why the IL-6 levels in sera from PTP1B$^{-/-}$ mice were elevated compared to wild type mice upon TLR9-specific stimulation. The numbers of cDC and pDC, which are the main source of IFNα and probably IL-12 upon TLR9-specific stimulation with CpG DNA *in vivo*, did not differ between wild type and PTP1B$^{-/-}$ mice[231]. Together, the experiments with total BM cells and the *in vivo* experiments strongly indicate that PTP1B regulates signaling of intracellular TLRs in pDC. To test whether the absence of PTP1B also affects IFNα and IL12-p40 responses upon TLR7-specific stimulation *in vivo*, mice could be injected with the TLR7 ligands R848 or Poly(U). Additionally, we currently investigate the role of PTP1B for type I IFN and proinflammatory cytokine responses upon MCMV infection of wild type and PTP1B$^{-/-}$ mice *in vivo*. So far, this study focused on the IFNα response upon *in vivo* stimulation of TLR9. In future experiments, analysis of the IFNβ response *in vivo* upon TLR stimulation or viral infection can easily be studied in the IFNβ$^{+/\Delta\beta\text{-luc}}$/PTP1B$^{-/-}$ reporter mouse line. This mouse line was generated during this study by crossing PTP1B$^{-/-}$ mice with IFNβ$^{\Delta\beta\text{-luc}}$ mice that expresses luciferase under transcriptional control of the IFNβ promoter[195]. Using these mice, the luciferase activity can be visualized with an *in vivo* imaging system (IVIS) upon injection of luciferin as well as *in vitro* with cells extracted from these mice.

There are different hypotheses that could explain the regulation of intracellular TLR signaling in pDC and the type I IFN response against MCMV in BMDM by PTP1B (Figure 45). First, PTP1B could act differently in pDC and BMDM and directly regulate TLRs and cytosolic PRRs or STING by distinct mechanisms. Second, PTP1B could regulate common features in the downstream signaling cascades of intracellular TLRs and cytosolic PRRs. Third, PTP1B could generally affect type I IFN responses by

regulating the type I IFN receptor complex or molecules downstream of type I IFN signaling.

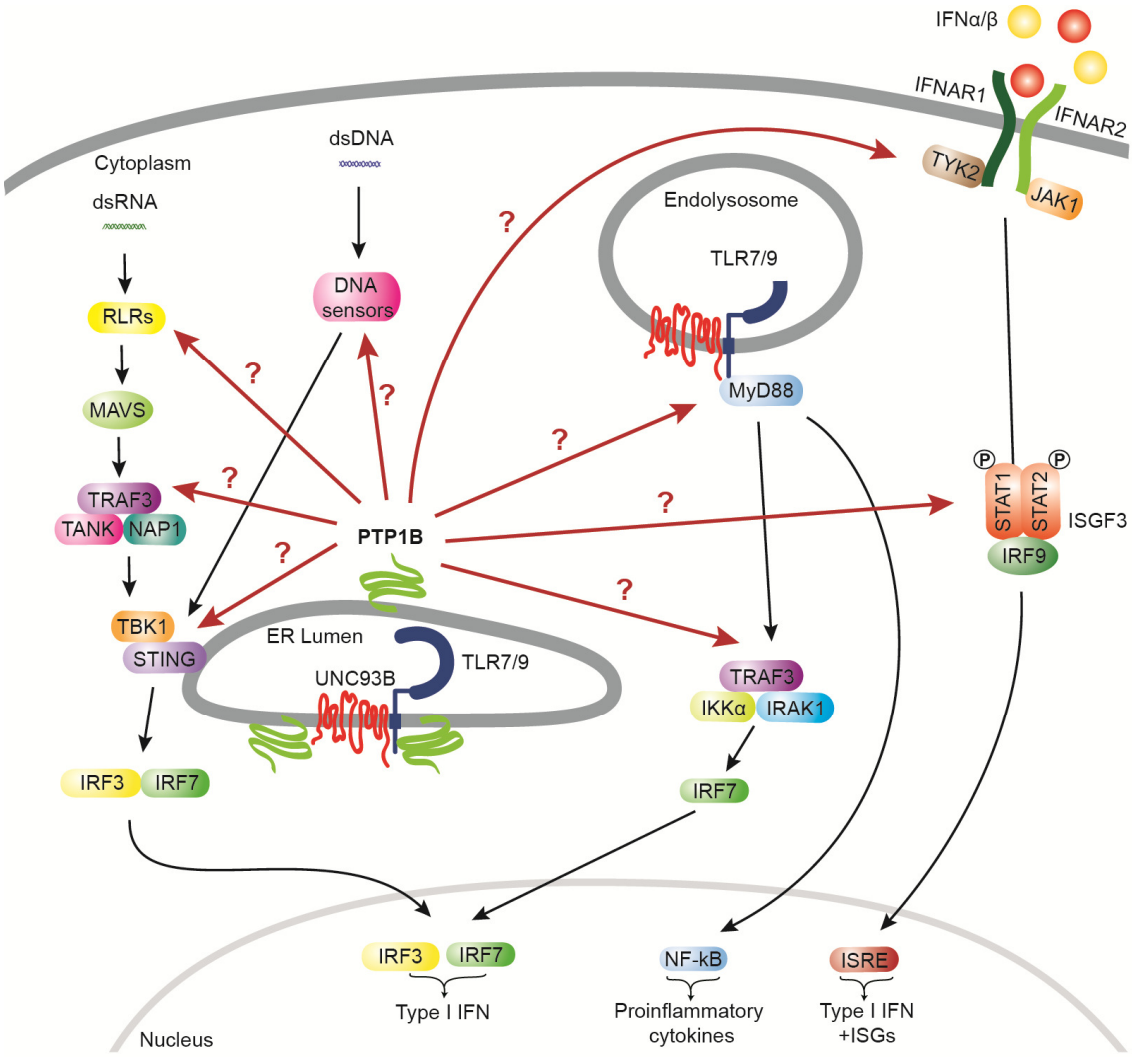

Figure 45: Possible mechanisms of regulation of type I IFN responses by PTP1B. PTP1B could directly regulate TLRs and cytosolic PRRs or STING, act on downstream signaling cascades of intracellular TLRs and cytosolic PRRs, or regulate the type I IFN receptor complex or molecules downstream of type I IFN signaling.

In order to investigate whether PTP1B directly affects trafficking of TLR9, mice expressing TLR9-GFP were crossed with PTP1B$^{-/-}$ mice. Using BMDM derived from these mice, it was shown that PTP1B does not regulate trafficking of TLR9 from the ER to the endolysosome in BMDM (Figure 42). Unfortunately, imaging of pDC, which are non-adherent cells, is very challenging and it is almost impossible to clearly visualize endosomal structures in these relatively small and round cells. Therefore, the possibility that PTP1B regulates trafficking of intracellular TLR9 in pDC cannot be excluded at this point.

The adaptor proteins AP-2 and AP-3 mediate trafficking of TLR9. TLR9 is thought to traffic to the endolysosome via the cell surface. At the cell surface, UNC93B recruits AP-2 which mediates the internalization of TLR9[78]. Upon internalization, TLR9 traffics to the endosomal compartment where it initiates the production of proinflammatory cytokines by recruitment of MyD88. To induce a type I IFN response, TLR9 traffics from the endosomal to a lysosomal compartment where it activates IRF7. This trafficking process is mediated by AP-3[88]. PTP1B could facilitate the recruitment of AP-2 or AP-3 by the UNC93B-TLR9 complex. Binding of AP-2 and AP-3A to RTKs has been reported to be inhibited by serine phosphorylation of AP-2 and AP-3A binding sites which prevents receptor endocytosis and late endolysosomal trafficking of RTKs[232,233]. Furthermore, AP-2-mediated endocytosis of the IFNα/β receptor chain 1 (IFNAR1) is regulated by PTP1B through dephosphorylation of Y466 which is part of the AP-2 binding motif in the cytosolic domain of human IFNAR1[234]. Since murine IFNAR1 lacks an analogous tyrosine-based motif, PTP1B does not regulate receptor endocytosis of IFNAR1 in murine cells[234]. These studies suggest that the recruitment of AP-2 and AP-3 to UNC93B-TLR9 complexes could be inhibited by tyrosine phosphorylation of UNC93B and TLR9 and that dephosphorylation by PTP1B could mediate binding of AP-2 or AP-3 and thereby positively regulates TLR9 signaling. However, proteolytic cleavage of TLR9 was intact in BMDM, cDC, and pDC derived from PTP1B$^{-/-}$ mice indicating that TLR9 at least reaches the endosomal compartment in these cell types also in the absence of PTP1B (Figure 43). Additionally, in the absence of PTP1B, the IFNα response in total BM cells was impaired upon stimulation of TLR7 (Figure 36), which uses a different route to traffic to the endolysosomal compartment than TLR9. TLR7 does not traffic via the cell surface, but directly recruits AP-4 which mediates its trafficking from the ER to the endolysosome[78]. These two observations do not support the hypothesis that PTP1B mediates the recruitment of AP-2 by UNC93B. AP-3 was not only reported to be required for TLR9, but also for TLR7 signaling[88]. However, AP-3-deficient mice still produced the proinflammatory cytokine IL-12p40 in response to injection of CpG DNA *in vivo*[88], but IL-12p40 levels in sera of PTP1B$^{-/-}$ mice were impaired compared to sera from wild type mice (Figure 39B). Therefore, it also seems unlikely that PTP1B regulates the recruitment of AP-3 by TLR7 or TLR9. In this regard, it would be interesting to test whether the adaptor protein MyD88 still interacts with TLR9 in the absence of PTP1B in FL-DC or sorted pDC. Altogether, PTP1B does not seem to regulate trafficking of intracellular TLRs.

We showed that UNC93B, TLR9, and Clptm could be potential substrates of PTP1B (Figure 44). Tyrosine phosphorylation of TLR9 has already been reported[222,223].

Unfortunately, tyrosine phosphorylation of TLR9, UNC93B, or Clptm by anti-pTyr immunoblotting could not be detected in this study. In order to enhance the amount of tyrosine phosphorylated proteins, cells could be treated with pervanadate, an irreversible inhibitor of tyrosine phosphatases[235], prior to cell lysis.

Whether the enzymatic activity of PTP1B is important for the regulation of the IFNα response in pDC is not clear. The protein tyrosine phosphatase non-receptor type 22 (Ptpn22) was recently reported to positively regulate the TLR-dependent type I IFN response in myeloid cells by promoting K63-linked ubiquitination of TRAF3[236]. This process is completely independent of the enzymatic phosphatase activity of Ptpn22, suggesting that PTP1B could also act downstream of TLR signaling and independently of its phosphatase activity. In order to study the requirement of the enzymatic function of PTP1B for the regulation of signaling of intracellular TLRs and cytosolic PRRs, an enzymatically inactive point mutant (D181A) of PTP1B can be used. However, primary BMDM or FL-DC derived from $PTP1B^{-/-}$ mice cannot be efficiently transduced with mutant (D181A) PTP1B and MEF derived from $PTP1B^{-/-}$ mice, which can be passaged several times and were effectively transduced with mutant PTP1B (Figure 38), do not express TLR9. Therefore, BMDM derived from $PTP1B^{-/-}$ mice are currently immortalized which should enable retroviral transduction of these cells (T. May, HZI). PTP1B inhibitors could also be used to study the role of PTP1B enzymatic activity for innate immune signaling, however, the use of PTP1B inhibitors in FL-DC was problematic due to cytotoxicity and unspecific side effects of the inhibitors (3.4.8).

Intracellular TLRs and cytosolic PRRs activate distinct downstream signaling cascades which involve different sets of proteins upon ligand binding. PTP1B-mediated regulation of proteins involved in signaling pathways downstream of TLR-dependent type I IFN signaling as well as cytosolic PRRs could explain how PTP1B regulates the TLR-independent IFNα response upon MCMV infection in BMDM as well as the TLR7- and TLR9-dependent IFNα response in pDC. TRAF3 is required for the activation of IRF7 downstream of TLR7 and TLR9 signaling in pDC. TRAF3 is also crucial for the signaling cascade downstream of MAVS. MAVS is activated upon interaction with the cytosolic RNA sensors RIG-I or MDA5 and induces the activation of IRF3 and IRF7 via STING[237]. An interaction between STING and TRAF3 has been shown in transfected HEK 293T cells[113]. A direct role for TRAF3 for STING-mediated signaling downstream of cytosolic DNA sensors or for RIG-I and MDA5 in sensing of MCMV has not been described so far. However, preliminary results with BMDM derived from $MAVS^{-/-}$ mice suggest that RLRs such as RIG-I or MDA5 are involved in the IFNα response upon MCMV infection (Baca Chan, unpublished results). Therefore, regulation of TRAF3 by

PTP1B, for example through a mechanism similar to the one that has been described for the phosphatase Ptpn22, could possibly explain the impairment of the IFNα response observed upon MCMV infection of PTP1B-deficient BMDM.

In order to systematically investigate whether PTP1B acts downstream of TLRs or cytosolic PRRs, the phosphorylation and translocation of IRF3 and IRF7 upon stimulation of TLRs or cytosolic PRRs should be analyzed in wild type and PTP1B-deficient cells. Unfortunately, the available antibodies against IRF7 or phospho-IRF7 are not very sensitive which makes the analysis of endogenous IRF7 difficult. IRF3 and IRF7 are activated by TBK1 which becomes serine phosphorylated upon activation[238]. Furthermore, IRF7 has been reported to interact with and to be ubiquitinated by TRAF6[239,240]. Therefore, the phosphorylation of TBK1, the interaction between IRF7 and TRAF6, and the ubiquitination of IRF7 could be analyzed in presence and absence of PTP1B.

Recently, it was shown that the spleen tyrosine kinase (Syk) differentially regulates TLR4-dependent signaling pathways through TRAF6 and TRAF3[241]. Syk negatively regulated the TRAF6- and TAK1-dependent proinflammatory cytokine pathway upon TLR4 stimulation on the cell surface, whereas it positively regulated TRAF3- and TBK1-dependent type I IFN production upon internalization of TLR4. It was shown that Syk interactes with TRAF3, TRAF6, TAK1, and TBK1 and inhibites K63-linked polyubiquitination of TRAF6. In contrast, Syk increased K63-specific autopoly-ubiquitination of TRAF3 and thereby stimulated the activation of TBK1-IRF3 signaling and the production of type I IFN. The authors of this study suggest that Syk could generally be involved in the regulation of TLR signaling since it associated with TLR3, TLR4, and TLR9 and because TRAF3, TRAF6, TAK1, and TBK1 are common molecules involved in TLR signaling[241]. Furthermore, cytosolic PRRs also signal via TBK1 which indicates that Syk could also regulate signaling pathways initiated by cytosolic DNA or RNA sensors. Upon activation, Syk becomes phosphorylated. PTP1B could either counteract the mechanism by which Syk positively regulates type I IFN signaling and negatively regulates the production of proinflammatory cytokines or it could regulate Syk itself by dephosphorylation. In order to find out whether PTP1B affects Syk activation or Syk mediated regulation of TLR signaling, the phosphorylation status of Syk and K63-linked polyubiquitination of TRAF3 and TRAF6 in the presence and absence of PTP1B could be analyzed.

Upon secretion, type I IFN binds to the IFN receptor complex which consists of IFNAR1 and IFNAR2 and thereby further activates the production of type I IFN in an autocrine and paracrine manner. The IFN receptor complex recruits Janus kinase 1 (JAK1) and

tyrosine kinase 2 (TYK2). JAK1 and TYK2 phosphorylate signal transducer and activator of transcription 1 (STAT1) and STAT2 leading to the formation of IFN-stimulated gene factor 3 complexes (ISGF3) with IRF9 which translocate into the nucleus and initiate gene transcription via IFN-stimulated response elements (ISRE)[242]. It has been shown that 6 h after i.v. injection of CpG DNA, mice deficient of IFNAR show severely impaired serum levels of type I IFN compared to wild type mice[243]. Therefore, PTP1B could directly regulate IFNAR or regulate signaling molecules downstream of IFNAR. As mentioned earlier, it is known that PTP1B positively regulates AP-2-mediated endocytosis of IFNAR1 by dephosphorylation of the AP-2 binding motif in human, but not in murine cells[234]. However, a similar mechanism in murine cells, for example on IFNAR2, would lead to increased IFNAR signaling and type I IFN production in the absence of PTP1B, because IFNAR could not be internalized to terminate its signaling. A conserved tyrosine motif in the cytoplasmic domain of IFNAR2 has been identified to mediate the recruitment of STAT1 and STAT2 and therefore plays a critical role for the response to type I IFN[244]. However, targeting of this tyrosine motif by PTP1B would decrease binding of STATs to IFNAR2 and would therefore also lead to increased type I IFN production in the absence of PTP1B.

TYK2, which is required for IFNAR signaling, is a known substrate of PTP1B[187]. TYK2 is also activated upon induction of the IL-12 signaling pathway[245]. However, dephosphorylation of TYK2 negatively regulates the production of type I IFN and IL-12. Therefore, the effect of PTP1B on TYK2 cannot explain the observations that IFNα and IL-12 responses are impaired in the absence of PTP1B which have been reported here. Nevertheless, the regulation of IFNAR or of components of the IFNAR signaling pathway could explain the effects on the TLR-independent type I IFN response upon MCMV infection of BMDM and the TLR7- and the TLR9-depdendent IFNα response in pDC observed in the absence of PTP1B. In addition to PTP1B, several molecules which negatively regulate type I IFN signaling have been described[246-249]. Inhibition of one of these negative regulators by PTP1B could counteract their downregulatory effects. In order to find out whether signaling of IFNAR is intact in the absence of PTP1B, the phosphorylation status of STAT1 and STAT2 in lysates of BMDM derived from $PTP1B^{-/-}$ mice could be analyzed upon stimulation of IFNAR with IFNα or IFNβ.

The identification of PTP1B interaction partners might help to find proteins involved in innate immune signaling which are targeted by PTP1B and could therefore give important insights into the mechanism by which PTP1B regulates type I IFN responses.

In order to identify binding partners of PTP1B, mass spectrometry analysis with BMDM stably expressing HA-PTP1B could be performed.

In this study it was demonstrated that PTP1B interacts with UNC93B, TLR9, TLR7, and Clptm in macrophages and that the expression of PTP1B is upregulated upon TLR stimulation. The type I IFN, but not proinflammatory cytokine responses, upon MCMV infection of primary BMDM were significantly impaired in the absence of PTP1B. In addition, compared to wild type controls, the IFNα response in PTP1B-deficient bone marrow cells was impaired upon stimulation of TLR7 or TLR9 and IFNα and IL-12p40 responses in PTP1B-deficient mice were impaired upon stimulation of TLR9 *in vivo*. In summary, these data show that PTP1B is a critical regulator of the TLR-independent type I IFN response upon MCMV infection of BMDM and the TLR7- and TLR9-depdendent IFNα response in pDC. The exact mechanism by which PTP1B differentially regulates the type I IFN response in these two cell types will be investigated in further studies.

5. Abstract

Toll-like receptors (TLRs) are key players of the innate immune system. Localized at the cell surface or intracellularly, they trigger immune responses upon recognition of pathogenic patterns. After their synthesis in the endoplasmic reticulum (ER), intracellular TLRs 3, 7, and 9 need to move to the endolysosome to meet their ligands. On their way they are escorted by the polytopic membrane protein UNC93B. UNC93B interacts with TLRs 3, 7, and 9 and delivers them from the ER to the endolysosome where they initiate the expression of proinflammatory cytokines and type I interferon (IFN) upon encounter of nucleic acids. In 3d mice, which express a missense mutant of UNC93B (H412R), binding of UNC93B to TLRs is disrupted and UNC93B H412R as well as intracellular TLRs fail to leave the ER. How function and trafficking of UNC93B-TLR complexes is regulated is not entirely understood. A comparison of innate immune cells derived from UNC93B knockout and 3d mice showed that the phenotype of cells from UNC93B knockout mice does not differ from the 3d phenotype. In a proteomics approach, cleft lip and palate transmembrane protein (Clptm), three prime repair exonuclease 1 (Trex1), and the protein tyrosine phosphatase 1B (PTP1B) have been identified as novel binding partners of UNC93B in macrophages. Co-immuno-precipitation experiments verified interactions between UNC93B, the previously uncharacterized protein Clptm, as well as the negative regulator of cytosolic DNA responses Trex1. PTP1B is known to be crucial for intracellular trafficking of receptor tyrosine kinases, but had not been linked to regulation of TLR signaling. Interaction of PTP1B with UNC93B, Clptm, TLR7, and TLR9 was verified by co-immunoprecipitation. The TLR-independent type I IFN response upon infection of bone marrow-derived macrophages with mouse cytomegalovirus, as well as the TLR7- and TLR9-dependent IFNα responses in plasmacytoid dendritic cells (pDC) were impaired in cells derived from PTP1B knockout mice compared to wild type cells. Furthermore, PTP1B knockout mice showed significantly reduced IFNα and interleukin (IL)-12p40 responses compared to wildtype mice upon stimulation of TLR9 by intravenous administration of CpG oligonucleotides *in vivo*. This suggests that PTP1B is a critical regulator of the TLR7- and TLR9-dependent IFNα response in pDC as well as the TLR-independent type I IFN response in macrophages.

I List of abbreviations

5`ppp-dsRNA	5`triphosphate double stranded RNA
7-AAD	7-Aminoactinomycin
aa	amino acid
AIM2	absent in melanoma 2
AMPK	adenosine monophosphate-activated protein kinase
AP	adaptor protein
AP-1	activator protein 1
AP-2/AP-3/AP-4	adaptor protein 2/adaptor protein 3/adaptor protein 4
APC	antigen presenting cells
APS	ammonium persulfate
ASC	apoptosis-associated speck-like protein containing a CARD domain
ATCC	American Type Culture Collection
BM	bone marrow
BMDM	bone marrow-derived macrophages
bp	base pair
BSA	bovine serum albumin
CARD	caspase recruitment domain
CD	cluster of differentiation
cDC	conventional dendritic cells
CDN	cyclic dinucleotides
cGAMP	cyclic guanosine monophosphate-adenosine monophosphate
cGAS	cGAMP synthase
Clptm	cleft lip and palate associated transmembrane protein
CLR	C-type lectin receptor
CRISPR	clustered regularly interspaced short palindromic repeat
C-terminus	carboxy-terminus
DAI	DNA-dependent activator of IFN-regulatory factors
DAMP	damage- or danger-associated molecular pattern
DC	dendritic cells
DDX	DEAD box helicase
DHX	DExD/H-box helicase
DNA	deoxyribonucleic acid
DNA-PK	DNA-dependent protein kinase
dsDNA	double-stranded DNA
dsRNA	double-stranded RNA
EGFR	epidermal growth factor receptor
ELISA	enzyme-linked immunosorbent assay
Endo H	Endoglycosidase H

ENU	*N*-ethyl-*N*-nitrosourea
ER	endoplasmic reticulum
ESCRT	endosomal sorting complex required for transport
FACS	fluorescence-activated cell sorting
FCS	fetal calf serum
FELASA	Federation of European Laboratory Animal Science Associations
FL-DC	Flt3 ligand-induced dendritic cells
Flt3	Fms-like tyrosine kinase 3
FRET	fluorescence resonance energy transfer
GFP	green fluorescent protein
GRP94 (gp96)	glucose-regulated protein of 94 kDa
HA	hemagglutinin
HBS	HEPES-buffered saline
HCMV	human cytomegalovirus
HEK	human embryonic kidney
HRP	horseradish peroxidase
HRS	hepatocyte growth factor-regulated tyrosine kinase substrate
HSV	herpes simplex virus
IC_{50}	half maximal inhibitory concentration
IFI16	IFNγ-inducible protein 16
IFN	interferon
IFNAR	IFNα/β receptor
IKK	IκB kinase
IL	interleukin
IRAK	IL-1 receptor-associated kinase
IRF	interferon regulatory factor
ISD	interferon stimulatory DNA
ISG	interferon-stimulated gene
ISGF3	IFN-stimulated gene factor 3 complexes
ISRE	IFN-stimulated response elements
JAK1/JAK2	Janus kinase 1/Janus kinase 2
kDa	kilodalton
KSHV	Kaposi`s sarcoma-associated herpesvirus
LBP	LPS-binding protein
LC-MS/MS	liquid chromatography and mass spectrometry
LGP2	laboratory of genetics and physiology 2
LPS	lipopolysaccharide
LRO	lysosome-related organelle
LRR	leucine-rich repeat
LRRFIP1	leucine-rich repeat flightless-interacting protein 1
LTA	lipotechoic acid

MACS	magnetic-activated cell sorting
MAPK	mitogen-activated protein kinase
MAVS	mitochondrial antiviral signaling protein
MCMV	mouse cytomegalovirus
MCSF (CSF-1)	macrophage colony-stimulating factor (colony-stimulating factor 1)
MD-2	myeloid differentiation factor 2
MDA5	melanoma differentiation-associated gene-5
MEF	mouse embryonic fibroblasts
MGC	Mammalian Gene Collection
MHV-68	murine herpesvirus 68
miR-30	microRNA-30
MOI	multiplicity of infection
MRE11	meiotic recombination 11
mRNA	messenger RNA
MSCV	murine stem cell virus
MVB	multivesicular body
MyD88	myeloid differentiation primary response gene 88
NAP1	NAK-associated protein 1
NEAA	non-essential amino acids
NEMO	NF-κB essential modulator
NF-κB	nuclear factor kappa-light-chain-enhancer of activated B cells
NK cell	natural killer cell
NLR	NOD-like receptor
NOD	nucleotide-binding oligomerization domain
N-terminus	amino-terminus
ODN	oligonucleotide
P/S	penicillin/streptomycin
PAGE	polyacrylamide gel electrophoresis
PAMP	pathogen-associated molecular pattern
PBS	Phosphate-buffered saline
PCR	polymerase chain reaction
pDC	plasmacytoid dendritic cell
PNGase F	Peptide-*N*-Glycosidase F
Poly(I:C)	polyinosinic-polycytidylic acid
Poly(U)	polyuridylic acid
PRAT4A	protein associated with TLR4
PRR	pattern recognition receptor
PTP	protein tyrosine phosphatase
PTP1B	protein tyrosine phosphatase 1B
Ptpn22	protein tyrosine phosphatase non-receptor type 22
pTyr	phosphotyrosine

PYHIN	pyrin and HIN domain-containing protein
qPCR	real-time quantitative PCR
R848	resiquimod
RIG-I	retinoic acid-inducible gene-I
RIP1	receptor-interacting protein 1
RLR	RIG-I-like receptor
RNA	ribonucleic acid
RNA Pol III	RNA Polymerase III
Rpl8	murine ribosomal protein L8
rpm	rounds per minute
RT	room temperature
RTK	receptor tyrosine kinase
shRNA	small hairpin RNA
ssRNA	single-stranded RNA
STAM2	signal transducing adaptor molecule 2
STAT	signal transducer and activator of transcription
STING	stimulator of interferon genes
Syk	spleen tyrosine kinase
TAB	TAK1-binding protein
TAK1	transforming growth factor β-activated kinase 1
TANK	TNFR-associated factor family member-associated NF-κB activator
TBK1	TANK-binding kinase 1
TBS	Tris-buffered saline
TBS-T	TBS/0.1% Tween 20
TC-PTP	T cell PTP
TEV	tobacco etch virus
TIR domain	Toll-interleukin-1 receptor domain
TIRAP	TIR domain-containing adaptor protein
TLR	Toll-like receptor
TMB	3,3',5,5'-Tetramethylbenzidine
TNF	tumor necrosis factor
TRADD	TNF receptor type 1-associated Death domain protein
TRAF	tumor necrosis factor receptor-associated factor
TRAM	TRIF-related adaptor molecule
Trex1	three prime repair exonuclease 1
TRIF	TIR domain-containing adaptor inducing IFNβ
TYK2	tyrosine kinase 2
ULK1	UNC-51-like kinase 1
WT	wild type

II List of tables

III List of figures

IV List of references

1. Medzhitov R. Recognition of microorganisms and activation of the immune response. *Nature* 2007, **449**(7164)**:** 819-826.
2. Iwasaki A, Medzhitov R. Regulation of adaptive immunity by the innate immune system. *Science* 2010, **327**(5963)**:** 291-295.
3. Schenten D, Medzhitov R. The control of adaptive immune responses by the innate immune system. *Advances in immunology* 2011, **109:** 87-124.
4. Medzhitov R, Janeway CA, Jr. Decoding the patterns of self and nonself by the innate immune system. *Science* 2002, **296**(5566)**:** 298-300.
5. Lemaitre B, Nicolas E, Michaut L, Reichhart J-M, Hoffmann JA. The Dorsoventral Regulatory Gene Cassette spätzle/Toll/cactus Controls the Potent Antifungal Response in Drosophila Adults. *Cell* 1996, **86**(6)**:** 973-983.
6. Medzhitov R, Preston-Hurlburt P, Janeway CA. A human homologue of the Drosophila Toll protein signals activation of adaptive immunity. *Nature* 1997, **388**(6640)**:** 394-397.
7. Hardison SE, Brown GD. C-type lectin receptors orchestrate antifungal immunity. *Nature immunology* 2012, **13**(9)**:** 817-822.
8. Kato H, Takahasi K, Fujita T. RIG-I-like receptors: cytoplasmic sensors for non-self RNA. *Immunological Reviews* 2011, **243**(1)**:** 91-98.
9. Keating SE, Baran M, Bowie AG. Cytosolic DNA sensors regulating type I interferon induction. *Trends in immunology* 2011, **32**(12)**:** 574-581.
10. Takeuchi O, Akira S. Pattern recognition receptors and inflammation. *Cell* 2010, **140**(6)**:** 805-820.
11. Schroder K, Tschopp J. The inflammasomes. *Cell* 2010, **140**(6)**:** 821-832.
12. Anderson KV, Jürgens G, Nüsslein-Volhard C. Establishment of dorsal-ventral polarity in the Drosophila embryo: Genetic studies on the role of the Toll gene product. *Cell* 1985, **42**(3)**:** 779-789.
13. Poltorak A. Defective LPS Signaling in C3H/HeJ and C57BL/10ScCr Mice: Mutations in Tlr4 Gene. *Science* 1998, **282**(5396)**:** 2085-2088.
14. O'Neill LA, Golenbock D, Bowie AG. The history of Toll-like receptors - redefining innate immunity. *Nature reviews Immunology* 2013, **13**(6)**:** 453-460.
15. Kawai T, Akira S. The role of pattern-recognition receptors in innate immunity: update on Toll-like receptors. *Nature immunology* 2010, **11**(5)**:** 373-384.
16. Broz P, Monack DM. Newly described pattern recognition receptors team up against intracellular pathogens. *Nature reviews Immunology* 2013, **13**(8)**:** 551-565.
17. Takeuchi O, Kaufmann A, Grote K, Kawai T, Hoshino K, Morr M, Mühlradt PF, Akira S. Cutting Edge: Preferentially the R-Stereoisomer of the Mycoplasmal Lipopeptide Macrophage-Activating Lipopeptide-2 Activates Immune Cells Through a Toll-Like Receptor 2- and MyD88-Dependent Signaling Pathway. *The Journal of Immunology* 2000, **164**(2)**:** 554-557.
18. Gantner BN, Simmons RM, Canavera SJ, Akira S, Underhill DM. Collaborative induction of inflammatory responses by dectin-1 and Toll-like receptor 2. *The Journal of experimental medicine* 2003, **197**(9)**:** 1107-1117.
19. Takeuchi O, Kawai T, Mühlradt PF, Morr M, Radolf JD, Zychlinsky A, Takeda K, Akira S. Discrimination of bacterial lipoproteins by Toll-like receptor 6. *International immunology* 2001, **13**(7)**:** 933-940.
20. Hayashi F, Smith KD, Ozinsky A, Hawn TR, Yi EC, Goodlett DR, Eng JK, Akira S, Underhill DM, Aderem A. The innate immune response to bacterial flagellin is mediated by Toll-like receptor 5. *Nature* 2001, **410**(6832)**:** 1099-1103.
21. Alexopoulou L, Holt AC, Medzhitov R, Flavell RA. Recognition of double-stranded RNA and activation of NF-[kappa]B by Toll-like receptor 3. *Nature* 2001, **413**(6857)**:** 732-738.
22. Diebold SS, Kaisho T, Hemmi H, Akira S, Reis e Sousa C. Innate antiviral responses by means of TLR7-mediated recognition of single-stranded RNA. *Science* 2004, **303**(5663)**:** 1529-1531.

23. Heil F, Hemmi H, Hochrein H, Ampenberger F, Kirschning C, Akira S, Lipford G, Wagner H, Bauer S. Species-specific recognition of single-stranded RNA via toll-like receptor 7 and 8. *Science* 2004, **303**(5663)**:** 1526-1529.
24. Hemmi H, Takeuchi O, Kawai T, Kaisho T, Sato S, Sanjo H, Matsumoto M, Hoshino K, Wagner H, Takeda K, Akira S. A Toll-like receptor recognizes bacterial DNA. *Nature* 2000, **408**(6813)**:** 740-745.
25. Oldenburg M, Kruger A, Ferstl R, Kaufmann A, Nees G, Sigmund A, Bathke B, Lauterbach H, Suter M, Dreher S, Koedel U, Akira S, Kawai T, Buer J*, et al.* TLR13 recognizes bacterial 23S rRNA devoid of erythromycin resistance-forming modification. *Science* 2012, **337**(6098)**:** 1111-1115.
26. Liu L, Botos I, Wang Y, Leonard JN, Shiloach J, Segal DM, Davies DR. Structural Basis of Toll-Like Receptor 3 Signaling with Double-Stranded RNA. *Science* 2008, **320**(5874)**:** 379-381.
27. Lu J, Sun PD. The structure of the TLR5-flagellin complex: a new mode of pathogen detection, conserved receptor dimerization for signaling. *Science signaling* 2012, **5**(216)**:** pe11.
28. Park BS, Song DH, Kim HM, Choi BS, Lee H, Lee JO. The structural basis of lipopolysaccharide recognition by the TLR4-MD-2 complex. *Nature* 2009, **458**(7242)**:** 1191-1195.
29. Tanji H, Ohto U, Shibata T, Miyake K, Shimizu T. Structural Reorganization of the Toll-Like Receptor 8 Dimer Induced by Agonistic Ligands. *Science* 2013, **339**(6126)**:** 1426-1429.
30. Jin MS, Lee JO. Structures of the toll-like receptor family and its ligand complexes. *Immunity* 2008, **29**(2)**:** 182-191.
31. Jin MS, Kim SE, Heo JY, Lee ME, Kim HM, Paik SG, Lee H, Lee JO. Crystal structure of the TLR1-TLR2 heterodimer induced by binding of a tri-acylated lipopeptide. *Cell* 2007, **130**(6)**:** 1071-1082.
32. Kang JY, Nan X, Jin MS, Youn SJ, Ryu YH, Mah S, Han SH, Lee H, Paik SG, Lee JO. Recognition of lipopeptide patterns by Toll-like receptor 2-Toll-like receptor 6 heterodimer. *Immunity* 2009, **31**(6)**:** 873-884.
33. Ozinsky A, Underhill DM, Fontenot JD, Hajjar AM, Smith KD, Wilson CB, Schroeder L, Aderem A. The repertoire for pattern recognition of pathogens by the innate immune system is defined by cooperation between toll-like receptors. *Proceedings of the National Academy of Sciences of the United States of America* 2000, **97**(25)**:** 13766-13771.
34. Andrade WA, Souza Mdo C, Ramos-Martinez E, Nagpal K, Dutra MS, Melo MB, Bartholomeu DC, Ghosh S, Golenbock DT, Gazzinelli RT. Combined action of nucleic acid-sensing Toll-like receptors and TLR11/TLR12 heterodimers imparts resistance to Toxoplasma gondii in mice. *Cell host & microbe* 2013, **13**(1)**:** 42-53.
35. O'Neill LA, Bowie AG. The family of five: TIR-domain-containing adaptors in Toll-like receptor signalling. *Nature reviews Immunology* 2007, **7**(5)**:** 353-364.
36. Barbalat R, Lau L, Locksley RM, Barton GM. Toll-like receptor 2 on inflammatory monocytes induces type I interferon in response to viral but not bacterial ligands. *Nature immunology* 2009, **10**(11)**:** 1200-1207.
37. Kagan JC, Su T, Horng T, Chow A, Akira S, Medzhitov R. TRAM couples endocytosis of Toll-like receptor 4 to the induction of interferon-beta. *Nature immunology* 2008, **9**(4)**:** 361-368.
38. Yamamoto M, Sato S, Hemmi H, Hoshino K, Kaisho T, Sanjo H, Takeuchi O, Sugiyama M, Okabe M, Takeda K, Akira S. Role of adaptor TRIF in the MyD88-independent toll-like receptor signaling pathway. *Science* 2003, **301**(5633)**:** 640-643.
39. Bonham KS, Orzalli MH, Hayashi K, Wolf AI, Glanemann C, Weninger W, Iwasaki A, Knipe DM, Kagan JC. A Promiscuous Lipid-Binding Protein Diversifies the Subcellular Sites of Toll-like Receptor Signal Transduction. *Cell* 2014, **156**(4)**:** 705-716.
40. Leifer CA, Kennedy MN, Mazzoni A, Lee C, Kruhlak MJ, Segal DM. TLR9 Is Localized in the Endoplasmic Reticulum Prior to Stimulation. *The Journal of Immunology* 2004, **173**(2)**:** 1179-1183.

41. Latz E, Schoenemeyer A, Visintin A, Fitzgerald KA, Monks BG, Knetter CF, Lien E, Nilsen NJ, Espevik T, Golenbock DT. TLR9 signals after translocating from the ER to CpG DNA in the lysosome. *Nature immunology* 2004, **5**(2)**:** 190-198.
42. Rigby RE, Webb LM, Mackenzie KJ, Li Y, Leitch A, Reijns MAM, Lundie RJ, Revuelta A, Davidson DJ, Diebold S, Modis Y, MacDonald AS, Jackson AP. RNA:DNA hybrids are a novel molecular pattern sensed by TLR9. *The EMBO journal* 2014, **33**(6)**:** 542-558.
43. Barton GM, Kagan JC, Medzhitov R. Intracellular localization of Toll-like receptor 9 prevents recognition of self DNA but facilitates access to viral DNA. *Nature immunology* 2006, **7**(1)**:** 49-56.
44. Mouchess ML, Arpaia N, Souza G, Barbalat R, Ewald SE, Lau L, Barton GM. Transmembrane mutations in Toll-like receptor 9 bypass the requirement for ectodomain proteolysis and induce fatal inflammation. *Immunity* 2011, **35**(5)**:** 721-732.
45. Subramanian S, Tus K, Li QZ, Wang A, Tian XH, Zhou J, Liang C, Bartov G, McDaniel LD, Zhou XJ, Schultz RA, Wakeland EK. A Tlr7 translocation accelerates systemic autoimmunity in murine lupus. *Proceedings of the National Academy of Sciences of the United States of America* 2006, **103**(26)**:** 9970-9975.
46. Pisitkun P, Deane JA, Difilippantonio MJ, Tarasenko T, Satterthwaite AB, Bolland S. Autoreactive B cell responses to RNA-related antigens due to TLR7 gene duplication. *Science* 2006, **312**(5780)**:** 1669-1672.
47. Deane JA, Pisitkun P, Barrett RS, Feigenbaum L, Town T, Ward JM, Flavell RA, Bolland S. Control of toll-like receptor 7 expression is essential to restrict autoimmunity and dendritic cell proliferation. *Immunity* 2007, **27**(5)**:** 801-810.
48. Funami K, Matsumoto M, Oshiumi H, Akazawa T, Yamamoto A, Seya T. The cytoplasmic 'linker region' in Toll-like receptor 3 controls receptor localization and signaling. *International immunology* 2004, **16**(8)**:** 1143-1154.
49. Nishiya T, Kajita E, Miwa S, Defranco AL. TLR3 and TLR7 are targeted to the same intracellular compartments by distinct regulatory elements. *The Journal of biological chemistry* 2005, **280**(44)**:** 37107-37117.
50. Kajita E, Nishiya T, Miwa S. The transmembrane domain directs TLR9 to intracellular compartments that contain TLR3. *Biochemical and biophysical research communications* 2006, **343**(2)**:** 578-584.
51. Leifer CA, Brooks JC, Hoelzer K, Lopez J, Kennedy MN, Mazzoni A, Segal DM. Cytoplasmic targeting motifs control localization of toll-like receptor 9. *The Journal of biological chemistry* 2006, **281**(46)**:** 35585-35592.
52. Tabeta K, Hoebe K, Janssen EM, Du X, Georgel P, Crozat K, Mudd S, Mann N, Sovath S, Goode J, Shamel L, Herskovits AA, Portnoy DA, Cooke M*, et al.* The Unc93b1 mutation 3d disrupts exogenous antigen presentation and signaling via Toll-like receptors 3, 7 and 9. *Nature immunology* 2006, **7**(2)**:** 156-164.
53. Casrouge A, Zhang SY, Eidenschenk C, Jouanguy E, Puel A, Yang K, Alcais A, Picard C, Mahfoufi N, Nicolas N, Lorenzo L, Plancoulaine S, Senechal B, Geissmann F*, et al.* Herpes simplex virus encephalitis in human UNC-93B deficiency. *Science* 2006, **314**(5797)**:** 308-312.
54. Brinkmann MM, Spooner E, Hoebe K, Beutler B, Ploegh HL, Kim YM. The interaction between the ER membrane protein UNC93B and TLR3, 7, and 9 is crucial for TLR signaling. *The Journal of cell biology* 2007, **177**(2)**:** 265-275.
55. Kim YM, Brinkmann MM, Paquet ME, Ploegh HL. UNC93B1 delivers nucleotide-sensing toll-like receptors to endolysosomes. *Nature* 2008, **452**(7184)**:** 234-238.
56. Lee BL, Moon JE, Shu JH, Yuan L, Newman ZR, Schekman R, Barton GM. UNC93B1 mediates differential trafficking of endosomal TLRs. *eLife Sciences* 2013, **2**.
57. Pifer R, Benson A, Sturge CR, Yarovinsky F. UNC93B1 is essential for TLR11 activation and IL-12-dependent host resistance to Toxoplasma gondii. *The Journal of biological chemistry* 2011, **286**(5)**:** 3307-3314.
58. Shi Z, Cai Z, Sanchez A, Zhang T, Wen S, Wang J, Yang J, Fu S, Zhang D. A novel Toll-like receptor that recognizes vesicular stomatitis virus. *The Journal of biological chemistry* 2011, **286**(6)**:** 4517-4524.

59. Koblansky AA, Jankovic D, Oh H, Hieny S, Sungnak W, Mathur R, Hayden MS, Akira S, Sher A, Ghosh S. Recognition of profilin by Toll-like receptor 12 is critical for host resistance to Toxoplasma gondii. *Immunity* 2013, **38**(1)**:** 119-130.
60. Fukui R, Saitoh S, Matsumoto F, Kozuka-Hata H, Oyama M, Tabeta K, Beutler B, Miyake K. Unc93B1 biases Toll-like receptor responses to nucleic acid in dendritic cells toward DNA- but against RNA-sensing. *The Journal of experimental medicine* 2009, **206**(6)**:** 1339-1350.
61. Fukui R, Saitoh S, Kanno A, Onji M, Shibata T, Ito A, Onji M, Matsumoto M, Akira S, Yoshida N, Miyake K. Unc93B1 restricts systemic lethal inflammation by orchestrating Toll-like receptor 7 and 9 trafficking. *Immunity* 2011, **35**(1)**:** 69-81.
62. Chockalingam A, Brooks JC, Cameron JL, Blum LK, Leifer CA. TLR9 traffics through the Golgi complex to localize to endolysosomes and respond to CpG DNA. *Immunology and cell biology* 2009, **87**(3)**:** 209-217.
63. Kim J, Huh J, Hwang M, Kwon E-H, Jung D-J, Brinkmann MM, Jang MH, Ploegh HL, Kim Y-M. Acidic Amino Acid Residues in the Juxtamembrane Region of the Nucleotide-Sensing TLRs Are Important for UNC93B1 Binding and Signaling. *The Journal of Immunology* 2013.
64. Onji M, Kanno A, Saitoh S, Fukui R, Motoi Y, Shibata T, Matsumoto F, Lamichhane A, Sato S, Kiyono H, Yamamoto K, Miyake K. An essential role for the N-terminal fragment of Toll-like receptor 9 in DNA sensing. *Nature communications* 2013, **4:** 1949.
65. Guerrier T, Pochard P, Lahiri A, Youinou P, Pers JO, Jamin C. TLR9 expressed on plasma membrane acts as a negative regulator of human B cell response. *Journal of autoimmunity* 2014.
66. Lindau D, Mussard J, Wagner BJ, Ribon M, Ronnefarth VM, Quettier M, Jelcic I, Boissier MC, Rammensee HG, Decker P. Primary blood neutrophils express a functional cell surface Toll-like receptor 9. *European journal of immunology* 2013, **43**(8)**:** 2101-2113.
67. Yang Y, Liu B, Dai J, Srivastava PK, Zammit DJ, Lefrancois L, Li Z. Heat shock protein gp96 is a master chaperone for toll-like receptors and is important in the innate function of macrophages. *Immunity* 2007, **26**(2)**:** 215-226.
68. Takahashi K, Shibata T, Akashi-Takamura S, Kiyokawa T, Wakabayashi Y, Tanimura N, Kobayashi T, Matsumoto F, Fukui R, Kouro T, Nagai Y, Takatsu K, Saitoh S, Miyake K. A protein associated with Toll-like receptor (TLR) 4 (PRAT4A) is required for TLR-dependent immune responses. *The Journal of experimental medicine* 2007, **204**(12)**:** 2963-2976.
69. Lee CC, Avalos AM, Ploegh HL. Accessory molecules for Toll-like receptors and their function. *Nature reviews Immunology* 2012, **12**(3)**:** 168-179.
70. Chiang CY, Engel A, Opaluch AM, Ramos I, Maestre AM, Secundino I, De Jesus PD, Nguyen QT, Welch G, Bonamy GM, Miraglia LJ, Orth AP, Nizet V, Fernandez-Sesma A*, et al.* Cofactors required for TLR7- and TLR9-dependent innate immune responses. *Cell host & microbe* 2012, **11**(3)**:** 306-318.
71. Park B, Brinkmann MM, Spooner E, Lee CC, Kim YM, Ploegh HL. Proteolytic cleavage in an endolysosomal compartment is required for activation of Toll-like receptor 9. *Nature immunology* 2008, **9**(12)**:** 1407-1414.
72. Ewald SE, Lee BL, Lau L, Wickliffe KE, Shi GP, Chapman HA, Barton GM. The ectodomain of Toll-like receptor 9 is cleaved to generate a functional receptor. *Nature* 2008, **456**(7222)**:** 658-662.
73. Ewald SE, Engel A, Lee J, Wang M, Bogyo M, Barton GM. Nucleic acid recognition by Toll-like receptors is coupled to stepwise processing by cathepsins and asparagine endopeptidase. *The Journal of experimental medicine* 2011, **208**(4)**:** 643-651.
74. Avalos AM, Kirak O, Oelkers JM, Pils MC, Kim YM, Ottinger M, Jaenisch R, Ploegh HL, Brinkmann MM. Cell-specific TLR9 trafficking in primary APCs of transgenic TLR9-GFP mice. *Journal of immunology* 2013, **190**(2)**:** 695-702.
75. Latz E, Verma A, Visintin A, Gong M, Sirois CM, Klein DC, Monks BG, McKnight CJ, Lamphier MS, Duprex WP, Espevik T, Golenbock DT. Ligand-induced conformational changes allosterically activate Toll-like receptor 9. *Nature immunology* 2007, **8**(7)**:** 772-779.

76. Garcia-Cattaneo A, Gobert FX, Muller M, Toscano F, Flores M, Lescure A, Del Nery E, Benaroch P. Cleavage of Toll-like receptor 3 by cathepsins B and H is essential for signaling. *Proceedings of the National Academy of Sciences* 2012, **109**(23)**:** 9053-9058.
77. Qi R, Singh D, Kao CC. Proteolytic Processing Regulates Toll-like Receptor 3 Stability and Endosomal Localization. *Journal of Biological Chemistry* 2012, **287**(39)**:** 32617-32629.
78. Lee BL, Barton GM. Trafficking of endosomal Toll-like receptors. *Trends in cell biology* 2014.
79. Sepulveda FE, Maschalidi S, Colisson R, Heslop L, Ghirelli C, Sakka E, Lennon-Dumenil AM, Amigorena S, Cabanie L, Manoury B. Critical role for asparagine endopeptidase in endocytic Toll-like receptor signaling in dendritic cells. *Immunity* 2009, **31**(5)**:** 737-748.
80. Peter ME, Kubarenko AV, Weber AN, Dalpke AH. Identification of an N-terminal recognition site in TLR9 that contributes to CpG-DNA-mediated receptor activation. *Journal of immunology* 2009, **182**(12)**:** 7690-7697.
81. Fukuda K, Watanabe T, Tokisue T, Tsujita T, Nishikawa S, Hasegawa T, Seya T, Matsumoto M. Modulation of double-stranded RNA recognition by the N-terminal histidine-rich region of the human toll-like receptor 3. *The Journal of biological chemistry* 2008, **283**(33)**:** 22787-22794.
82. Toscano F, Estornes Y, Virard F, Garcia-Cattaneo A, Pierrot A, Vanbervliet B, Bonnin M, Ciancanelli MJ, Zhang SY, Funami K, Seya T, Matsumoto M, Pin JJ, Casanova JL*, et al.* Cleaved/associated TLR3 represents the primary form of the signaling receptor. *Journal of immunology* 2013, **190**(2)**:** 764-773.
83. Honda K, Ohba Y, Yanai H, Negishi H, Mizutani T, Takaoka A, Taya C, Taniguchi T. Spatiotemporal regulation of MyD88-IRF-7 signalling for robust type-I interferon induction. *Nature* 2005, **434**(7036)**:** 1035-1040.
84. Kerkmann M, Rothenfusser S, Hornung V, Towarowski A, Wagner M, Sarris A, Giese T, Endres S, Hartmann G. Activation with CpG-A and CpG-B Oligonucleotides Reveals Two Distinct Regulatory Pathways of Type I IFN Synthesis in Human Plasmacytoid Dendritic Cells. *The Journal of Immunology* 2003, **170**(9)**:** 4465-4474.
85. Guiducci C, Ott G, Chan JH, Damon E, Calacsan C, Matray T, Lee KD, Coffman RL, Barrat FJ. Properties regulating the nature of the plasmacytoid dendritic cell response to Toll-like receptor 9 activation. *The Journal of experimental medicine* 2006, **203**(8)**:** 1999-2008.
86. Vollmer J, Weeratna R, Payette P, Jurk M, Schetter C, Laucht M, Wader T, Tluk S, Liu M, Davis HL, Krieg AM. Characterization of three CpG oligodeoxynucleotide classes with distinct immunostimulatory activities. *European journal of immunology* 2004, **34**(1)**:** 251-262.
87. Kim S, Kaiser V, Beier E, Bechheim M, Guenthner-Biller M, Ablasser A, Berger M, Endres S, Hartmann G, Hornung V. Self-priming determines high type I IFN production by plasmacytoid dendritic cells. *European journal of immunology* 2014, **44**(3)**:** 807-818.
88. Sasai M, Linehan MM, Iwasaki A. Bifurcation of Toll-like receptor 9 signaling by adaptor protein 3. *Science* 2010, **329**(5998)**:** 1530-1534.
89. Blasius AL, Arnold CN, Georgel P, Rutschmann S, Xia Y, Lin P, Ross C, Li X, Smart NG, Beutler B. Slc15a4, AP-3, and Hermansky-Pudlak syndrome proteins are required for Toll-like receptor signaling in plasmacytoid dendritic cells. *Proceedings of the National Academy of Sciences of the United States of America* 2010, **107**(46)**:** 19973-19978.
90. Paludan SR, Bowie AG, Horan KA, Fitzgerald KA. Recognition of herpesviruses by the innate immune system. *Nature reviews Immunology* 2011, **11**(2)**:** 143-154.
91. Szomolanyi-Tsuda E, Liang X, Welsh RM, Kurt-Jones EA, Finberg RW. Role for TLR2 in NK cell-mediated control of murine cytomegalovirus in vivo. *J Virol* 2006, **80**(9)**:** 4286-4291.
92. Krug A, French AR, Barchet W, Fischer JA, Dzionek A, Pingel JT, Orihuela MM, Akira S, Yokoyama WM, Colonna M. TLR9-dependent recognition of MCMV by IPC and DC generates coordinated cytokine responses that activate antiviral NK cell function. *Immunity* 2004, **21**(1)**:** 107-119.

93. Tabeta K, Georgel P, Janssen E, Du X, Hoebe K, Crozat K, Mudd S, Shamel L, Sovath S, Goode J, Alexopoulou L, Flavell RA, Beutler B. Toll-like receptors 9 and 3 as essential components of innate immune defense against mouse cytomegalovirus infection. *Proceedings of the National Academy of Sciences of the United States of America* 2004, **101**(10)**:** 3516-3521.
94. Zucchini N, Bessou G, Traub S, Robbins SH, Uematsu S, Akira S, Alexopoulou L, Dalod M. Cutting Edge: Overlapping Functions of TLR7 and TLR9 for Innate Defense against a Herpesvirus Infection. *The Journal of Immunology* 2008, **180**(9)**:** 5799-5803.
95. Michaud F, Coulombe F, Gaudreault É, Kriz J, Gosselin J. Involvement of TLR2 in Recognition of Acute Gammaherpesvirus-68 Infection. *PloS one* 2010, **5**(10)**:** e13742.
96. Guggemoos S, Hangel D, Hamm S, Heit A, Bauer S, Adler H. TLR9 Contributes to Antiviral Immunity during Gammaherpesvirus Infection. *The Journal of Immunology* 2008, **180**(1)**:** 438-443.
97. Satoh T, Kato H, Kumagai Y, Yoneyama M, Sato S, Matsushita K, Tsujimura T, Fujita T, Akira S, Takeuchi O. LGP2 is a positive regulator of RIG-I- and MDA5-mediated antiviral responses. *Proceedings of the National Academy of Sciences of the United States of America* 2010, **107**(4)**:** 1512-1517.
98. Kawai T, Takahashi K, Sato S, Coban C, Kumar H, Kato H, Ishii KJ, Takeuchi O, Akira S. IPS-1, an adaptor triggering RIG-I- and Mda5-mediated type I interferon induction. *Nature immunology* 2005, **6**(10)**:** 981-988.
99. Zhu Z, Zhang X, Wang G, Zheng H. The Laboratory of Genetics and Physiology 2: Emerging Insights into the Controversial Functions of This RIG-I-Like Receptor. *BioMed research international* 2014, **2014:** 960190.
100. Pichlmair A, Schulz O, Tan CP, Naslund TI, Liljestrom P, Weber F, Reis e Sousa C. RIG-I-mediated antiviral responses to single-stranded RNA bearing 5'-phosphates. *Science* 2006, **314**(5801)**:** 997-1001.
101. Kato H, Takeuchi O, Mikamo-Satoh E, Hirai R, Kawai T, Matsushita K, Hiiragi A, Dermody TS, Fujita T, Akira S. Length-dependent recognition of double-stranded ribonucleic acids by retinoic acid-inducible gene-I and melanoma differentiation-associated gene 5. *The Journal of experimental medicine* 2008, **205**(7)**:** 1601-1610.
102. Ablasser A, Bauernfeind F, Hartmann G, Latz E, Fitzgerald KA, Hornung V. RIG-I-dependent sensing of poly(dA:dT) through the induction of an RNA polymerase III-transcribed RNA intermediate. *Nature immunology* 2009, **10**(10)**:** 1065-1072.
103. Chiu YH, Macmillan JB, Chen ZJ. RNA polymerase III detects cytosolic DNA and induces type I interferons through the RIG-I pathway. *Cell* 2009, **138**(3)**:** 576-591.
104. Kato H, Sato S, Yoneyama M, Yamamoto M, Uematsu S, Matsui K, Tsujimura T, Takeda K, Fujita T, Takeuchi O, Akira S. Cell type-specific involvement of RIG-I in antiviral response. *Immunity* 2005, **23**(1)**:** 19-28.
105. Kato H, Takeuchi O, Sato S, Yoneyama M, Yamamoto M, Matsui K, Uematsu S, Jung A, Kawai T, Ishii KJ, Yamaguchi O, Otsu K, Tsujimura T, Koh CS*, et al.* Differential roles of MDA5 and RIG-I helicases in the recognition of RNA viruses. *Nature* 2006, **441**(7089)**:** 101-105.
106. Luber CA, Cox J, Lauterbach H, Fancke B, Selbach M, Tschopp J, Akira S, Wiegand M, Hochrein H, O'Keeffe M, Mann M. Quantitative proteomics reveals subset-specific viral recognition in dendritic cells. *Immunity* 2010, **32**(2)**:** 279-289.
107. Stetson DB, Medzhitov R. Recognition of cytosolic DNA activates an IRF3-dependent innate immune response. *Immunity* 2006, **24**(1)**:** 93-103.
108. Ishii KJ, Coban C, Kato H, Takahashi K, Torii Y, Takeshita F, Ludwig H, Sutter G, Suzuki K, Hemmi H, Sato S, Yamamoto M, Uematsu S, Kawai T*, et al.* A Toll-like receptor-independent antiviral response induced by double-stranded B-form DNA. *Nature immunology* 2006, **7**(1)**:** 40-48.
109. Takaoka A, Wang Z, Choi MK, Yanai H, Negishi H, Ban T, Lu Y, Miyagishi M, Kodama T, Honda K, Ohba Y, Taniguchi T. DAI (DLM-1/ZBP1) is a cytosolic DNA sensor and an activator of innate immune response. *Nature* 2007, **448**(7152)**:** 501-505.
110. Ishii KJ, Kawagoe T, Koyama S, Matsui K, Kumar H, Kawai T, Uematsu S, Takeuchi O, Takeshita F, Coban C, Akira S. TANK-binding kinase-1 delineates innate and adaptive immune responses to DNA vaccines. *Nature* 2008, **451**(7179)**:** 725-729.

111. Upton JW, Kaiser WJ, Mocarski ES. DAI/ZBP1/DLM-1 complexes with RIP3 to mediate virus-induced programmed necrosis that is targeted by murine cytomegalovirus vIRA. *Cell host & microbe* 2012, **11**(3)**:** 290-297.
112. Ishikawa H, Barber GN. STING is an endoplasmic reticulum adaptor that facilitates innate immune signalling. *Nature* 2008, **455**(7213)**:** 674-678.
113. Zhong B, Yang Y, Li S, Wang YY, Li Y, Diao F, Lei C, He X, Zhang L, Tien P, Shu HB. The adaptor protein MITA links virus-sensing receptors to IRF3 transcription factor activation. *Immunity* 2008, **29**(4)**:** 538-550.
114. Jin L, Waterman PM, Jonscher KR, Short CM, Reisdorph NA, Cambier JC. MPYS, a novel membrane tetraspanner, is associated with major histocompatibility complex class II and mediates transduction of apoptotic signals. *Molecular and cellular biology* 2008, **28**(16)**:** 5014-5026.
115. Sun W, Li Y, Chen L, Chen H, You F, Zhou X, Zhou Y, Zhai Z, Chen D, Jiang Z. ERIS, an endoplasmic reticulum IFN stimulator, activates innate immune signaling through dimerization. *Proceedings of the National Academy of Sciences of the United States of America* 2009, **106**(21)**:** 8653-8658.
116. Tanaka Y, Chen ZJ. STING specifies IRF3 phosphorylation by TBK1 in the cytosolic DNA signaling pathway. *Science signaling* 2012, **5**(214)**:** ra20.
117. Ishikawa H, Ma Z, Barber GN. STING regulates intracellular DNA-mediated, type I interferon-dependent innate immunity. *Nature* 2009, **461**(7265)**:** 788-792.
118. Sun L, Wu J, Du F, Chen X, Chen ZJ. Cyclic GMP-AMP synthase is a cytosolic DNA sensor that activates the type I interferon pathway. *Science* 2013, **339**(6121)**:** 786-791.
119. Wu J, Sun L, Chen X, Du F, Shi H, Chen C, Chen ZJ. Cyclic GMP-AMP Is an Endogenous Second Messenger in Innate Immune Signaling by Cytosolic DNA. *Science* 2012, **339**(6121)**:** 826-830.
120. Ablasser A, Schmid-Burgk JL, Hemmerling I, Horvath GL, Schmidt T, Latz E, Hornung V. Cell intrinsic immunity spreads to bystander cells via the intercellular transfer of cGAMP. *Nature* 2013, **503**(7477)**:** 530-534.
121. Ahn J, Gutman D, Saijo S, Barber GN. STING manifests self DNA-dependent inflammatory disease. *Proceedings of the National Academy of Sciences* 2012, **109**(47)**:** 19386-19391.
122. Gall A, Treuting P, Elkon KB, Loo YM, Gale M, Jr., Barber GN, Stetson DB. Autoimmunity initiates in nonhematopoietic cells and progresses via lymphocytes in an interferon-dependent autoimmune disease. *Immunity* 2012, **36**(1)**:** 120-131.
123. Saitoh T, Fujita N, Hayashi T, Takahara K, Satoh T, Lee H, Matsunaga K, Kageyama S, Omori H, Noda T, Yamamoto N, Kawai T, Ishii K, Takeuchi O*, et al.* Atg9a controls dsDNA-driven dynamic translocation of STING and the innate immune response. *Proceedings of the National Academy of Sciences of the United States of America* 2009, **106**(49)**:** 20842-20846.
124. Konno H, Konno K, Barber GN. Cyclic dinucleotides trigger ULK1 (ATG1) phosphorylation of STING to prevent sustained innate immune signaling. *Cell* 2013, **155**(3)**:** 688-698.
125. Hornung V, Ablasser A, Charrel-Dennis M, Bauernfeind F, Horvath G, Caffrey DR, Latz E, Fitzgerald KA. AIM2 recognizes cytosolic dsDNA and forms a caspase-1-activating inflammasome with ASC. *Nature* 2009, **458**(7237)**:** 514-518.
126. Fernandes-Alnemri T, Yu JW, Datta P, Wu J, Alnemri ES. AIM2 activates the inflammasome and cell death in response to cytoplasmic DNA. *Nature* 2009, **458**(7237)**:** 509-513.
127. Burckstummer T, Baumann C, Bluml S, Dixit E, Durnberger G, Jahn H, Planyavsky M, Bilban M, Colinge J, Bennett KL, Superti-Furga G. An orthogonal proteomic-genomic screen identifies AIM2 as a cytoplasmic DNA sensor for the inflammasome. *Nature immunology* 2009, **10**(3)**:** 266-272.
128. Roberts TL, Idris A, Dunn JA, Kelly GM, Burnton CM, Hodgson S, Hardy LL, Garceau V, Sweet MJ, Ross IL, Hume DA, Stacey KJ. HIN-200 Proteins Regulate Caspase Activation in Response to Foreign Cytoplasmic DNA. *Science* 2009, **323**(5917)**:** 1057-1060.

129. Unterholzner L, Keating SE, Baran M, Horan KA, Jensen SB, Sharma S, Sirois CM, Jin T, Latz E, Xiao TS, Fitzgerald KA, Paludan SR, Bowie AG. IFI16 is an innate immune sensor for intracellular DNA. *Nature immunology* 2010, **11**(11)**:** 997-1004.
130. Rathinam VA, Jiang Z, Waggoner SN, Sharma S, Cole LE, Waggoner L, Vanaja SK, Monks BG, Ganesan S, Latz E, Hornung V, Vogel SN, Szomolanyi-Tsuda E, Fitzgerald KA. The AIM2 inflammasome is essential for host defense against cytosolic bacteria and DNA viruses. *Nature immunology* 2010, **11**(5)**:** 395-402.
131. Kerur N, Veettil MV, Sharma-Walia N, Bottero V, Sadagopan S, Otageri P, Chandran B. IFI16 acts as a nuclear pathogen sensor to induce the inflammasome in response to Kaposi Sarcoma-associated herpesvirus infection. *Cell host & microbe* 2011, **9**(5)**:** 363-375.
132. Zhang Z, Yuan B, Bao M, Lu N, Kim T, Liu YJ. The helicase DDX41 senses intracellular DNA mediated by the adaptor STING in dendritic cells. *Nature immunology* 2011, **12**(10)**:** 959-965.
133. Parvatiyar K, Zhang Z, Teles RM, Ouyang S, Jiang Y, Iyer SS, Zaver SA, Schenk M, Zeng S, Zhong W, Liu ZJ, Modlin RL, Liu YJ, Cheng G. The helicase DDX41 recognizes the bacterial secondary messengers cyclic di-GMP and cyclic di-AMP to activate a type I interferon immune response. *Nature immunology* 2012, **13**(12)**:** 1155-1161.
134. Kim T, Pazhoor S, Bao M, Zhang Z, Hanabuchi S, Facchinetti V, Bover L, Plumas J, Chaperot L, Qin J, Liu YJ. Aspartate-glutamate-alanine-histidine box motif (DEAH)/RNA helicase A helicases sense microbial DNA in human plasmacytoid dendritic cells. *Proceedings of the National Academy of Sciences of the United States of America* 2010, **107**(34)**:** 15181-15186.
135. Yang P, An H, Liu X, Wen M, Zheng Y, Rui Y, Cao X. The cytosolic nucleic acid sensor LRRFIP1 mediates the production of type I interferon via a beta-catenin-dependent pathway. *Nature immunology* 2010, **11**(6)**:** 487-494.
136. Zhang X, Brann TW, Zhou M, Yang J, Oguariri RM, Lidie KB, Imamichi H, Huang DW, Lempicki RA, Baseler MW, Veenstra TD, Young HA, Lane HC, Imamichi T. Cutting edge: Ku70 is a novel cytosolic DNA sensor that induces type III rather than type I IFN. *Journal of immunology* 2011, **186**(8)**:** 4541-4545.
137. Ferguson BJ, Mansur DS, Peters NE, Ren H, Smith GL, Medzhitov R. DNA-PK is a DNA sensor for IRF-3-dependent innate immunity. *eLife* 2012, **1**.
138. Kondo T, Kobayashi J, Saitoh T, Maruyama K, Ishii KJ, Barber GN, Komatsu K, Akira S, Kawai T. DNA damage sensor MRE11 recognizes cytosolic double-stranded DNA and induces type I interferon by regulating STING trafficking. *Proceedings of the National Academy of Sciences of the United States of America* 2013, **110**(8)**:** 2969-2974.
139. Paludan SR, Bowie AG. Immune sensing of DNA. *Immunity* 2013, **38**(5)**:** 870-880.
140. Okabe Y, Kawane K, Akira S, Taniguchi T, Nagata S. Toll-like receptor-independent gene induction program activated by mammalian DNA escaped from apoptotic DNA degradation. *The Journal of experimental medicine* 2005, **202**(10)**:** 1333-1339.
141. Stetson DB, Ko JS, Heidmann T, Medzhitov R. Trex1 prevents cell-intrinsic initiation of autoimmunity. *Cell* 2008, **134**(4)**:** 587-598.
142. Crow YJ, Hayward BE, Parmar R, Robins P, Leitch A, Ali M, Black DN, van Bokhoven H, Brunner HG, Hamel BC, Corry PC, Cowan FM, Frints SG, Klepper J*, et al.* Mutations in the gene encoding the 3′-5′ DNA exonuclease TREX1 cause Aicardi-Goutières syndrome at the AGS1 locus. *Nature Genetics* 2006, **38**(8)**:** 917-920.
143. Lee-Kirsch MA, Gong M, Chowdhury D, Senenko L, Engel K, Lee YA, de Silva U, Bailey SL, Witte T, Vyse TJ, Kere J, Pfeiffer C, Harvey S, Wong A*, et al.* Mutations in the gene encoding the 3'-5' DNA exonuclease TREX1 are associated with systemic lupus erythematosus. *Nat Genet* 2007, **39**(9)**:** 1065-1067.
144. Rice G, Newman WG, Dean J, Patrick T, Parmar R, Flintoff K, Robins P, Harvey S, Hollis T, O'Hara A, Herrick AL, Bowden AP, Perrino FW, Lindahl T*, et al.* Heterozygous mutations in TREX1 cause familial chilblain lupus and dominant Aicardi-Goutieres syndrome. *American journal of human genetics* 2007, **80**(4)**:** 811-815.
145. Yang YG, Lindahl T, Barnes DE. Trex1 exonuclease degrades ssDNA to prevent chronic checkpoint activation and autoimmune disease. *Cell* 2007, **131**(5)**:** 873-886.

146. Yan N, Regalado-Magdos AD, Stiggelbout B, Lee-Kirsch MA, Lieberman J. The cytosolic exonuclease TREX1 inhibits the innate immune response to human immunodeficiency virus type 1. *Nature immunology* 2010, **11**(11)**:** 1005-1013.
147. Gehrke N, Mertens C, Zillinger T, Wenzel J, Bald T, Zahn S, Tuting T, Hartmann G, Barchet W. Oxidative damage of DNA confers resistance to cytosolic nuclease TREX1 degradation and potentiates STING-dependent immune sensing. *Immunity* 2013, **39**(3)**:** 482-495.
148. Morita M, Stamp G, Robins P, Dulic A, Rosewell I, Hrivnak G, Daly G, Lindahl T, Barnes DE. Gene-targeted mice lacking the Trex1 (DNase III) 3'-->5' DNA exonuclease develop inflammatory myocarditis. *Molecular and cellular biology* 2004, **24**(15)**:** 6719-6727.
149. Hasan M, Koch J, Rakheja D, Pattnaik AK, Brugarolas J, Dozmorov I, Levine B, Wakeland EK, Lee-Kirsch MA, Yan N. Trex1 regulates lysosomal biogenesis and interferon-independent activation of antiviral genes. *Nature immunology* 2013, **14**(1)**:** 61-71.
150. Pereira-Lopes S, Celhar T, Sans-Fons G, Serra M, Fairhurst AM, Lloberas J, Celada A. The exonuclease Trex1 restrains macrophage proinflammatory activation. *Journal of immunology* 2013, **191**(12)**:** 6128-6135.
151. Xu J, Zoltick PW, Gamero AM, Gallucci S. TLR ligands up-regulate Trex1 expression in murine conventional dendritic cells through type I Interferon and NF-kappaB-dependent signaling pathways. *J Leukoc Biol* 2014.
152. Alonso A, Sasin J, Bottini N, Friedberg I, Friedberg I, Osterman A, Godzik A, Hunter T, Dixon J, Mustelin T. Protein tyrosine phosphatases in the human genome. *Cell* 2004, **117**(6)**:** 699-711.
153. Feldhammer M, Uetani N, Miranda-Saavedra D, Tremblay ML. PTP1B: a simple enzyme for a complex world. *Critical reviews in biochemistry and molecular biology* 2013, **48**(5)**:** 430-445.
154. Frangioni JV, Beahm PH, Shifrin V, Jost CA, Neel BG. The nontransmembrane tyrosine phosphatase PTP-1B localizes to the endoplasmic reticulum via its 35 amino acid C-terminal sequence. *Cell* 1992, **68**(3)**:** 545-560.
155. Woodford-Thomas T, Rhodes J, Dixon J. Expression of a protein tyrosine phosphatase in normal and v-src-transformed mouse 3T3 fibroblasts. *The Journal of cell biology* 1992, **117**(2)**:** 401-414.
156. Frangioni JV, Oda A, Smith M, Salzman EW, Neel BG. Caplpain-catalyzed cleavage and subcellular relocation of protein phosphotyrosine phosphatase 1B (PTP-1B) in human platelets. *Embo J* 1993, **12**(12)**:** 4843-4856.
157. Ferrari E, Tinti M, Costa S, Corallino S, Nardozza AP, Chatraryamontri A, Ceol A, Cesareni G, Castagnoli L. Identification of new substrates of the protein-tyrosine phosphatase PTP1B by Bayesian integration of proteome evidence. *The Journal of biological chemistry* 2011, **286**(6)**:** 4173-4185.
158. Stuible M, Tremblay ML. In control at the ER: PTP1B and the down-regulation of RTKs by dephosphorylation and endocytosis. *Trends in cell biology* 2010, **20**(11)**:** 672-679.
159. Tonks NK, Diltz CD, Fischer EH. Characterization of the major protein-tyrosine-phosphatases of human placenta. *Journal of Biological Chemistry* 1988, **263**(14)**:** 6731-6737.
160. Cicirelli MF, Tonks NK, Diltz CD, Weiel JE, Fischer EH, Krebs EG. Microinjection of a protein-tyrosine-phosphatase inhibits insulin action in Xenopus oocytes. *Proceedings of the National Academy of Sciences* 1990, **87**(14)**:** 5514-5518.
161. Maegawa H, Ide R, Hasegawa M, Ugi S, Egawa K, Iwanishi M, Kikkawa R, Shigeta Y, Kashiwagi A. Thiazolidine Derivatives Ameliorate High Glucose-induced Insulin Resistance via the Normalization of Protein-tyrosine Phosphatase Activities. *Journal of Biological Chemistry* 1995, **270**(13)**:** 7724-7730.
162. Ahmad F, Li P-M, Meyerovitch J, Goldstein BJ. Osmotic Loading of Neutralizing Antibodies Demonstrates a Role for Protein-tyrosine Phosphatase 1B in Negative Regulation of the Insulin Action Pathway. *Journal of Biological Chemistry* 1995, **270**(35)**:** 20503-20508.
163. Chen H, Wertheimer SJ, Lin CH, Katz SL, Amrein KE, Burn P, Quon MJ. Protein-tyrosine Phosphatases PTP1B and Syp Are Modulators of Insulin-stimulated

Translocation of GLUT4 in Transfected Rat Adipose Cells. *Journal of Biological Chemistry* 1997, **272**(12)**:** 8026-8031.

164. Seely BL, Staubs PA, Reichart DR, Berhanu P, Milarski KL, Saltiel AR, Kusari J, Olefsky JM. Protein Tyrosine Phosphatase 1B Interacts With the Activated Insulin Receptor. *Diabetes* 1996, **45**(10)**:** 1379-1385.
165. Bandyopadhyay D, Kusari A, Kenner KA, Liu F, Chernoff J, Gustafson TA, Kusari J. Protein-Tyrosine Phosphatase 1B Complexes with the Insulin Receptor in Vivo and Is Tyrosine-phosphorylated in the Presence of Insulin. *Journal of Biological Chemistry* 1997, **272**(3)**:** 1639-1645.
166. Elchebly M. Increased Insulin Sensitivity and Obesity Resistance in Mice Lacking the Protein Tyrosine Phosphatase-1B Gene. *Science* 1999, **283**(5407)**:** 1544-1548.
167. Klaman LD, Boss O, Peroni OD, Kim JK, Martino JL, Zabolotny JM, Moghal N, Lubkin M, Kim Y-B, Sharpe AH, Stricker-Krongrad A, Shulman GI, Neel BG, Kahn BB. Increased Energy Expenditure, Decreased Adiposity, and Tissue-Specific Insulin Sensitivity in Protein-Tyrosine Phosphatase 1B-Deficient Mice. *Molecular and cellular biology* 2000, **20**(15)**:** 5479-5489.
168. Iversen LF, Moller KB, Pedersen AK, Peters GH, Petersen AS, Andersen HS, Branner S, Mortensen SB, Moller NP. Structure determination of T cell protein-tyrosine phosphatase. *The Journal of biological chemistry* 2002, **277**(22)**:** 19982-19990.
169. Lorenzen JA, Dadabay CY, Fischer EH. COOH-terminal sequence motifs target the T cell protein tyrosine phosphatase to the ER and nucleus. *The Journal of cell biology* 1995, **131**(3)**:** 631-643.
170. Lam MH, Michell BJ, Fodero-Tavoletti MT, Kemp BE, Tonks NK, Tiganis T. Cellular stress regulates the nucleocytoplasmic distribution of the protein-tyrosine phosphatase TCPTP. *The Journal of biological chemistry* 2001, **276**(40)**:** 37700-37707.
171. You-Ten KE, Muise ES, Itié A, Michaliszyn E, Wagner J, Jothy S, Lapp WS, Tremblay ML. Impaired Bone Marrow Microenvironment and Immune Function in T Cell Protein Tyrosine Phosphatase–deficient Mice. *The Journal of experimental medicine* 1997, **186**(5)**:** 683-693.
172. Galic S, Klingler-Hoffmann M, Fodero-Tavoletti MT, Puryer MA, Meng TC, Tonks NK, Tiganis T. Regulation of Insulin Receptor Signaling by the Protein Tyrosine Phosphatase TCPTP. *Molecular and cellular biology* 2003, **23**(6)**:** 2096-2108.
173. Bourdeau A, Dube N, Tremblay ML. Cytoplasmic protein tyrosine phosphatases, regulation and function: the roles of PTP1B and TC-PTP. *Current opinion in cell biology* 2005, **17**(2)**:** 203-209.
174. Heinonen KM, Bourdeau A, Doody KM, Tremblay ML. Protein tyrosine phosphatases PTP-1B and TC-PTP play nonredundant roles in macrophage development and IFN-gamma signaling. *Proceedings of the National Academy of Sciences of the United States of America* 2009, **106**(23)**:** 9368-9372.
175. Tiganis T. PTP1B and TCPTP--nonredundant phosphatases in insulin signaling and glucose homeostasis. *The FEBS journal* 2013, **280**(2)**:** 445-458.
176. Flint AJ, Tiganis T, Barford D, Tonks NK. Development of “substrate-trapping” mutants to identify physiological substrates of protein tyrosine phosphatases. *Proceedings of the National Academy of Sciences* 1997, **94**(5)**:** 1680-1685.
177. Eden ER, Huang F, Sorkin A, Futter CE. The role of EGF receptor ubiquitination in regulating its intracellular traffic. *Traffic* 2012, **13**(2)**:** 329-337.
178. Haj FG, Verveer PJ, Squire A, Neel BG, Bastiaens PI. Imaging sites of receptor dephosphorylation by PTP1B on the surface of the endoplasmic reticulum. *Science* 2002, **295**(5560)**:** 1708-1711.
179. Eden ER, White IJ, Tsapara A, Futter CE. Membrane contacts between endosomes and ER provide sites for PTP1B-epidermal growth factor receptor interaction. *Nature cell biology* 2010, **12**(3)**:** 267-272.
180. Yudushkin IA, Schleifenbaum A, Kinkhabwala A, Neel BG, Schultz C, Bastiaens PI. Live-cell imaging of enzyme-substrate interaction reveals spatial regulation of PTP1B. *Science* 2007, **315**(5808)**:** 115-119.
181. Anderie I, Schulz I, Schmid A. Direct interaction between ER membrane-bound PTP1B and its plasma membrane-anchored targets. *Cellular signalling* 2007, **19**(3)**:** 582-592.

182. Monteleone MC, Gonzalez Wusener AE, Burdisso JE, Conde C, Caceres A, Arregui CO. ER-bound protein tyrosine phosphatase PTP1B interacts with Src at the plasma membrane/substrate interface. *PloS one* 2012, **7**(6)**:** e38948.
183. Lammers R, Bossenmaier B, Cool DE, Tonks NK, Schlessinger J, Fischer EH, Ullrich A. Differential activities of protein tyrosine phosphatases in intact cells. *Journal of Biological Chemistry* 1993, **268**(30)**:** 22456-22462.
184. Stuible M, Abella JV, Feldhammer M, Nossov M, Sangwan V, Blagoev B, Park M, Tremblay ML. PTP1B targets the endosomal sorting machinery: dephosphorylation of regulatory sites on the endosomal sorting complex required for transport component STAM2. *The Journal of biological chemistry* 2010, **285**(31)**:** 23899-23907.
185. Eden ER, Burgoyne T, Edgar JR, Sorkin A, Futter CE. The relationship between ER-multivesicular body membrane contacts and the ESCRT machinery. *Biochemical Society transactions* 2012, **40**(2)**:** 464-468.
186. Komada M, Kitamura N. The Hrs/STAM complex in the downregulation of receptor tyrosine kinases. *Journal of biochemistry* 2005, **137**(1)**:** 1-8.
187. Myers MP, Andersen JN, Cheng A, Tremblay ML, Horvath CM, Parisien JP, Salmeen A, Barford D, Tonks NK. TYK2 and JAK2 are substrates of protein-tyrosine phosphatase 1B. *The Journal of biological chemistry* 2001, **276**(51)**:** 47771-47774.
188. Heinonen KM, Dube N, Bourdeau A, Lapp WS, Tremblay ML. Protein tyrosine phosphatase 1B negatively regulates macrophage development through CSF-1 signaling. *Proceedings of the National Academy of Sciences of the United States of America* 2006, **103**(8)**:** 2776-2781.
189. Lumeng CN, Saltiel AR. Inflammatory links between obesity and metabolic disease. *The Journal of clinical investigation* 2011, **121**(6)**:** 2111-2117.
190. Zabolotny JM, Kim YB, Welsh LA, Kershaw EE, Neel BG, Kahn BB. Protein-tyrosine phosphatase 1B expression is induced by inflammation in vivo. *The Journal of biological chemistry* 2008, **283**(21)**:** 14230-14241.
191. Nieto-Vazquez I, Fernandez-Veledo S, de Alvaro C, Lorenzo M. Dual role of interleukin-6 in regulating insulin sensitivity in murine skeletal muscle. *Diabetes* 2008, **57**(12)**:** 3211-3221.
192. González-Rodríguez Á, Más-Gutierrez JA, Mirasierra M, Fernandez-Pérez A, Lee YJ, Ko HJ, Kim JK, Romanos E, Carrascosa JM, Ros M, Vallejo M, Rondinone CM, Valverde ÁM. Essential role of protein tyrosine phosphatase 1B in obesity-induced inflammation and peripheral insulin resistance during aging. *Aging Cell* 2012, **11**(2)**:** 284-296.
193. Hornung V, Bauernfeind F, Halle A, Samstad EO, Kono H, Rock KL, Fitzgerald KA, Latz E. Silica crystals and aluminum salts activate the NALP3 inflammasome through phagosomal destabilization. *Nature immunology* 2008, **9**(8)**:** 847-856.
194. Valenzuela DM, Murphy AJ, Frendewey D, Gale NW, Economides AN, Auerbach W, Poueymirou WT, Adams NC, Rojas J, Yasenchak J, Chernomorsky R, Boucher M, Elsasser AL, Esau L*, et al.* High-throughput engineering of the mouse genome coupled with high-resolution expression analysis. *Nat Biotech* 2003, **21**(6)**:** 652-659.
195. Lienenklaus S, Cornitescu M, Zietara N, Lyszkiewicz M, Gekara N, Jablonska J, Edenhofer F, Rajewsky K, Bruder D, Hafner M, Staeheli P, Weiss S. Novel reporter mouse reveals constitutive and inflammatory expression of IFN-beta in vivo. *Journal of immunology* 2009, **183**(5)**:** 3229-3236.
196. Honda K, Sakaguchi S, Nakajima C, Watanabe A, Yanai H, Matsumoto M, Ohteki T, Kaisho T, Takaoka A, Akira S, Seya T, Taniguchi T. Selective contribution of IFN-alpha/beta signaling to the maturation of dendritic cells induced by double-stranded RNA or viral infection. *Proceedings of the National Academy of Sciences of the United States of America* 2003, **100**(19)**:** 10872-10877.
197. Hemmi H, Kaisho T, Takeuchi O, Sato S, Sanjo H, Hoshino K, Horiuchi T, Tomizawa H, Takeda K, Akira S. Small anti-viral compounds activate immune cells via the TLR7 MyD88-dependent signaling pathway. *Nature immunology* 2002, **3**(2)**:** 196-200.
198. Shi G-P, Villadangos JA, Dranoff G, Small C, Gu L, Haley KJ, Riese R, Ploegh HL, Chapman HA. Cathepsin S Required for Normal MHC Class II Peptide Loading and Germinal Center Development. *Immunity* 1999, **10**(2)**:** 197-206.

199. Mathys S, Schroeder T, Ellwart J, Koszinowski UH, Messerle M, Just U. Dendritic Cells under Influence of Mouse Cytomegalovirus Have a Physiologic Dual Role: to Initiate and to Restrict T Cell Activation. *Journal of Infectious Diseases* 2003, **187**(6)**:** 988-999.
200. Scheibe E, Lienenklaus S, May T, Magalhães V, Weiss S, Brinkmann M. Measurement of Mouse Cytomegalovirus-Induced Interferon-β with Immortalized Luciferase Reporter Cells. In: Bailer SM, Lieber D (eds). *Virus-Host Interactions*, vol. 1064. Humana Press, 2013, pp 355-366.
201. Bussey KA, Reimer E, Todt H, Denker B, Gallo A, Konrad A, Ottinger M, Adler H, Stürzl M, Brune W, Brinkmann MM. The gammaherpesviruses KSHV and MHV68 modulate the TLR-induced proinflammatory cytokine response. *Journal of Virology* 2014 (under revision).
202. Paddison PJ, Cleary M, Silva JM, Chang K, Sheth N, Sachidanandam R, Hannon GJ. Cloning of short hairpin RNAs for gene knockdown in mammalian cells. *Nat Meth* 2004, **1**(2)**:** 163-167.
203. Livak KJ, Schmittgen TD. Analysis of relative gene expression data using real-time quantitative PCR and the 2(-Delta Delta C(T)) Method. *Methods* 2001, **25**(4)**:** 402-408.
204. Tabeta K, Hoebe K, Janssen EM, Xia Y, Beutler B. Respond to "No antigen-presentation defect in Unc93b13d/3d (3d) mice". *Nature immunology* 2013, **14**(11)**:** 1102-1103.
205. Ivashkiv LB, Donlin LT. Regulation of type I interferon responses. *Nature reviews Immunology* 2014, **14**(1)**:** 36-49.
206. Gilliet M, Cao W, Liu YJ. Plasmacytoid dendritic cells: sensing nucleic acids in viral infection and autoimmune diseases. *Nature reviews Immunology* 2008, **8**(8)**:** 594-606.
207. Edwards AD, Diebold SS, Slack EMC, Tomizawa H, Hemmi H, Kaisho T, Akira S, Sousa CRe. Toll-like receptor expression in murine DC subsets: lack of TLR7 expression by CD8α+ DC correlates with unresponsiveness to imidazoquinolines. *European journal of immunology* 2003, **33**(4)**:** 827-833.
208. Hornung V, Rothenfusser S, Britsch S, Krug A, Jahrsdörfer B, Giese T, Endres S, Hartmann G. Quantitative Expression of Toll-Like Receptor 1–10 mRNA in Cellular Subsets of Human Peripheral Blood Mononuclear Cells and Sensitivity to CpG Oligodeoxynucleotides. *The Journal of Immunology* 2002, **168**(9)**:** 4531-4537.
209. Brasel K, De Smedt T, Smith JL, Maliszewski CR. Generation of murine dendritic cells from flt3-ligand–supplemented bone marrow cultures. *Blood* 2000, **96**(9)**:** 3029-3039.
210. Gilliet M, Boonstra A, Paturel C, Antonenko S, Xu X-L, Trinchieri G, O'Garra A, Liu Y-J. The Development of Murine Plasmacytoid Dendritic Cell Precursors Is Differentially Regulated by FLT3-ligand and Granulocyte/Macrophage Colony-Stimulating Factor. *The Journal of experimental medicine* 2002, **195**(7)**:** 953-958.
211. Hornung V, Ellegast J, Kim S, Brzozka K, Jung A, Kato H, Poeck H, Akira S, Conzelmann KK, Schlee M, Endres S, Hartmann G. 5'-Triphosphate RNA is the ligand for RIG-I. *Science* 2006, **314**(5801)**:** 994-997.
212. Takeuchi T, Kuro-o M, Miyazawa H, Ohtsuki Y, Yamamoto H. Transgenic expression of a novel thymic epithelial cell antigen stimulates abberant development of thymocytes. *The Journal of Immunology* 1997, **159**(2)**:** 726-733.
213. Yoshiura K-i, Machida J, Daack-Hirsch S, Patil SR, Ashworth LK, Hecht JT, Murray JC. Characterization of a Novel Gene Disrupted by a Balanced Chromosomal Translocation t(2;19)(q11.2;q13.3) in a Family with Cleft Lip and Palate. *Genomics* 1998, **54**(2)**:** 231-240.
214. Rossi MR, Hawthorn L, Platt J, Burkhardt T, Cowell JK, Ionov Y. Identification of inactivating mutations in the JAK1, SYNJ2, and CLPTM1 genes in prostate cancer cells using inhibition of nonsense-mediated decay and microarray analysis. *Cancer genetics and cytogenetics* 2005, **161**(2)**:** 97-103.
215. Ouyang S, Song X, Wang Y, Ru H, Shaw N, Jiang Y, Niu F, Zhu Y, Qiu W, Parvatiyar K, Li Y, Zhang R, Cheng G, Liu ZJ. Structural analysis of the STING adaptor protein reveals a hydrophobic dimer interface and mode of cyclic di-GMP binding. *Immunity* 2012, **36**(6)**:** 1073-1086.
216. Barber GN. STING-dependent cytosolic DNA sensing pathways. *Trends in immunology* 2014, **35**(2)**:** 88-93.

217. Matthews W, Jordan CT, Wiegand GW, Pardoll D, Lemischka IR. A receptor tyrosine kinase specific to hematopoietic stem and progenitor cell-enriched populations. *Cell* 1991, **65**(7)**:** 1143-1152.
218. Lantz KA, Hart SG, Planey SL, Roitman MF, Ruiz-White IA, Wolfe HR, McLane MP. Inhibition of PTP1B by trodusquemine (MSI-1436) causes fat-specific weight loss in diet-induced obese mice. *Obesity* 2010, **18**(8)**:** 1516-1523.
219. Asselin-Paturel C, Brizard G, Pin J-J, Brière F, Trinchieri G. Mouse Strain Differences in Plasmacytoid Dendritic Cell Frequency and Function Revealed by a Novel Monoclonal Antibody. *The Journal of Immunology* 2003, **171**(12)**:** 6466-6477.
220. Cisse B, Caton ML, Lehner M, Maeda T, Scheu S, Locksley R, Holmberg D, Zweier C, den Hollander NS, Kant SG, Holter W, Rauch A, Zhuang Y, Reizis B. Transcription factor E2-2 is an essential and specific regulator of plasmacytoid dendritic cell development. *Cell* 2008, **135**(1)**:** 37-48.
221. Dube N, Bourdeau A, Heinonen KM, Cheng A, Loy AL, Tremblay ML. Genetic ablation of protein tyrosine phosphatase 1B accelerates lymphomagenesis of p53-null mice through the regulation of B-cell development. *Cancer research* 2005, **65**(21)**:** 10088-10095.
222. Sanjuan MA, Rao N, Lai KT, Gu Y, Sun S, Fuchs A, Fung-Leung WP, Colonna M, Karlsson L. CpG-induced tyrosine phosphorylation occurs via a TLR9-independent mechanism and is required for cytokine secretion. *The Journal of cell biology* 2006, **172**(7)**:** 1057-1068.
223. Chockalingam A, Rose WA, Hasan M, Ju CH, Leifer CA. Cutting Edge: A TLR9 Cytoplasmic Tyrosine Motif Is Selectively Required for Proinflammatory Cytokine Production. *The Journal of Immunology* 2011, **188**(2)**:** 527-530.
224. Salmeen A, Andersen JN, Myers MP, Tonks NK, Barford D. Molecular Basis for the Dephosphorylation of the Activation Segment of the Insulin Receptor by Protein Tyrosine Phosphatase 1B. *Molecular cell* 2000, **6**(6)**:** 1401-1412.
225. Bresnahan WA. A Subset of Viral Transcripts Packaged Within Human Cytomegalovirus Particles. *Science* 2000, **288**(5475)**:** 2373-2376.
226. Li S, Wang L, Berman M, Kong YY, Dorf ME. Mapping a dynamic innate immunity protein interaction network regulating type I interferon production. *Immunity* 2011, **35**(3)**:** 426-440.
227. Mali P, Yang L, Esvelt KM, Aach J, Guell M, DiCarlo JE, Norville JE, Church GM. RNA-guided human genome engineering via Cas9. *Science* 2013, **339**(6121)**:** 823-826.
228. Sauer JD, Sotelo-Troha K, von Moltke J, Monroe KM, Rae CS, Brubaker SW, Hyodo M, Hayakawa Y, Woodward JJ, Portnoy DA, Vance RE. The N-ethyl-N-nitrosourea-induced Goldenticket mouse mutant reveals an essential function of Sting in the in vivo interferon response to Listeria monocytogenes and cyclic dinucleotides. *Infection and immunity* 2011, **79**(2)**:** 688-694.
229. Mosmann T. Rapid colorimetric assay for cellular growth and survival: Application to proliferation and cytotoxicity assays. *Journal of Immunological Methods* 1983, **65**(1–2)**:** 55-63.
230. Dalod M, Salazar-Mather TP, Malmgaard L, Lewis C, Asselin-Paturel C, Brière F, Trinchieri G, Biron CA. Interferon α/β and Interleukin 12 Responses to Viral Infections: Pathways Regulating Dendritic Cell Cytokine Expression In Vivo. *The Journal of experimental medicine* 2002, **195**(4)**:** 517-528.
231. Asselin-Paturel C, Boonstra A, Dalod M, Durand I, Yessaad N, Dezutter-Dambuyant C, Vicari A, O'Garra A, Biron C, Briere F, Trinchieri G. Mouse type I IFN-producing cells are immature APCs with plasmacytoid morphology. *Nature immunology* 2001, **2**(12)**:** 1144-1150.
232. Kittler JT, Chen G, Honing S, Bogdanov Y, McAinsh K, Arancibia-Carcamo IL, Jovanovic JN, Pangalos MN, Haucke V, Yan Z, Moss SJ. Phospho-dependent binding of the clathrin AP2 adaptor complex to GABAA receptors regulates the efficacy of inhibitory synaptic transmission. *Proceedings of the National Academy of Sciences of the United States of America* 2005, **102**(41)**:** 14871-14876.
233. Matsuda S, Kakegawa W, Budisantoso T, Nomura T, Kohda K, Yuzaki M. Stargazin regulates AMPA receptor trafficking through adaptor protein complexes during long-term depression. *Nature communications* 2013, **4**.

234. Carbone CJ, Zheng H, Bhattacharya S, Lewis JR, Reiter AM, Henthorn P, Zhang Z-Y, Baker DP, Ukkiramapandian R, Bence KK, Fuchs SY. Protein tyrosine phosphatase 1B is a key regulator of IFNAR1 endocytosis and a target for antiviral therapies. *Proceedings of the National Academy of Sciences* 2012, **109**(47)**:** 19226-19231.

235. Huyer G, Liu S, Kelly J, Moffat J, Payette P, Kennedy B, Tsaprailis G, Gresser MJ, Ramachandran C. Mechanism of Inhibition of Protein-tyrosine Phosphatases by Vanadate and Pervanadate. *Journal of Biological Chemistry* 1997, **272**(2)**:** 843-851.

236. Wang Y, Shaked I, Stanford SM, Zhou W, Curtsinger JM, Mikulski Z, Shaheen ZR, Cheng G, Sawatzke K, Campbell AM, Auger JL, Bilgic H, Shoyama FM, Schmeling DO*, et al.* The autoimmunity-associated gene PTPN22 potentiates toll-like receptor-driven, type 1 interferon-dependent immunity. *Immunity* 2013, **39**(1)**:** 111-122.

237. Hacker H, Tseng PH, Karin M. Expanding TRAF function: TRAF3 as a tri-faced immune regulator. *Nature reviews Immunology* 2011, **11**(7)**:** 457-468.

238. Kishore N, Huynh QK, Mathialagan S, Hall T, Rouw S, Creely D, Lange G, Caroll J, Reitz B, Donnelly A, Boddupalli H, Combs RG, Kretzmer K, Tripp CS. IKK-i and TBK-1 are enzymatically distinct from the homologous enzyme IKK-2: comparative analysis of recombinant human IKK-i, TBK-1, and IKK-2. *The Journal of biological chemistry* 2002, **277**(16)**:** 13840-13847.

239. Kawai T, Sato S, Ishii KJ, Coban C, Hemmi H, Yamamoto M, Terai K, Matsuda M, Inoue J, Uematsu S, Takeuchi O, Akira S. Interferon-alpha induction through Toll-like receptors involves a direct interaction of IRF7 with MyD88 and TRAF6. *Nature immunology* 2004, **5**(10)**:** 1061-1068.

240. Ning S, Campos AD, Darnay BG, Bentz GL, Pagano JS. TRAF6 and the three C-terminal lysine sites on IRF7 are required for its ubiquitination-mediated activation by the tumor necrosis factor receptor family member latent membrane protein 1. *Molecular and cellular biology* 2008, **28**(20)**:** 6536-6546.

241. Lin YC, Huang DY, Chu CL, Lin YL, Lin WW. The tyrosine kinase Syk differentially regulates Toll-like receptor signaling downstream of the adaptor molecules TRAF6 and TRAF3. *Science signaling* 2013, **6**(289)**:** ra71.

242. Platanias LC. Mechanisms of type-I- and type-II-interferon-mediated signalling. *Nature reviews Immunology* 2005, **5**(5)**:** 375-386.

243. Asselin-Paturel C, Brizard G, Chemin K, Boonstra A, O'Garra A, Vicari A, Trinchieri G. Type I interferon dependence of plasmacytoid dendritic cell activation and migration. *The Journal of experimental medicine* 2005, **201**(7)**:** 1157-1167.

244. Zhao W, Lee C, Piganis R, Plumlee C, de Weerd N, Hertzog PJ, Schindler C. A Conserved IFN-α Receptor Tyrosine Motif Directs the Biological Response to Type I IFNs. *The Journal of Immunology* 2008, **180**(8)**:** 5483-5489.

245. Bacon CM, McVicar DW, Ortaldo JR, Rees RC, O'Shea JJ, Johnston JA. Interleukin 12 (IL-12) induces tyrosine phosphorylation of JAK2 and TYK2: differential use of Janus family tyrosine kinases by IL-2 and IL-12. *The Journal of experimental medicine* 1995, **181**(1)**:** 399-404.

246. Fenner JE, Starr R, Cornish AL, Zhang JG, Metcalf D, Schreiber RD, Sheehan K, Hilton DJ, Alexander WS, Hertzog PJ. Suppressor of cytokine signaling 1 regulates the immune response to infection by a unique inhibition of type I interferon activity. *Nature immunology* 2006, **7**(1)**:** 33-39.

247. David M, Chen HE, Goelz S, Larner AC, Neel BG. Differential regulation of the alpha/beta interferon-stimulated Jak/Stat pathway by the SH2 domain-containing tyrosine phosphatase SHPTP1. *Molecular and cellular biology* 1995, **15**(12)**:** 7050-7058.

248. You M, Yu D-H, Feng G-S. Shp-2 Tyrosine Phosphatase Functions as a Negative Regulator of the Interferon-Stimulated Jak/STAT Pathway. *Molecular and cellular biology* 1999, **19**(3)**:** 2416-2424.

249. Malakhova OA, Kim KI, Luo JK, Zou W, Kumar KGS, Fuchs SY, Shuai K, Zhang DE. UBP43 is a novel regulator of interferon signaling independent of its ISG15 isopeptidase activity. *The EMBO journal* 2006, **25**(11)**:** 2358-2367.

V Appendix

Table 14: List of potential interaction partners of wild type (WT) and mutant (H412R) UNC93B.

Protein Description	Interaction with UNC93B		Protein Accession
5'-3' exoribonuclease 2		H412R	gi|117606214
78 kDa glucose-regulated protein	WT	H412R	gi|2506545
A disintegrin and metalloprotease domain 17		H412R	gi|110347485
AAA-ATPase TOB3		H412R	gi|30725845
ADP-ribosylation factor-like 10C	WT	H412R	gi|13385518
ADP-ribosylation factor-like 8A	WT	H412R	gi|23956194
AGP7		H412R	gi|22550098
AHNAK nucleoprotein isoform 1		H412R	gi|61743961
ARP3 actin-related protein 3 homolog	WT	H412R	gi|23956222
ATP synthase, H+ transporting mitochondrial F1 complex, beta subunit	WT	H412R	gi|31980648
ATP synthase, H+ transporting, mitochondrial F0 complex, subunit d		H412R	gi|21313679
ATP-binding cassette, sub-family F (GCN20), member 2		H412R	gi|23956078
ATP-binding cassette, subfamily E, member 1		H412R	gi|114205431
ATP-dependent glucokinase	WT	H412R	gi|21312406
ATPase type 13A1	WT	H412R	gi|18875382
ATPase, Ca++ transporting, slow twitch 2 isoform a	WT	H412R	gi|158635979
ATPase, H+ transporting, lysosomal V1 subunit A	WT	H412R	gi|31560731
Abhydrolase domain containing 6	WT	H412R	gi|31560264
Achalasia, adrenocortical insufficiency, alacrimia	WT	H412R	gi|23510311
Actin related protein 2/3 complex, subunit 1B		H412R	gi|160837788
Actin, beta-like 2		H412R	gi|30425250
Actin-like 6A		H412R	gi|189181668
Actinin alpha 4		H412R	gi|11230802
Actinin, alpha 1		H412R	gi|61097906
Acyl-CoA synthetase long-chain family member 3 isoform b		H412R	gi|209977076
Acyl-CoA synthetase long-chain family member 5	WT	H412R	gi|58218988
Acyl-CoA thioesterase 9		H412R	gi|31980998
Adaptor protein complex AP-1, beta 1 subunit	WT	H412R	gi|88853578
Adaptor protein complex AP-1, gamma 1 subunit	WT	H412R	gi|56744242
Adaptor protein complex AP-2, alpha 1 subunit isoform b		H412R	gi|116256510
Adaptor protein complex AP-2, alpha 2 subunit	WT	H412R	gi|163644277
Adaptor protein complex AP-2, mu1	WT	H412R	gi|6753074
Adenylosuccinate lyase	WT	H412R	gi|29788764
Adenylosuccinate synthetase 1		H412R	gi|6671519
Adenylosuccinate synthetase, non muscle		H412R	gi|31560737
Alanyl-tRNA synthetase		H412R	gi|34610207
Aldehyde dehydrogenase family 3, subfamily A2	WT	H412R	gi|75677435
Aldo-keto reductase family 1, member B3 (aldose reductase)	WT	H412R	gi|160707894
All-trans-13,14-dihydroretinol saturase	WT	H412R	gi|52627143
Alpha glucosidase 2 alpha neutral subunit	WT	H412R	gi|6679891
Alpha isoform of regulatory subunit B55, protein phosphatase 2	WT	H412R	gi|110625886
Alpha-N-acetylglucosaminidase	WT		gi|7305299
Amplified in osteosarcoma	WT	H412R	gi|29243990
Ankycorbin		H412R	gi|13507620
Ankyrin repeat and FYVE domain containing 1		H412R	gi|85702366
Ankyrin repeat domain 39	WT	H412R	gi|58037099
Annexin A5	WT	H412R	gi|6753060

Arachidonate 5-lipoxygenase	WT	H412R	gi|62526037
Arsenate resistance protein 2 isoform 3		H412R	gi|158186674
Arylacetamide deacetylase-like 1		H412R	gi|30520239
Asparaginyl-tRNA synthetase		H412R	gi|29789191
Aspartyl beta-hydroxylase isoform 1	WT	H412R	gi|125628659
Aspartyl-tRNA synthetase isoform 1	WT	H412R	gi|211065507
Ataxia telangiectasia mutated homolog		H412R	gi|163838660
Atlastin GTPase 3	WT	H412R	gi|31559920
B Chain B, Porcine E-Trypsin (E.C.3.4.21.4)	WT	H412R	gi|999627
B aggressive lymphoma		H412R	gi|13384918
B-cell receptor-associated protein 29	WT	H412R	gi|6671620
BCL2-associated athanogene 5	WT		gi|58037205
BRCA1/BRCA2-containing complex, subunit 3		H412R	gi|22165366
Bcl2-associated X protein		H412R	gi|6680770
Branched chain aminotransferase 1, cytosolic isoform 2		H412R	gi|161016828
Bri3 binding protein	WT	H412R	gi|58037467
C-src tyrosine kinase	WT	H412R	gi|31560712
CCR4-NOT transcription complex, subunit 1 isoform 2		H412R	gi|189458844
CDK5 regulatory subunit associated protein 3		H412R	gi|13384788
CDNA sequence BC022641		H412R	gi|31712002
CDP-diacylglycerol--inositol 3-phosphatidyltransferase (phosphatidylinositol synthase)	WT	H412R	gi|28076897
CNDP dipeptidase 2	WT	H412R	gi|31981273
Calcium/calmodulin-dependent protein kinase II, delta isoform 1	WT	H412R	gi|70906479
Calreticulin	WT	H412R	gi|6680836
Carbamoyl-phosphate synthetase 2, aspartate transcarbamylase, and dihydroorotase		H412R	gi|51093867
Casein kinase 1, alpha 1		H412R	gi|22165382
Cathepsin A isoform a	WT	H412R	gi|84042525
Cathepsin S preproprotein	WT		gi|160707996
Cathepsin Z preproprotein	WT	H412R	gi|11968166
Cell division cycle 37 homolog		H412R	gi|7949018
Cell division cycle 5-like		H412R	gi|22779899
Centromere/kinetochore protein zw10		H412R	gi|22165349
Chaperonin containing Tcp1, subunit 5 (epsilon)		H412R	gi|6671702
Chaperonin containing Tcp1, subunit 7 (eta)		H412R	gi|31982472
Chaperonin subunit 2 (beta)	WT	H412R	gi|126521835
Checkpoint kinase 1 homolog	WT	H412R	gi|31542385
Chloride channel CLIC-like 1		H412R	gi|21704070
Chondroitin sulfate proteoglycan 6		H412R	gi|36031035
Chromodomain helicase DNA binding protein 4		H412R	gi|39204553
Chromosome segregation 1-like		H412R	gi|12963737
Cleft lip and palate associated transmembrane protein 1	WT	H412R	gi|103472025
Coatomer protein complex subunit alpha		H412R	gi|31981828
Coatomer protein complex, subunit beta 1		H412R	gi|15426055
Coatomer protein complex, subunit beta 2 (beta prime)	WT	H412R	gi|29789080
Coatomer protein complex, subunit gamma 2		H412R	gi|8567340
Coatomer protein complex, subunit gamma isoform 1		H412R	gi|8567338
Coiled-coil domain containing 115		H412R	gi|58037169
Coiled-coil domain containing 47	WT	H412R	gi|125628650
Cold shock domain protein A long isoform		H412R	gi|47059495
Coronin, actin binding protein 1B		H412R	gi|6753494
Coronin, actin binding protein 1C	WT	H412R	gi|31542413
Crystallin, zeta (quinone reductase)-like 1		H412R	gi|21617847
Cullin 3		H412R	gi|7710014
Cullin 4A	WT	H412R	gi|167466258
Cyclin H	WT	H412R	gi|12963599

Cytidine 5'-triphosphate synthase		H412R	gi|172072613
Cytochrome P450 reductase	WT	H412R	gi|6679421
Cytochrome P450, family 51	WT	H412R	gi|71061451
Cytochrome b5 type B precursor	WT	H412R	gi|31542438
Cytoplasmic FMR1 interacting protein 1	WT	H412R	gi|164698474
Cytoskeleton-associated protein 4	WT	H412R	gi|62526118
D6Wsu176e protein	WT	H412R	gi|42734496
DEAD (Asp-Glu-Ala-Asp) box polypeptide 1		H412R	gi|19527256
DEAD (Asp-Glu-Ala-Asp) box polypeptide 39		H412R	gi|38372907
DEAH (Asp-Glu-Ala-His) box polypeptide 8		H412R	gi|56699440
DEK oncogene (DNA binding)		H412R	gi|29789160
DENN/MADD domain containing 2A		H412R	gi|27369652
DH and coiled-coil domain-containing protein ENSP00000381780 homolog	WT		gi|123792451
Dedicator of cyto-kinesis 2	WT	H412R	gi|117553625
Dehydrogenase/reductase (SDR family) member 1	WT	H412R	gi|31980844
Dehydrogenase/reductase (SDR family) member 8	WT	H412R	gi|16716597
Deltex 3-like		H412R	gi|133930784
Deoxyuridine triphosphatase		H412R	gi|21281687
Desmin		H412R	gi|33563250
Diaphorase 1	WT		gi|19745150
Dihydrolipoamide branched chain transacylase E2	WT	H412R	gi|170172520
Dihydrolipoamide dehydrogenase		H412R	gi|31982856
DnaJ (Hsp40) homolog, subfamily A, member 1		H412R	gi|6680297
DnaJ (Hsp40) homolog, subfamily A, member 2		H412R	gi|9789937
DnaJ (Hsp40) homolog, subfamily B, member 11	WT	H412R	gi|110625998
DnaJ (Hsp40) homolog, subfamily B, member 12	WT	H412R	gi|31982701
DnaJ (Hsp40) homolog, subfamily C, member 10		H412R	gi|119508443
DnaJ (Hsp40) homolog, subfamily C, member 11		H412R	gi|164565394
Dynactin 1		H412R	gi|118601017
Dynactin 2		H412R	gi|28076935
Dynein cytoplasmic 1 intermediate chain 2		H412R	gi|6753658
Dynein cytoplasmic 1 light intermediate chain 1		H412R	gi|22122795
EF hand domain containing 2		H412R	gi|31981086
ER lipid raft associated 1	WT	H412R	gi|31981799
Elongation factor Tu GTP binding domain containing 2 isoform b	WT	H412R	gi|158508674
Enolase 2, gamma neuronal	WT	H412R	gi|7305027
Epidermal growth factor receptor pathway substrate 8		H412R	gi|75677397
ErbB3-binding protein 1		H412R	gi|6755100
Eukaryotic translation elongation factor 1 delta isoform b	WT	H412R	gi|54287684
Eukaryotic translation initiation factor 2, subunit 1 alpha	WT		gi|13385624
Eukaryotic translation initiation factor 3 subunit 6 interacting protein	WT	H412R	gi|51093840
Eukaryotic translation initiation factor 3, subunit 10 (theta)		H412R	gi|146219837
Eukaryotic translation initiation factor 3, subunit 9	WT	H412R	gi|29789343
Eukaryotic translation initiation factor 3, subunit C		H412R	gi|22203755
Eukaryotic translation initiation factor 3, subunit F	WT	H412R	gi|21313620
Eukaryotic translation initiation factor 3, subunit G		H412R	gi|31980808
Eukaryotic translation initiation factor 4A, isoform 3		H412R	gi|20149756
Eukaryotic translation initiation factor 5B	WT	H412R	gi|84043961
Excision repair cross-complementing rodent repair deficiency, complementation group 2		H412R	gi|31542614
Exportin 1, CRM1 homolog	WT	H412R	gi|78190507
Exportin 5		H412R	gi|24429570
F-box protein 22		H412R	gi|139948465
FK506 binding protein 11	WT	H412R	gi|15277331
Fatty acyl CoA reductase 1		H412R	gi|74096448
Ferredoxin reductase	WT	H412R	gi|6679767

Fibronectin type III domain containing 3a	WT		gi|83745139
Filamin, alpha	WT	H412R	gi|125347376
Flightless I homolog		H412R	gi|11528490
Formin-like 1 isoform 1		H412R	gi|118136290
Fucokinase isoform 2		H412R	gi|41281971
GPI anchor attachment protein 1	WT	H412R	gi|6754046
GTP binding protein 7 (putative)		H412R	gi|188528646
Gelsolin		H412R	gi|28916693
Gem (nuclear organelle) associated protein 5		H412R	gi|27369782
Glucosamine-6-phosphate deaminase 1	WT	H412R	gi|188219582
Glucose phosphate isomerase 1	WT	H412R	gi|6680067
Glucosidase 1	WT	H412R	gi|31981106
Glutamic pyruvate transaminase (alanine aminotransferase) 2		H412R	gi|27805389
Glutaminyl-tRNA synthetase	WT	H412R	gi|55741703
Glutamyl-prolyl-tRNA synthetase	WT	H412R	gi|82617575
Glutaredoxin 3	WT		gi|31981269
Glyceraldehyde-3-phosphate dehydrogenase	WT	H412R	gi|6679937
Glycerol phosphate dehydrogenase 2, mitochondrial		H412R	gi|31981769
Glycyl-tRNA synthetase		H412R	gi|93102417
GrpE-like 2, mitochondrial	WT	H412R	gi|29789124
Guanine monphosphate synthetase	WT	H412R	gi|85861218
Guanine nucleotide binding protein, alpha 13	WT		gi|89001109
Guanine nucleotide binding protein, alpha q polypeptide	WT		gi|84662745
Guanine nucleotide-binding protein, beta-1 subunit	WT		gi|6680045
Guanine nucleotide-binding protein, beta-2 subunit	WT	H412R	gi|13937391
HECT domain containing 1		H412R	gi|205277432
HIV TAT specific factor 1	WT	H412R	gi|23956212
Heat shock protein 105	WT	H412R	gi|114145505
Heat shock protein 4	WT	H412R	gi|112293266
Hect domain and RLD 4		H412R	gi|32451488
Hematopoietic cell specific Lyn substrate 1		H412R	gi|6680187
Heme oxygenase (decycling) 2	WT	H412R	gi|209862939
Heterogeneous nuclear ribonucleoprotein A1 isoform b		H412R	gi|85060507
Heterogeneous nuclear ribonucleoprotein A2/B1 isoform 1		H412R	gi|109134362
Heterogeneous nuclear ribonucleoprotein C		H412R	gi|8393544
Heterogeneous nuclear ribonucleoprotein F		H412R	gi|19527048
Heterogeneous nuclear ribonucleoprotein H1		H412R	gi|10946928
Heterogeneous nuclear ribonucleoprotein K	WT	H412R	gi|13384620
Heterogeneous nuclear ribonucleoprotein L		H412R	gi|183980004
Heterogeneous nuclear ribonucleoprotein L-like		H412R	gi|110347535
Heterogeneous nuclear ribonucleoprotein M isoform b		H412R	gi|158186704
Heterogeneous nuclear ribonucleoprotein R		H412R	gi|33859724
Heterogeneous nuclear ribonucleoprotein U		H412R	gi|160333923
Hexokinase 1		H412R	gi|6754206
Hexokinase 2		H412R	gi|7305143
Hexokinase 3	WT	H412R	gi|84370288
High density lipoprotein binding protein		H412R	gi|19527028
Histocompatibility 13	WT	H412R	gi|18034682
Histone deacetylase 1		H412R	gi|6680193
Hydrogen/potassium-exchanging ATPase 12A		H412R	gi|157168326
Hydroxymethylglutaryl-CoA synthase 1	WT	H412R	gi|31981842
Hydroxysteroid (17-beta) dehydrogenase 4	WT	H412R	gi|31982273
Hypothetical protein LOC217370	WT	H412R	gi|21450219
Hypothetical protein LOC223665	WT	H412R	gi|21735489
Hypothetical protein LOC224171		H412R	gi|125858491
Hypothetical protein LOC230866 isoform 1	WT	H412R	gi|31542273

Hypothetical protein LOC230866 isoform 2	WT	H412R	gi|85861260
Hypothetical protein LOC28088		H412R	gi|21703842
Hypothetical protein LOC67490		H412R	gi|21312946
Hypothetical protein LOC73694	WT		gi|158937256
Hypoxia up-regulated 1		H412R	gi|157951706
IlvB (bacterial acetolactate synthase)-like	WT	H412R	gi|30424591
Implantation-associated protein	WT		gi|148747202
Importin 11	WT	H412R	gi|31541898
Importin 5	WT	H412R	gi|29789199
Importin 9		H412R	gi|112734861
Influenza virus NS1A binding protein isoform 3		H412R	gi|87239996
Inhibitor of kappa light polypeptide enhancer in B-cells, kinase complex-associated protein		H412R	gi|158937298
Inner membrane protein, mitochondrial		H412R	gi|70608131
Inorganic pyrophosphatase 2		H412R	gi|22203753
Inosine 5'-phosphate dehydrogenase 2		H412R	gi|31981382
Inositol 1,4,5-triphosphate receptor 1		H412R	gi|146198792
Integrin linked kinase		H412R	gi|6754342
Interferon-induced protein 44-like		H412R	gi|190359774
Intergral membrane protein 1	WT	H412R	gi|148747128
Interleukin 16		H412R	gi|52138550
Isocitrate dehydrogenase 3, beta subunit	WT	H412R	gi|18700024
Isoleucyl-tRNA synthetase		H412R	gi|29789383
Junction-mediating and regulatory protein		H412R	gi|61098108
KH-type splicing regulatory protein (FUSE binding protein 2)		H412R	gi|163954948
Karyopherin (importin) alpha 2		H412R	gi|6754474
Kelch domain containing 5		H412R	gi|124486991
Kelch-like 25		H412R	gi|170671742
Keratin complex 1, acidic, gene 10	WT	H412R	gi|112983636
Kinectin 1		H412R	gi|144922638
Kinesin family member 21B		H412R	gi|86990454
Kinesin family member 2C		H412R	gi|31981665
Kinesin family member 5A		H412R	gi|84781727
Lamin B receptor	WT	H412R	gi|19527034
Lanosterol synthase	WT	H412R	gi|22122469
Lectin, mannose-binding 2	WT	H412R	gi|34328278
Lectin, mannose-binding 2-like	WT		gi|61656186
Lectin, mannose-binding, 1	WT	H412R	gi|21312570
Leucine aminopeptidase 3		H412R	gi|31981147
Leucine carboxyl methyltransferase 2		H412R	gi|198278410
Leucine rich repeat (in FLII) interacting protein 1 isoform 1		H412R	gi|162417949
Leucine rich repeat (in FLII) interacting protein 2		H412R	gi|110625827
Leucine rich repeat containing 47		H412R	gi|41152116
Leucine rich repeat containing 59	WT	H412R	gi|19527026
Leucine rich repeat containing 8D		H412R	gi|170650657
Leucine rich repeat protein 4, neuronal		H412R	gi|22122701
Leucine zipper protein 5		H412R	gi|91208439
Leucyl-tRNA synthetase		H412R	gi|120537241
Ligase I, DNA, ATP-dependent		H412R	gi|133892807
Lymphocyte specific 1 isoform 2		H412R	gi|11225264
Lymphoid-restricted membrane protein		H412R	gi|162287383
Lysophosphatidylcholine acyltransferase 2	WT	H412R	gi|27370522
Lysophosphatidylcholine acyltransferase 3	WT	H412R	gi|21699058
Lysophosphatidylcholine acyltransferase 4		H412R	gi|46402175
Lysyl-tRNA synthetase isoform 1	WT	H412R	gi|195963321
MCG129058		H412R	gi|148679865

MCG13955		H412R	gi|148704913
MMS19 (MET18 S. cerevisiae)		H412R	gi|15100156
Major facilitator superfamily domain containing 10	WT	H412R	gi|13386144
Mannose-6-phosphate receptor, cation dependent		H412R	gi|14916479
Mannosidase, alpha, class 2C, member 1	WT	H412R	gi|30794150
Membrane bound C2 domain containing protein		H412R	gi|33859650
Methionine-tRNA synthetase		H412R	gi|51491852
Methylenetetrahydrofolate dehydrogenase (NADP+ dependent) 1-like	WT	H412R	gi|31559887
Methylenetetrahydrofolate dehydrogenase 1		H412R	gi|20270275
Minichromosome maintenance complex component 7		H412R	gi|10242373
Minichromosome maintenance deficient 3		H412R	gi|33859484
Minichromosome maintenance deficient 5, cell division cycle 46		H412R	gi|112293273
Mitochondrial trifunctional protein, beta subunit	WT	H412R	gi|21704100
MutS homolog 6		H412R	gi|6754744
Myo-inositol 1-phosphate synthase A1		H412R	gi|12963757
Myosin IC isoform b		H412R	gi|124494244
Myosin IE		H412R	gi|68299824
Myosin IG		H412R	gi|30410767
Myosin XVIIIa		H412R	gi|22094119
Myosin, heavy polypeptide 9, non-muscle isoform 1		H412R	gi|114326446
N-acetyltransferase 10		H412R	gi|23346561
N-ethylmaleimide sensitive fusion protein		H412R	gi|31543349
N-ethylmaleimide sensitive fusion protein attachment protein alpha	WT	H412R	gi|13385392
NAD(P) dependent steroid dehydrogenase-like	WT		gi|31982437
NADH dehydrogenase (ubiquinone) flavoprotein 1		H412R	gi|19526814
NOD9 protein		H412R	gi|30410746
Nardilysin		H412R	gi|31559918
Neuroplastin	WT		gi|153945724
Nicalin homolog	WT	H412R	gi|33469043
Nodal modulator 1	WT	H412R	gi|27151748
Non-SMC condensin I complex, subunit D2		H412R	gi|22165392
Non-metastatic cells 6, protein expressed in (nucleoside-diphosphate kinase)		H412R	gi|9055290
Nuclear VCP-like		H412R	gi|33468981
Nuclear factor of kappa light polypeptide gene enhancer in B-cells 2, p49/p100		H412R	gi|9506921
Nuclear matrix protein SNEV		H412R	gi|19527358
Nuclease sensitive element binding protein 1		H412R	gi|113205059
Nucleophosmin 1	WT		gi|6679108
Nucleoporin 160		H412R	gi|10946932
Nucleoporin 85		H412R	gi|108773813
Nucleoporin 93		H412R	gi|27369533
Nucleoporin 98	WT		gi|39930413
Nudix (nucleoside diphosphate linked moiety X)-type motif 5		H412R	gi|8393853
O-linked N-acetylglucosamine transferase	WT	H412R	gi|46909607
On-SMC condensin I complex, subunit G		H412R	gi|169234780
PAP associated domain containing 1		H412R	gi|21312970
PREDICTED: hypothetical protein	WT	H412R	gi|149273161
PREDICTED: similar to 2310014H01Rik protein		H412R	gi|149269292
PREDICTED: similar to 2310022K01Rik protein		H412R	gi|149256963
PREDICTED: similar to Rab3 GTPase-activating protein non-catalytic subunit (Rab3 GTPase-activating protein 150 kDa subunit) (Ra		H412R	gi|94364680
PREDICTED: similar to Small subunit processome component 20 homolog (Down-regulated in metastasis protein) isoform 4		H412R	gi|149261463
PREDICTED: similar to Tripartite motif protein 21 isoform 2	WT		gi|149257887
Paraoxonase 3	WT	H412R	gi|27370510
Pentatricopeptide repeat domain 3		H412R	gi|33469980
Peptidase (mitochondrial processing) alpha	WT	H412R	gi|27502349
Peptidylprolyl isomerase B	WT		gi|71774133

Phosphatidylinositol 3-kinase catalytic delta polypeptide	WT	H412R	gi|71067116
Phosphatidylinositol 3-kinase, regulatory subunit, polypeptide 1 isoform 2	WT	H412R	gi|117320524
Phosphatidylinositol 3-kinase, regulatory subunit, polypeptide 2 (p85 beta)		H412R	gi|6679321
Phosphatidylinositol glycan, class T		H412R	gi|120587021
Phosphofructokinase, liver, B-type		H412R	gi|31560653
Phosphofructokinase, platelet		H412R	gi|9790051
Phosphogluconate dehydrogenase	WT	H412R	gi|124486895
Phosphoglycerate dehydrogenase like 1		H412R	gi|90568036
Phospholipase A2, activating protein		H412R	gi|114431250
Phospholipase C, gamma 2		H412R	gi|26986603
Phosphoribosylglycinamide formyltransferase	WT	H412R	gi|93102415
Phosphorylase kinase beta		H412R	gi|40789096
Pitrilysin metallepetidase 1	WT		gi|21699068
Plastin 1 (I-isoform)	WT	H412R	gi|85986577
Platelet-activating factor acetylhydrolase, isoform 1b, beta1 subunit	WT	H412R	gi|7305363
Poly (ADP-ribose) polymerase family, member 1	WT	H412R	gi|20806109
Poly-U binding splicing factor 60 isoform b		H412R	gi|76677895
Polymerase (DNA directed), delta 2, regulatory subunit		H412R	gi|6679413
Polypyrimidine tract binding protein 1 isoform 2		H412R	gi|116517303
Prenylcysteine oxidase 1 like	WT	H412R	gi|27370248
Procollagen-proline, 2-oxoglutarate 4-dioxygenase (proline 4-hydroxylase), alpha 1 polypeptide		H412R	gi|33859596
Progesterone receptor membrane component	WT	H412R	gi|31980806
Proteasome (prosome, macropain) 26S subunit, ATPase 2		H412R	gi|33859604
Proteasome (prosome, macropain) 26S subunit, ATPase 3		H412R	gi|6679503
Proteasome (prosome, macropain) subunit, beta type 2	WT	H412R	gi|31981327
Proteasome 26S ATPase subunit 4	WT	H412R	gi|124248577
Proteasome 26S ATPase subunit 6		H412R	gi|27754103
Proteasome 26S non-ATPase subunit 1	WT	H412R	gi|74315975
Proteasome 26S non-ATPase subunit 12		H412R	gi|13385384
Proteasome 26S non-ATPase subunit 13	WT	H412R	gi|6755210
Proteasome 26S non-ATPase subunit 2	WT	H412R	gi|19882201
Proteasome 26S non-ATPase subunit 3		H412R	gi|19705424
Protein kinase C substrate 80K-H	WT		gi|6679465
Protein kinase, cAMP dependent regulatory, type I, alpha		H412R	gi|30794476
Protein phosphatase 1, catalytic subunit, alpha	WT	H412R	gi|13994195
Protein phosphatase 1, regulatory (inhibitor) subunit 12A		H412R	gi|95772123
Protein phosphatase 1, regulatory subunit 12C		H412R	gi|124249341
Protein phosphatase 1, regulatory subunit 9B		H412R	gi|50053703
Protein phosphatase 2 (formerly 2A), regulatory subunit A (PR 65), beta isoform isoform b		H412R	gi|77539776
Protein phosphatase 2a, catalytic subunit, alpha isoform	WT	H412R	gi|9506983
Protein tyrosine phosphatase, non-receptor type 1	WT	H412R	gi|133505845
Protein tyrosine phosphatase, non-receptor type 6 isoform b		H412R	gi|118130785
Purine rich element binding protein A	WT	H412R	gi|6679573
Putative membrane protein	WT	H412R	gi|87116677
Pyruvate dehydrogenase complex, component X		H412R	gi|28201978
RAB1, member RAS oncogene family	WT	H412R	gi|6679587
RAB11a, member RAS oncogene family	WT	H412R	gi|31980840
RAB1B, member RAS oncogene family	WT	H412R	gi|21313162
RAB21, member RAS oncogene family	WT		gi|33859751
RAB2B protein	WT		gi|30525051
RAB6B, member RAS oncogene family	WT	H412R	gi|30424655
RAB7, member RAS oncogene family	WT	H412R	gi|148747526
RAD50 homolog		H412R	gi|153945822
RANBP4		H412R	gi|19745156
RAP1, GTP-GDP dissociation stimulator 1 isoform a	WT		gi|100818161

RAP2B, member of RAS oncogene family	WT		gi|13386338
RIKEN cDNA 2310001A20	WT		gi|21313668
RIKEN cDNA 2310044H10	WT		gi|37574074
Ras homolog gene family, member A		H412R	gi|31542143
Ras-GTPase-activating protein SH3-domain binding protein		H412R	gi|7305075
Regulator of nonsense transcripts 1 isoform a		H412R	gi|170784813
Required for meiotic nuclear division 1 homolog		H412R	gi|86198296
Reticulocalbin 2	WT	H412R	gi|114205428
Reticulon 4 isoform A		H412R	gi|34610235
Retinol dehydrogenase 11	WT		gi|19482172
Rho GTPase activating protein 9		H412R	gi|90093351
Rho guanine nucleotide exchange factor (GEF) 11		H412R	gi|51491850
Rho-associated coiled-coil forming kinase 2		H412R	gi|134949013
Rho/rac guanine nucleotide exchange factor (GEF) 2		H412R	gi|170650647
Ribonucleotide reductase M1		H412R	gi|31982026
Ribosomal RNA processing 12 homolog		H412R	gi|40789092
Ribosomal protein 10		H412R	gi|16418339
Ribosomal protein L12		H412R	gi|160333553
Ribosomal protein L13	WT		gi|33186863
Ribosomal protein L21	WT		gi|31560385
Ribosomal protein L23a		H412R	gi|46430508
Ribosomal protein L24		H412R	gi|18250296
Ribosomal protein L26	WT	H412R	gi|6677777
Ribosomal protein L3		H412R	gi|7305441
Ribosomal protein S6	WT	H412R	gi|6677809
Ribosome binding protein 1 isoform a	WT	H412R	gi|124486712
RuvB-like protein 1	WT	H412R	gi|9790083
RuvB-like protein 2	WT	H412R	gi|6755382
SEC22 vesicle trafficking protein-like 1	WT	H412R	gi|6755448
SERPINE1 mRNA binding protein 1 isoform 2		H412R	gi|165932377
SMC1 structural maintenance of chromosomes 1-like 1		H412R	gi|9790237
SPECC1-like		H412R	gi|49274627
STIP1 homology and U-box containing protein 1	WT	H412R	gi|9789907
SWI/SNF related, matrix associated, actin dependent regulator of chromatin, subfamily d, member 2 isoform 1		H412R	gi|194328773
Saccharomyces cerevisiae Nip7p homolog		H412R	gi|13928674
Sel1 (suppressor of lin-12) 1 homolog isoform a	WT	H412R	gi|84875513
Serine (or cysteine) proteinase inhibitor, clade B, member 6a		H412R	gi|6678097
Serine palmitoyltransferase subunit 1	WT	H412R	gi|29244577
Serine palmitoyltransferase, long chain base subunit 2	WT	H412R	gi|6755656
Seryl-aminoacyl-tRNA synthetase 2	WT	H412R	gi|12963765
Signal recognition particle receptor		H412R	gi|27229036
Signal sequence receptor, alpha	WT	H412R	gi|165377206
Signal sequence receptor, delta	WT		gi|6678145
Signal transducer and activator of transcription 1		H412R	gi|114326482
Signal transducer and activator of transcription 5A		H412R	gi|6755672
Signal-induced proliferation associated gene 1		H412R	gi|61556720
Signaling molecule ATTP	WT	H412R	gi|104294890
Silencer-associated factor	WT		gi|110626163
Sjogren syndrome antigen B		H412R	gi|158636012
Smooth muscle cell associated protein-1		H412R	gi|19527172
Solute carrier family 33 (acetyl-CoA transporter), member 1	WT	H412R	gi|31543730
Solute carrier family 39, member 7		H412R	gi|118150670
Sorting and assembly machinery component 50 homolog	WT	H412R	gi|30519943
Sorting nexin 5		H412R	gi|18034769
Source of immunodominant MHC-associated peptides	WT	H412R	gi|61651673

Spectrin alpha 2		H412R	gi|115496850
Spectrin beta 2 isoform 2		H412R	gi|117938334
Sperm antigen with calponin homology and coiled-coil domains 1	WT	H412R	gi|71979930
Sperm antigen with calponin homology and coiled-coil domains 1		H412R	gi|117949789
Sphingomyelin phosphodiesterase 2, neutral	WT		gi|6678031
Sphingosine phosphate lyase 1	WT	H412R	gi|31543694
Splicing factor 3a, subunit 1		H412R	gi|165932270
Splicing factor 3b, subunit 2	WT	H412R	gi|30794206
Splicing factor 3b, subunit 4	WT	H412R	gi|23346437
Staphylococcal nuclease domain containing 1		H412R	gi|77404392
Structural maintenance of chromosomes 2		H412R	gi|62990166
Structural maintenance of chromosomes 4		H412R	gi|29789347
Succinate-CoA ligase, GDP-forming, alpha subunit		H412R	gi|9845299
Superkiller viralicidic activity 2-like 2		H412R	gi|21312352
T-cell, immune regulator 1	WT		gi|209863008
TAP binding protein isoform 1	WT	H412R	gi|70778974
TAR DNA binding protein isoform 5		H412R	gi|56682935
TNF receptor-associated protein 1		H412R	gi|13385998
TRNA splicing endonuclease 34		H412R	gi|13195596
Tetratricopeptide repeat domain 27		H412R	gi|164519039
Thioredoxin 1	WT	H412R	gi|6755911
Thioredoxin domain containing 10	WT	H412R	gi|117606385
Thioredoxin domain containing 5		H412R	gi|83921612
Thioredoxin interacting protein isoform 1	WT	H412R	gi|60687518
Thioredoxin-related transmembrane protein 2	WT	H412R	gi|21313210
Three prime repair exonuclease 1	WT	H412R	gi|59624981
Threonyl-tRNA synthetase 2, mitochondrial		H412R	gi|21313644
Thymopoietin isoform delta	WT	H412R	gi|121949767
Toll-like receptor 13	WT		gi|45429999
Toll-like receptor 2	WT		gi|158749638
Toll-like receptor 3	WT		gi|31543872
Toll-like receptor 7	WT		gi|18875360
Toll-like receptor 9	WT		gi|157057166
Toll-like receptor 9	WT		gi|20140793
Torsin A interacting protein 1	WT		gi|21450141
Transferrin receptor		H412R	gi|11596855
Transforming growth factor beta regulated gene 4		H412R	gi|194394227
Transgelin 2		H412R	gi|30519911
Translation initiation factor eIF-2B subunit alpha/beta/delta-like protein	WT	H412R	gi|31541890
Translocase of inner mitochondrial membrane 50 homolog	WT	H412R	gi|22094989
Translocation protein 1	WT	H412R	gi|39930429
Transmembrane emp24 domain-containing protein 10	WT	H412R	gi|21312062
Transmembrane emp24 protein transport domain containing 9	WT	H412R	gi|145966911
Transmembrane protein 109		H412R	gi|19527378
Transmembrane protein 214	WT		gi|31559970
Transmembrane protein 33 isoform 1	WT	H412R	gi|22267448
Transmembrane protein 43	WT	H412R	gi|21311891
Transmembrane protein 55b	WT		gi|84095197
Transporter 1, ATP-binding cassette, sub-family B		H412R	gi|7305539
Tripartite motif protein 27	WT	H412R	gi|125347389
Tripartite motif protein 28		H412R	gi|170295840
Tripartite motif-containing 32		H412R	gi|27477053
Tropomodulin 3		H412R	gi|8394460
Tropomyosin 1, alpha, isoform CRA_k		H412R	gi|148694203
Tropomyosin 4		H412R	gi|47894398
Tropomyosin alpha-3 chain		H412R	gi|20178336

Ts translation elongation factor, mitochondrial		H412R	gi|21313468
Tu translation elongation factor, mitochondrial	WT	H412R	gi|27370092
Tubulin folding cofactor B		H412R	gi|170650659
Tubulin, beta 4	WT	H412R	gi|31981939
Tubulin, beta 6		H412R	gi|27754056
Tubulin-specific chaperone d	WT	H412R	gi|28077067
Tubulin-specific chaperone e		H412R	gi|31543843
Tumor protein, translationally-controlled 1		H412R	gi|6678437
Tumor suppressor candidate 3	WT	H412R	gi|124248487
Tyrosyl-tRNA synthetase	WT	H412R	gi|165377181
UBX domain containing 8	WT	H412R	gi|158533976
UDP glucuronosyltransferase 1 family, polypeptide A7C	WT	H412R	gi|47059123
UDP-glucose ceramide glucosyltransferase-like 1	WT	H412R	gi|45387933
UMP-CMP kinase	WT	H412R	gi|165377065
UPF0510 protein C19orf63 homolog	WT		gi|166215193
USO1 homolog, vesicle docking protein		H412R	gi|23956096
Ubiquilin 2		H412R	gi|34328236
Ubiquitin specific peptidase 7		H412R	gi|154146209
Ubiquitin-conjugating enzyme E2M	WT	H412R	gi|21704162
Ubiquitin-conjugating enzyme E2Q		H412R	gi|170172548
Ubiquitin-like modifier activating enzyme 6	WT	H412R	gi|27370032
Ubiquitin-like with PHD and ring finger domains 1 isoform B		H412R	gi|162287241
Unnamed protein product		H412R	gi|74214757
Uridine monophosphate synthetase		H412R	gi|33859498
Vac14 homolog		H412R	gi|31542488
Vacuolar H+ATPase B2	WT	H412R	gi|19705578
Vacuolar protein sorting 16		H412R	gi|46852153
Vacuolar protein sorting 35		H412R	gi|13928670
Valosin containing protein	WT	H412R	gi|30023842
Valyl-tRNA synthetase	WT	H412R	gi|34328204
Vav 1 oncogene		H412R	gi|31981440
Vesicle amine transport protein 1 homolog (T californica)		H412R	gi|33859662
Vesicle-associated membrane protein, associated protein A	WT	H412R	gi|94721328
Vimentin		H412R	gi|31982755
Voltage-dependent anion channel 1	WT	H412R	gi|6755963
Voltage-dependent anion channel 2	WT	H412R	gi|6755965
WD repeat domain 36 isoform 2		H412R	gi|158517942
WD repeat domain 6		H412R	gi|13878227
Werner helicase interacting protein 1		H412R	gi|31981384
Williams-Beuren syndrome chromosome region 16 homolog		H412R	gi|15809010
Wiskott-Aldrich syndrome homolog		H412R	gi|6678581
XTP3-transactivated protein B		H412R	gi|114205437
YME1-like 1		H412R	gi|7305635
Zinc metalloproteinase, STE24 homolog		H412R	gi|27370012

Table 15: List of potential Clptm interaction partners.

Protein Description	Protein Accession
5'-methylthioadenosine phosphorylase	gi|45544618
7-dehydrocholesterol reductase	gi|6681179
ATP synthase, H+ transporting, mitochondrial F1 complex, alpha subunit, isoform 1	gi|6680748
ATP-binding cassette, subfamily G, member 1	gi|6752940
ATPase type 13A1	gi|18875382
ATPase, Ca++ transporting, slow twitch 2 isoform a	gi|158635979

ATPase, H+ transporting, V0 subunit D isoform 1	gi|31981304
ATPase, H+ transporting, lysosomal accessory protein 1	gi|9055172
Acetyl-Coenzyme A acyltransferase 1B	gi|22122797
Acyl-Coenzyme A dehydrogenase, medium chain	gi|6680618
Aldolase A, fructose-bisphosphate	gi|6671539
Alpha-1,3-mannosyltransferase ALG3	gi|22122365
Annexin A5	gi|6753060
Archain 1	gi|148747410
Arylacetamide deacetylase-like 1	gi|30520239
Asparaginase like 1	gi|31560239
Atlastin GTPase 3	gi|31559920
B-cell receptor-associated protein 31	gi|31981310
Basic leucine zipper and W2 domains 1	gi|13385296
Basigin isoform 2	gi|116014342
Bri3 binding protein	gi|58037467
CD5 antigen-like precursor	gi|160358823
CLPTM1-like	gi|22122537
COX4 neighbor	gi|6754870
Calcium binding protein P22	gi|9790225
Calnexin	gi|160333216
Casein alpha s1	gi|30794348
Chaperonin subunit 8 (theta)	gi|126723461
Chemokine (C-X3-C) receptor 1	gi|87299632
Chloride channel CLIC-like 1	gi|21704070
Chromosome segregation 1-like	gi|12963737
Cleft lip and palate associated transmembrane protein 1	gi|103472025
Coatomer protein complex subunit alpha	gi|31981828
Coatomer protein complex, subunit beta 1	gi|15426055
Coatomer protein complex, subunit beta 2 (beta prime)	gi|29789080
Coatomer protein complex, subunit gamma isoform 1	gi|8567338
Coiled-coil domain containing 115	gi|58037169
Coiled-coil domain containing 47	gi|125628650
Coronin, actin binding protein 1A	gi|6753492
Cytochrome P450 reductase	gi|6679421
Cytochrome P450, family 20, subfamily A, polypeptide 1	gi|74271886
Cytochrome b-245, beta polypeptide	gi|161333819
Cytochrome b-5	gi|13385268
Cytochrome b5 type B precursor	gi|31542438
Damage specific DNA binding protein 1	gi|7657011
Dehydrogenase/reductase (SDR family) member 13	gi|117647267
Der1-like domain family, member 2	gi|15808990
Dihydrolipoamide S-succinyltransferase (E2 component of 2-oxo-glutarate complex)	gi|21313536
DnaJ (Hsp40) homolog, subfamily B, member 11	gi|110625998
DnaJ (Hsp40) homolog, subfamily B, member 12	gi|31982701
Dolichyl-di-phosphooligosaccharide-protein glycotransferase	gi|46195798
ER lipid raft associated 1	gi|31981799
ER lipid raft associated 2	gi|23956396
Emerin	gi|6679641
Enolase 2, gamma neuronal	gi|7305027
Env polypeptide	gi|200091
Epsilon subunit of coatomer protein complex	gi|10946972
Equilibrative nucleoside transporter 1	gi|12584968
Eukaryotic translation initiation factor 3, subunit 6	gi|45476573
FK506 binding protein 52	gi|6753882
Fibrinogen, alpha polypeptide isoform 1	gi|167555029
Galactokinase 1	gi|93102413

Guanine nucleotide binding protein (G protein), beta polypeptide 2 like 1	gi|6680047
HCLS1 associated X-1	gi|6754160
Heat shock protein 1 (chaperonin)	gi|183396771
Heme oxygenase (decycling) 2	gi|209862939
Hemoglobin alpha 1 chain	gi|145301578
Histidine ammonia lyase	gi|6754152
Hydrogen/potassium-exchanging ATPase 4A	gi|110225337
Hypothetical protein 4732456N10	gi|29244176
Hypothetical protein LOC215900	gi|31982193
Hypothetical protein LOC230866 isoform 1	gi|31542273
Implantation-associated protein	gi|148747202
Importin 5	gi|29789199
Intergral membrane protein 1	gi|148747128
Isoleucyl-tRNA synthetase	gi|29789383
L-arginine:glycine amidinotransferase	gi|13385454
LAG1 homolog, ceramide synthase 2	gi|22095015
Lectin, mannose-binding 2	gi|34328278
Leucine rich repeat containing 59	gi|19527026
Low density lipoprotein receptor-related protein associated protein 1	gi|63999380
Major facilitator superfamily domain containing 10	gi|13386144
Malectin	gi|188497650
Membrane magnesium transporter 1	gi|22122803
Na+/K+ -ATPase alpha 1 subunit	gi|21450277
Na+/K+ -ATPase alpha 2 subunit	gi|30409956
Neuroplastin	gi|153945724
Nucleolin	gi|84875537
PREDICTED: DnaJ (Hsp40) homolog, subfamily B, member 14	gi|149251954
PREDICTED: hypothetical protein LOC72512 isoform 13	gi|94404729
Paraoxonase 3	gi|27370510
Peripheral myelin protein 2	gi|71892436
Phosphatidylinositol glycan anchor biosynthesis, class S	gi|41351529
Phosphoglycerate dehydrogenase	gi|52353955
Phosphoribosylaminoimidazole carboxylase, phosphoribosylaminoimidazole succinocarboxamide synthetase	gi|13385434
Presenilin 2	gi|190684663
Presenilin-like protein 3	gi|23094389
Progressive ankylosis	gi|157951668
Prolactin regulatory element binding protein	gi|158749640
Proliferating cell nuclear antigen	gi|7242171
Proteasome 26S ATPase subunit 4	gi|124248577
Proteasome 26S ATPase subunit 6	gi|27754103
Proteasome 26S non-ATPase subunit 11	gi|134053905
Protein disulfide-isomerase A3	gi|112293264
Protein phosphatase 2a, catalytic subunit, alpha isoform	gi|9506983
Protein tyrosine phosphatase, non-receptor type 1	gi|133505845
Pyrophosphatase	gi|27754065
RAB1, member RAS oncogene family	gi|6679587
RAB18, member RAS oncogene family	gi|30841008
RAB1B, member RAS oncogene family	gi|21313162
RAB7, member RAS oncogene family	gi|148747526
RIKEN cDNA 2310044H10	gi|37574074
RIKEN cDNA 2900064A13	gi|19526956
RNA polymerase II transcriptional coactivator	gi|6755364
Ribophorin I	gi|31543605
Ribophorin II	gi|34996495
Ribosomal protein S19	gi|12963511

RuvB-like protein 1	gi|9790083
RuvB-like protein 2	gi|6755382
SAC1 (supressor of actin mutations 1, homolog)-like	gi|13507622
SEC22 vesicle trafficking protein-like 1	gi|6755448
Sec11-like 1	gi|9910550
Serine (or cysteine) proteinase inhibitor, clade A, member 1a	gi|6678079
Signal peptidase complex subunit 2 homolog	gi|13385134
Signal recognition particle receptor, B subunit	gi|6678137
Signal sequence receptor, alpha	gi|165377206
Signal sequence receptor, delta	gi|6678145
Signal sequence receptor, gamma	gi|21312968
Solute carrier family 11 (proton-coupled divalent metal ion transporters), member 1	gi|190877473
Solute carrier family 16, member 1	gi|6677995
Solute carrier family 16, member 3	gi|84697028
Solute carrier family 16, member 6 isoform a	gi|71067107
Solute carrier family 19 (sodium/hydrogen exchanger), member 1	gi|13654260
Solute carrier family 2 (facilitated glucose transporter), member 6	gi|153945872
Solute carrier family 38, member 10	gi|31541852
Solute carrier family 6 (neurotransmitter transporter, betaine/GABA), member 12	gi|92110009
Solute carrier organic anion transporter family, member 4a1	gi|22507335
Splicing factor 3b, subunit 4	gi|23346437
Squalene epoxidase	gi|6678127
Sterol O-acyltransferase 1	gi|84619697
Succinate dehydrogenase Fp subunit	gi|54607098
Succinate dehydrogenase complex, subunit B, iron sulfur (Ip)	gi|34328286
Succinate-CoA ligase, GDP-forming, alpha subunit	gi|9845299
Succinate-Coenzyme A ligase, GDP-forming, beta subunit	gi|165972309
T-complex protein 1	gi|110625624
Thioredoxin domain containing 1	gi|33859722
Thioredoxin domain containing 10	gi|117606385
Thioredoxin-related transmembrane protein 2	gi|21313210
Three prime repair exonuclease 1	gi|59624981
Thymopoietin isoform beta	gi|121949769
Thymopoietin isoform delta	gi|121949767
Thymopoietin isoform zeta	gi|121949779
Torsin A interacting protein 1	gi|21450141
Transmembrane emp24 domain-containing protein 10	gi|21312062
Transmembrane emp24 protein transport domain containing 5	gi|21746165
Transmembrane protein 111	gi|28827824
Transmembrane protein 120A	gi|29789387
Transmembrane protein 38B	gi|21312532
Transmembrane protein 85	gi|13386014
Tropomyosin 1, alpha	gi|31560030
Tropomyosin 3, gamma	gi|40254525
Tumor differentially expressed protein 1	gi|213385301
Tyrosine 3-monooxygenase/tryptophan 5-monooxygenase activation protein, zeta polypeptide	gi|6756041
UBX domain containing 8	gi|158533976
Ubiquinol-cytochrome c reductase core protein 1	gi|46593021
Unc93 homolog B	gi|23956094
Unnamed protein product	gi|74226916
Vesicle-associated membrane protein, associated protein A	gi|94721328
Vesicle-associated membrane protein, associated protein B and C	gi|31543940
Zinc metalloproteinase, STE24 homolog	gi|27370012

Peptides of selected proteins found by large scale immunoprecipitation and mass spectrometry analysis of wild type UNC93B:

Clptm (peptide coverage 26.3%)

MAAAQEADGAGSAVVAAGGGSSGQVTSNGSIGRDTPAETQPQNPPPQPAPNAWQVIKGVLFRIFIIWAIS
SWFRRGPSPQDQSGPGGAPRVASRNLFPKDTLMNLHVYISEHEHFTDFNATSALFWEQHDLVYGDWTSGE
NSDGCYEHFAELDIPQSVQQNGSIYIHVYFTKSGFHPDPRQKALYRRLATVHMSRMINKYKRRRFQKTKN
LLTGETEADPEMIKRAEDYGPVEVISHWHPNITININVDDHTPWVKGSVPPPLDQYVKFDAVSGDYYPIIY
FNDYWNLQKDYYPINESLASLPLRVSFCPLSLWRWQLYAAQSTKSPWNFLGDELYEQSDEEQDSVKVALL
ETSPYLLALTIIVSIVHSVFEFLAFKNDIQFWNSRQSLEGLSVRSVFFGVFQSFVVLLYILDNETNFVVQ
VSVFIGVLIDLWKITKVMDVRLDREHRVAGIFPCPTFKDKSTYIESSTKVYDDMAFRYLSWILFPLLGCY
AVYSLLYLEHKGWYSWVLSMLYGFLLTFGFITMTPQLFINYKLKSVAHLPWRMLTYKALNTFIDDLFAFV
IKMPVMYRIGCLRDDVVFFIYLYQRWIYRVDPTRVNEFGMSGEDVSAAASRAQASTAAGALTPAPSTAVS
GEDASTVPKATSGACTASQPQEAPPKPAEDKKKD

PTP1B (peptide coverage 7.8%)

MEMEKEFEEIDKAGNWAAIYQDIRHEASDFPCKVAKLPKNKNRNRYRDVSPFDHSRIKLHQEDNDYINAS
LIKMEEAQRSYILTQGPLPNTCGHFWEMVWEQKSRGVVMLNRIMEKGSLKCAQYWPQQEEKEMVFDDTGL
KLTLISEDVKSYYTVRQLELENLTTKETREILHFHYTTWPDFGVPESPASFLNFLFKVRESGSLSLEHGP
IVVHCSAGIGRSGTFCLADTCLLLMDKRKDPSSVDIKKVLLEMRRFRMGLIQTADQLRFSYLAVIEGAKF
IMGDSSVQDQWKELSREDLDLPPEHVPPPPRPPKRTLEPHNGKCKELFSSHQWVSEETCGDEDSLAREEG
RAQSSAMHSVSSMSPDTEVRRRMVGGGLQSAQASVPTEEELSSTEEEHKAHWPSHWKPFLVNVCMATLLA
TGAYLCYRVCFH

Trex1 (peptide coverage 10.2%)

MGSQTLPHGHMQTLIFLDLEATGLPSSRPEVTELCLLAVHRRALENTSISQGHPPPVPRPPRVVDKLSLC
IAPGKACSPGASEITGLSKAELEVQGRQRFDDNLAILLRAFLQRQPQPCCLVAHNGDRYDFPLLQTELAR
LSTPSPLDGTFCVDSIAALKALEQASSPSGNGSRKSYSLGSIYTRLYWQAPTDSHTAEGDVLTLLSICQW
KPQALLQWVDEHARPFSTVKPMYGTPATTGTTNLRPHAATATTPLATANGSPSNGRSRRPKSPPPEKVPE
APSQEGLLAPLSLLTLLTLAIATLYGLFLASPGQ

Peptides of selected proteins found by large scale immunoprecipitation and mass spectrometry analysis of mutant (H412R) UNC93B:

Clptm (peptide coverage 27.7%)

MAAAQEADGAGSAVVAAGGGSSGQVTSNGSIGRDTPAETQPQNPPPQPAPNAWQVIKGVLFRIFIIWAIS
SWFRRGPSPQDQSGPGGAPRVASRNLFPKDTLMNLHVYISEHEHFTDFNATSALFWEQHDLVYGDWTSGE
NSDGCYEHFAELDIPQSVQQNGSIYIHVYFTKSGFHPDPRQKALYRRLATVHMSRMINKYKRRRFQKTKN
LLTGETEADPEMIKRAEDYGPVEVISHWHPNITININVDDHTPWVKGSVPPPLDQYVKFDAVSGDYYPIIY
FNDYWNLQKDYYPINESLASLPLRVSFCPLSLWRWQLYAAQSTKSPWNFLGDELYEQSDEEQDSVKVALL
ETSPYLLALTIIVSIVHSVFEFLAFKNDIQFWNSRQSLEGLSVRSVFFGVFQSFVVLLYILDNETNFVVQ
VSVFIGVLIDLWKITKVMDVRLDREHRVAGIFPCPTFKDKSTYIESSTKVYDDMAFRYLSWILFPLLGCY
AVYSLLYLEHKGWYSWVLSMLYGFLLTFGFITMTPQLFINYKLKSVAHLPWRMLTYKALNTFIDDLFAFV
IKMPVMYRIGCLRDDVVFFIYLYQRWIYRVDPTRVNEFGMSGEDVSAAASRAQASTAAGALTPAPSTAVS
GEDASTVPKATSGACTASQPQEAPPKPAEDKKKD

PTP1B (peptide coverage 30.6%)

MEMEKEFEEIDKAGNWAAIYQDIRHEASDFPCKVAKLPKNKNRNRYRDVSPFDHSRIKLHQEDNDYINAS
LIKMEEAQRSYILTQGPLPNTCGHFWEMVWEQKSRGVVMLNRIMEKGSLKCAQYWPQQEEKEMVFDDTGL
KLTLISEDVKSYYTVRQLELENLTTKETREILHFHYTTWPDFGVPESPASFLNFLFKVRESGSLSLEHGP
IVVHCSAGIGRSGTFCLADTCLLLMDKRKDPSSVDIKKVLLEMRRFRMGLIQTADQLRFSYLAVIEGAKF
IMGDSSVQDQWKELSREDLDLPPEHVPPPPRPPKRTLEPHNGKCKELFSSHQWVSEETCGDEDSLAREEG
RAQSSAMHSVSSMSPDTEVRRRMVGGGLQSAQASVPTEEELSSTEEEHKAHWPSHWKPFLVNVCMATLLA
TGAYLCYRVCFH

Trex1 (peptide coverage 16.6%)

MGSQTLPHGHMQTLIFLDLEATGLPSSRPEVTELCLLAVHRRALENTSISQGHPPPVPRPPRVVDKLSLC
IAPGKACSPGASEITGLSKAELEVQGRQRFDDNLAILLRAFLQRQPQPCCLVAHNGDRYDFPLLQTELAR
LSTPSPLDGTFCVDSIAALKALEQASSPSGNGSRKSYSLGSIYTRLYWQAPTDSHTAEGDVLTLLSICQW
KPQALLQWVDEHARPFSTVKPMYGTPATTGTTNLRPHAATATTPLATANGSPSNGRSRRPKSPPPEKVPE
APSQEGLLAPLSLLTLLTLAIATLYGLFLASPGQ

Peptides of selected proteins found by large scale immunoprecipitation and mass spectrometry analysis of Clptm:

PTP1B (peptide coverage 24.7%)

MEMEKEFEEIDKAGNWAAIYQDIRHEASDFPCKVAKLPKNKNRNRYRDVSPFDHSRIKLHQEDNDYINAS
LIKMEEAQRSYILTQGPLPNTCGHFWEMVWEQKSRGVVMLNRIMEKGSLKCAQYWPQQEEKEMVFDDTGL
KLTLISEDVKSYYTVRQLELENLTTKETREILHFHYTTWPDFGVPESPASFLNFLFKVRESGSLSLEHGP
IVVHCSAGIGRSGTFCLADTCLLLMDKRKDPSSVDIKKVLLEMRRFRMGLIQTADQLRFSYLAVIEGAKF
IMGDSSVQDQWKELSREDLDLPPEHVPPPPRPPKRTLEPHNGKCKELFSSHQWVSEETCGDEDSLAREEG
RAQSSAMHSVSSMSPDTEVRRRMVGGGLQSAQASVPTEEELSSTEEEHKAHWPSHWKPFLVNVCMATLLA
TGAYLCYRVCFH

Trex1 (peptide coverage 26.4%)

MGSQTLPHGHMQTLIFLDLEATGLPSSRPEVTELCLLAVHRRALENTSISQGHPPPVPRPPRVVDKLSLC
IAPGKACSPGASEITGLSKAELEVQGRQRFDDNLAILLRAFLQRQPQPCCLVAHNGDRYDFPLLQTELAR
LSTPSPLDGTFCVDSIAALKALEQASSPSGNGSRKSYSLGSIYTRLYWQAPTDSHTAEGDVLTLLSICQW
KPQALLQWVDEHARPFSTVKPMYGTPATTGTTNLRPHAATATTPLATANGSPSNGRSRRPKSPPPEKVPE
APSQEGLLAPLSLLTLLTLAIATLYGLFLASPGQ

STING (peptide coverage 10.8%)

MPYSNLHPAIPRPRGHRSKYVALIFLVASLMILWVAKDPPNHTLKYLALHLASHELGLLLKNLCCLAEEL
CHVQSRYQGSYWKAVRACLGCPIHCMAMILLSSYFYFLQNTADIYLSWMFGLLVLYKSLSMLLGLQSLTP
AEVSAVCEEKKLNVAHGLAWSYYIGYLRLILPGLQARIRMFNQLHNNMLSGAGSRRLYILFPLDCGVPDN
LSVVDPNIRFRDMLPQQNIDRAGIKNRVYSNSVYEILENGQPAGVCILEYATPLQTLFAMSQDAKAGFSR
EDRLEQAKLFCRTLEEILEDVPESRNNCRLIVYQEPTDGNSFSLSQEVLRHIRQEEKEEVTMNAPMTSVA
PPPSVLSQEPRLLISGMDQPLPLRTDLI

Danksagung/Acknowledgment

An dieser Stelle möchte ich mich bei allen bedanken, die mich bei der Anfertigung meiner Doktorarbeit unterstützt haben:

Zuerst möchte ich mich bei Prof. Dr. Melanie M. Brinkmann bedanken, die mich während meiner Doktorarbeit hervorragend betreut hat. Besonders möchte ich mich dafür bedanken, dass sie jederzeit für mich ansprechbar war und mich stets gefördert, aber auch oft sehr gefordert und die Entstehung dieser Arbeit damit erst ermöglich hat.

Ich möchte mich auch bei Prof. Dr. Ralf-Rainer Mendel für die Übernahme der Mentorenschaft für diese Arbeit sowie bei Prof. Dr. Martin Korte für die Übernahme des Prüfungsvorsitzes bedanken.
Außerdem möchte ich mich bei Prof. Dr. Ingo Schmitz, Dr. Maximiliano Gutierrez und Prof. Dr. med. Mathias Hornef für die vielen Anregungen und hilfreichen Diskussionen im Rahmen meiner Thesis Committee Meetings bedanken.

Ein besonderer Dank geht an unsere technischen Assistentinnen Christine Standfuß-Gabisch und Brigitte Denker, die mir während meiner Arbeit bei der Durchführung unzähliger Versuche geholfen haben. Ich bedanke mich auch bei Matthias Ottinger, der mich bei der Planung und Durchführung der *in vivo* Versuche tatkräftig unterstützt hat.

Außerdem möchte mich ganz herzlich bei der gesamten Arbeitsgruppe VIMM inklusive aller ehemaligen Gruppenmitglieder für die gute und produktive Zusammenarbeit bedanken. Christine, Brigitte, Ulrike, Vladimir, Sripriya, Helene, Kendra, Baca und Margit, es hat mir viel Freude gemacht mit euch zu arbeiten. Vor allem wird mir aber auch die Zeit, in der wir nicht unbedingt gearbeitet haben sehr positiv in Erinnerung bleiben. Ich möchte ich mich auch bei den drei Bachelor- und Masterstudenten Olga, Christoph und Ann-Kristin bedanken, die ich während der Zeit meiner Doktorarbeit betreut habe, und die alle einen kleinen Teil zu dieser Arbeit beigetragen haben.

Ein besonderes Dankeschön geht auch an Stefan, dafür, dass er während der gesamten Zeit dieser Arbeit eine wichtige Stütze für mich war und mir immer mit sehr viel Geduld zugehört und mich weiter ermutigt hat.

Nicht zuletzt danke ich auch meiner Familie, die mich nicht nur während der letzten dreieinhalb Jahre meiner Doktorarbeit immer unterstützt hat.